



HAL
open science

Synthesis and study of compounds able to activate MAIT cells

Thomas Yvorra

► **To cite this version:**

Thomas Yvorra. Synthesis and study of compounds able to activate MAIT cells. Medicinal Chemistry. Université Paris sciences et lettres, 2020. English. NNT : 2020UPSJT011 . tel-03200069

HAL Id: tel-03200069

<https://theses.hal.science/tel-03200069>

Submitted on 16 Apr 2021

HAL is a multi-disciplinary open access archive for the deposit and dissemination of scientific research documents, whether they are published or not. The documents may come from teaching and research institutions in France or abroad, or from public or private research centers.

L'archive ouverte pluridisciplinaire **HAL**, est destinée au dépôt et à la diffusion de documents scientifiques de niveau recherche, publiés ou non, émanant des établissements d'enseignement et de recherche français ou étrangers, des laboratoires publics ou privés.



THÈSE DE DOCTORAT
DE L'UNIVERSITÉ PSL

Préparée à l'Institut Curie
UMR3666/U1143 - Chimie & Biologie de la Cellule

**Synthèse et étude de composés susceptibles d'activer
les cellules MAIT**

Soutenue par

Thomas Yvorra

Le 24 Novembre 2020

Ecole doctorale n° 563

**Médicament, Toxicologie,
Chimie, Imageries**

Spécialité

Chimie thérapeutique

Composition du jury :

| | |
|---|---------------------------|
| Ana-Maria LENNON-DUMENIL DR, Institut Curie - INSERM | <i>Président</i> |
| Maria DUCA CR, Université Côte d'Azur | <i>Rapporteur</i> |
| Sho YAMASAKI Professeur, Osaka University | <i>Rapporteur</i> |
| Nicolas WILLAND Professeur, Université de Lille | <i>Examineur</i> |
| Olivier LANTZ Directeur scientifique, Institut Curie | <i>Examineur</i> |
| Frédéric SCHMIDT DR, Institut Curie | <i>Directeur de thèse</i> |

Acknowledgements

First of all, I want to acknowledge Dr Maria Duca, Dr Ana-Maria Lennon-Duménil, Pr Sho Yamasaki and Pr Nicolas Willand for having accepted to be part of the jury of my thesis.

I am grateful to my PhD director Dr Frédéric Schmidt and also to Dr Olivier Lantz for the opportunity they offered me to do my thesis at Institut Curie under their supervision along the past 3 years. I also thank the ANR for financial support.

I sincerely thank Anke Steinmetz, Yannick Benedetti, Jidong Zhang from Sanofi, and Pascal Retailleau from Institut de Chimie des Substances Naturelles for their significant contribution to this work.

Special thanks should go to Bhanudas Dasari for his precious help and for the passionate discussions we had. I am also grateful to Jean-Claude and Raphaël for their scientific advice.

Of course, I want to address a great thanks to my PhD labmates: Steve, Anne B., Antoine and Jo. Thank you for all the good moments we spent together. I also thank Siau, Hari, Anne L., Christine, Sylvie, Stéphanie, Julio, Ludo, Sylvain, Fabien, Tati, Stefan, Boom, Justine, Romain, Sebastian, Yannick and Yasmina. Thank you for your permanent good mood and all your help.

Thanks should also go to the colleagues from the biology laboratory with a special thanks to Aurélie and Yara for their help with experiments. Thank you Anastasia, Marion, François, Francesca, Laurie, Emanuele for your help and your kindness.

I want to thank my intern students Louise-Marie and Mélinda. Thank you for your great implication at work. It was really an enriching experience to supervise you during your internship.

Then I thank all my family for having supported me during these long student years. Thanks to my parents Nathalie, Christophe and my step-parents François, Marie; to my grandparents Bonnie et Jean, Papi et Mamie Guerzi, Papi Pomme; to my brothers Adri and Clément; to Estelle, Maxou, Anne, Rachid, Soso, Oncle Ben, Habibi Touret and Loulou.

I want to finish by acknowledging my wife Selma for her tremendous support. Thank you for all the things you have done for me. I wish to dedicate this thesis to you and our wonderful daughter Assia.

Table of contents

| | |
|--|-----------|
| LIST OF FIGURES | 9 |
| LIST OF SCHEMES..... | 13 |
| LIST OF TABLES | 14 |
| LIST OF ABBREVIATIONS..... | 15 |
| GENERAL INTRODUCTION | 19 |
| INTRODUCTION: MAIT CELLS..... | 21 |
| I. MAIT CELL BIOLOGY OVERVIEW | 21 |
| A. MAIT cell development..... | 21 |
| B. MAIT cell phenotype..... | 22 |
| C. Frequency and localization..... | 22 |
| D. Effector functions | 23 |
| II. MAIT CELL LIGANDS AND ACTIVATION | 23 |
| A. TCR-MR1 dependent modulation of MAIT cell activity..... | 23 |
| 1. <i>MHC class I-related (MR1) protein</i> | 23 |
| 2. <i>MAIT cell inhibitory ligands derived from folic acid (vitamin B9)</i> | 24 |
| 3. <i>MAIT cell stimulatory ligands derived from the riboflavin (vitamin B2) pathway</i> | 25 |
| 4. <i>Molecular basis for MR1 binding and TCR recognition</i> | 27 |
| 5. <i>Antigen processing</i> | 29 |
| B. TCR-independent activation of MAIT cells | 30 |
| C. Summary on MAIT cell activation | 31 |
| III. MAIT CELLS AS POTENTIAL THERAPEUTIC TARGETS..... | 33 |
| A. Protection against infectious diseases | 33 |
| 1. <i>Bacterial infections</i> | 33 |
| 2. <i>Viral infections</i> | 33 |
| B. Other roles of MAIT cells in non-infectious diseases | 34 |
| 1. <i>Auto-immune and inflammatory diseases</i> | 34 |
| 2. <i>Cancer</i> | 34 |
| 3. <i>Graft-versus-host-disease (GvHD)</i> | 34 |
| C. Development of immunotherapies targeting MAIT cells | 35 |
| IV. OVERVIEW OF THE RESEARCH AIMING TO FIND NEW ANTIGENS OF MAIT CELLS..... | 37 |

| | | |
|--|--|-----------|
| A. | Synthesis of new MAIT cell competitive antagonists..... | 37 |
| B. | Analytical study and synthesis of new stable agonists of 5-OP-RU..... | 37 |
| C. | Identification of drugs and drug-like molecules able to modulate MAIT cell activity..... | 39 |
| D. | Design of 5-OP-RU analogues to unravel the structural basis for the recognition of MAIT cell antigens by MR1 and the TCR | 40 |
| RESEARCH WORK | | 45 |
| I. INTRODUCTION | | 45 |
| II. SYNTHESIS AND STUDY OF STABLE ANALOGUES OF 5-OP-RU..... | | 47 |
| A. | Synthesis and chemical study of 5-A-RU and 5-OP-RU | 47 |
| 1. | <i>Bibliographic review.....</i> | 47 |
| 2. | <i>Syntheses of 5-A-RU.....</i> | 52 |
| 3. | <i>Analytical study of 5-A-RU.....</i> | 54 |
| 4. | <i>Synthesis of 5-OP-RU</i> | 57 |
| B. | Design, synthesis and biological evaluation of new stable analogues of 5-OP-RU | 58 |
| 1. | <i>Medicinal chemistry strategy.....</i> | 58 |
| 2. | <i>Chemical modulation of the α-iminocarbonyl group.....</i> | 60 |
| 3. | <i>Pharmacomodulation of the D-ribitylamine moiety</i> | 65 |
| 4. | <i>Synthesis of stable fused bicyclic analogues of 5-OP-RU.....</i> | 66 |
| C. | Biological evaluation..... | 69 |
| 1. | <i>Description of the tests used for the biological evaluation of the molecules</i> | 69 |
| 2. | <i>Results.....</i> | 70 |
| D. | Structure-activity relationships | 76 |
| III. PRODRUG STRATEGY AND VECTORIZATION OF 5-A-RU | | 77 |
| A. | Introduction and rationale | 77 |
| B. | Design, synthesis and biological evaluation of a new prodrug of 5-A-RU | 77 |
| 1. | <i>Design of an enzymatically cleavable prodrug of 5-A-RU</i> | 77 |
| 2. | <i>Chemical synthesis.....</i> | 78 |
| 3. | <i>Biochemical and biological evaluation of the prodrugs</i> | 88 |
| C. | Design, synthesis and biological evaluation of a self-immolative prodrug of 5-A-RU..... | 91 |
| 1. | <i>Rationale and bibliography</i> | 91 |
| 2. | <i>Design of the self-immolative prodrug.....</i> | 93 |
| 3. | <i>Chemical synthesis of the prodrug.....</i> | 93 |
| 4. | <i>Biological evaluation.....</i> | 96 |
| D. | Summary and conclusion | 97 |

| | |
|--|------------|
| IV. DESIGN AND SYNTHESIS OF A NEW CHEMICAL PROBE FOR THE STUDY OF MAIT CELL BIOLOGY | 99 |
| A. Introduction | 99 |
| 1. <i>Rationale and goals</i> | 99 |
| 2. <i>Bio-orthogonal chemistry</i> | 99 |
| 3. <i>Design of the chemical probe</i> | 104 |
| B. Synthesis of the chemical probe | 106 |
| 1. <i>Synthesis strategy</i> | 106 |
| 2. <i>Initial synthesis route with attempts to functionalize D-ribose by an amine and an alkyne</i> | 107 |
| 3. <i>Second strategy: synthesis of an azido precursor of protected D-ribitylamine</i> | 108 |
| 4. <i>Synthesis of ethinyl-5-A-RU and ethinyl-5-OP-RU</i> | 109 |
| 5. <i>Diastereomers 71a and 71b separation and identification</i> | 110 |
| C. Biological evaluation and validation of the chemical probes | 112 |
| 1. <i>Rationale and goals</i> | 112 |
| 2. <i>Biological evaluation of the diastereomeric mixture 73</i> | 112 |
| 3. <i>Biological evaluation of the two diastereomers 73a and 73b</i> | 113 |
| 4. <i>In vitro validation of the use of 73 as a chemical probe for the study of MAIT cell biology</i> | 115 |
| D. Summary and conclusion | 116 |
| V. GENERAL CONCLUSION AND PERSPECTIVES | 117 |
| EXPERIMENTAL PART | 119 |
| I. CHEMISTRY | 119 |
| A. General aspects | 119 |
| B. Protocol and product characterizations | 120 |
| C. Molecular modelling | 193 |
| D. X-ray crystallography | 193 |
| E. Biochemical assay | 194 |
| II. BIOLOGY | 194 |
| A. Cell culture | 194 |
| B. Bone marrow dendritic cells (BMDCs) | 194 |
| C. Mice | 195 |
| D. MR1 up-regulation assay | 195 |
| E. MAIT cell activation assay | 195 |
| F. Competition assay | 196 |
| G. MR1 tetramer staining assay | 196 |
| 1. <i>MR1 tetramer preparation</i> | 196 |

| | |
|---|------------|
| 2. Tetramer staining assay..... | 196 |
| H. Click chemistry experiments..... | 197 |
| APPENDICES | 199 |
| Appendix A : Flow cytometry gating strategy for MR1 up-regulation assay..... | 199 |
| Appendix B : Flow cytometry gating strategy for MAIT cell activation assay..... | 200 |
| Appendix C: Molecular modelling of clickable analogues of 5-A-RU..... | 201 |
| Appendix D : Crystallographic data of compound 71a | 202 |
| BIBLIOGRAPHY | 205 |

List of figures

| | |
|---|----|
| Figure 1: Main T cell subsets and their antigen presentation mode | 19 |
| Figure 2: Intrathymic development of T cells..... | 21 |
| Figure 3: Human classical MAIT cell phenotype | 22 |
| Figure 4: Frequency and localization of MAIT cells..... | 23 |
| Figure 5: Different modes of antigen presentation to conventional and non-conventional T cells..... | 24 |
| Figure 6: Formation of 6-Fp MR1 ligand from photodegradation of folic acid | 25 |
| Figure 7: Riboflavin and ribityllumazine biosynthesis pathways..... | 26 |
| Figure 8: Chemical structure of hypothetical MAIT cell agonists..... | 26 |
| Figure 9: MAIT cell pyrimidine adduct antigen biosynthesis..... | 27 |
| Figure 10: Structural basis of MR1-binding and TCR recognition of 6-Fp | 28 |
| Figure 11: Structural basis of MR1-binding and TCR recognition of MAIT cell vitamin B2-derivative antigens..... | 29 |
| Figure 12: MR1 trafficking and antigen processing | 30 |
| Figure 13: Summary of MAIT cell activation process..... | 31 |
| Figure 14: Chemical structure of synthetic MAIT cell inhibitory ligands..... | 37 |
| Figure 15: Analytical study and biological evaluation of 3a-c | 38 |
| Figure 16: Chemical structure of compounds 9-11 | 39 |
| Figure 17: Chemical structure of drugs and drug-like molecules able to modulate MAIT cell functions | 40 |
| Figure 18: Chemical structure of the different AMLs..... | 41 |
| Figure 19: Chemical structure and biological evaluation of glyco-analogues of 5-OP-RU and RL-6-Me-7-OH | 43 |
| Figure 20: Chemical structure and biological evaluation of 6-alkylamino analogues of 5-OP-RU | 44 |
| Figure 21: Objectives of the research project | 46 |
| Figure 22: ¹ H NMR analysis of 5-A-RU in DMSO-d ₆ | 55 |

| | |
|---|-----|
| Figure 23: Proposed degradation mechanism of 5-A-RU by oxidation of the primary aromatic amine | 56 |
| Figure 24: Summary of the different pharmacomodulations envisioned to obtain stable potent analogues of 5-OP-RU | 59 |
| Figure 25: Chemical structure of different alkyl anionic analogues of 5-OP-RU | 60 |
| Figure 26: Docking analysis of 13 inside the MR1-TCR binding groove in comparison with 5-OE-RU.. | 60 |
| Figure 27: Chemical structure of D-ribitylamine modified analogues of 5-OP-RU | 65 |
| Figure 28: MAIT cell activation assay | 70 |
| Figure 29: MR1 up-regulation evaluation of newly synthesized ligands..... | 71 |
| Figure 30: MR1 up-regulation evaluation of 30 and 31 | 72 |
| Figure 31 : MAIT cell staining assay with MR1-5-OP-RU and MR1- 13 tetramers..... | 73 |
| Figure 32: MAIT cell activation by 30 in comparison with 5-OP-RU and 5-A-RU..... | 74 |
| Figure 33: Competitive inhibition of 5-OP-RU by compound C | 75 |
| Figure 34: Competition assay with 30 and 31 | 75 |
| Figure 35: Design of the 5-A-RU prodrug | 78 |
| Figure 36: UPLC-MS analysis of the coupling reaction between 44 and AMC | 83 |
| Figure 37: UPLC-MS analysis of the reaction between 44 and ethynyl-5-A-RU 72 | 85 |
| Figure 38: ¹ H NMR analysis of a. 72 ; b. conjugate 47 | 86 |
| Figure 39: Analysis of the coupling reactions to CML beads (48 and 49) | 87 |
| Figure 40: Cathepsin L cleavage assay of 46 and 48 | 88 |
| Figure 41: UPLC-MS analysis of Cathepsin L cleavage of 46 | 89 |
| Figure 42: Biological evaluation of 47 and 49 on MAIT cells..... | 90 |
| Figure 43: <i>In vivo</i> MAIT cell activation in mice with 5-A-RU and 5-A-RU prodrug (10)..... | 92 |
| Figure 44: Chemical structure of CI-072 | 92 |
| Figure 45: Chemical structure of the self-immolative prodrug of 5-A-RU | 93 |
| Figure 46: Biological evaluation of the different prodrugs on murine MAIT cells..... | 97 |
| Figure 47: Bio-orthogonal reactions | 100 |

| | |
|--|-----|
| Figure 48: Most efficient and commonly used bio-orthogonal reactions..... | 101 |
| Figure 49: Detailed mechanism of CuAAC reaction | 103 |
| Figure 50: Chemical structure of CuAAC ligands | 103 |
| Figure 51: Chemical structure of envisioned ethinyl-functionalized analogues of 5-OP-RU | 104 |
| Figure 52: Poses of ethinyl-5-A-RU docked to MR1/TCR complex in comparison to the crystal structure of the ternary complex of 5-OE-RU..... | 105 |
| Figure 53: Preparative HPLC chromatogram of 71 (separation of the two diastereomers) | 111 |
| Figure 54: ORTEP view of one conformer of compound 71a | 112 |
| Figure 55: Biological evaluation of the diastereomeric mixture 73 | 113 |
| Figure 56: MR1 up-regulation in the presence of 5-OP-RU, 73a or 73b | 114 |
| Figure 57: MAIT cell activation by 5-OP-RU (12), 73a and 73b | 115 |
| Figure 58: Epifluorescence microscopy images showing 73 conjugated to azide-AF ₄₈₈ fluorophore in WT3-m cells or WT3-WT cells..... | 116 |
| Figure 59: Other possible pharmacomodulations of 5-OP-RU | 117 |

List of schemes

| | |
|--|-----|
| Scheme 1: First synthesis of 5-A-RU by Plaut and co-workers | 48 |
| Scheme 2: Different modifications of the initial synthesis of 5-A-RU (by Plaut and co-workers) for the synthesis of lumazine derivatives | 49 |
| Scheme 3: Recent modifications of the synthesis of 5-A-RU to make 5-OP-RU for MAIT cell study.... | 50 |
| Scheme 4: Synthesis of 5-A-RU in protected series | 52 |
| Scheme 5: Synthesis of 5-A-RU in non-protected series | 53 |
| Scheme 6: Syntheses of 12a (5-OP-RU in DMSO) and 12b (5-OP-RU in water) | 58 |
| Scheme 7: Attempt to introduce the iodoethane side chain to get 17 | 61 |
| Scheme 8: Synthesis of 13 | 62 |
| Scheme 9: Initial synthesis of the vinylsulfonate analogue of 5-OP-RU | 63 |
| Scheme 10: Synthetic route towards vinylsulfonate analogue of 5-OP-RU | 64 |
| Scheme 11: Synthesis of compounds 29 , 31 and 32 from Sanofi's chemical precursors | 66 |
| Scheme 12: Synthesis of purinetrione analogue of 5-OP-RU 37 | 67 |
| Scheme 13: Synthesis of 43 | 68 |
| Scheme 14: Synthesis of formylumazine analogue of 5-OP-RU | 69 |
| Scheme 15: Solid phase peptide synthesis of 44 | 79 |
| Scheme 16: synthesis of 46 (44 -AMC conjugate) | 82 |
| Scheme 17: Synthesis of 47 (44 -ethinyl-5-A-RU conjugate)..... | 85 |
| Scheme 18: Synthesis of CML bead conjugates 48 and 49 | 87 |
| Scheme 19: Chemical structure and synthesis of Fmoc-NH-Val-Cit-PAB-5-A-RU conjugate..... | 91 |
| Scheme 20: Synthesis of prodrug linkers 51 and 53 | 94 |
| Scheme 21: Synthesis of 5-A-RU prodrugs 58 and 59 | 95 |
| Scheme 22: Synthesis of CML bead conjugate 60 | 96 |
| Scheme 23: Ethinyl-5-OP-RU chemical synthesis strategy | 106 |
| Scheme 24: Initial synthesis of ethinyl-D-ribitylamine..... | 107 |
| Scheme 25: Attempts to selectively deprotect the primary alcohol of 61 | 108 |

| | |
|---|-----|
| Scheme 26: Synthesis of ethinyl-D-ribitylamine..... | 109 |
| Scheme 27: Synthesis of ethinyl-5-OP-RU 73 | 110 |

List of tables

| | |
|--|----|
| Table 1: Chemical stability, MR1 up-regulation, MAIT cell activity and binding affinity of AMLs..... | 42 |
| Table 2 : Attempts for the chemical coupling of AMC with 44 | 80 |
| Table 3: Attempts for the chemical coupling of 5-A-RU and 72 to 44 | 84 |

List of abbreviations

A

ACN: acetonitrile

AcOH: acetic acid

Ac-6-Fp: acetyl-6-formylpterin

ADC: antibody drug conjugate

AMC: 7-amino-4-methylcoumarin

AMLs: altered metabolite ligands

APCs: antigen presenting cells

B

BMDCs: bone marrow dendritic cells

BTES: 3-(4-((bis((1-(tert-butyl)-1H-1,2,3-triazol-4-yl)methyl)amino)methyl)-1H-1,2,3-triazol-1-yl)propane-1-sulfonic acid

C

CCR5: C-C chemokine receptor 5

CCR6: C-C chemokine receptor 6

CL: Cathepsin L

CML: carboxylate-modified latex beads

CuAAC: copper(I)-assisted azide-alkyne cycloaddition

CXCR6: C-X-C chemokine receptor 6

D

DCF: diclofenac

DCM: dichloromethane

DIPEA or DIEA: *N,N*-diisopropylethylamine

DMF: *N,N*-dimethylformamide

DMP: Dess-Martin periodinane

DMSO: dimethylsulfoxide

E

EC₅₀: half maximal effective concentration

EDC: 1-éthyl-3-(3-diméthylaminopropyl)carbodiimide

EtOAc: ethyl acetate

EtOH: ethanol

ER: endoplasmic reticulum

F

Fmoc: fluorenylmethyloxycarbonyl

G

GvHD: graft-versus-host disease

H

HOBt: 1-hydroxybenzotriazole

HPLC: high performance liquid chromatography

HR-MS: high-resolution mass spectrometry

I

IED-DA: inverse electron-demand Diels-Alder reaction

INF γ : interferon γ

L

LB: latex beads

M

MAITs: Mucosal-associated invariant T cells

MeOH: methanol

MES: 2-(*N*-morpholino)ethanesulfonic acid

MetG: methylglyoxal

MFI: mean fluorescence intensity

MHC: major histocompatibility complex

MR1: MHC class I-related protein

Mtb: *Mycobacterium tuberculosis*

MS: mass spectrometry

N

NIS: *N*-iodosuccinimide

iNKTs: invariant natural killer T cells

NMR: nuclear magnetic resonance

O

ON: overnight

P

PBMCs: peripheral blood mononuclear cells

Pbf: 2,2,4,6,7-pentamethyldihydrobenzofuran-5-sulfonyl

PBS: phosphate-buffered saline

Pd/c: palladium on charcoal

PEG: polyethylene glycol

PLZF: pro-myelocytic leukemia zinc finger

PRR: pattern recognition receptor

PyBOP: benzotriazol-1-yl-oxytripyrrolidinophosphonium hexafluorophosphate

R

ROR γ t: RAR (retinoic acid receptor)-related orphan receptor γ

RP-HPLC: reverse phase high-performance liquid chromatography

RL-6-Me-7-OH: 7-hydroxy-6-methyl-8-D-ribityllumazine

RL-6,7-diMe: 6,7-dimethyl-8-D-ribityllumazine

rRL-6-CH₂OH: reduced 6-hydroxymethyl-8-D-ribityllumazine

RPMI: Roswell Park Memorial Institute medium

rt: room temperature

S

SPAAC: strain-promoted azide-alkyne cycloaddition

SAR: structure-activity relationships

T

T-bet: T-box transcription factor TBX21

TBS or TBDMS: *tert*-butyldimethylsilyl ether

TBTA: tris((1-benzyl-4-triazolyl)methyl)amine

TCFH: chloro-*N,N,N',N'*-tetramethylformamidium hexafluorophosphate

TCO: *trans*-cyclooctene

TCR: T-cell receptor

TFA: trifluoroacetic acid

TFE: 2,2,2-trifluoroethanol

THF: tetrahydrofuran

THPTA: Tris(3-hydroxypropyltriazolylmethyl)amine

TLR: toll-like receptor

TMS: trimethylsilyl

TNBS: 2,4,6-trinitrobenzenesulfonic acid

TNF α : tumor necrosis factor α

U

UPLC-MS: ultra-performance liquid chromatography mass spectrometry

Other:

5-A-RU: 5-amino-6-D-ribitylaminouracil

5-N-RU: 5-nitro-6-D-ribitylaminouracil

5-MOP-RU: 5-(1-methyl-2-oxopropylideneamino)-6-D-ribitylaminouracil

5-OP-RU: 5-(2-oxopropylideneamino)-6-D-ribitylaminouracil

5-OE-RU: 5-(2-oxoethylideneamino)-6-D-ribitylaminouracil

5-F-SA: 5-formaldehyde salicylic acid

3-F-SA: 3-formaldehyde salicylic acid

6-Fp: 6-formylpterin

α -GalCer: α -galactosylceramide

β 2m: β 2-microglobulin

2-OH-1-NA: 2-hydroxy-naphthaldehyde

2,4-DA-6-Fp: 2,4-diamino-6-formylpteridine

General introduction

The immune system is an essential host defense system developed by vertebrates to fight against micro-organism aggressions. The immune system is commonly divided into innate and adaptive (or acquired) responses. The innate immunity is a rapid, first line response to infection led by diverse effector cells such as macrophages, granulocytic cells (neutrophils, eosinophils, basophils, mast cells) and antimicrobial proteins of the complement system. In case they fail to control the infection, a second line of defense called adaptive immunity is triggered leading to a more specific and powerful immune response. The two major effector cells involved in this response are T and B lymphocytes. Once activated, T cells are able to differentiate to effector phenotypes owning diverse essential immune roles like CD4⁺ helper T cells (T_H1, T_H2, T_H17, T_{reg} cells) or cytotoxic CD8⁺ T cells. They also indirectly enable the production of highly specific antibodies as well as the development of an effector memory phenotype through B cell activation.

The activation of conventional T lymphocytes (CD4⁺ and CD8⁺ T cells) is mediated by the presentation of a wide repertoire of antigenic peptides to their $\alpha\beta$ TCR (heterodimeric T-cell receptor) by highly polymorphic major histocompatibility complex (MHC) molecules expressed by antigen presenting cells (APCs). Yet, in the 1990's a new class of unconventional T lymphocytes, commonly called innate-like T cells, was discovered. Unlike conventional T lymphocytes, innate-like T cells are restricted by a limited number of specific antigens presented by non-polymorphic analogues of the MHC (Figure 1).

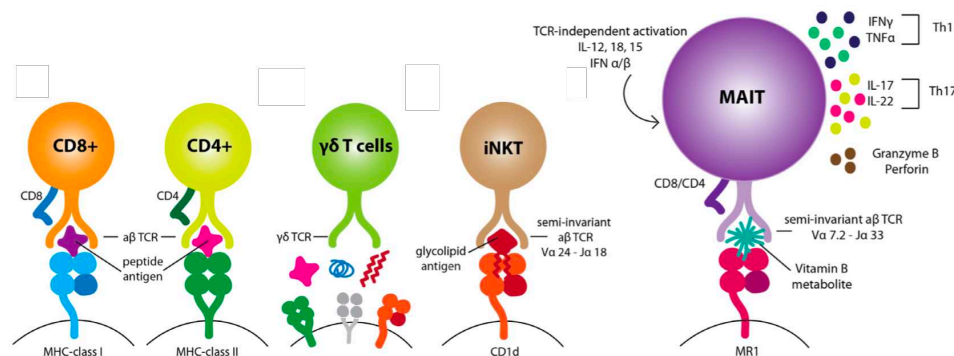


Figure 1: Main T cell subsets and their antigen presentation mode¹

There are two distinct innate-like $\alpha\beta$ T cell populations. iNKT cells (invariant Natural Killer T cells) that are activated by glycolipidic antigens presented by the CD1d molecule. And MAIT cells (Mucosal-Associated Invariant T cells) that were initially identified on the basis of a semi-invariant TCR in human (V α 7.2-J α 33) and mice (V α 19-J α 33), associated with a limited repertoire of β chains^{2,3,4}. In 2003, it was discovered that the MAIT cell TCR was restricted to the non-polymorphic, highly

evolutionary conserved MR1 (MHC class I-related) protein discovered a few years before in 1995⁵. Later in 2014, highly unstable microbial antigens of MAIT cells derived from the vitamin B2 biosynthesis pathway were discovered by Corbett *et al.*⁶.

Research on MAIT cells has dramatically expanded over the past two decades as we are becoming aware of how important this T cell population is, especially for their potential therapeutic applications as antimicrobial agents. Research has been primarily focused on studying the biology of MAIT cells while few researchers have explored MAIT cell antigens. It is now essential to improve our knowledge of these unique antigens and to overcome their chemical instability. This is why, we have decided to focus on synthesizing and studying new compounds that are able to activate MAIT cells, both for medicinal chemistry and chemical biology purposes. Through this work, we aim to increase our knowledge of MAIT cell's biology, as well as to learn crucial information about their therapeutic potential.

We will first give an overview of MAIT cell biology and we will provide a detailed presentation of MAIT cell antigens. We will then introduce our main research objectives and share our results.

Introduction: MAIT cells

I. MAIT cell biology overview

A. MAIT cell development

MAIT cell development occurs in the thymus (Figure 2). Unlike conventional T lymphocytes that are selected by thymic epithelial cells expressing MHC I or II, MAIT cells (and iNKT cells) are selected by MR1-expressing double positive (DP) CD4⁺CD8⁺ thymocytes^{7,8}. The corresponding cells undergo a three stage intrathymic development leading to the expression of diverse characteristic cell-surface markers like C-type lectin CD161 and transcription factors such as PLZF, ROR γ t or T-bet⁹. The nature and requirement of an exogenous ligand for MAIT cell development in the thymus remained unclear until recently. Legoux *et al.* found that the intrathymic development of MAIT cells is governed by commensal bacteria and is dependent on MAIT cell unique microbial ligand that can travel from mucosal tissues to the thymus where it is captured by MR1 for thymic selection¹⁰. MAIT cells finally exit the thymus and continue their maturation depending on commensal bacteria⁴.

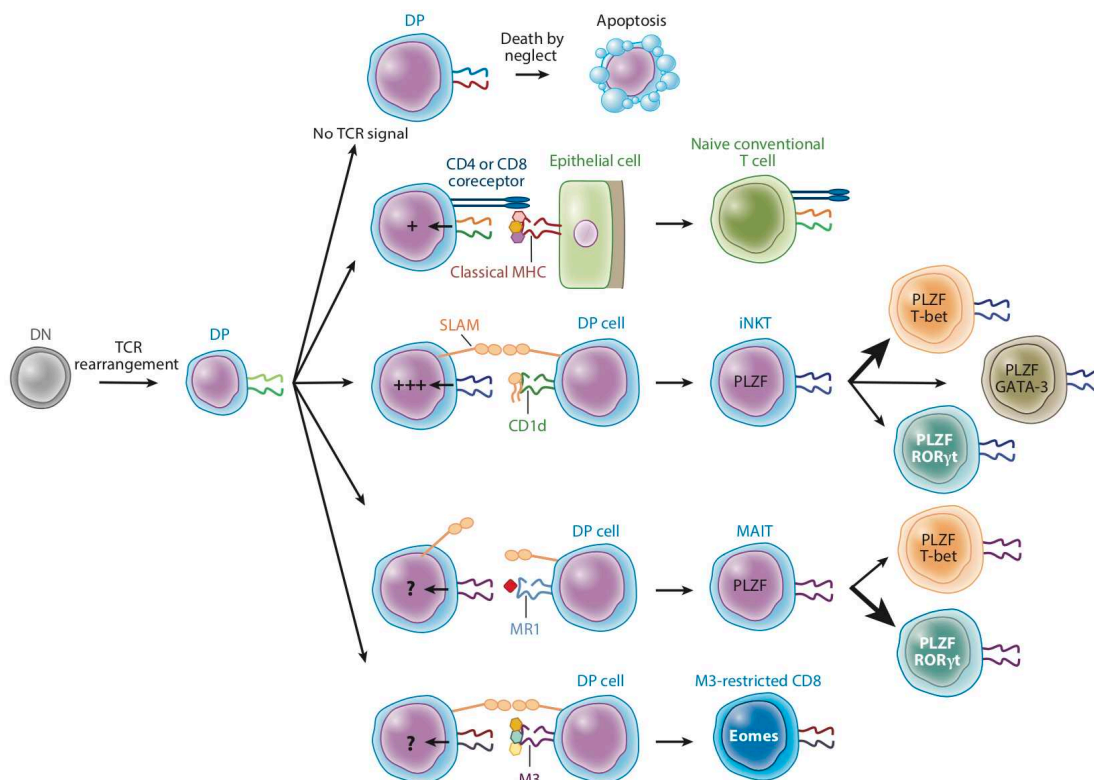


Figure 2: Intrathymic development of T cells¹¹

B. MAIT cell phenotype

MAIT cells are commonly identified and classified according to the different cellular markers they express. MR1 tetramer loaded with MAIT cell antigens and monoclonal antibody specific for the V α 7.2 chain of the MAIT cell TCR are also widely used for the phenotypic analysis¹².

As described before, most of MAIT cells express a semi-invariant TCR with V α 7.2-J α 33/12/20 α chain associated with a limited repertoire of β chains (V β 2-13 in humans) (Figure 3). After thymic maturation, most of human MAIT cells are identified as CD3⁺ V α 7.2⁺ CD161^{high} and CD8⁺ $\alpha\alpha$ or double negative T cells (CD4⁻CD8⁻)¹³. MAIT cells also produce tissue homing chemokine receptors CCR6, CXCR6, CCR5 allowing them to migrate to different parts of the organism (mostly to the liver, gut and lung)¹⁴. They express several interleukin receptors like IL-18R, IL-12R and exhibit an effector memory phenotype with CD45RO and CD95. MAIT cells also express several transcription factors like ROR γ t or PLZF, the latter being essential for stage progression during thymic development⁹.

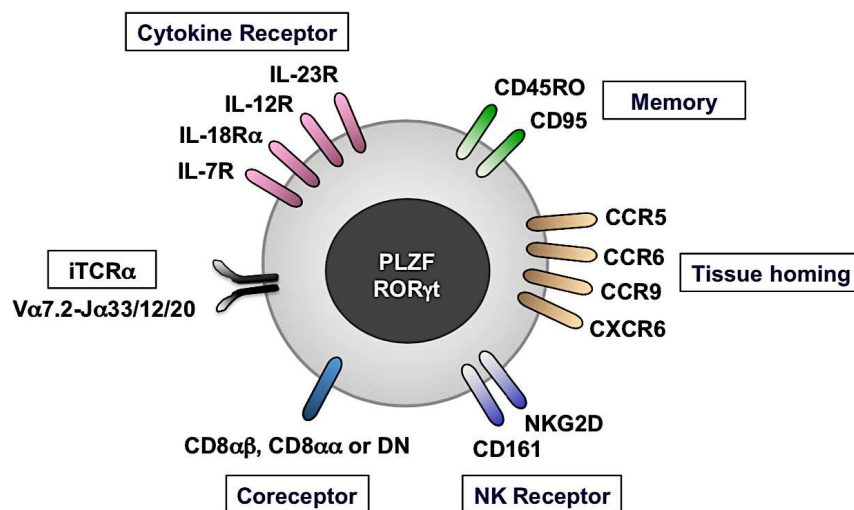


Figure 3: Human classical MAIT cell phenotype¹⁵

C. Frequency and localization

Overall, MAIT cells represent a large part of T cells though their frequency varies in different organs (Figure 4). They are mostly found in human liver (20-50% of T-cells), gastro-intestinal tract (3-5% of intestinal T cells), peripheral blood (1-10% of T cells) and lungs (2-4% of T cells)¹⁶.

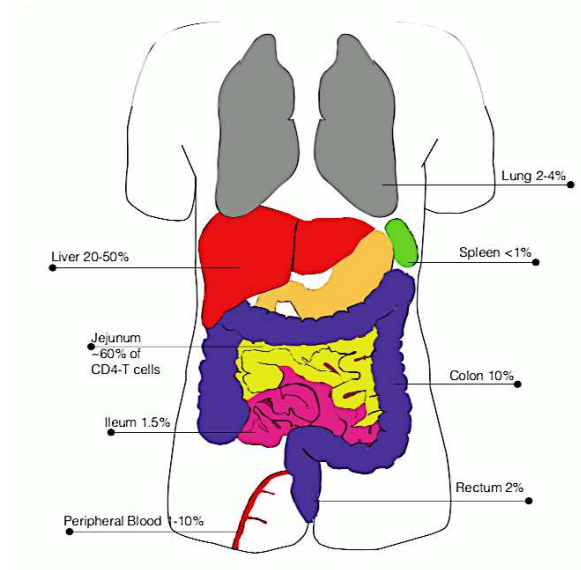


Figure 4: Frequency and localization of MAIT cells¹⁶

D. Effector functions

Upon stimulation, MAIT cells produce and secrete several cytokines, mostly $TNF\alpha$, $INF\gamma$ and IL-17. MAIT cells exert cytotoxic functions as they are able to kill infected cells in a MR1-dependent manner through perforin and granzyme B secretion^{17,18}. Activated MAIT cells can also trigger the activation of other immune cells such as B lymphocytes and dendritic cells, thus eliciting the recruitment of adaptive immune cells¹⁹.

II. MAIT cell ligands and activation

A. TCR-MR1 dependent modulation of MAIT cell activity

1. MHC class I-related (MR1) protein

The major histocompatibility complex (MHC) protects vertebrates by assuring the presentation of a wide array of antigenic peptides to T lymphocytes triggering an adaptive immune response. The MHC is subdivided into two classes (I and II) (Figure 5). Immunogenic peptide-MHC class I complexes are presented at the surface of nucleated cells to cytotoxic $CD8^+$ T cells, while MHC class II complexes are expressed by antigen presenting cells (APCs) and recognized by $CD4^+$ T cells to coordinate and regulate effector cells²⁰. The MHC-encoding genes are highly polymorphic to allow the presentation a vast repertoire of antigenic peptides to conventional T cells. In contrast, some MHC-like molecules are responsible for a specific presentation of a limited number of antigens to innate-

like T cells like iNKT cells and MAIT cells. iNKT cells recognize the MHC analogue CD1d molecule that present lipidic and glycolipidic antigens (like α -GalCer) to the TCR while MAIT cells are restricted to MR1 that present small microbial antigens derived from several vitamin metabolism.

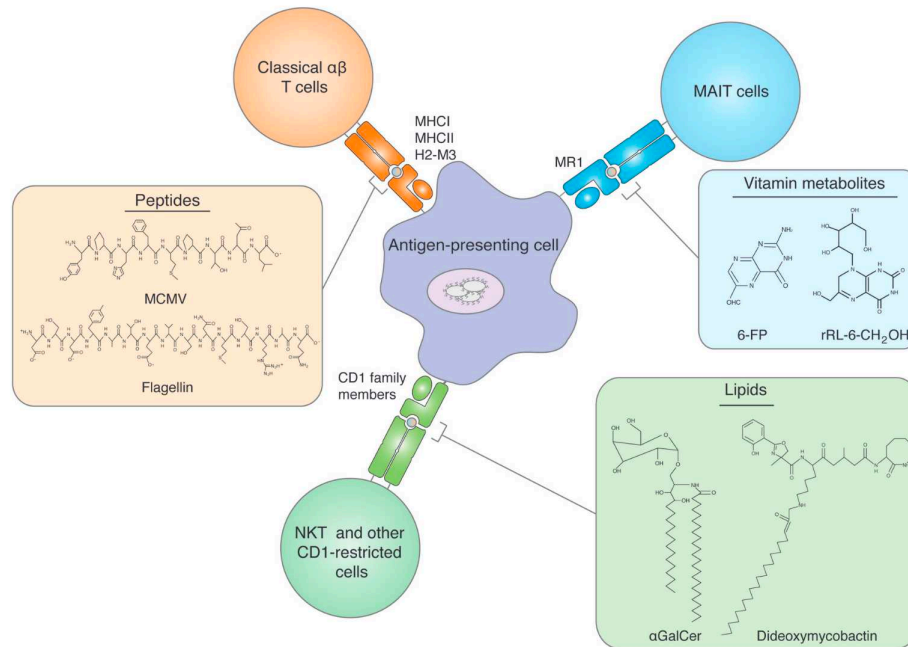


Figure 5: Different modes of antigen presentation to conventional and non-conventional T cells²¹

For humans, MR1 gene is ubiquitously expressed and is located on chromosome 1 near the CD1d gene. It is also highly conserved among mammalian species (90% sequence homology between mouse and human)²². Similarly to MHC class I, MR1 is constituted of three α domains ($\alpha 1$, $\alpha 2$ and $\alpha 3$), a transmembrane domain and an intracytoplasmic tail. To be fully functional, MR1 must bind both to a molecule of $\beta 2$ -microglobulin ($\beta 2m$) and to its antigens.

2. MAIT cell inhibitory ligands derived from folic acid (vitamin B9)

Identifying MAIT cell ligands was initially based on observing the MR1-mediated antimicrobial activity of MAIT cells against several strains of yeasts and bacteria (but not of viruses), meaning that MAIT cell ligands were produced by such micro-organisms^{23,24}. Later, Kjer-Nielsen *et al.* found that a small amount of MR1 was folded in the presence of $\beta 2m$ and RPMI 1640, a common cell culture media, even in the absence of microbes²⁵. RPMI medium contains many components including several vitamins, produced exclusively by yeasts and bacteria but not by animal cells. After having separately tested the different components of this culture media, they found that a significant amount of MR1 was folded in the presence of vitamin B9, also known as folic acid. Mass spectrometry analysis of the folded complex showed that it was actually 6-formylpterine (6-Fp), a photodegradation product of

vitamin B9 formed upon exposure to UV light that was bound to MR1 instead of folic acid (Figure 6). However, 6-Fp was not able to activate Jurkat.MAIT cell line (immortalized human CD4⁺ T lymphocyte cell line expressing human MAIT cell TCR chains) and the molecule inhibited the activation of MAIT cells by *Salmonella tiphymurium* supernatant.

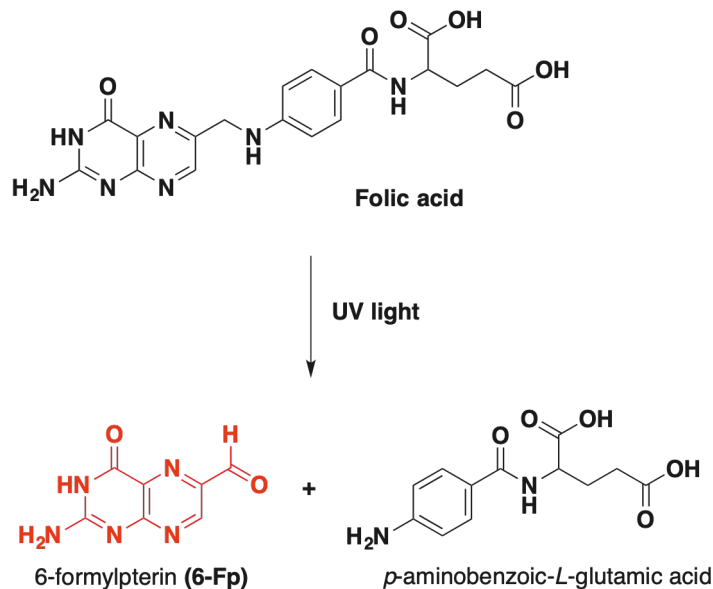


Figure 6: Formation of 6-Fp MR1 ligand from photodegradation of folic acid²⁶

3. MAIT cell stimulatory ligands derived from the riboflavin (vitamin B2) pathway

Bacterial culture of *S. tiphymurium* in vitamin B9 free media (to avoid any competition between stimulatory antigens and 6-Fp) allowed to isolate MR1 complex with the stimulatory antigen bound to the protein. Elution of the ligand followed by mass spectrometry analysis identified two ribityllumazine compounds derived from the riboflavin (vitamin B2) pathway as potential MAIT cell agonists: 7-hydroxy-6-methyl-8-D-ribityllumazine (RL-6-Me-7-OH) and 6,7-dimethyl-8-D-ribityllumazine (RL-6,7-diMe) (blue frame in Figure 7).

These two products were synthesized and tested for Jurkat.MAIT cell activation. Both compounds were active but with lower potency in comparison to *S. tiphymurium* supernatants. This meant that the chemical structure of the more potent MAIT cells agonist still was not elucidated.

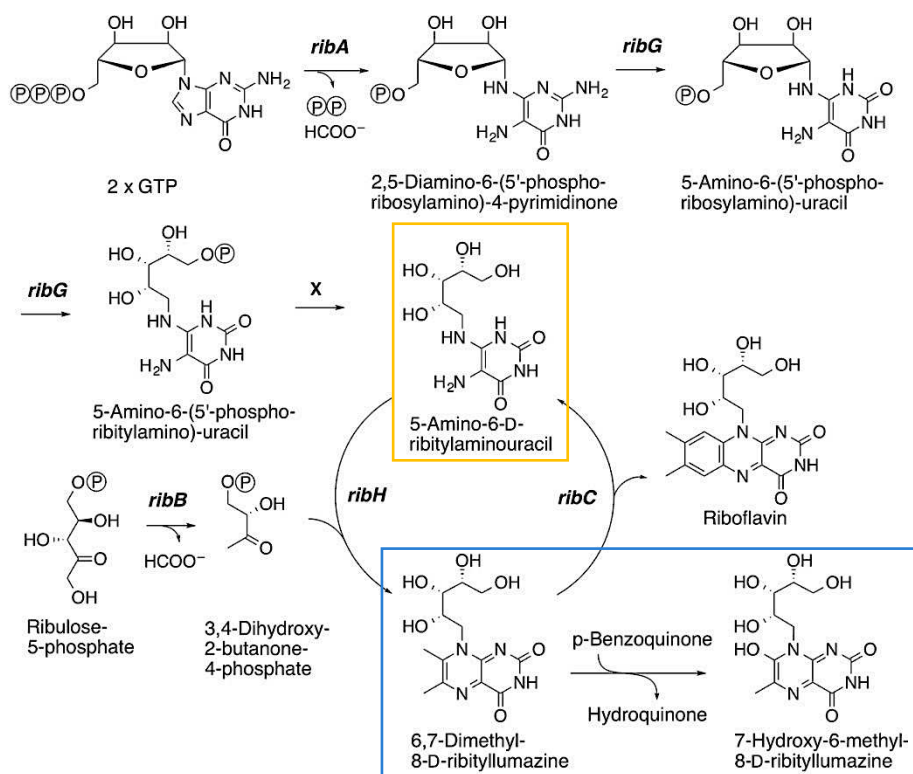


Figure 7: Riboflavin and ribityllumazine biosynthesis pathways²⁷

Three other molecules with similar chemical structure but distinct from the riboflavin pathway were then proposed as potential MAIT cell agonists: rRL-6-CH₂OH, rRL-6-Me-7-OH and 5-OP-RU (with the latter initially thought to be too unstable in water) (Figure 8). rRL-6-CH₂OH was synthesized and it potently activated MAIT cells but crystallographic analyses of the ternary complex (ligand bound to MR1 and the TCR) showed that it was actually a single ring molecule present in the binding pocket instead of the double lumazine rings, meaning rRL-6-CH₂OH was not the potent antigen they were looking for.

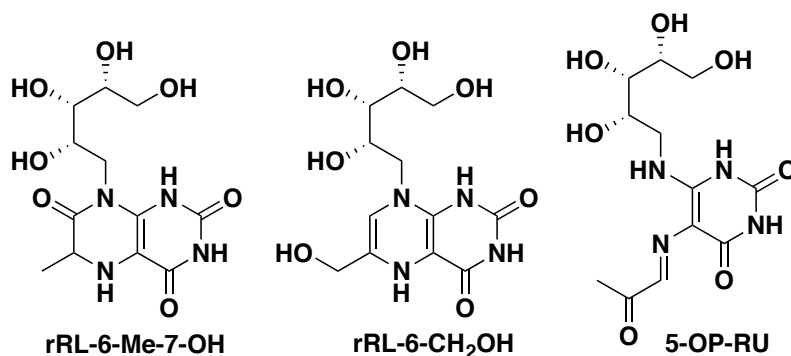


Figure 8: Chemical structure of hypothetical MAIT cell agonists

A genetic approach was complementary used to help identify the ligands⁶. The riboflavin pathway relies on different genes called *rib* genes that are grouped in a same bacterial operon of Gram-positive bacteria (Figure 7). A set of individual *rib* gene deficient bacteria (*Lactococcus lactis*) was cultivated to assess the importance of the different biosynthetic intermediates for MAIT cell activation. While supernatants of *ribB* and *ribH* mutants did not induce lower MAIT cell activation than the wild-type strain, *ribA* and *ribG* mutants clearly did. This result pointed out that the molecule 5-A-RU (5-amino-6-D-ribitylaminouracil, yellow frame in Figure 7) is a key intermediate in the synthesis of MAIT cell stimulatory ligands. In the riboflavin pathway, 5-A-RU can react through a non-enzymatic reaction with 3,4-dihydroxy-2-butanone-4-phosphate to give the unstable intermediate 5-MOP-RU that spontaneously cyclizes to RL-6,7-DiMe (Figure 9). By analogy to this reaction, it was thought that 5-A-RU could react with other small endogenous metabolites such as glyoxal or methylglyoxal (derived from the glycolysis pathway) that would give respectively compounds 5-OE-RU and 5-OP-RU (the latter was discussed earlier). The two unstable pyrimidine adducts were synthesized and showed the highest potency to activate MAIT cells, confirming the elucidation of the chemical structure of the most potent MAIT cell antigens.

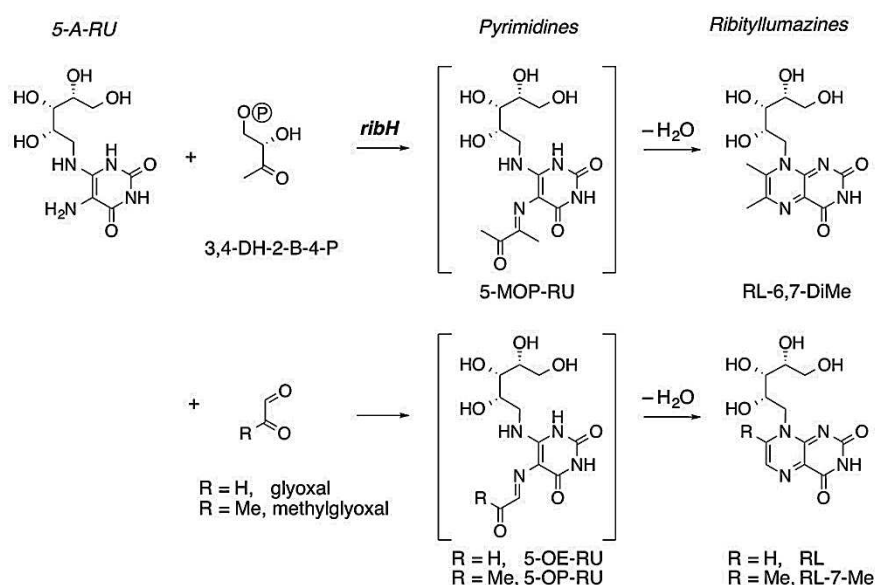


Figure 9: MAIT cell pyrimidine adduct antigen biosynthesis²⁷

4. Molecular basis for MR1 binding and TCR recognition

Figure 10 and Figure 11 show respectively radiocrystallographic images of the ternary structures of 6-Fp and stimulatory MAIT cell agonists (5-OP-RU, 5-OE-RU, RL-6-Me-7-OH) bound to MR1 and to the MAIT cell TCR. 6-Fp is deeply inserted in the binding groove of MR1 where it has many hydrophobic interactions with Tyr7, Tyr62, Trp69 and Trp156 (mediated by their aromatic core) (Figure

10c). 6-Fp also interacts with MR1 through Van der Waals interactions with Arg9, Arg94 and Ile96 residues. Most importantly, 6-Fp covalently binds to Lys43 of MR1 by forming an unusual imine (also commonly called Schiff base). This covalent bond is essential for the binding to MR1 as it will be described later. 6-Fp is deeply inserted inside MR1 cleft because of this covalent linkage, resulting in an inaccessibility to the MAIT cell TCR. Thus, even if the molecule can interact with Tyr95 α by water mediated interaction, it is too weak to efficiently bind to the TCR and activate MAIT cells (Figure 10b).

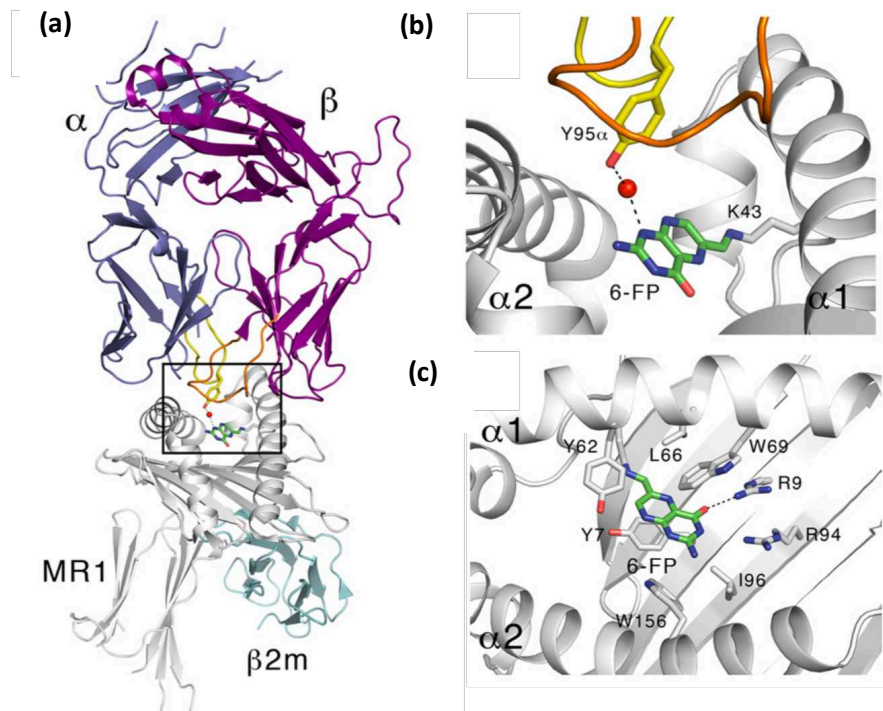


Figure 10: Structural basis of MR1-binding and TCR recognition of 6-Fp (a) ternary structure of MR1 presenting 6-Fp to the MAIT cell TCR; (b) contact between the MR1 bound antigen 6-Fp and the TCR; (c) interactions of 6-Fp with MR1²⁷

Like 6-Fp, pyrimidine adduct antigens (5-OP-RU and 5-OE-RU) form a Schiff base with Lys43 of MR1 but this time, the ribityl chain mediates strong interaction with the TCR (Figure 11c,d,e,g,h). Indeed, the four hydroxyls groups create a hydrogen bond network with both the TCR and MR1. The stimulatory ligands interact especially with Tyr95 α of the TCR CDR3 α loop and with diverse residues of MR1 (Arg9, Tyr152, Gln153). Ribityllumazine antigens finally have the same non-covalent interactions but are unable to form the Schiff base with Lys43 (Figure 11c,f). This is probably responsible for a different orientation of the molecule in the binding cleft, leading to a less efficient interaction with the TCR compared to 5-OP-RU and 5-OE-RU.

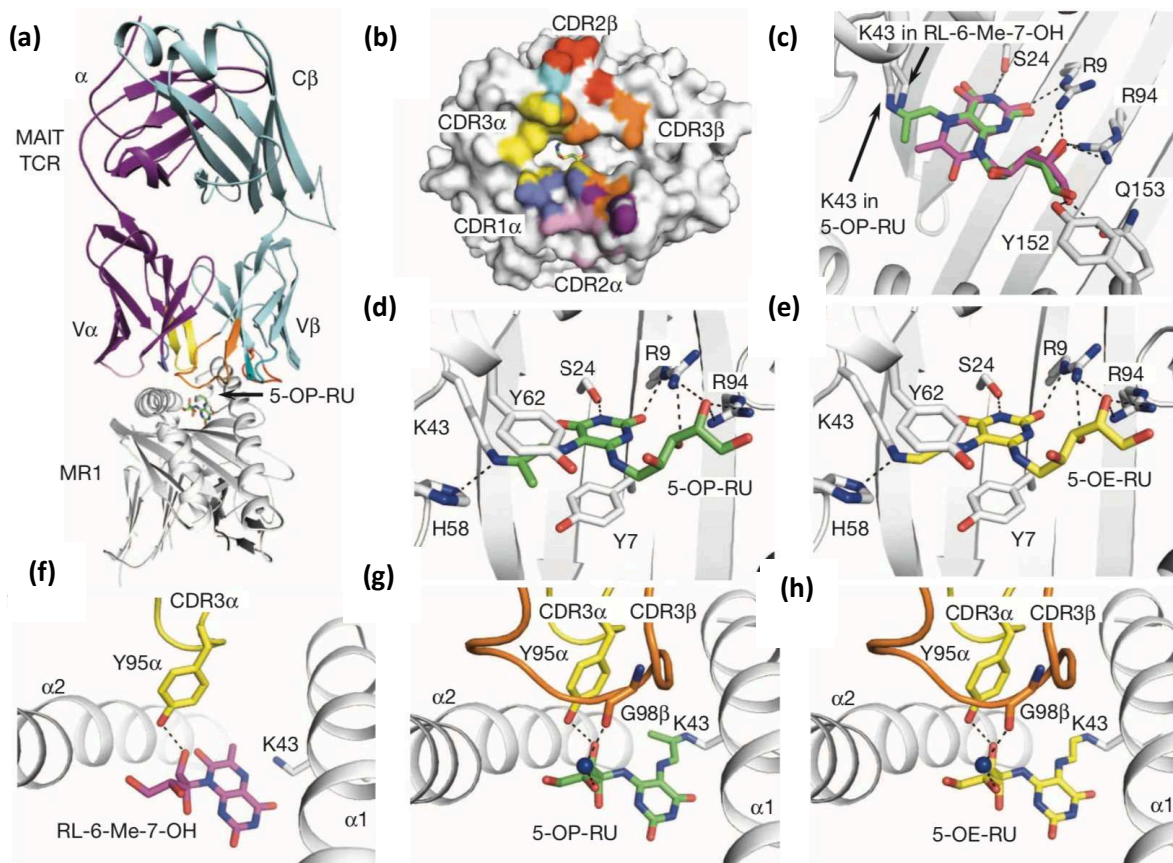


Figure 11: Structural basis of MR1-binding and TCR recognition of MAIT cell vitamin B2-derivative antigens. (a-c): MAIT TCR-MR1-antigen docking (a), MAIT TCR footprint on MR1 surface (b) and 5-OP-RU and RL-6-Me-7-OH overlay (c); (d-h): MR1 contacting 5-OP-RU (d) and 5-OE-RU (e), MAIT TCR contacting RL-6-Me-7-OH (f), 5-OP-RU (g) or 5-OE-RU (h)⁶

5. Antigen processing

To conclude on the mechanisms of antigen presentation and interaction with their targets, it is important to understand how the antigens are processed inside APCs to allow the presentation by MR1 to the TCR. In 2016, McWilliams *et al.* showed that the imine bond formed between Lys43 of MR1 and vitamin B-derivative antigens acted as a molecular switch allowing MR1 to egress the endoplasmic reticulum (ER) where it is sequestered at steady state²⁸. This mechanism seems to rely on the neutralization of the positively charged amino group of Lys43 through the formation of the Schiff base (Lys43Ala mutants displaying a neutral alanine instead of a positively charged lysine spontaneously folded and reached the cell membrane even without antigens) (Figure 12). Once the ligand is bound to MR1, the resulting complex traffics through ER and Golgi apparatus to reach the cell membrane where antigen presentation to the TCR occurs. The complex is finally degraded upon cellular internalization or MR1 is recycled leading potentially to an ER independent loading of antigens on MR1 inside endosomes²⁹.

Some questions still remain around how antigens reach the ER where MR1 resides at steady state. Indeed, MAIT cell antigens are exogenously produced by microbes, they are not produced by APCs themselves. They can be released either by microbes in the extracellular environment, in the lumen of phagosomes containing endocytosed bacteria or they can come from the cytosol of cells infected by intracytosolic bacteria. In both cases, we do not yet know how they manage to reach the ER. We also don't know which cellular machinery is involved in this process (one hypothesis would involve transporters expressed at cell and/or endosome membranes).

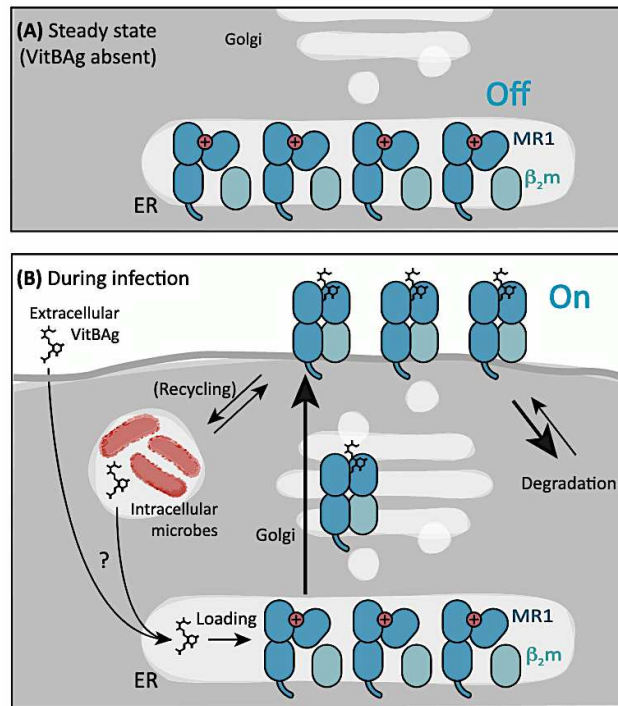


Figure 12: MR1 trafficking and antigen processing (A) at steady state (absence of antigens); (B) in the presence of Vitamin B-derivative antigens³⁰

B. TCR-independent activation of MAIT cells

In addition to the TCR-dependent activation, MAIT cells can be activated in a TCR-independent manner (like iNKT cells) through innate inflammatory and antiviral cytokine stimulation (mostly IL-18, IL-12, IL-15 or IFN- α - β)^{1,31}. These cytokines are produced by APCs through triggering of toll-like receptor (TLR) or other pattern recognition receptors (PRR) in response to viral infection. Thus, it is likely that MAIT cells can sense virus infections. The ability of MAIT cells to recognize such cytokines would also naturally extend their implication to non-infectious diseases such as inflammatory and auto-immune diseases as it will be discussed later.

C. Summary on MAIT cell activation

To summarize, MAIT cells can be activated either in a TCR-dependent manner or through a TCR-independent mechanism relying on cytokines stimulation (Figure 13). TCR-independent activation of MAIT cells requires APCs to recognize TLR ligands, triggering the release of inflammatory cytokines (such as IL-12, IL-18). TCR-mediated activation of MAIT cells rely on the presentation of microbial antigens derived from the riboflavin biosynthesis pathway (5-OP-RU, 5-OE-RU). Antigen processing in APCs involves refolding of MR1 in the ER in the presence of these antigens that triggers trafficking of the complex to the cell membrane where it is recognized by the MAIT cell TCR. Cytokine-mediated co-stimulation can also occur. In all cases, MAIT cell activation lead to the secretion of pro-inflammatory cytokines such as IFN γ or TNF α and to the development of a cytotoxic phenotype (similar to CD8⁺ cytotoxic T cells).

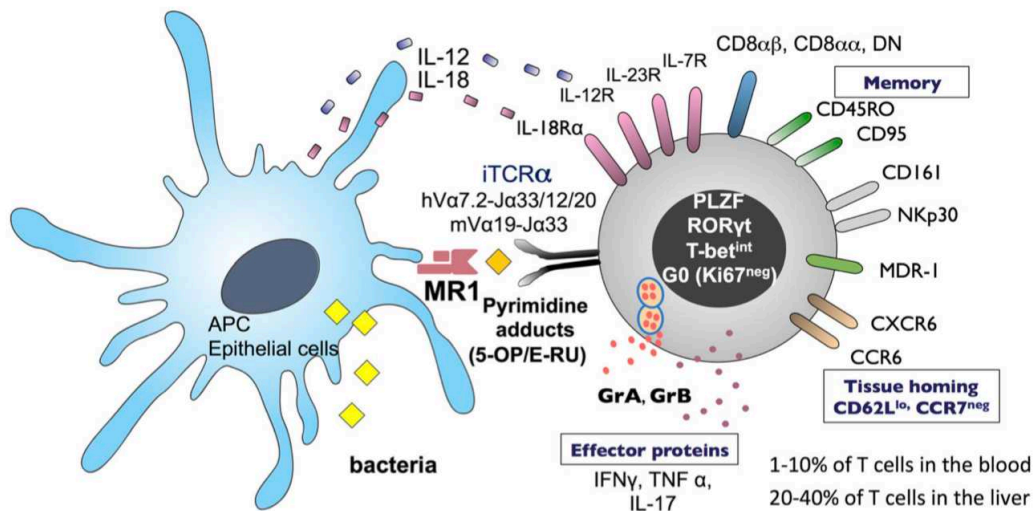


Figure 13: Summary of MAIT cell activation process³²

Having described the main characteristics of MAIT cells and how MAIT cells can sense infectious diseases, we will now discuss MAIT cells' immune roles, especially for infectious diseases, and provide some insight around their potential use in immunotherapy.

III. MAIT cells as potential therapeutic targets

A. Protection against infectious diseases

1. Bacterial infections

Many studies were conducted to understand how MAIT cells contribute to protective immunity against bacterial infection in human and mice. So far, the most studied bacterial infection has been tuberculosis due to *Mycobacterium tuberculosis* (Mtb). The first evidence that MAIT cells could recognize *Mycobacterium tuberculosis* was made by Gold *et al.* in 2010 (before the elucidation of MAIT cell antigens) with highlight of a MAIT cell population able to detect bacterially infected human cells²⁴. Other studies showed a decreased frequency of peripheral blood MAIT cells in patients infected by Mtb^{23,33–37}. This phenomenon was observed with other bacteria such as *Pseudomonas aeruginosa* in cystic fibrosis³⁸, *Vibrio cholerae*³⁹, *Shigella* in vaccine clinical trials¹⁸, *Helicobacter pylori*⁴⁰ and also in septic shocks⁴¹. MAIT cells were also able to accumulate in tissues infected by different bacteria (in human and mice)^{23,42,43}. An important study demonstrated a critical role of MAIT cells in the response of mouse model lung infection with live *Francisella tularensis*⁴⁴. MAIT cells could colonize and expand in the lungs at both early and intermediate stages and they still expanded after clearance of the bacteria. MAIT cells also produced pro-inflammatory cytokines IFN γ , TNF α and IL-17. Moreover, MR1 knockout mice showed higher bacterial burden correlated to a delay in the recruitment of IFN γ producing CD4⁺ and CD8⁺ T cells into the lungs. Another study in mice pointed out the protective effect of MAIT cells against pulmonary infection due to *Legionella longbeachae*⁴⁵.

Altogether, these data suggest that MAIT cells can migrate from peripheral blood to infected tissues where they could contribute to host defense against infections through direct cytotoxicity, secretion of pro-inflammatory cytokines (IFN γ , TNF α or IL-17) or other mediators that are yet to be discovered^{18,46}.

2. Viral infections

Recent data suggest that MAIT cells can be activated and expanded in a TCR-independent manner in the course of diverse viral infections including hepatitis C, dengue and *influenza virus*^{47,48}. Blood MAIT cells could secrete IFN γ , TNF α and granzymes after *in vitro* stimulation in an IL-18 dependent manner, most likely in synergy with IL-12, IL-15 and type I interferons⁴⁹. Like with bacterial infections, patients with early and chronic HIV infection showed a decreased frequency of peripheral blood MAIT cells compared to healthy individuals. This is due to a potential recruitment of MAIT cells in infected tissues upon viral infection^{50,51}.

B. Other roles of MAIT cells in non-infectious diseases

1. Auto-immune and inflammatory diseases

The involvement of MAIT cells in immunity is not restricted to infectious diseases since MAIT cells respond to various cytokine stimuli. MAIT cells are modulated in several auto-immune and inflammatory diseases such as multiple sclerosis, gastro-intestinal disorders (celiac disease and inflammatory bowel diseases), allergic diseases, asthma and metabolic diseases (type 1 and 2 diabetes)^{49,52}. Like for microbial infection, a decrease of MAIT cell frequency in peripheral blood was often found, probably reflecting a migration to inflamed sites in the course of immune-mediated diseases⁵³. However, there is no clear evidence of the protective or pathogenic role of MAIT cells in such diseases.

2. Cancer

MAIT cells' roles in malignant diseases have also been investigated (both for solid and hematological malignancies) but still remain poorly understood. Patients with cancer often showed a depletion of MAIT cell population in peripheral blood compared to healthy donors^{49,52,53}. In parallel, MAIT cells could infiltrate various tumors and metastases but it is unclear whether this phenomenon contributes to host protection or to pathogenesis. Furthermore, an impairment of MAIT cell cytokine profile was described several times, notably a decreased of INF- γ secretion and/or an increased production of cytokines supporting tumor growth like IL-17. A recent *in vivo* study on mice suggests a pro-tumorigenic effect of MAIT cells caused by the suppression of T and/or NK cells (partly due to IL-17 secretion) after interaction with MR1 molecules expressed on tumor cells⁵⁴. Pre-treatment of tumor cells with 5-OP-RU was also associated with an increase of lung metastasis.

3. Graft-versus-host-disease (GvHD)

MAIT cells are preferentially localized in organs implicated in GvHD (such as liver) justifying the investigations related to this disease. MAIT cells are unlikely to induce alloreactive response and GvHD since they are not directed towards polymorphic MHC molecules⁵⁵. Little data is available on this topic but one study showed that an early increase in the number of MAIT cells in peripheral blood after stem cell transplantation was associated with a reduced risk of GvHD⁵³.

C. Development of immunotherapies targeting MAIT cells

As depicted above, MAIT cells have important immune functions since they seem to be involved in the response to many diseases. MAIT cells could represent attractive targets for cancer immunotherapy because of their secretory capacity and their ability to recruit other immune cells. However, more investigation is required to assess the safety and the efficacy of this therapeutic strategy. If MAIT cells appeared to induce pro-tumorigenic effect as it was supposed in the study discussed above⁵⁴, a direct inhibition of MR1 could be envisioned with inhibitory ligands. Another promising therapeutic option under study is the development of CAR (chimeric antigen receptor)-MAIT cells.

The antimicrobial activity of MAIT cells is without any doubt the best-documented immune role of MAIT cells. There is strong evidence that MAIT cells help fight several bacterial (and perhaps viral) diseases. Thus, they potentially represent an interesting therapeutic target for innovative antimicrobial immunotherapies. They could especially be a good target for new antimicrobial mucosal vaccines. Indeed, most existing vaccines are administered through the systemic route and they may not confer an effective and durable mucosal immunity⁵⁶. Targeting MAIT cells with new mucosal vaccines could overcome this issue since this population of T cells is abundant at mucosal sites (lungs, gastro-intestinal tract...). We could consider directly targeting MAIT cells with such vaccines since they display a memory phenotype. Another option (perhaps more relevant) would be to harness MAIT cells as vaccine adjuvants in order to boost systemic vaccine efficacy.

It is clear that the feasibility of such vaccine would rely on the discovery of more stable MAIT cell agonists than the very unstable ones we have (5-OP-RU, 5-OE-RU). Having understood this critical element, several research teams deeply investigated MAIT cell antigens to unravel the molecular basis of interaction with MR1 and the MAIT cell TCR. A better knowledge of the structure-activity relationships of MAIT cell antigens would greatly help design new stable MAIT cell ligands. A review of all the research completed in this field is presented in the following and final section of this introductory chapter.

IV. Overview of the research aiming to find new antigens of MAIT cells

A. Synthesis of new MAIT cell competitive antagonists

Several analogues of 6-Fp were synthesized, the first being acetyl-6-formylpterin (Ac-6-Fp). It proved to be much more potent than 6-Fp to inhibit MAIT cell activation, presumably due to a higher chemical stability (Figure 14)⁵⁷. Soudais *et al.* reported later the synthesis and biological evaluation of two other analogues of 6-Fp that they called Compound A (2-amino-4-hydroxy-6-formylpteridine dimethyl acetal) and Compound C (2-acetylamino-4-hydroxy-6-formylpteridine dimethyl acetal). While Compound A did not show inhibitory activity, Compound C showed a concentration-dependent activity similar to Ac-6-Fp for MR1 up-regulation (reflecting the binding affinity to MR1) and inhibition of MAIT cell activation.

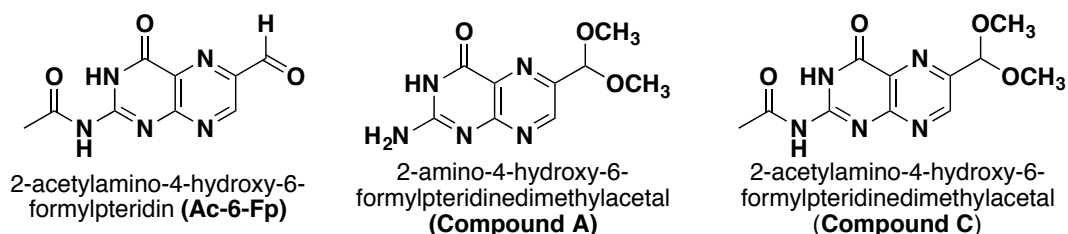


Figure 14: Chemical structure of synthetic MAIT cell inhibitory ligands

B. Analytical study and synthesis of new stable agonists of 5-OP-RU

The α -iminocarbonyl moiety of pyrimidine adduct antigens is prone to hydrolysis and cyclisation to give thermodynamically stable but far less antigenic ribityllumazines. Mak *et al.* investigated the underlying mechanism causing this instability to overcome this problem. For this purpose, they studied the effect of the solvent on the formation and the stability of three different pyrimidine adduct derivatives (**3a-c**) synthesized through condensation reaction between 5-A-RU and small dicarbonyl metabolites: butane-2,3-dione (**3a**), glyoxal (5-OE-RU **3b**) and methylglyoxal (5-OP-RU **3c**). In PBS (pH 8.0, 15°C), **3a** underwent degradation in less than five minutes while **3b** had a half-life of 18 minutes. **3c** (5-OP-RU) was more stable than the two other compounds with a half-life of 14 hours even if the stability decreased with lower pH and higher temperature. Under physiological conditions (PBS, pH 7.4, 37°C), the half-life of **3c** was only 88 minutes. Among the three molecules, 5-OP-RU (**3c**) was the most potent, consistent with a lower instability compared to the other ones (Figure 15b). Altogether, these results suggest that the use of 5-OP-RU is more suitable than the other molecules to study MAIT cells, in terms of both stability and biological activity.

Then, the authors deeply studied the kinetic of formation of 5-OP-RU and the influence of the solvent used for the reaction. They showed that the condensation reaction between methylglyoxal and 5-A-RU in PBS (pH 7.4, 37°C) reached a maximum concentration of 5-OP-RU corresponding to only 1.1% conversion after 5 minutes. The same reaction done in DMSO led to total conversion of the starting material to 5-OP-RU after 2 days. Furthermore, the imine formed in DMSO was reasonably stable with more than 90% of the product remaining unchanged after 2 days at 22°C. A mechanism was proposed in which the reaction should be under thermodynamic control in water. *Trans* kinetic product **3** would rehydrate to give **6**, followed by cyclisation via **7** (or *cis* **3**) giving at the end thermodynamic product lumazines **4** (Figure 15a). In polar aprotic solvent DMSO, the reaction should be under kinetic control where *trans* **3** product should form faster than *cis* **3**. Once formed, *trans* **3** is unlikely to isomerize because of a high energy barrier for the isomerization thus stabilizing the pyrimidine antigens.

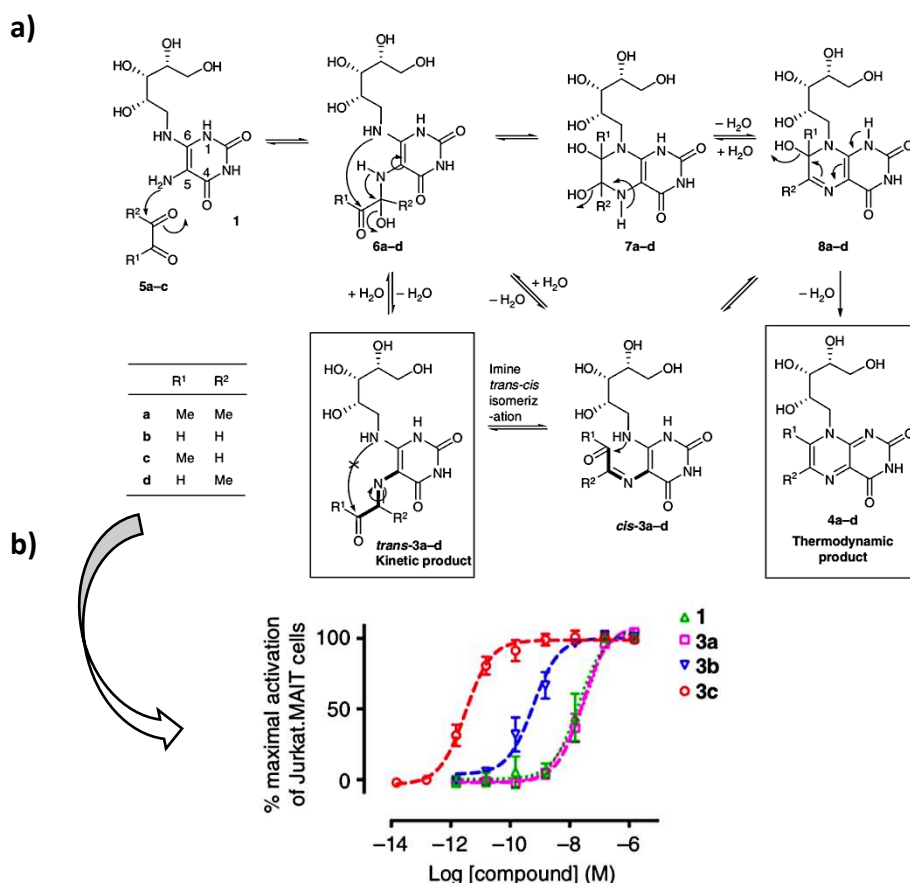


Figure 15: Analytical study and biological evaluation of 3a-c; a) Study of the mechanisms of antigenic pyrimidine adducts synthesis in water or DMSO; b) biological evaluation of 3a-c (on Jurkat.MAIT cell line)⁵⁸

The same study reported the design and synthesis of three potential stable analogues of 5-OP-RU. They synthesized two N-methylated products keeping either the α -iminocarbonyl group (**9**) or replacing the imine function by an alkene (**10**). The third molecule **11** contained an alkyl ribityl chain

lacking the reactive secondary amino group and the imine was also replaced by an alkene like for **10** (Figure 16).

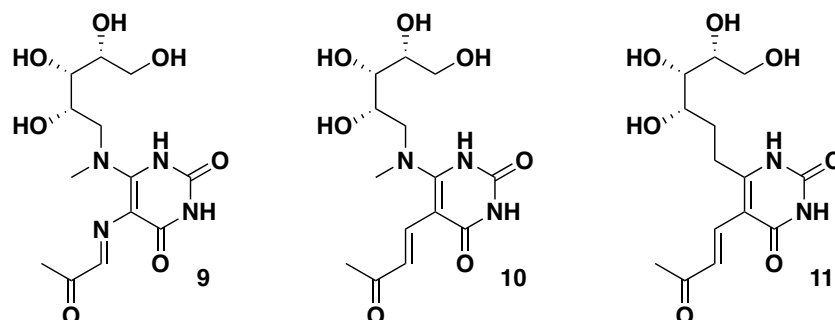


Figure 16: Chemical structure of compounds 9-11

Surprisingly, **9** was even less stable than 5-OP-RU under physiological conditions while **10** was slightly more stable though it also rapidly formed quaternary ammonium cyclized species like **9**. In contrast, compound **11** was completely stable. Biological evaluation on Jurkat.MAIT cells showed an important loss of potency for the three molecules in comparison to 5-OP-RU (EC_{50} 1.6 pM). **11** (EC_{50} 1.6 nM) and **9** (EC_{50} 14 nM) displayed similar potencies (1000-fold less active than 5-OP-RU) while **10** was poorly active ($EC_{50} > 10 \mu\text{M}$).

C. Identification of drugs and drug-like molecules able to modulate MAIT cell activity

Another study identified several drugs and drug-like molecules able to modulate the functions of MAIT cells⁵⁹. Multiple *in silico* screening were done to identify new MR1 binding ligands and MAIT cell agonists. 81 compounds of the *in silico* hits were biologically evaluated. Among them, several molecules could up-regulate MR1 and/or activate MAIT cells. Compounds 3-formaldehyde-salicylic acid (3-F-SA), 5-formaldehyde-salicylic acid (5-F-SA), 2-hydroxy-naphthaldehyde (2-OH-1-NA) and 2,4-diamino-6-formylpteridine (2,4-DA-6-Fp, obtained from the photodegradation of antineoplastic drug aminopterin) were able to up-regulate MR1 of C1R.MR1 cells (C1R human lymphoblastoid cells overexpressing MR1). 3-F-SA and 2-OH-1-NA inhibited Jurkat.MAIT cells while 5-F-SA moderately activated specific clones of Jurkat.MAIT cells (depending on the nature of the TCR β chain).

The well-known and commonly used drug diclofenac (used for the treatment of inflammatory diseases) was also able to activate one clone of Jurkat.MAIT cells *in vitro* without up-regulating MR1. This activity was actually most likely due to its metabolites 4'-hydroxy-diclofenac (4'-OH-DCF) and mostly 5-hydroxy-diclofenac (5-OH-DCF) that were rapidly formed in cells.

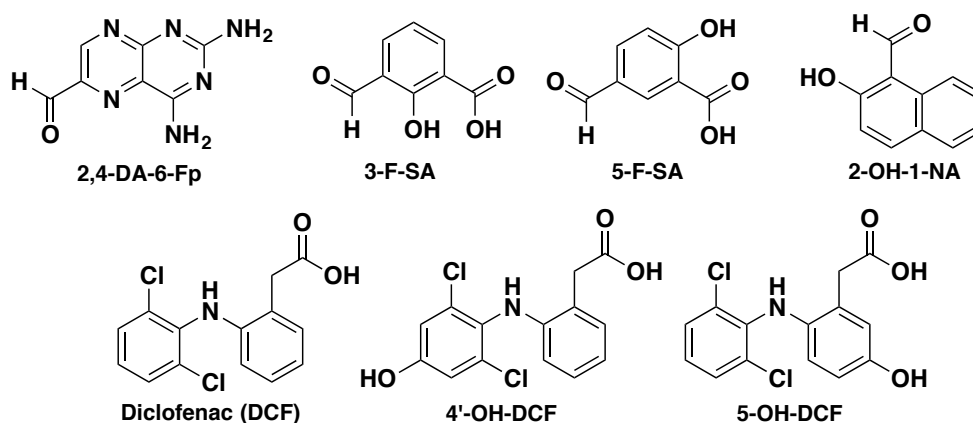


Figure 17: Chemical structure of drugs and drug-like molecules able to modulate MAIT cell functions

Interestingly, crystallographic data showed that all the inhibitory compounds bearing an aromatic aldehyde functional group were able to form a Schiff base with Lys43 of MR1 like 5-OP-RU whereas diclofenac and its metabolites did not form such chemical bond. The inhibitory compounds did not directly interact with the TCR in the MR1-TCR complex like 6-Fp, thus explaining their inhibitory effect. In contrast, diclofenac and its metabolites could make few interactions with the TCR but their mode of binding was different and less effective than the one of 5-OP-RU leading to a weak activation of Jurkat.MAIT cells. Nevertheless, this study proved that MR1 can present other compounds than pyrimidine adduct antigens and folic acid derivatives to the MAIT cell TCR. Thus, it offers the possibility of discovering new small molecules able to modulate MAIT cell activity. It finally gave some insight about the poorly understood contribution of the β chain to the TCR binding of the ligands, since DCF and 5-F-SA only activated one clone of Jurkat.MAIT cells bearing a specific TCR β chain (Jurkat.MAIT-A-F7 cell strain).

D. Design of 5-OP-RU analogues to unravel the structural basis for the recognition of MAIT cell antigens by MR1 and the TCR

A large survey was recently published in which the authors studied structure-activity relationships (SAR) of twenty 5-OP-RU altered metabolites ligands (AMLs) compared to 5-OP-RU and its degradation product RL-7-Me⁶⁰. Among these molecules, the chemical synthesis of deoxy AMLs (2'-D-5-OP-RU, 3'-D-5-OP-RU, 4'-D-5-OP-RU 5'-D-5-OP-RU) and their corresponding lumazine degradation products (2'-D-RL-7-Me, 3'-D-RL-7-Me, 4'-D-RL-7-Me, 5'-D-RL-7-Me, respectively) was previously described by Ler *et al.*⁶¹. They additionally synthesized series of pyrimidine and lumazine ligands bearing a monohydroxy ribityl chain (2'-OH-ethyl-5-OP-U, 2'-OH-ethyl-L-6-Me, 3'-OH-ethyl-5-OP-U...). Finally, a ribityl-less analogue and JYM72 (previously discussed as compound **11**⁵⁸) were also included in the study (Figure 18).

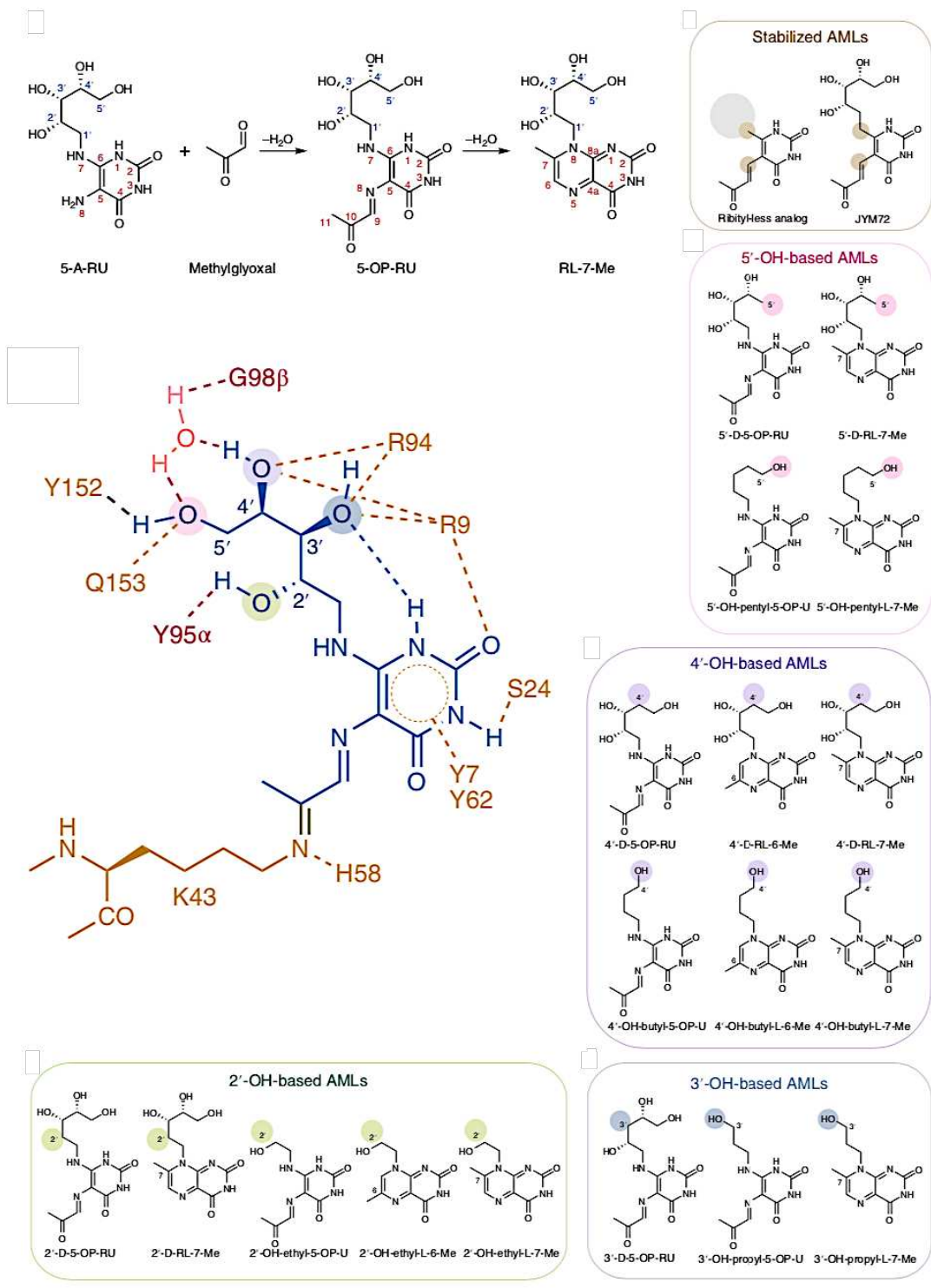


Figure 18: Chemical structure of the different AMLs⁶⁰

The chemical stability, MR1 up-regulation, MAIT cell activation, and binding affinity (K_d value) were assessed using two different Jurkat.MAIT cell lines (A-F7 and #6) bearing a different TCR β chain (Table 1).

Table 1: Chemical stability, MR1 up-regulation, MAIT cell activity and binding affinity of AMLs⁶⁰

| | $t_{1/2}$ | MR1 upregulation at 10 μ M (% max at 6 h) | A-F7 (TRAV1-2-TRBV6-1) TCR | | | #6 (TRAV1-2-TRBV6-4) TCR | | |
|----------------------------------|-----------|---|----------------------------|------------------|---------------------------|--------------------------|------------------|---------------------------|
| | | | Max activity (%) | EC ₅₀ | K _d (μ M) | Max activity (%) | EC ₅₀ | K _d (μ M) |
| Strong agonists | | | | | | | | |
| 5-OP-RU | 88 min | 50 | 100 | 8.3 pM | 2.2 \pm 0.3 | 100 | 0.9 pM | 2.7 \pm 0.3 |
| 4'-D-5-OP-RU | 69 min | 65 | 100 | 24 pM | 4.3 \pm 0.6 | 82 | 33 pM | 14.9 \pm 0.9 |
| 5'-D-5-OP-RU | 162 min | 54 | 95 | 10 pM | 3.7 \pm 0.3 | 75 | 165 pM | 16.9 \pm 0.9 |
| Moderate agonists | | | | | | | | |
| JYM72 | >100 h | 64 | 90 | 1.5 nM | 10.7 \pm 0.7 | 59 | ND | 24.1 \pm 1.4 |
| 3'-D-5-OP-RU | 300 min | 52 | 85 | ND | 25.1 \pm 0.4 | 43 | ND | 53.6 \pm 2.5 |
| 2'-D-5-OP-RU | 49 min | 39 | 60 | ND | 35.1 \pm 0.9 | 20 | ND | 64.1 \pm 4.6 |
| 2'-OH-ethyl-5-OP-U | 35 min | 71 | 63 | >50 nM | 25.2 \pm 1.5 | 26 | ND | 60.5 \pm 4.7 |
| 3'-OH-propyl-5-OP-U | 61 min | 78 | 42 | >40 nM | 60.2 \pm 2.5 | 5 | ND | ND |
| Weak agonist/non-activating AMLs | | | | | | | | |
| Ribityl-less analog | >100 h | 79 | 18 | ND | 97.5 \pm 7.2 | 11 | ND | ND |
| 4'-OH-butyl-5-OP-U | 47 min | 79 | 8 | ND | ND | 5 | ND | ND |
| 5'-OH-pentyl-5-OP-U | 49 min | 75 | 3 | ND | ND | 1 | ND | ND |
| Ac-6-FP | >100 h | 73 | 0 | ND | ND | 2 | ND | ND |

The upregulation and activation data are shown as the mean from $n=3$ independent experiments. Steady-state K_d values are presented as the mean \pm s.e.m. from $n=2$ independent experiments. ND, not determined (owing to the curve not reaching a plateau); max, maximum.

The different pyrimidine adduct AMLs showed almost the same instability as 5-OP-RU while the ribityl-less analogue and JYM72 were highly stable ($t_{1/2}>100$ h in PBS, pH 7.4, 37°C). All the compounds could up-regulate MR1 with the ribityl-less analogue showing the best potency. Ribityllumazine analogues displayed the slower kinetic of up-regulation, most likely because they were unable to form a Schiff base with Lys43 of MR1. Unstable AMLs reached a maximum up-regulation after 4-8h while stable ribityl-less analogue and JYM72 continued to up-regulate MR1 after 24h. All these results suggest that concentration and time-dependent MR1 up-regulation rely on the stability of the ligands and on their ability to form a covalent bond with Lys43 of MR1. Thus, the ribityl chain does not seem to be a prerequisite for inducing strong MR1 up-regulation and it might be rather deleterious.

MAIT cell activation assay showed that 4'-D-5-OP-RU and 5'-D-5-OP-RU could still activate MAIT cells with strong potency close to the one of 5-OP-RU while 4'-OH-butyl-5-OP-U and 5'-OH-pentyl-5-OP-U did not activate MAIT cells. This means that 4'-OH and 5'-OH are probably not essentials for the binding to the MAIT cell TCR. On the contrary, 2'-OH and 3'-OH seem to be very important for MAIT cell activation since compounds lacking one of these hydroxyl groups (2'-D-5-OP-RU and 3'-D-5-OP-RU) were not active. Finally, the different lumazine compounds showed only moderate MAIT cell activation presumably due to the absence of covalent linkage to Lys43 though they maintained weak interaction with the TCR.

To finish, the authors gave some information about the structural basis explaining the structure-activity relationships of the AMLs by studying ternary structures of the ligands interacting with MR1 and the TCR. They affirmed that the 2'-OH and 5'-OH groups of 5-OP-RU formed an essential interaction triad with Tyr95 of the TCR α and Tyr152 of MR1. According to them, AMLs that perturbed

these interactions were subject to a dramatic loss of potency. The strong potency of 4'-D-5-OP-RU and 5'-D-5-OP-RU was theoretically explained by conformational malleability and dynamic compensations inside the binding groove allowing to maintain this interaction triad. The moderate AMLs displayed an altered interaction triad causing a decrease of biological activity while the weak or non-agonistic AMLs like 4'-OH-butyl-5-OP-U and 5'-OH-pentyl-5-OP-U simply could not interact properly with the TCR because they lack 2'-OH and 3'-OH groups.

A second recent study described the synthesis and study of new glyco-analogues of 5-OP-RU and RL-6-Me-7-OH to give insight about the influence of the chemical changes on MAIT cell activation^{26,62}. Several analogues with different absolute configuration, with 2'-OH deoxygenation or displaying longer ribityl chain were synthesized (Figure 19).

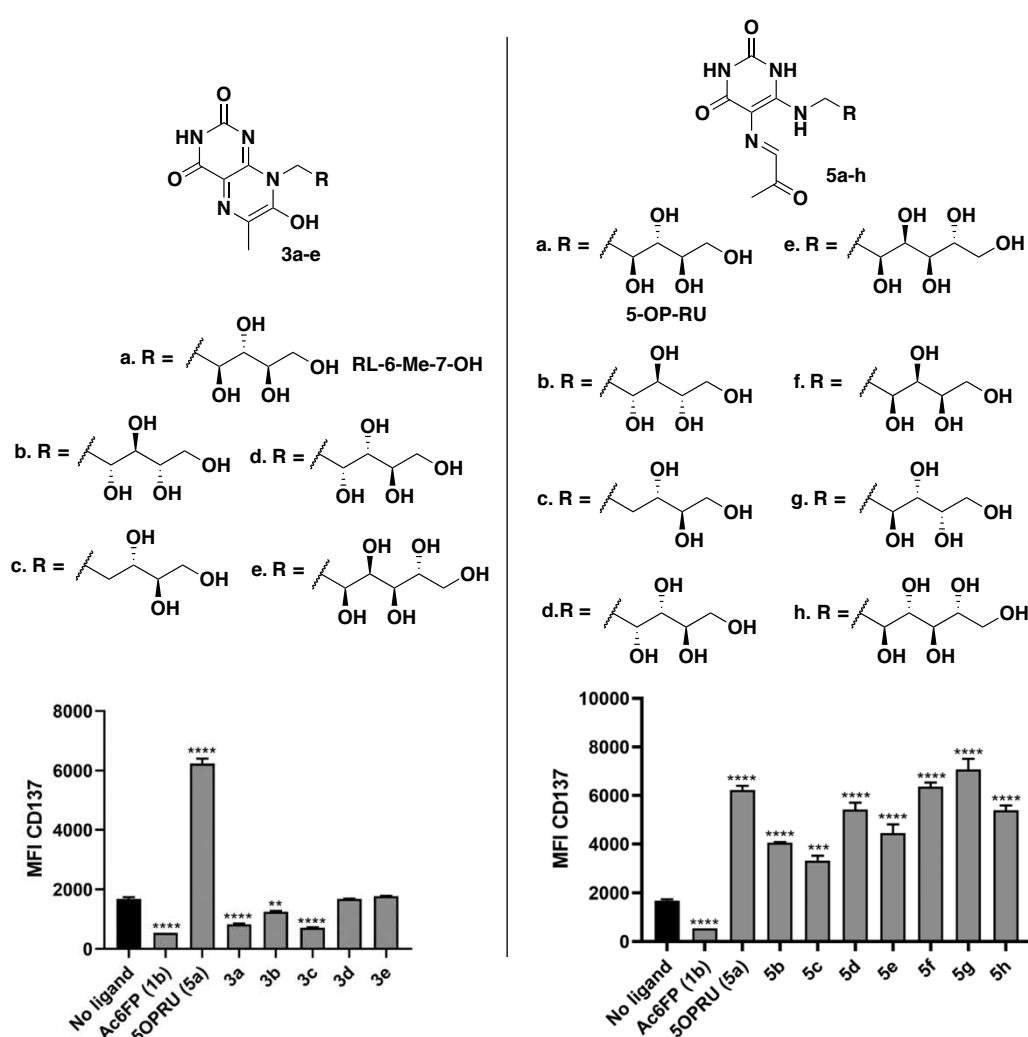


Figure 19: Chemical structure and biological evaluation of glyco-analogues of 5-OP-RU (10 μ M) and RL-6-Me-7-OH (100 μ M) (adapted from Braganza et al.)⁶²

Ribityllumazine analogues (100 μ M concentration like 6-Fp) were able to up-regulate MR1 of NiH.c19 presenting cells but they did not activate MAIT cells (measured by the MFI of CD137 of 6C2

MAIT cell line). In contrast, all the glyco-analogues of 5-OP-RU were active at 10 μ M concentration. **5d**, **5f**, **5g** and **5h** displayed a similar activity compared to 5-OP-RU while **5b**, **5e** and especially **5c** (lacking 2'-OH) were less potent than 5-OP-RU. A virtual docking study was done to help explain these results. It showed that **5c** and **5e** probably did not interact with Tyr95 of the TCR α , thus explaining the low activity. The authors emitted the theory that the more the compounds could make interactions with Tyr95 α residue, the more potent they were.

The same research groups recently published a second survey in which they synthesized several molecules by modulating the 6-aminoalkyl (ribityl) chain⁶³. They produced three aminoalkyl derivatives with a single terminal alcohol (**3b-d**), a N-methylated analogue (**3e**) and three aminoalkyl products without any hydroxyl group (**3f-h**).

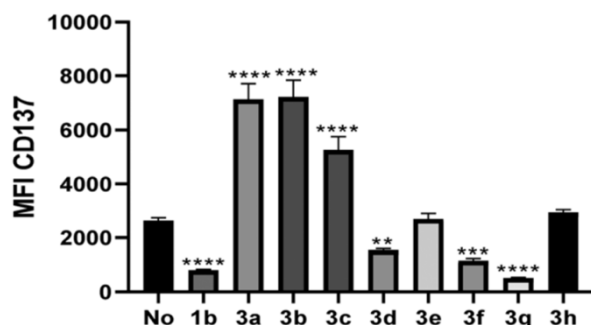
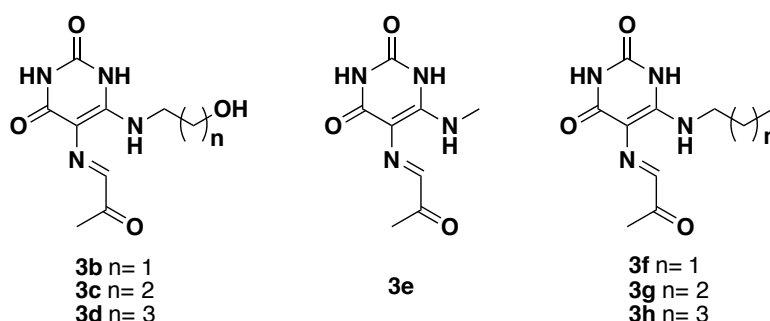


Figure 20: Chemical structure and biological evaluation of 6-alkylamino analogues of 5-OP-RU; 1b is Ac-6-Fp and 3a is 5-OP-RU (adapted from Braganza et al.)⁶³

Biological evaluation of these molecules revealed a high potency of **3b** and **3c** at activating MAIT cell line 6C2 similarly to 5-OP-RU (10 μ M concentration). The authors suggested that **3b** is of high interest for the study of MAIT cells since it is as potent as 5-OP-RU and its synthesis is easier and faster compared to the synthesis of 5-OP-RU. However, these data are contradictory with the one of Awad *et al.* (described above)⁶⁰. They produced and tested the same monohydroxy analogue **3b** but the biological evaluation showed almost no Jurkat.MAIT cell activation. The use of different biological models by the two research groups (different MR1 expressing cells and MAIT cells) could explain these divergent results. Thus, further investigation is required to confirm these observations.

Research work

I. Introduction

As described earlier, MAIT cells could become attractive targets for new immunotherapies against infectious diseases (mucosal vaccines) and presumably other pathologies like cancers. However, more investigation is required to validate this therapeutic approach and many questions around MAIT cell biology and ligands must be addressed.

The recent discovery of MAIT cell highly potent antigens (5-OP-RU and 5-OE-RU) was a major breakthrough in the field. The thorough investigation of MAIT cell antigens, at the interface of chemistry and biology, provided some valuable information, especially around the molecular basis governing their interaction with MR1 and the MAIT cell TCR. Despite all these discoveries, we still lack stable highly potent analogues of MAIT cell antigens. Today, it is one of the main hurdles limiting the efficient study of MAIT cells as potential therapeutic targets. Thus, we urgently need to find original research approaches in order to produce new potent antigen of MAIT cells.

We wanted to address this major issue by adopting two different medicinal chemistry approaches. The first one consisted in doing original pharmacomodulations on 5-OP-RU chemical structure (Figure 21). All our work was focused on 5-OP-RU (like most studies on MAIT cells) since it is the most potent MAIT cell antigen and it is also more stable than 5-OE-RU⁵⁸. By doing pharmacomodulations of 5-OP-RU, we aimed at obtaining stable products with comparable activity to 5-OP-RU. The second strategy relied on designing prodrugs of 5-A-RU, the biosynthetic precursor of 5-OP-RU able to generate 5-OP-RU *in situ* after condensation with endogenous methylglyoxal. Our final objective was to develop new chemical probes that could help understand MAIT cell biology. For this Chemical Biology approach, we designed a unique clickable analogue of 5-OP-RU that can be used to track MAIT cell ligands inside biological tissues and cells.

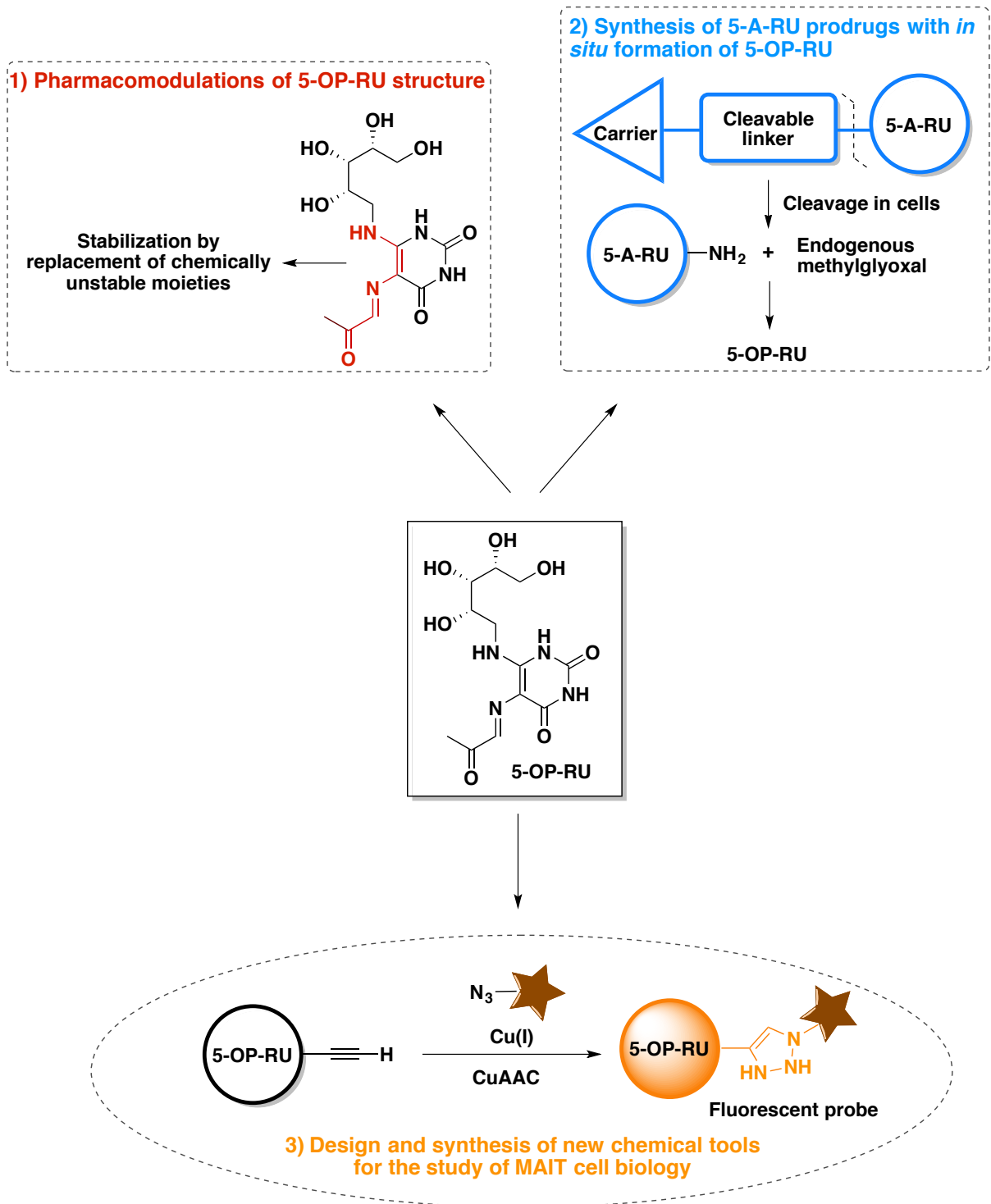


Figure 21: Objectives of the research project

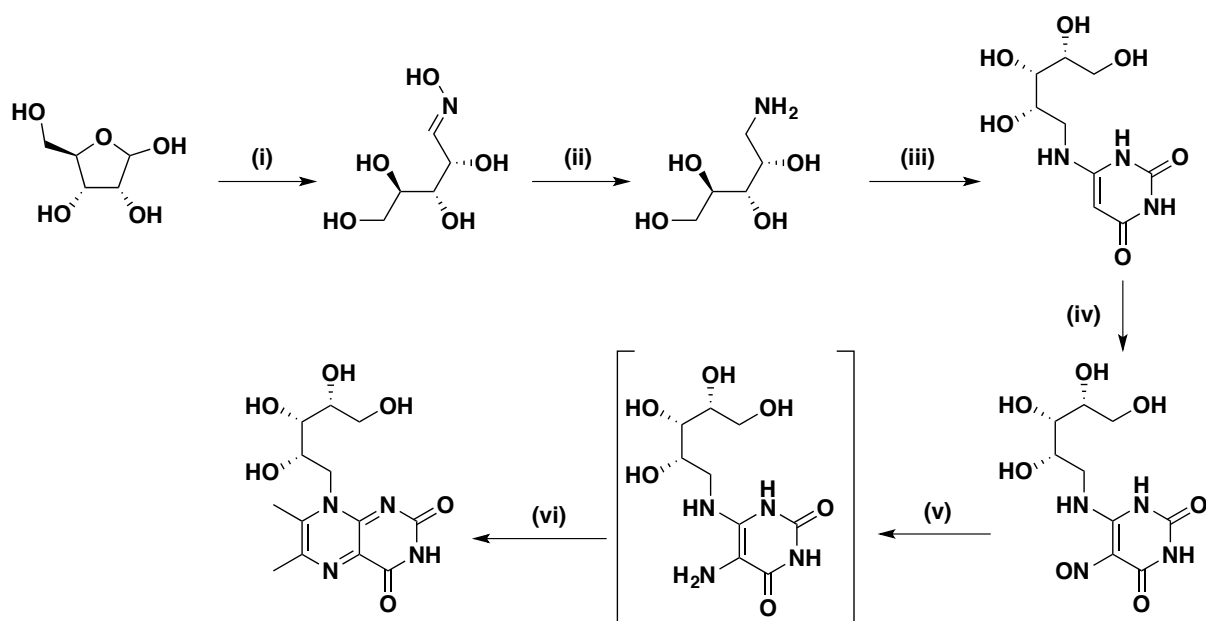
II. Synthesis and study of stable analogues of 5-OP-RU

A. Synthesis and chemical study of 5-A-RU and 5-OP-RU

1. Bibliographic review

5-OP-RU is unstable in physiological media and therefore very difficult to isolate for further use in biology. The molecule is commonly formed *in situ* prior to addition on cells by condensation between synthetic 5-A-RU and commercial methylglyoxal. Unlike 5-OP-RU, 5-A-RU was discovered many years ago and has been extensively used as a chemical intermediate for the synthesis of riboflavin and lumazine analogues. Several research groups have developed efficient synthesis routes towards 5-A-RU since the late 1950's and all this precious work has been exploited to synthesize 5-OP-RU for the study of MAIT cells. All published chemical routes rely first on the synthesis of the D-ribitylamine tail, followed by its coupling to the uracil heterocycle and amine functionalization. The main syntheses of 5-A-RU are presented in this section.

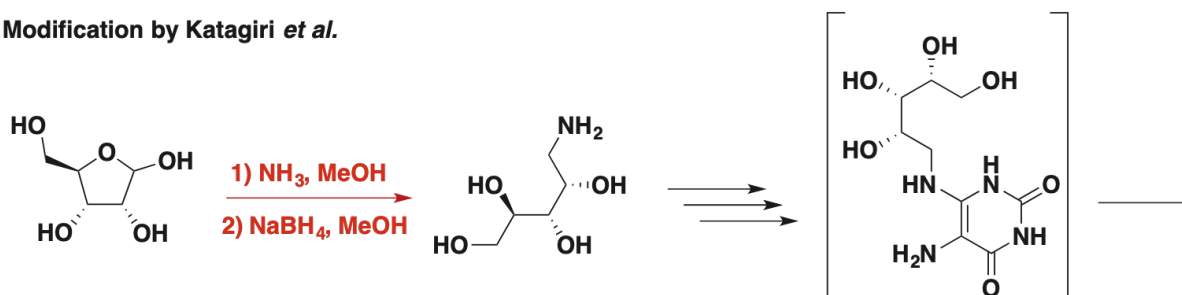
The initial syntheses of 5-A-RU were described by Maley and Plaut⁶⁴ and Winestock and Plaut⁶⁵ (Scheme 1). 5-A-RU was used as an intermediate for the synthesis of 6,7-dimethyl-8-ribityllumazine. Their syntheses started from D-ribose and went through a D-ribityloxime intermediate, which was then reduced by hydrogenation with platinum oxide heterogeneous catalyst. D-ribitylamine reacted with 6-chlorouracil and position 5 of the molecule was functionalized by a nitroso group. Reduction of the nitroso with sodium dithionite afforded 5-A-RU, which was directly used without isolation for the last step of the synthesis.



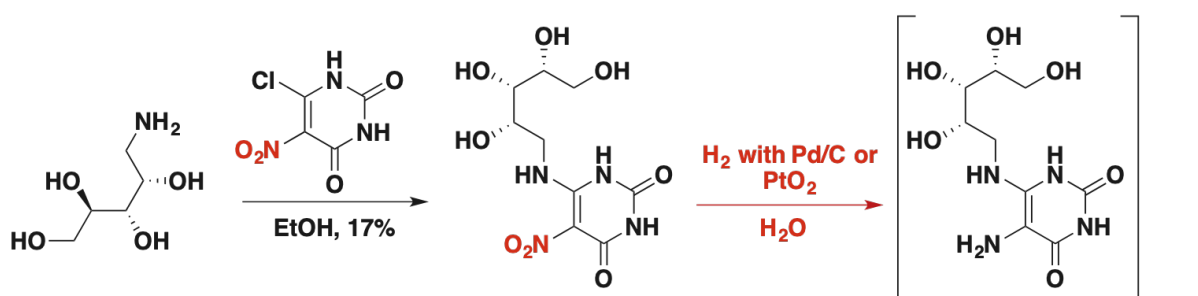
Scheme 1: First synthesis of 5-A-RU by Plaut and co-workers. Reagents and conditions: $\text{NH}_2\text{OH}\cdot\text{HCl}$, NaOMe in EtOH (yield not mentioned); (ii) H_2 , PtO_2 in AcOH; (iii) 6-chlorouracil, 128°C , 44%; (iv) HNO_2 in H_2O , 72%; (v) $\text{Na}_2\text{S}_2\text{O}_4$ in H_2O (product not isolated); (vi) biacetyl

5-A-RU was used for the synthesis of other molecules and several modifications of the initial synthesis were done keeping the same synthesis strategy (Scheme 2). Katagiri *et al.* proposed a different synthesis of the D-ribitylamine chain by reductive amination with ammoniac and sodium borohydride⁶⁶. Other variations were performed by Wood and co-workers with the use 6-chloro-5-nitrouracil instead of 6-chlorouracil for the coupling reaction with D-ribitylamine in ethanol^{67,68}. The nitro group at ortho position of the chloro allowed the reaction to proceed at room temperature in contrast to the synthesis of Plaut and co-workers that required strong heating at 128°C . Reduction of the nitro was done by hydrogenation either with platinum oxide or with palladium on charcoal (Pd/C). Later, Cushman *et al.* described hydrogenation of the nitroso precursor in aqueous HCl to get a more stable form of 5-A-RU as hydrochloride salts (instability issues will be discussed later)⁶⁹.

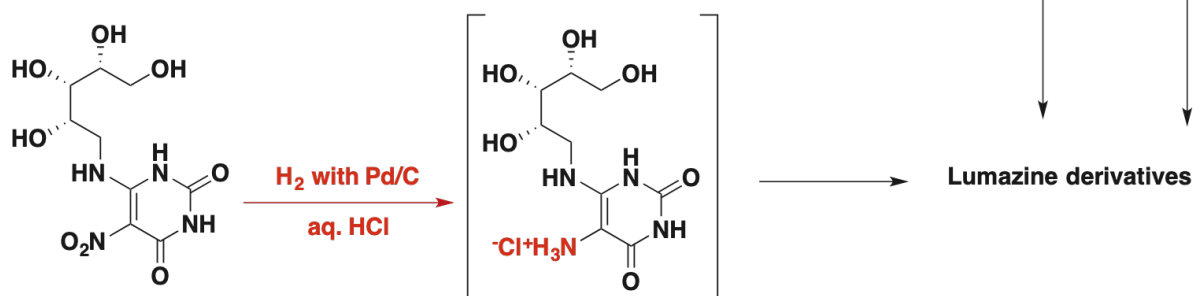
Modification by Katagiri *et al.*



Modification by Wood and co-workers



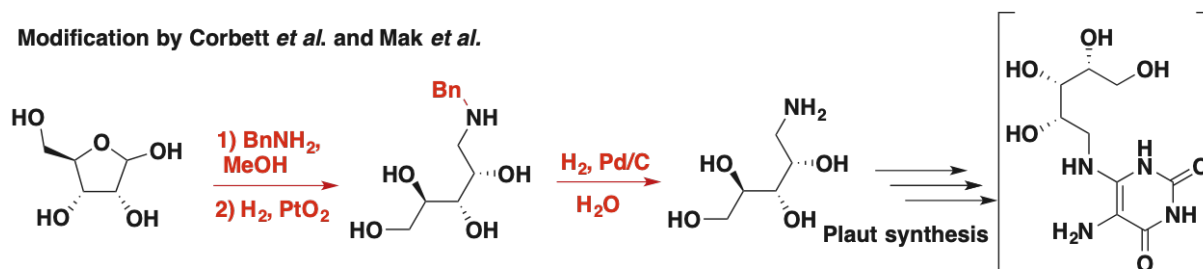
Modification by Cushman *et al.*



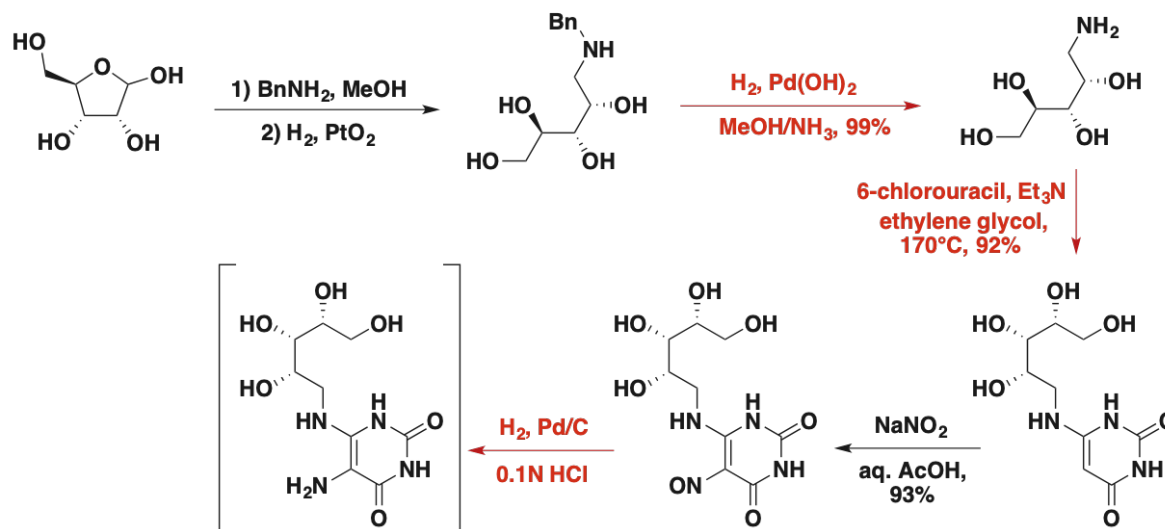
Scheme 2: Different modifications of the initial synthesis of 5-A-RU (by Plaut and co-workers) for the synthesis of lumazine derivatives. Modifications are highlighted in red

Relying on these published syntheses and chemical procedures, 5-A-RU as a precursor of 5-OP-RU could be efficiently synthesized. The initial syntheses of 5-OP-RU were done by Corbett *et al.*⁶ and Mak *et al.*⁵⁸ (research group that initially identified MAIT cell antigens). To make 5-OP-RU, they produced 5-A-RU precursor by adapting the synthesis of Plaut and co-workers. They synthesized the D-ribitylamine moiety by forming a D-ribitylbenzylamine intermediate instead of an oxime through the reaction of D-ribose with benzylamine, followed by hydrogenation reaction with platinum oxide catalyst (Scheme 3). Then, D-ribitylbenzylamine was reduced to D-ribitylamine by hydrogenation over Pd/c in water.

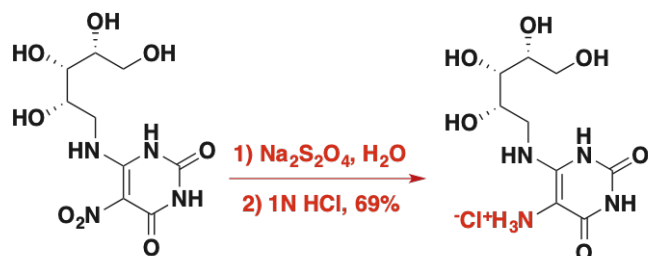
Modification by Corbett *et al.* and Mak *et al.*



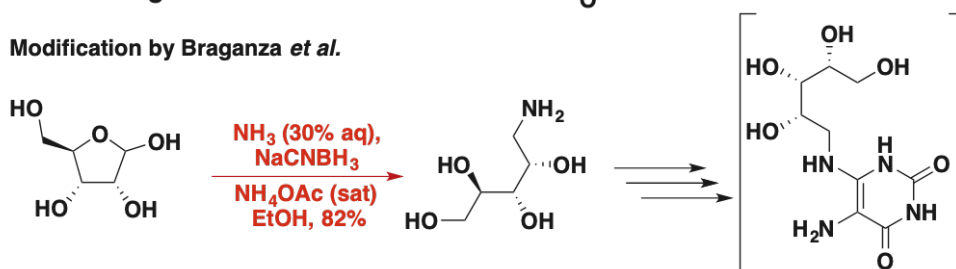
Modification by Lange *et al.*



Modification by Li *et al.*



Modification by Braganza *et al.*



Scheme 3: Recent modifications of the synthesis of 5-A-RU to make 5-OP-RU. Modifications are highlighted in red.

Modification of this synthesis was recently done by Lange *et al.* that aimed to produce a prodrug of 5-A-RU⁷⁰. They reduced D-ribitylbenzylamine by hydrogenation using Pd(OH)_2 instead of Pd/C (in a mixture of methanol and ammoniac) to afford D-ribitylamine in high yield (99%). The same authors also proposed an efficient coupling reaction with 6-chlorouracil using ethylene glycol as

solvent and triethylamine as base. According to them, less equivalent of D-ribitylamine were necessary (1.3 eq) for the reaction in comparison to the other syntheses available (at least 2 eq required) and the reaction was almost quantitative (92% yield). The last change was the reduction of the nitroso group by hydrogenation in 0.1 N HCl (like the synthesis of Cushman *et al.*). 5-A-RU hydrochloride salts were obtained after a careful work-up under inert atmosphere followed by lyophilization. The salts were then directly used in synthesis without further purification.

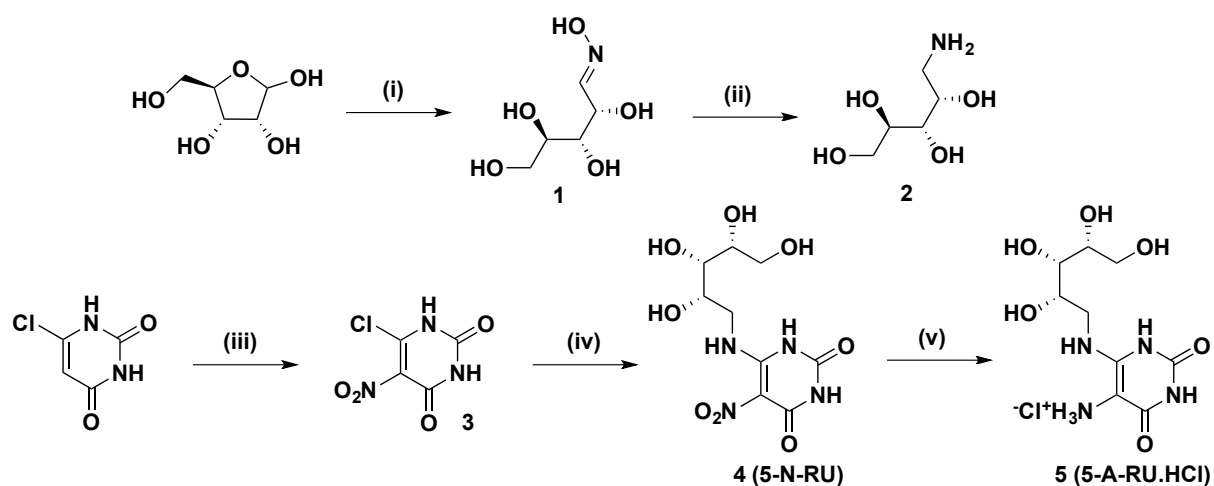
Li *et al.*⁷¹ also developed a synthetic route aiming to obtain 5-A-RU.HCl as a more stable precursor of 5-OP-RU. After reduction of the nitroso group with sodium dithionite, they could purify the product by reverse phase HPLC and they finally added few volumes of 1N HCl to form the salts (69% yield). Finally, Braganza *et al.*⁶² recently published the synthesis of glyco-analogues of 5-OP-RU (discussed in section **IV.D**). Like Katagiri *et al.*, they did a reductive amination with ammoniac, but this time with milder sodium cyanoborohydride as reducing agent instead of sodium borohydride, and in a saturated solution of ammonium acetate in ethanol.

To summarize, different synthetic routes towards 5-A-RU have been described, and several improvements were achieved over the past decades by different research groups. Most of the changes focused on overcoming the stability issues of 5-A-RU (isolation of hydrochloride salts). Another difficulty of all the syntheses was the high polarity of the molecules due to the presence of many polar functional groups (hydroxyl groups and secondary amine of D-ribitylamine, lactam functions of the uracil ring). This made the purification of both chemical intermediates and 5-A-RU tedious (classical normal phase chromatography was not applicable). In our lab, a different synthesis with fully protected D-ribitylamine was developed (set-up by previous M2 intern Marie Flamme). We commonly used this synthetic pathway to produce protected D-ribitylamine as an essential synthetic intermediate for the synthesis of stable analogues of 5-OP-RU. We also adapted a shorter synthesis route of 5-A-RU made by Li *et al.* allowing to synthesize grams of 5-A-RU nitro precursor and giving at the end more stable hydrochloride salts of 5-A-RU. The two different syntheses will be described in details bellow.

2. Syntheses of 5-A-RU

a) *5-A-RU synthesis in non-protected series*

In this synthesis adapted from Li *et al.*⁷¹, the uracil moiety and D-ribitylamine were synthesized separately. The synthesis of D-ribitylamine started from the reaction between D-ribose and hydroxylamine in ethanol to form oxime **1** (Scheme 4). It was then reduced to **2** by hydrogenation over PtO₂ in acetic acid. Compound **3** was synthesized by nitration of 6-chlorouracil in a mixture of fuming nitric acid and sulfuric acid. The coupling reaction between **2** and **3** was done under basic conditions with potassium hydroxide (KOH) to give nitro precursor **4** also commonly called 5-N-RU. Product **5** (5-A-RU.HCl) was obtained after hydrogenation over Pd/C in water and conversion to hydrochloride salts was done by adding of few drops of 1N HCl followed by water evaporation under vacuum.

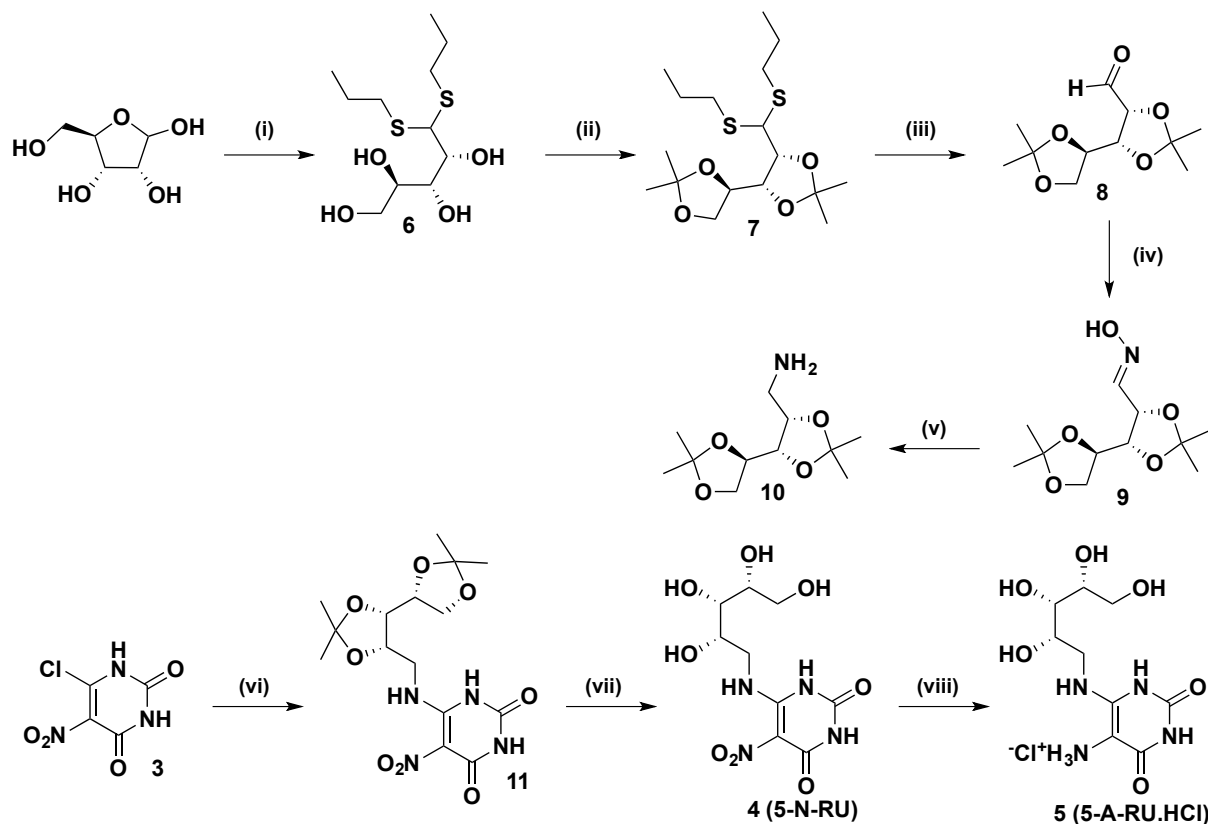


Scheme 4: Synthesis of 5-A-RU in non-protected series. Conditions and reagents: (i) NH₂OH.HCl, NaOMe in EtOH, 70°C, 78%; (ii) PtO₂, H₂ in AcOH, 103% (product isolated with few impurities); (iii) HNO₃, H₂SO₄, 73%; (iv) **2**, KOH 2N in EtOH/H₂O, 45%; (v) 1) Pd/C, H₂ in H₂O 2) 1N HCl, 94%

b) *5-A-RU synthesis in protected series*

The synthesis of 5-A-RU in protected series was done by adapting protocols from the literature⁷². The synthesis started also from D-ribose but this time by a thioketal protection of the aldehyde function using *n*-propanethiol in concentrated hydrochloric acid (37% HCl) leading to **6**. The four hydroxyl groups were subsequently protected by dimethyl acetal (**7**) and thioketal groups were removed under oxidative conditions to afford **8** with 76% yield. Reaction with hydroxylamine gave oxime **9** that was reduced using LiAlH₄ in tetrahydrofuran (THF) to obtain protected D-ribitylamine **10**. The sugar moiety was coupled to **3** in dichloromethane (DCM) with triethylamine, and the acetal groups were removed under acidic conditions giving **4**. 5-A-RU.HCl (**5**) was finally obtained by

hydrogenation and it was isolated as hydrochloride salts after 1N HCl addition and drying under vacuum.



Scheme 5: Synthesis of 5-A-RU in non-protected series. Reagents and conditions: (i) *n*-PrSH in 37% HCl, 47%; (ii) 2,2-dimethoxypropane, *p*-TsOH in acetone, 53%; (iii) I₂, NaHCO₃ in acetone/H₂O, 76%; (iv) NH₂OH.HCl, NaHCO₃ in EtOH/H₂O, 77%; (v) LiAlH₄ in THF, reflux, 76%; (vi) **10**, Et₃N in DCM, 93%, (vii) TFA/H₂O, 94%; (viii) **1** Pd/C, H₂ in H₂O, 2) 1N HCl, 94%

c) Comparison of the two different syntheses of **5**

The protected synthesis of **5** required more synthetic steps than the non-protected synthesis but it was technically easier to perform. Classical way of purification (normal phase chromatography) was successful whereas purifications in non-protected series were more difficult and less efficient (resin-exchange chromatography). Furthermore, the synthesis in protected series enabled the use of common organic solvents that were easy to handle (acetone, DCM, THF). In contrast, the synthesis in non-protected series required acetic acid and ammoniac as solvents that were difficult to completely remove under vacuum. Ultimately, both syntheses are useful, one to quickly obtain high amounts of precursor **4** (non-protected series) and the other to obtain the same product with high purity and to produce the strategic intermediate **10** that was extensively used for the synthesis of 5-OP-RU analogues.

3. Analytical study of 5-A-RU

In the literature, 5-A-RU is briefly described as an unstable compound prone to oxidation, but there is no additional information about the underlying degradation mechanisms⁷³. Because 5-A-RU is a key intermediate in the synthesis of MAIT cell antigens, we wanted to investigate this chemical instability. Analytical study of 5-A-RU was challenging because of the high polarity and hygroscopic properties of the molecule making classical analyses (HPLC, NMR...) difficult to realize. Still, some analyses were successfully performed in collaboration with a research team from Sanofi.

First, we ran UPLC-MS analysis of 5-A-RU. Product **4** was reduced by hydrogenation reaction to give 5-A-RU (neutral form), which was then filtered on celite, dried and directly used for analysis. We first noticed that the molecule co-eluted with the solvent peak, making the chromatographical analysis difficult. Still, MS (ESI+) analysis showed unambiguously the corresponding m/z 277 of 5-A-RU. After only a few minutes, a new peak appeared in ESI+ with m/z 294 while the m/z 277 peak of 5-A-RU decreased rapidly to finally disappear. The same analysis made by Sanofi's research team formed the same product with m/z 294 peak. These results, combined, suggest a very quick transformation of 5-A-RU.

We next carried out ¹H NMR analysis of 5-A-RU in DMSO-d₆ (Figure 22). 5-A-RU was again freshly synthesized and four different analyses were made: (i) freshly synthesized 5-A-RU; (ii) 5-A-RU kept under solid form in air for 48h; (iii) 5-A-RU dissolved in DMSO-d₆ for 48h; (iv) 5-A-RU kept in water for 48h, then lyophilized and analyzed. Sample (i) showed the presence of pure 5-A-RU as expected. After 48h in air (ii), slight differences of NMR signals were noticed but it was not clear whether degradation had occurred or not. The sample (iii) showed degradation with appearance of small new peaks in the region of OH-heteroatom protons of the ribityl moiety (4-6 ppm). Furthermore, the intensity of the signal of one NH of the uracil ring (10 ppm) was lower in (ii) and almost disappeared in (iii). The most important changes were for sample (iv) with a complete change of the NMR profile in the 4 to 6 ppm region and a complete disappearance of the two NH signals of the uracil ring. This was evidence of an important degradation of 5-A-RU in water.

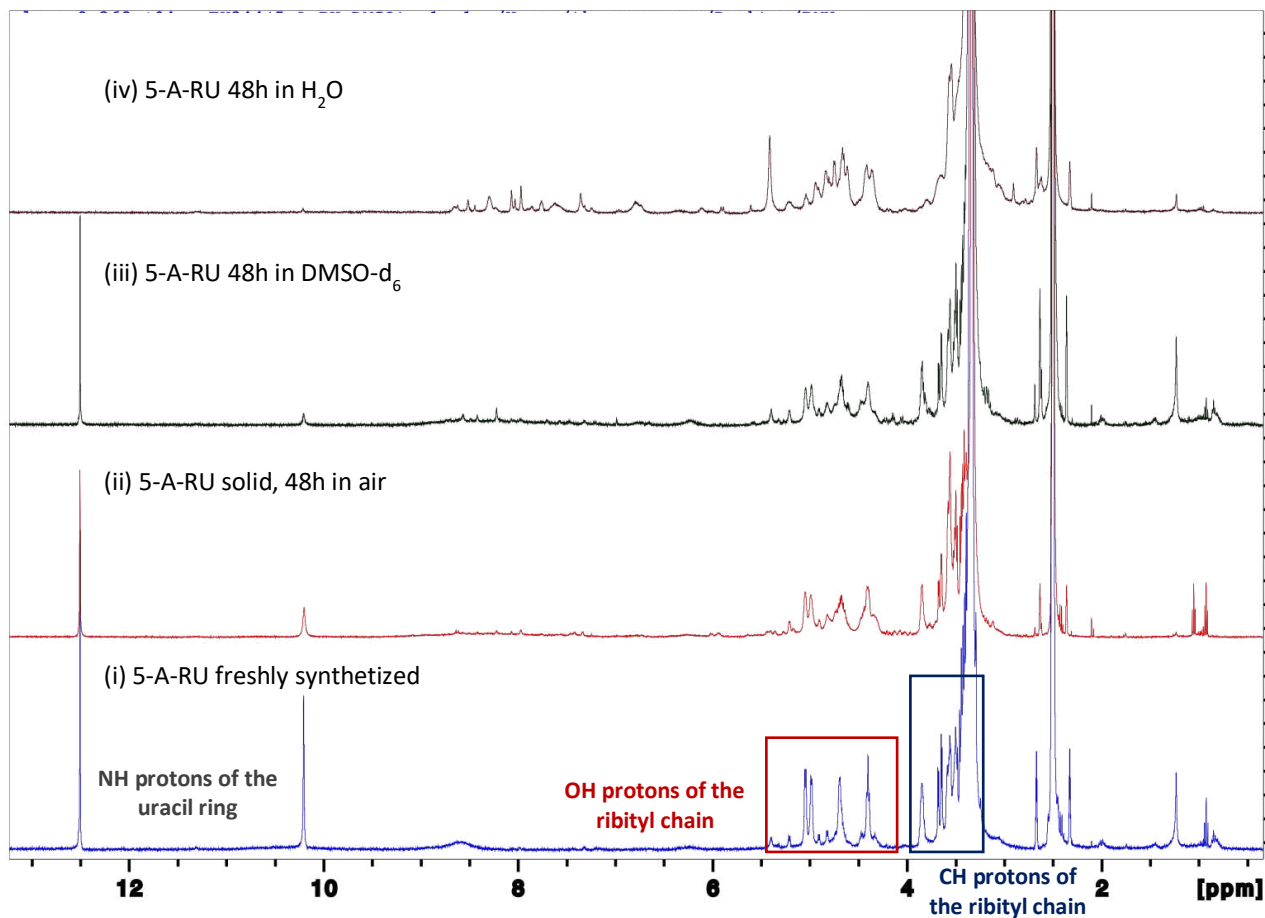


Figure 22: ^1H NMR analysis of 5-A-RU in DMSO-d_6

The two different spectrometric analyses of 5-A-RU seemed to confirm the high instability of the molecule in water. In collaboration with Sanofi, and by reviewing the literature, we were able to propose an hypothetical mechanism for the degradation of 5-A-RU⁷⁴ (Figure 23a). We hypothesized that the primary aromatic amine could oxidize in water to give an imine derivative ($M_w = 274$ g/mol). The product would then react with water to give at the end an equilibrium between keto and dihydroxy product, the latter matching the m/z 294 (ESI+). Lange *et al.* that proposed a different synthesis of 5-A-RU (described earlier) also investigated the instability of 5-A-RU⁷⁰. Similar to us, they strongly supported an autooxidation of the aromatic amine in water and found the same mass spectrometry (ESI+) peak m/z 294 but also m/z 275. They proposed a similar mechanism of degradation with an additional ending rearrangement to a five-membered ring after uracil ring opening (Figure 23b).

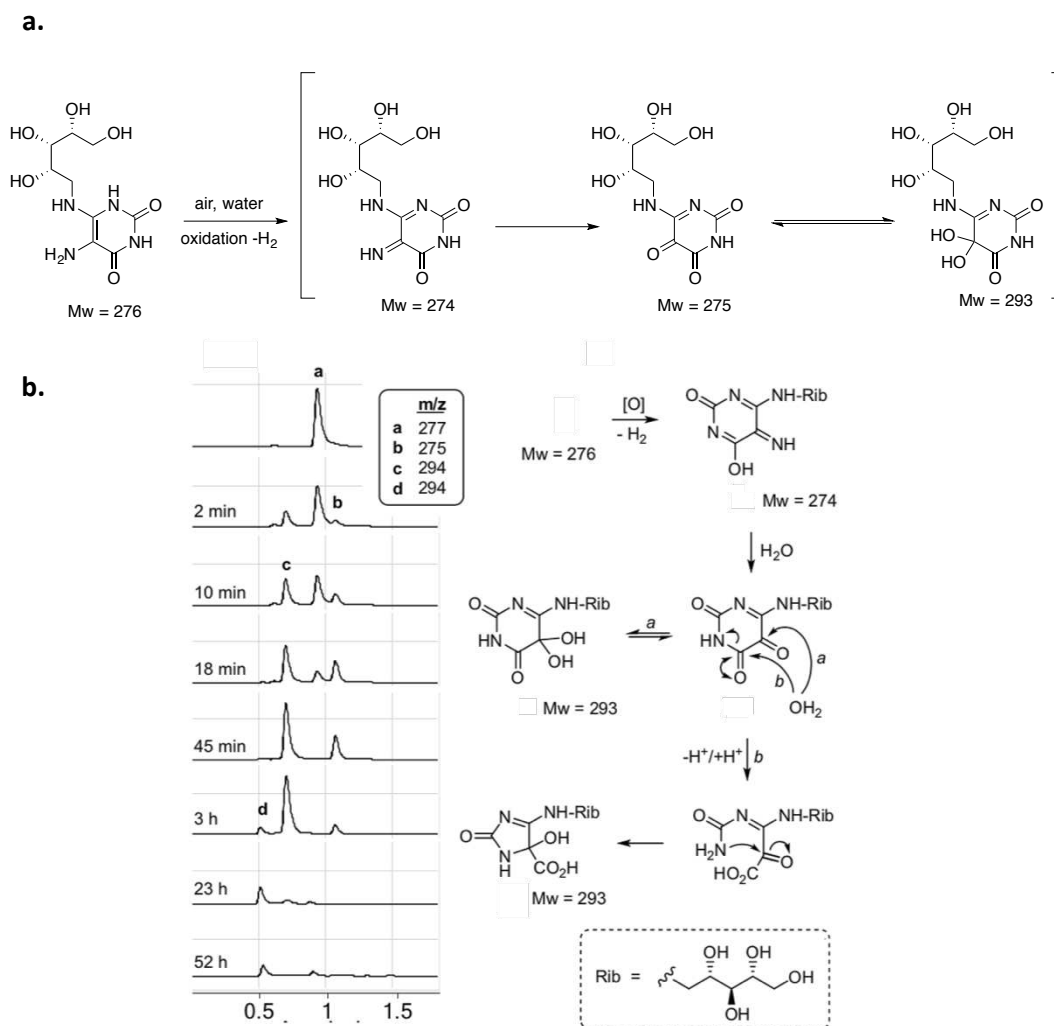


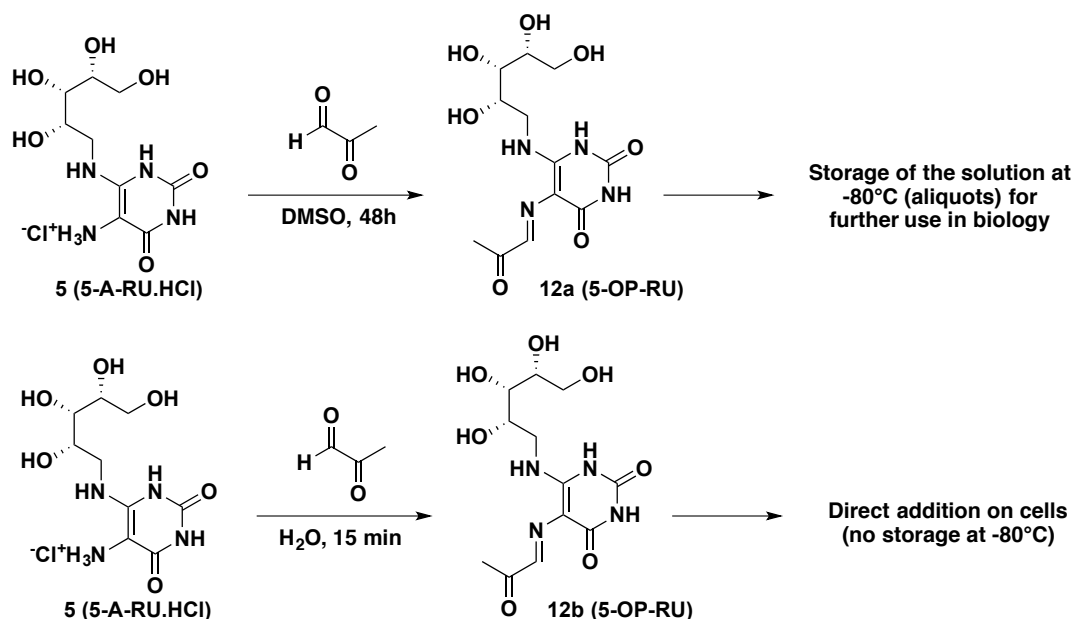
Figure 23: Proposed degradation mechanism of 5-A-RU by oxidation of the primary aromatic amine; a. Model proposed in collaboration with Sanofi; b. hypothesis from the literature⁷⁰

The analytical study of 5-A-RU gave some precious information about 5-A-RU degradation conditions. This knowledge allowed us to take all the precautions needed during the reduction of 5-N-RU to give 5-A-RU. Thus, it is crucial to carefully filter 5-A-RU solution on celite after hydrogenation to limit the contact with air as much as possible. The solution must be rapidly lyophilized and directly used without storage, or the more stable hydrochloride salts must be formed directly by adding aqueous HCl to freshly prepared 5-A-RU for storage (at -20°C and under inert atmosphere). Still, even under this form, degradation of some salts occurred, most likely due to the hygroscopic properties of 5-A-RU. Therefore, a fresh batch of 5-A-RU.HCl was made each time it was required and it was directly used in synthesis to ensure the purity of the product.

4. Synthesis of 5-OP-RU

As mentioned earlier, 5-OP-RU is unstable so it is very difficult to purify and isolate the molecule. Therefore, 5-OP-RU is commonly directly used on cells after condensation reaction between 5-A-RU and methylglyoxal without isolation of the product. A first option is to do the reaction in phosphate sodium buffer (PBS) or in culture medium just before the addition on cells. This was routinely done in the biology laboratory of Institut Curie and it enabled a strong activation of MAIT cells, confirming the success of the chemical reaction. However, the quantity of 5-OP-RU added on cells is rather approximate because of a quick degradation occurring and an incomplete conversion of 5-A-RU to 5-OP-RU during the reaction (as described by Mak *et al.*⁵⁸). The second option is to do the reaction in DMSO. Indeed, the conversion of 5-A-RU to 5-OP-RU is almost quantitative in this solvent. Furthermore, the degradation of 5-OP-RU in DMSO is slow after addition of water. This means that if 5-OP-RU formed in DMSO is quickly added on cells after dilution in aqueous media, no major degradation would occur. Thus, the concentration added on cells would be more reliable than the one of 5-OP-RU formed in water. We decided to prepare 5-OP-RU in water and DMSO to compare the biological activity of both batches.

The first batch of 5-OP-RU in DMSO (**12a**) was obtained by dissolving freshly synthesized 5-A-**5** in DMSO, then adding excess methylglyoxal (Scheme 6). The solution was left at room temperature for 48h (the reaction was monitored by UPLC-MS to confirm the quantitative formation of 5-OP-RU). After this time, the solution was aliquoted and freeze-dried at -80°C for further use in biological assays. The second batch in water (**12b**) was obtained by adding excess methylglyoxal to an aqueous solution of **5**. After 15 minutes, the solution containing 5-OP-RU was directly added on cells for the biological evaluation. Each time a fresh batch of **12b** in water was made because of the instability of the molecule in this solvent (the product was not stored at -80°C contrary to **12a**).



Scheme 6: Syntheses of 12a (5-OP-RU in DMSO) and 12b (5-OP-RU in water)

B. Design, synthesis and biological evaluation of new stable analogues of 5-OP-RU

1. Medicinal chemistry strategy

Three different strategies were envisioned to produce new stable analogues of 5-OP-RU (Figure 24). The first strategy consisted in fully replacing the unstable α -iminocarbonyl group by a stable side chain still susceptible to interact with MR1. The α -iminocarbonyl group is made of two unstable parts, a terminal ketone undergoing cyclization after nucleophilic attack by N7H group and an imine function sensitive to hydrolysis. We had the idea to replace both sensitive groups by an alkyl or a vinyl sulfonate side chain. The rationale behind this was the introduction of a negative charge (at physiological pH) carried by the sulfonate functional group. It would create an ionic interaction with positively charged Lys43 of MR1 instead of an imine that would trigger the trafficking of the complex from the ER to the plasma membrane.

The second strategy was a pharmacomodulation of the D-ribitylamine group. We aimed to replace the nucleophilic N7H group by less nucleophilic oxygen or carbon atoms or to form an amide derivative. Another idea was to increase the steric hindrance at C1' position by introducing a gem-dimethyl group. This would favor the formation of trans imine after reaction with methylglyoxal and limits the cyclization reaction. This part of the work was done in collaboration with Sanofi's drug discovery research team from Vitry-sur-Seine.

Our final strategy was to design and synthesize stable fused bicyclic heterocycle analogues of 5-OP-RU. Since several ribityllumazines and formylpterin derivatives showed biological activity (MR1 up-regulation and/or MAIT cell activation), we hypothesized that other fused heterocycles could be potent at activating MAIT cells. Ribityllumazine are far less potent than 5-OP-RU because they do not covalently bind to Lys43, while formylpterin derivatives can form a Schiff base with Lys43 of MR1 but do not interact with the MAIT cell TCR because they lack the essential D-ribitylamine tail. Thus, we attempted to design fused heterocycles that would conserve both the D-ribitylamine chain and the terminal electrophilic carbonyl group for MR1 interaction. We focused on purinetrione and pyrazolo[3,4-*d*]pyrimidine heterocycles, partly inspired by the work of Cushman and co-workers on the synthesis of riboflavin and lumazine synthase inhibitors^{73,75}. We also wanted to synthesize a ribityllumazine analogue bearing an additional aromatic aldehyde function like 6-Fp. This compound could interact with MR1 contrary to lumazine derivatives lacking such functional group, and it could interact with MR1 and the MAIT cell TCR through its ribityl chain.

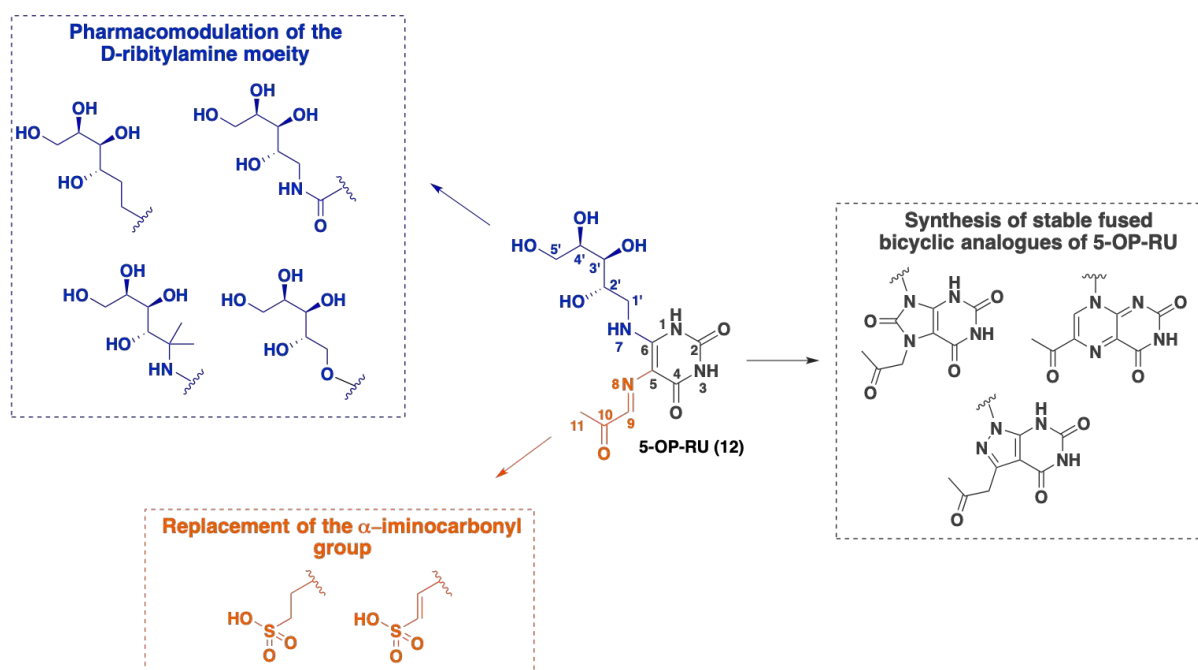


Figure 24: Summary of the different pharmacomodulations envisioned to obtain stable potent analogues of 5-OP-RU

The different synthesized molecules are detailed in the next section, followed by the biological evaluation and a discussion of the different results obtained (structure-activity relationships).

2. Chemical modulation of the α -iminocarbonyl group

a) *Synthesis of an alkylanionic analogue of 5-OP-RU*

i) *In silico study*

Three different analogues of 5-OP-RU bearing an ionizable function at physiological pH were initially envisioned bearing either sulfonate, phosphonate or carboxylate functions (Figure 25).

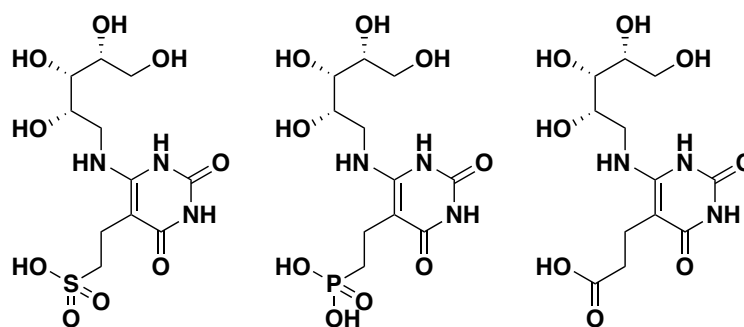


Figure 25: Chemical structure of different alkylanionic analogues of 5-OP-RU

Docking analysis of the three molecules was completed at Sanofi by Anke Steinmetz to help us choose the most promising molecule to synthesize. While no convincing poses were obtained with phosphonate and carboxylate analogues, the sulfonate derivative showed a very convincing analogy with 5-OP-RU binding mode inside the MR1-TCR binding groove (Figure 26).

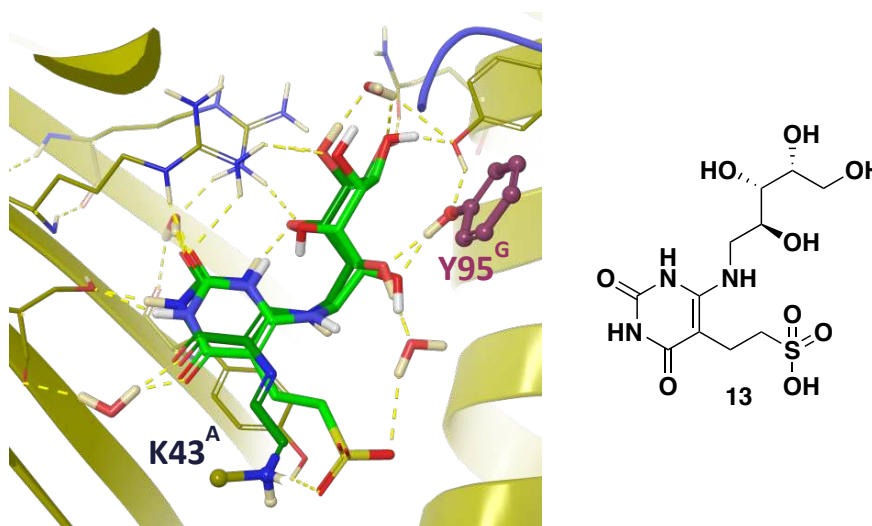


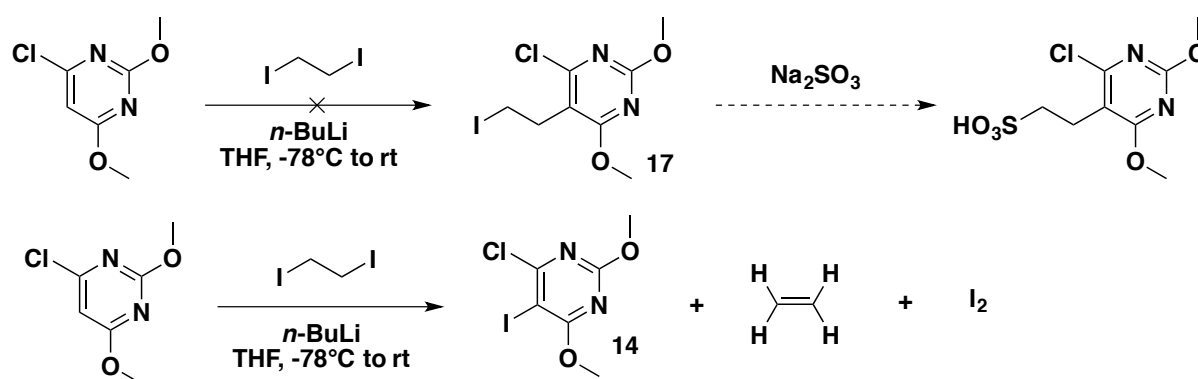
Figure 26: Docking analysis of 13 inside the MR1-TCR binding groove in comparison with 5-OE-RU (4NQE PDB file⁶) Protein is depicted by ribbon diagrams with MR1 chain A, TCR chains G and H colored in blue and plum, respectively. Selected amino acids and ligands are represented as ball-and-sticks or tubes

Critical interaction with Tyr95 (Y95) of the TCR was maintained as well as other Van der Waals interactions with MR1. Most importantly, the sulfonate moiety was able to interact with the amino group of Lys43 (K43) through an ionic interaction. These results motivated us to start synthesizing the sulfonate analogue **13**.

ii) Chemical synthesis of **13**

The synthesis of **13** was partly inspired by the one developed by Cushman *et al.*⁷⁶. They synthesized analogues of **13** with four, five and six-carbon side chains instead of the two-carbon alkyl chain of **13**. Since hydroxyls groups of the ribityl chain and lactam groups of the uracil ring are reactive moieties, they must be fully protected by appropriate protective groups. Protected D-ribitylamine **10** was already synthesized so we decided to use this molecule for the introduction of the ribityl moiety. The use of methyl ether protective groups was considered for the uracil ring because they are stable to most of reaction conditions. Furthermore, the corresponding protected molecule 6-chloro-2,4-dimethoxypyrimidinedione was commercially available and was considered as a strategic starting material.

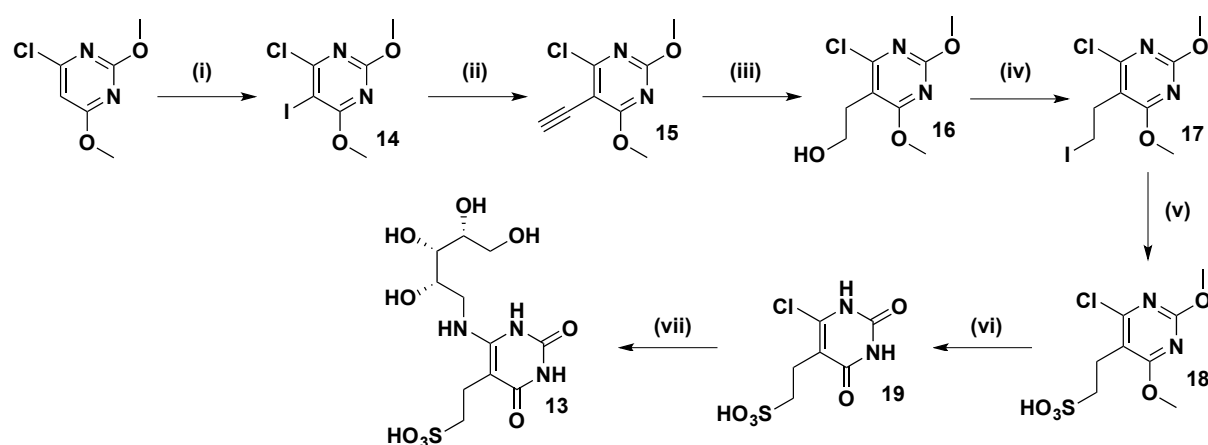
Following the synthesis from the literature, we attempted to add an iodoethane chain at the C5 position of the uracil ring by a nucleophilic substitution on 1,2-diiodoethane with the use of *n*-BuLi⁷⁶. Unfortunately, product **17** was not obtained and only the major iodinated product **14** was obtained⁷⁶ (Scheme 7). This phenomenon is likely explained by a nucleophilic attack of iodine driven by elimination of ethene⁷⁷.



Scheme 7: Attempt to introduce the iodoethane side chain to get **17**

We could obtain **17** using a different synthesis strategy (Scheme 8). The starting material was again 6-chloro-2,4-dimethoxypyrimidine. Iodination reaction under acidic conditions gave **14**⁷⁸. Then, we introduced a TMS-acetylene group at C5 position of the heterocycle by Sonogashira reaction to get the two-carbon side chain. The reaction was done in a mixture of diisopropylamine and THF at 70°C to enable the critical reduction of Pd(II) of Pd(PPh₃)₂Cl₂ to Pd(0) and also because the boiling point of this

mixture of solvents was ideal to give enough pressure in the sealed tube at 70°C so the reaction could work. Previous attempts done at higher temperatures or with DIPEA (diisopropylethylamine) instead of diisopropylamine failed. Product **15** was obtained after TMS removal with potassium methanolate. Then, hydroboration reaction with bis(pinacolato)diboron allowed to convert the terminal alkyne to a primary alcohol. However, a small amount of aldehyde was produced in addition to the desired intermediate. It was reduced with sodium borohydride to give only **16**. The latter compound was converted to **17** by replacement of the alcohol functional group by an iodo with the use of iodine, triphenylphosphine and imidazole reagents. **17** reacted with sodium sulfite in methanol at reflux to afford sulfonic acid **18** with 88% yield. The deprotection of methyl ether protective groups was done in a mixture of 37% HCl and acetic acid under reflux giving **19**. The coupling reaction with **10** proved to be challenging and it required harsh conditions (48h-heating at 120°C in ethanol in a sealed tube). Nevertheless, the final product **13** was obtained with 22% yield after acetal deprotection in a mixture of TFA/H₂O.

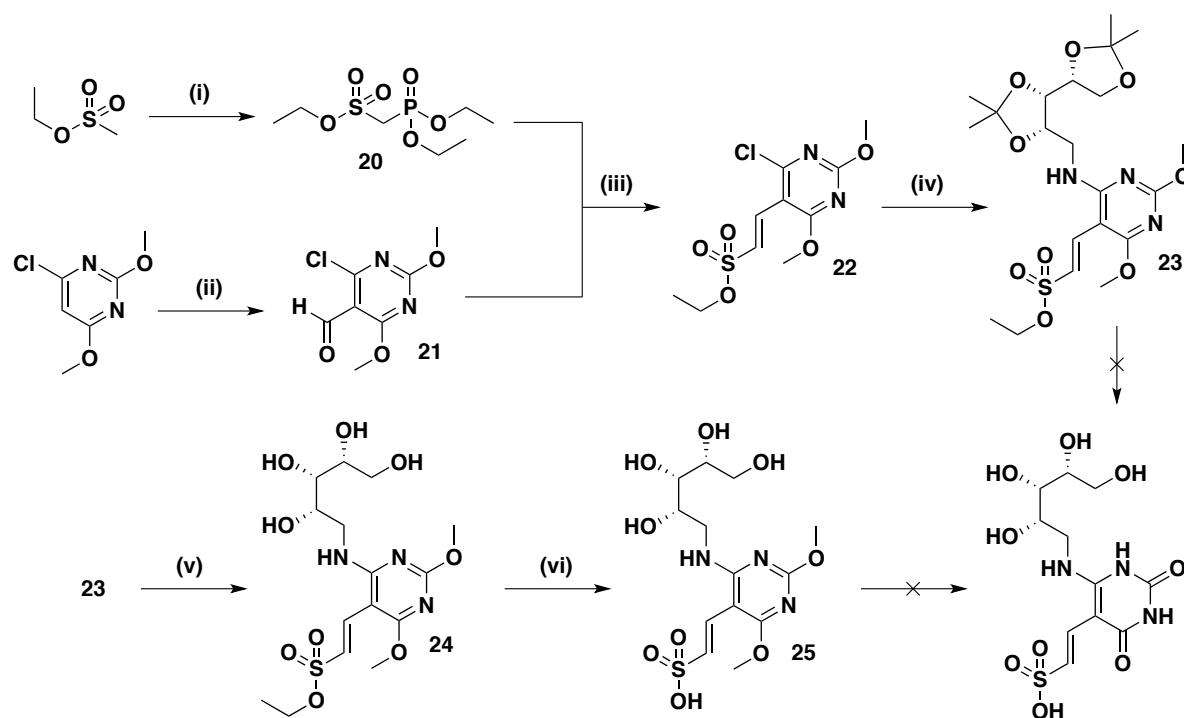


Scheme 8: Synthesis of 13. Reagents and conditions: (i) N-iodosuccinimide, AcOH, acetic anhydride in CH₃CN, 80°C, 81%; (ii) 1) TMS-acetylene, Pd(PPh₃)₂Cl₂, CuI in iPr₂NH / THF 1:1, 70°C; 2) K₂CO₃ in MeOH, 64%; (iii) 1) B₂Pin₂, Cs₂CO₃, MeOH in CH₃CN, 100 °C, sealed tube; 2) NaOH, H₂O₂; 3) NaBH₄ in MeOH 52%; (iv) PPh₃, I₂, imidazole in THF, 74%; (v) Na₂SO₃ in acetone/H₂O, reflux, 88%; (vi) 37% HCl, AcOH, reflux 65%; (vii) 1) **10** in EtOH, sealed tube; 2) TFA/H₂O 22%

b) Synthesis of vinylsulfonate analogue of 5-OP-RU

For the use of protective groups, we took into account the same considerations as for **13**. This time, we thought of introducing at an early stage a protected sulfonate derivative moiety by a Wittig reaction. Then, we planned to couple the protected sugar moiety (**10**) by Buchwald-Hartwig cross-coupling reaction to finally remove all the protecting groups to obtain the final product.

Methylethanesulfonate reacted with diethylphosphochloridate with the use of the strong base *n*-BuLi to give ylide precursor **20**⁷⁹ (Scheme 9). It is noteworthy to mention that the reaction mixture must be kept at -50°C since many side products were formed at higher temperature. Uracil derivative **21** was synthesized by a formylation reaction at -78°C from 6-chloro-2,4-dimethoxypyrimidine and DMF after *n*-BuLi deprotonation. Wittig reaction between **20** and **21** and with *t*-BuOK as a base afforded the protected vinylsulfonate compound **22** with the desired E configuration (like 5-OP-RU). This stereoselectivity is explained by the use of the Horner-Wadsworth-Emmons reagent **20**. Buchwald-Hartwig cross-coupling reaction between **22** and **10** afforded the fully protected precursor **23**. The last step of the synthesis consisted in the deprotection of all protective groups. One pot deprotection of all the groups failed under acidic conditions (HCl in MeOH at reflux, HBr/H₂O in MeOH at 60°C⁸⁰, TMSI in DCM) with only degradation products formed (notably with a loss of alkene ¹H NMR signals).

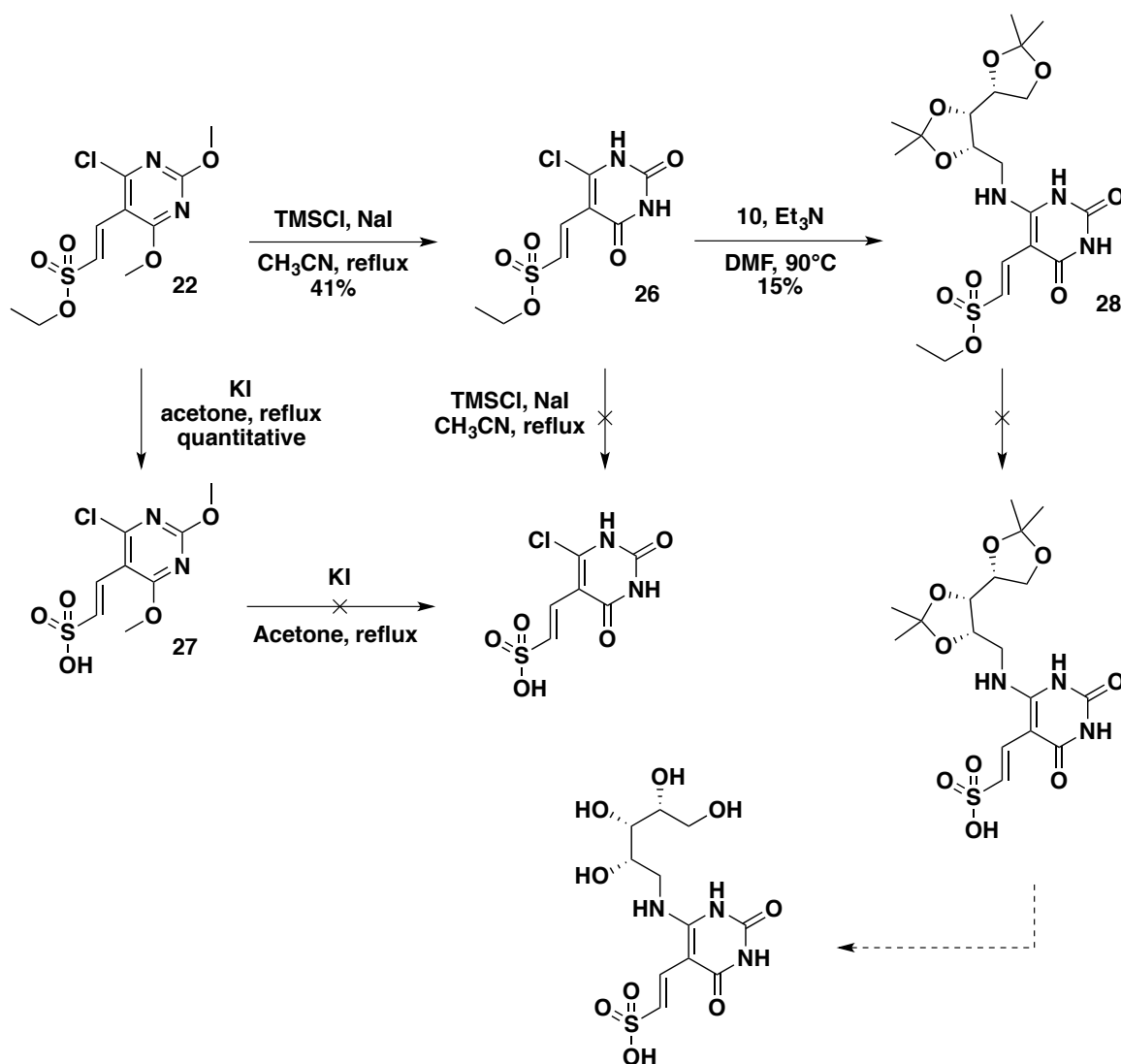


Scheme 9: Initial synthesis of the vinylsulfonate analogue of 5-OP-RU. Reagents and conditions: (i) diethylphosphochloridate, *n*-BuLi in THF, -78°C to -50°C, 63%; (ii) *n*-BuLi, DMF in THF, -78°C, 64%; (iii) *t*-BuOK in THF, 0°C to rt, 69%; (iv) **10**, Pd(dba)₃, Xantphos, Cs₂CO₃ in toluene, rt, 66%; (v) TFA/H₂O in CH₃CN, 0°C to rt, 47%; (vi) KI in acetone, reflux, 40%

We tried in a second attempt to sequentially remove each protecting group. The ribityl chain was easily deprotected in a mixture of TFA/H₂O in acetonitrile to give **24** and the sulfonic ester was successfully deprotected with potassium iodide in acetone at reflux (**25**), without any degradation observed. However, attempts to deprotect the two methyl ethers of **25** by using TMSI failed. NMR

analysis confirmed that demethylation worked but the molecule underwent degradation to give an unidentified mixture of products (still with loss of alkene NMR signals).

We suspected that the D-ribitylamine chain was responsible for this instability. We therefore tried to deprotect **22** before running the coupling reaction with **10**. We first tried the deprotection in a mixture of concentrated HCl and acetic acid at reflux. The corresponding m/z peak of the product was observed in UPLC-MS but the major product was dehydrated (m/z -18). Another attempt with HCl in methanol and heating at reflux also failed to give the desired product. We then tried milder conditions with Lewis acid TMSI formed *in situ* from TMSCl and NaI at room temperature. A selective deprotection of methyl ethers was observed in acetonitrile affording **26** but no deprotection of the sulfonic ester occurred (Scheme 10). This confirmed that the deprotection of the uracil ring must be done before introducing the sugar moiety.



Scheme 10: Synthetic route towards vinylsulfonate analogue of 5-OP-RU

We then tried to deprotect the sulfonic ester of **26** using the same conditions as the one used for **25** (potassium iodide in acetone at reflux) but it failed to give the corresponding product while the same reaction with **22** readily afforded **27**. These surprising results are likely explained by the low solubility of **26** in organic solvents compared to **22** and/or by a chelation of potassium by the uracil ring decreasing the reactivity of **26**. We managed to couple **10** to **26** giving **28**, though with a low yield. Indeed, the reaction required heating at 80°C to work but some degradation occurred at the same temperature. Contrary to **26**, compound **28** displayed a good solubility in common organic solvents including acetone. However, attempts to deprotect the sulfonic ester with potassium iodide only yielded to traces of the desired product (*m/z* peak detected in UPLC-MS). More vigorous conditions of deprotection were attempted with 37% HCl in methanol, 48% HBr/H₂O in methanol and TMSCl/NaI in acetonitrile (even with heating), but only degradation products were obtained each time.

3. Pharmacomodulation of the D-ribitylamine moiety

In collaboration with Sanofi's research team, we aimed to synthesize stable analogues of 5-OP-RU by modifying the ribityl chain of the molecule. Compounds **29**, **31** and **32** were synthesized at Institut Curie from chemical precursors provided by Sanofi and the stable analogue of 5-OP-RU **30** was directly tested in biology (Figure 27).

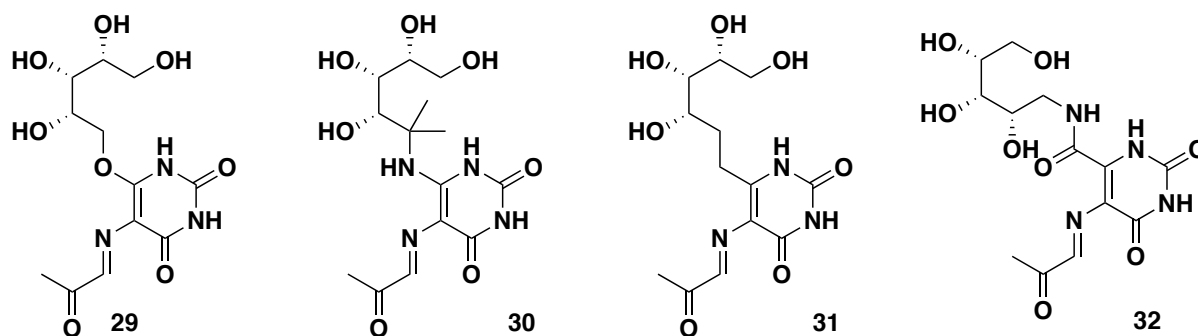
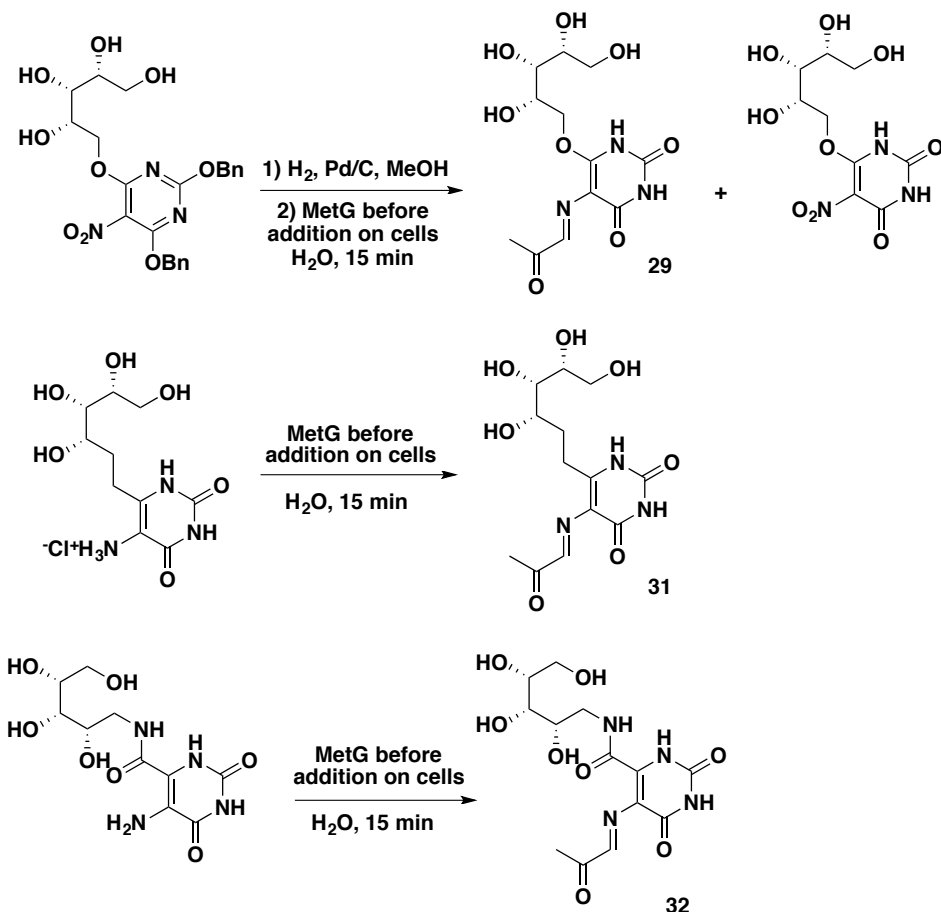


Figure 27: Chemical structure of D-ribitylamine modified analogues of 5-OP-RU

Small amounts of chemical precursors of **29**, **31** and **32** were furnished by Sanofi. **29** amino precursor was synthesized by one pot hydrogenation of the nitro group and deprotection of the benzyl protecting groups. Despite several attempts of hydrogenation (with Pd/C or Raney nickel), we always got a mixture of the desired product and the nitro precursor derivative as an impurity. This result was also observed by Sanofi's research group when using water as solvent instead of methanol and Lindlar palladium as catalyst. Nevertheless, we used this mixture for the reaction with methylglyoxal to form

29. The reaction with methylglyoxal was done right before addition on cells (like for **12b**). The same reaction was done to get products **31** and **32** (Scheme 11)



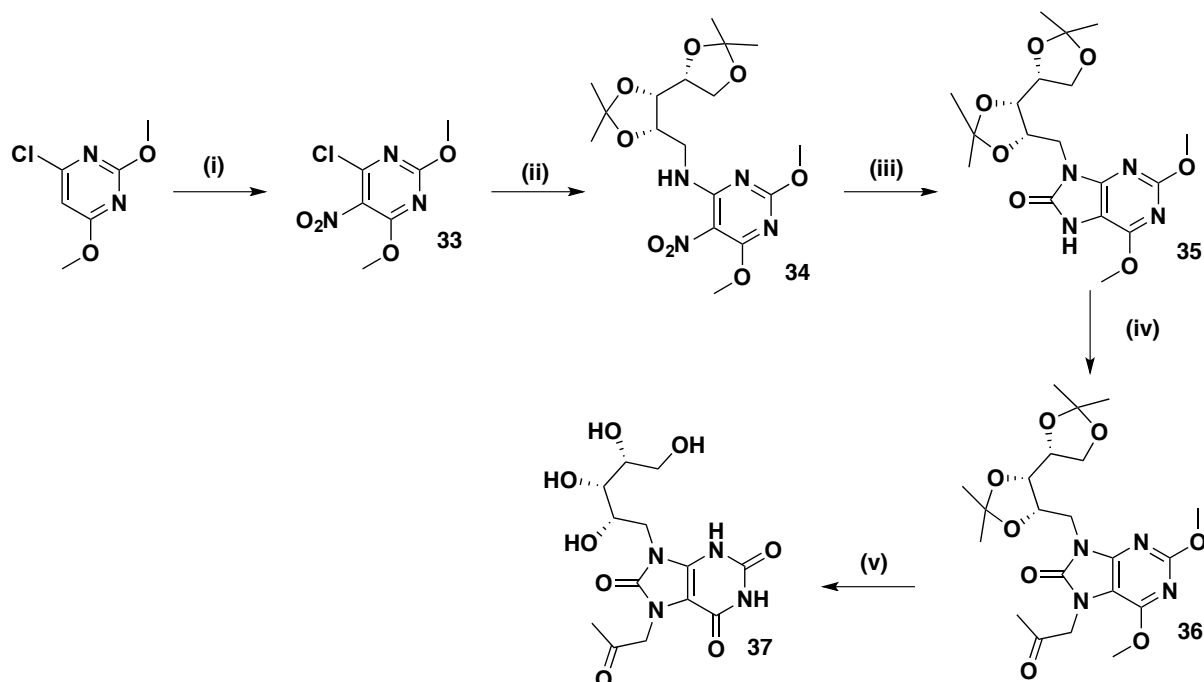
Scheme 11: Synthesis of compounds 29, 31 and 32 from Sanofi's chemical precursors

4. Synthesis of stable fused bicyclic analogues of 5-OP-RU

a) *Purinetrione analogue synthesis*

Purinetrione analogue of 5-OP-RU was designed by adapting a synthetic procedure from the literature⁷³. 6-chloro-2,4-dimethoxypyrimidine was again chosen as starting material (Scheme 12). Nitration was performed in a mixture of fuming nitric acid and sulfuric acid to afford **33**. Like for 5-N-RU (**4**), the presence of the nitro group at ortho position of the chloro helped with the introduction of the protected ribityl chain to give fully protected analogue of 5-N-RU **34**. Nitro reduction by hydrogenation with Pd/C followed by cyclization reaction using triphosgene led to the formation of **35**. Reaction of **35** with chloroacetone with prior deprotonation using sodium hydride afforded bicyclic

product **36**. Finally, acetal and methyl ether protective groups were removed by concentrated HCl in methanol at reflux to give the final product **37**.



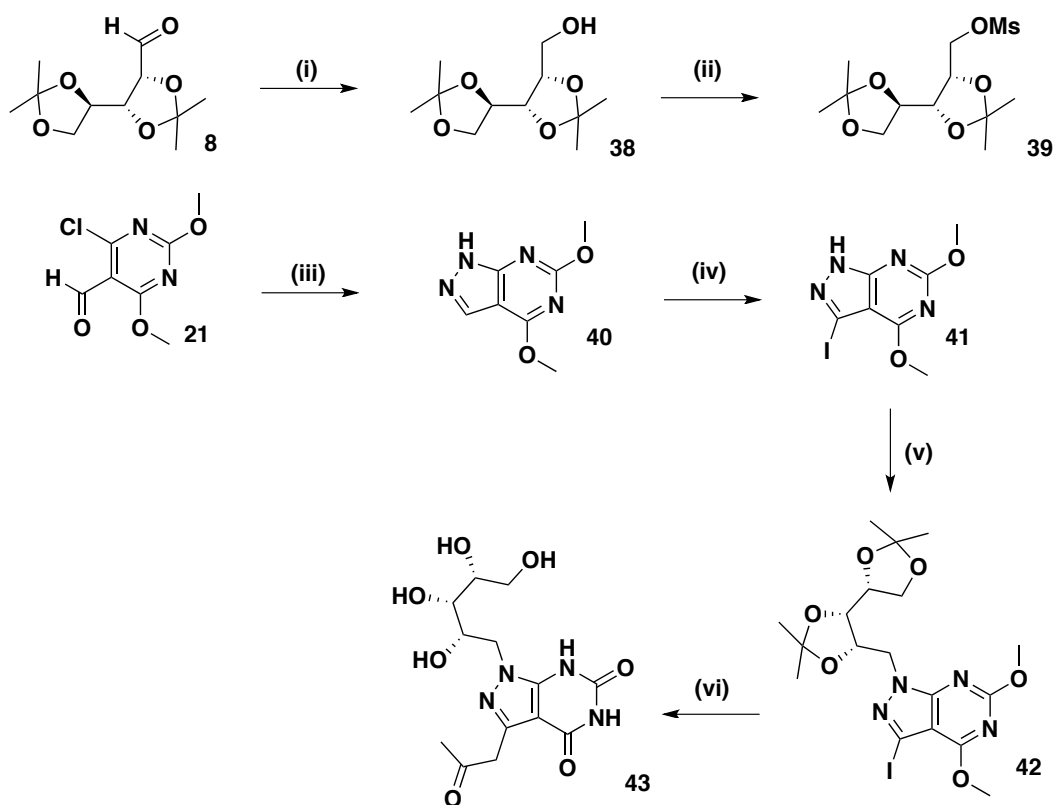
Scheme 12: Synthesis of 37. Reagents and conditions: (i) HNO₃, H₂SO₄, 80°C, 56%; (ii) **10**, Et₃N in DMF, 75%; (iii) 1) H₂, Pd/C in MeOH; 2) triphosgene, Et₃N in DCM, 0°C, 72%; (iv) chloroacetone, NaH in DMF, 94%; (v) 37% HCl in MeOH, reflux, 84%

b) *Pyrazolo[3,4-d]pyrimidine analogue synthesis*

43 was designed with a separated synthesis of the heterocycle bearing a free intracyclic nucleophilic amine that could react with an activated protected analogue of D-ribose (bearing a mesyl function). Like the other analogues, a protection of the sugar moiety and the uracil was required to avoid any side reaction. Once again, we chose to use an acetal protected D-ribose analogue and a methyl ether protected uracil, as it was efficient for the synthesis of the other analogues of 5-OP-RU. One challenging step of the synthesis was the introduction of the propan-2-one. Our strategy was to form an iodo precursor and to introduce the lateral chain by palladium-catalyzed cross-coupling reaction.

The sugar moiety was obtained from the reduction of **8** with sodium borohydride giving **38**, followed by mesylation with mesyl chloride in pyridine to get **39** (Scheme 13). Synthesis of the heterocycle moiety was started from the already synthesized compound **21**. Cyclization with hydrazine gave bicyclic product **40** with the pyrazolo[3,4-d]pyrimidine core. Iodination at C5 position with NIS in DMF at reflux gave **41**. The two synthons were then coupled to give **42**. Introduction of the propan-2-

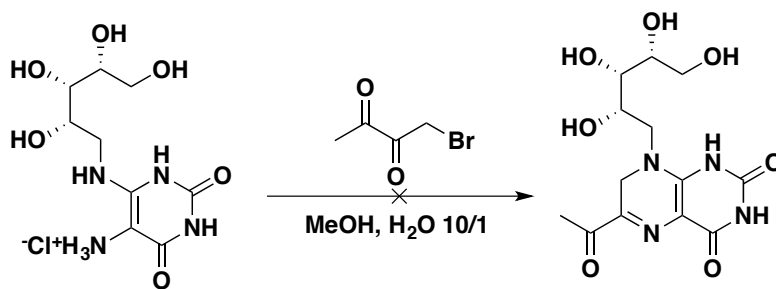
one side chain was done by Stille cross-coupling reaction. Unfortunately, the reaction was not efficient as only a small amount of compound was obtained, even after 24h heating in sealed tube (120°C) and several impurities were produced. Still, we continued the synthesis with the mixture by removing all protecting groups with 37% HCl in methanol. At last, only traces of the product **43** were obtained along with several impurities. Thus, the synthesis route must be optimized to get cleaner reactions and to obtain enough amounts of **43** for its chemical analyses and biological evaluation.



Scheme 13: Synthesis of 43. Reagents and conditions: (i) NaBH₄ in MeOH, 48%; (ii) MsCl in pyridine, 89%; (iii) H₂N-NH₂·H₂O in MeOH, reflux, 46%; (iv) NIS in DMF, 46%; (v) **39**, K₂CO₃ in DMF, 39%; (vi) 1) isopropenyl acetate, (t-Bu)₃SnMeO, P(o-tolyl)₃, PdCl₂(CH₃CN)₂ in toluene, 120°C sealed tube; 2) 37% HCl in methanol, only traces obtained

c) *Formyllumazine analogue*

Formyllumazine analogue of 5-OP-RU was synthesized directly through the reaction between 5-A-RU and bromo-2,3-butanedione in a mixture of methanol/water (Scheme 14). After 30 min, complete conversion of 5-A-RU to the desired bicyclic product was observed by UPLC-MS. However, after HPLC purification of the product, its aspect rapidly changed from a yellow powder to a brown paste in the fridge. NMR analysis confirmed that a degradation of the molecule had occurred. Thus, despite several attempts of synthesis, we were not able to get some amount of product for the biological evaluation.



Scheme 14: Synthesis of formyllumazine analogue of 5-OP-RU

C. Biological evaluation

1. Description of the tests used for the biological evaluation of the molecules

TCR-dependent activation of MAIT cells rely on the capacity of the ligands to bind MR1 and to efficiently recognize the TCR. The binding to MR1 is commonly evaluated in cells by measuring the up-regulation of MR1 at the cell membrane surface after incubation of APCs with diverse ligands. Increased amounts of MR1 protein at the cell membrane can be detected by flow cytometry by using a fluorophore conjugated anti-MR1 antibody (flow cytometry gating strategy for MR1 up-regulation assay is exposed in Appendix A). WT3-m cell line was used to do the biological evaluation. It is a murine embryonic fibroblastic cell line transfected with mouse MR1 gene (meaning the cells overexpress MR1). WT3-m cell line was already described and validated for this purpose⁸¹. The use of cells overexpressing MR1 was necessary because MR1 is endogenously expressed at a low level. Indeed, tests with wild type cells (WT3-WT) appeared not to be sensitive enough. MR1 up-regulation is a time and concentration-dependent process. These parameters must be carefully studied and determined before the experiments. In our case, we chose to incubate each ligand dilution for 2 hours, like it was previously done and to do a large panel of concentrations for each active molecule to get the maximum information⁸².

The second part of the biological evaluation is MAIT cell activation assay. To do so, we have to mimic an antigenic presentation *in vitro* with APCs and MAIT cells. Again, we used murine model with WT3-m as APCs and MAIT cells were obtained from mice. Unlike in humans, MAIT cells are very rare in mice. To overcome this issue, transgenic mice model expressing the iV α 19 chain of the MAIT cell TCR were generated several years ago¹³. They were generated on C α ^{-/-} background to prevent the use of endogenous TCR α chain. They can also express murine V β 8 or V β 6 chains (double transgenic mice) or not (single transgenic mice). In the first case, a monoclonal repertoire of T cells is obtained while single transgenic mice develop a polyclonal repertoire of T cells harboring different TCR β chains. In our study, we mostly (but not only) used double transgenic mice C α ^{-/-} iV α 19 V β 8⁺ to assess the biological

activity of the different molecules. MAIT cells were harvested from the spleen of these transgenic mice and put into 96-well plates with WT3-m cells and the ligands. Activation of MAIT cells was assessed by measuring an increased expression of activation markers CD69 (and CD25) (**Figure 28**) (flow cytometry gating strategy for MAIT cell activation assay is exposed in Appendix B).

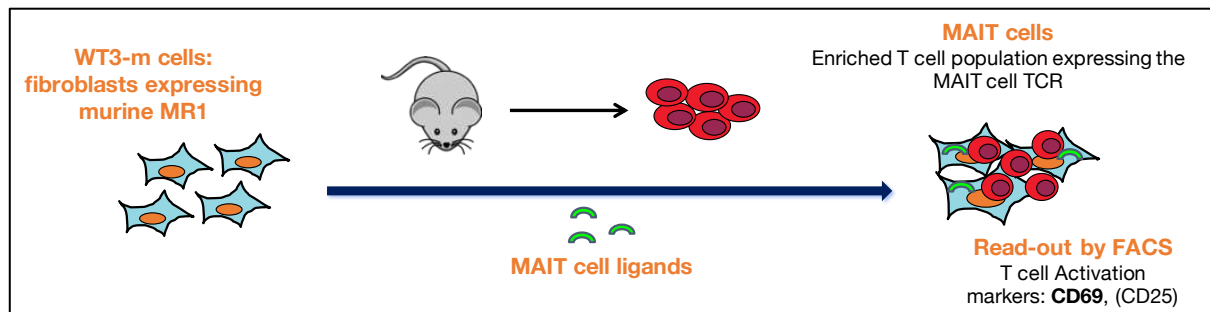


Figure 28: MAIT cell activation assay

2. Results

a) *MR1 up-regulation measurements*

The capacity of compounds **12a**, **12b**, **5**, compound C (2-Ac-6-Fp-diOMe), mixture **29**, **30**, **31**, **13** and **32** to up-regulate MR1 at the surface of WT3-m cells was assessed. A first simple screening with two concentrations (10 μ M and 0.1 μ M) was done (Figure 29). **12a** (5-OP-RU in DMSO) showed the strongest MR1 up-regulation, higher than **12b** (5-OP-RU in water), which is consistent with a more efficient synthesis of 5-OP-RU in DMSO and a higher chemical stability. Molecules **30** and compound C were also able to strongly up-regulate MR1 with similar potency. Finally, slight up-regulation was observed at 10 μ M for **31** and **5** (5-A-RU) whereas **29**, **13**, **32** and **37** did not up-regulate MR1.

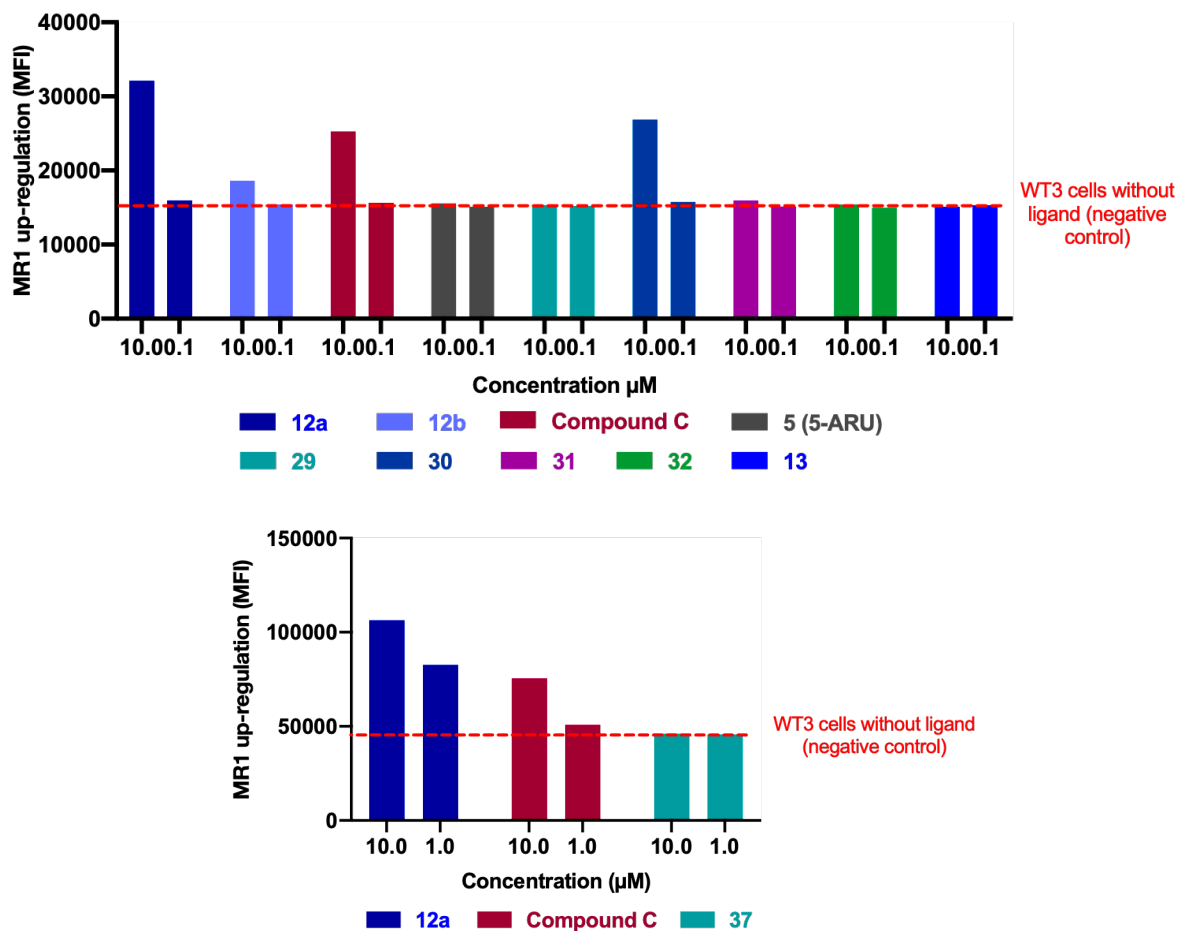


Figure 29: MR1 up-regulation evaluation of newly synthesized ligands

A second assay was done to get a more detailed dose-effect response of MR1 up-regulation with potent compounds **30** and **31** (Figure 30). The up-regulation of MR1 was concentration dependent and **12a** still showed the strongest up-regulation after 2 hours followed by **30**. This time, **31** induced a slight up-regulation of MR1 like compound C.

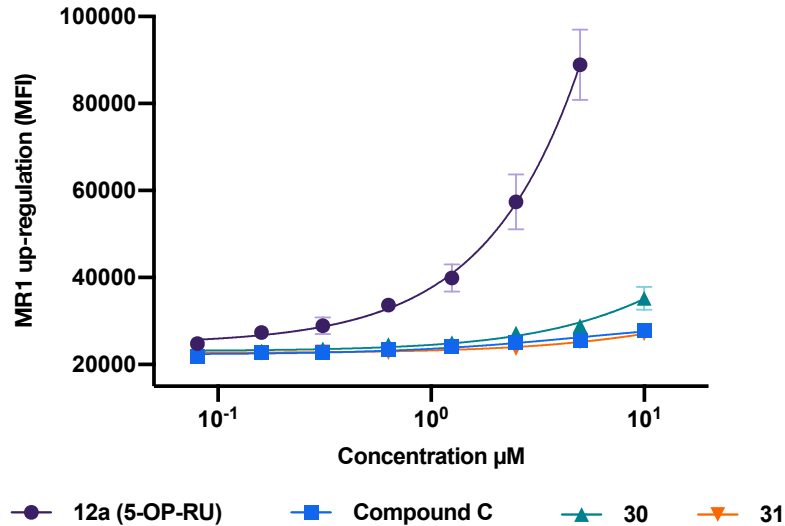


Figure 30: MR1 up-regulation evaluation of 30 and 31. Data displayed on the graphs are means \pm SD of technical duplicates

b) *MR1-13 tetramer formation and MAIT cell staining assay*

Since sulfonic acids are negatively charged at physiological pH (sulfonate form), this can result in difficulties for the molecules to cross lipidic barriers such as cell and vesicle membranes⁸³. We thought this could be an important drawback for antigen processing inside APCs. Therefore, the affinity of **13** for MR1 was assessed outside living cells by attempting to refold recombinant MR1 protein (produced at the recombinant protein platform of Institut Curie). Compound **13** efficiently refold MR1 to give a fully functional protein complex. This result demonstrated that **13** had some affinity for MR1 and likely confirmed the issue of cell membrane impermeability to **13**, responsible for the absence of MR1 up-regulation. We then wanted to know if the whole complex could bind to the MAIT cell TCR to determine whether **13** could activate MAIT cells. For this purpose, we managed to produce a MR1-**13** tetramer using a protocol provided by NIH tetramer core facility. MR1-**13** tetramer staining assay of murine MAIT cells ($C\alpha^{-/-}$ $iV\alpha 19$ $V\beta 8^{+}$ mice) was done in comparison to a staining with MR1-5-OP-RU tetramer. Unfortunately, no staining was observed with MR1-**13** tetramer while a significant MAIT cell staining was detected with MR1-5-OP-RU tetramer (Figure 31).

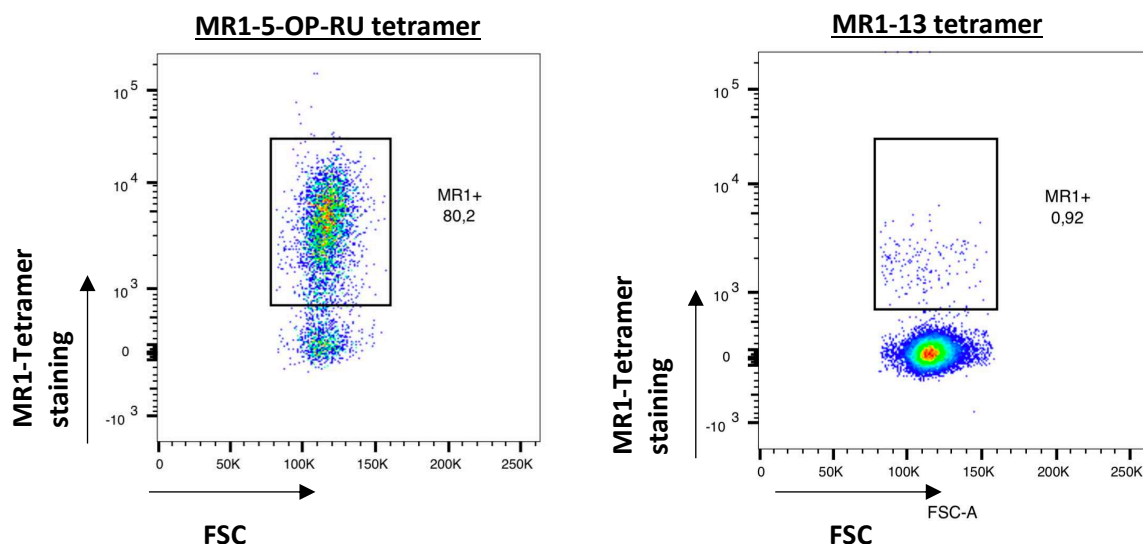


Figure 31 : MAIT cell staining assay with MR1-5-OP-RU and MR1-13 tetramers

c) *MAIT cell activation*

The different compounds were tested for murine MAIT cell activation. **12a** and **12b** were again used as positive controls and we also filled several wells with only WT3-m and MAIT cell suspensions for negative controls. It is important to mention that a background activation of MAIT cells from double transgenic mice was always obtained because of an auto-reactivity of the V β chain (usually 20% of activated cell background).

Compound **12a** (5-OP-RU in DMSO) showed again a higher potency than **12b** (5-OP-RU in water) (Figure 32). As predicted, all the compounds that did not up-regulate MR1 were unable to activate MAIT cells. Among the two molecules **30** and **31** that were able to up-regulate MR1, only **30** was slightly active though the activity was very low ($EC_{50} > 10 \mu\text{M}$) compared to 5-OP-RU ($EC_{50} \approx 6 \text{ nM}$) and even lower than 5-A-RU (submicromolar range EC_{50}).

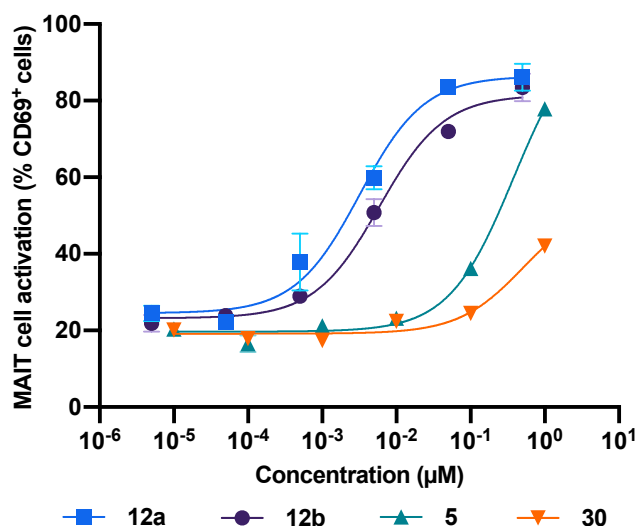


Figure 32: MAIT cell activation by 30 in comparison with 5-OP-RU and 5-A-RU. Data displayed on the graphs are means \pm SD of duplicates.

d) *Competition assays*

Since **30** and **31** could up-regulate MR1 and were more stable than 5-OP-RU, we thought these compounds could act as competitive inhibitors of 5-OP-RU. We set-up a competition assay to demonstrate this point. Our test relied on incubating WT3-m cells with the supposed competitors over a certain period of time and then adding 5-OP-RU on cells (at different concentrations). We first aimed to determine the best time interval between the addition of 5-OP-RU and the known competitor compound C, that would induce the maximum competition. Thus, we tested adding compound C to WT3-m cells either 4h before adding 5-OP-RU (t-4h), as well as 1h before (t-1h) and also tested adding the two compounds simultaneously (t). Compound C acted as competitive inhibitor of 5-OP-RU as it induced a shift of EC_{50} with the three different experimental conditions (Figure 33). Simultaneous addition of 5-OP-RU and compound C led to a less effective competition compared to an addition of compound C at t-1h or t-4h. As the two latter conditions induced a similar EC_{50} shift, we decided to choose a 1h interval between the addition of the competitive inhibitor and 5-OP-RU for the next experiments.

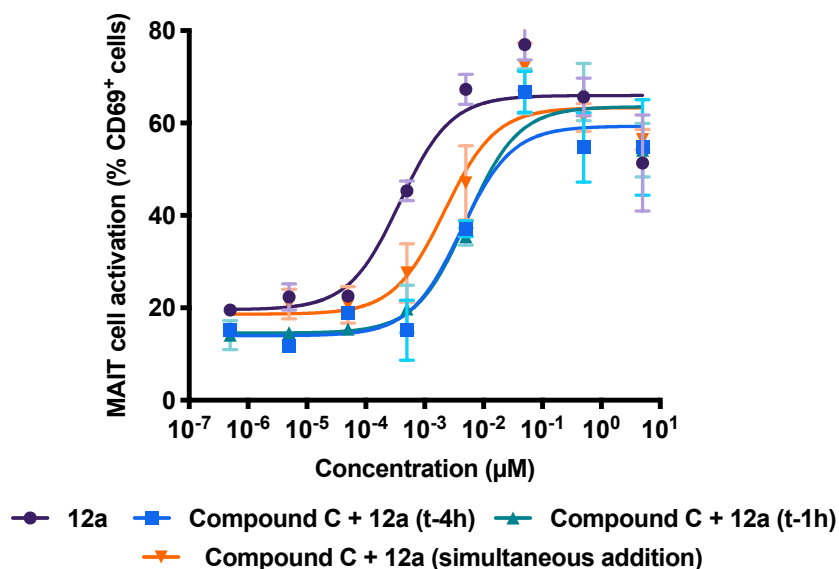


Figure 33: Competitive inhibition of 5-OP-RU by compound C (10 μM concentration). Data displayed on the graphs are means ± SD of duplicates.

Competition assay was done with **30** and **31** (Figure 34). Like in the precedent experiment, we used 10 μM concentration of each compound and a wide range of concentrations of 5-OP-RU (5 μM to 0.5 pM). Molecule **30** induced a shift of EC₅₀ of 5-OP-RU, similar to Compound C. Molecule **31** induced a more pronounced inhibition with a lower plateau reached at high concentration compared to 5-OP-RU alone. This probably results from a strong binding affinity of **31** to MR1 and stability of the complex leading to difficulties even at high concentrations of 5-OP-RU to displace **31** from MR1.

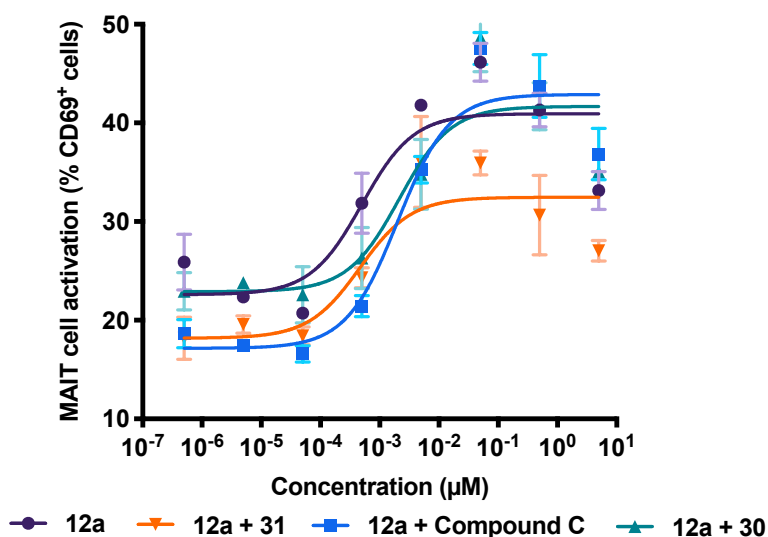


Figure 34: Competition assay with 30 and 31 (10 μM concentration). Data displayed on the graphs are means ± SD of duplicates.

D. Structure-activity relationships

All the pharmacomodulations performed had a strong impact on the potency of the different molecules. Pharmacomodulations of the ribityl moiety globally induced a decrease of MR1 up-regulation. Still, some compounds, **30** in particular (and to a lower extent **31**), were able to up-regulate MR1. These results confirm previous observations that the ribityl moiety is not mandatory for MR1 binding. In contrast, all these pharmacomodulations dramatically reduced or abolished MAIT cell activation. This is presumably explained by disturbances in the interaction made by 2'-OH and 3'-OH groups that are essential for the binding to both MR1 and the MAIT cell TCR. The same observations were described by Awad *et al.* with the altered metabolites ligands (AMLs) that they studied⁶⁰. We can conclude that this part of the ribityl moiety should not be modified in order to maintain a biological activity. Thus, it seems more relevant, though challenging, to do pharmacomodulations on the α -iminocarbonyl moiety to stabilize 5-OP-RU structure.

Alkylsulfonate analogue **13** had some affinity for MR1 since it enabled the refolding of MR1 recombinant protein. Thus, the incorporation of a negative charge carried by the sulfonic acid group seemed to allow an ionic interaction between **13** and Lys43 of MR1. However, the absence of MAIT cell TCR staining with MR1-**13** tetramer showed an absence or too weak of an interaction with the TCR. One hypothesis for this could be a lack of planarity of the alkylsulfonate side chain. In fact, the α -iminocarbonyl of 5-OP-RU is planar and this might be important to efficiently orient the ribityl chain towards the TCR after binding to MR1. In their study, Mak *et al.* supported the hypothesis of the importance of dihedral angles between α -iminocarbonyl, D-ribitylamine and uracil moieties⁵⁸. Thus, it would be very interesting to get the planar vinylsulfonate analogue of 5-OP-RU to confirm this hypothesis. The same idea could explain the lack of activity of purinetrione analogue **37** that is not entirely planar, thus probably blocking the interaction with both MR1 and the TCR.

A general conclusion after looking at the results we obtained and those from the literature is that it is very difficult to modify 5-OP-RU structure without dramatically losing potency for MAIT cell activation. Furthermore, chemical synthesis of 5-OP-RU analogues is tedious. It requires many synthetic steps, especially because of the high number of heteroatoms harbored by the molecules requiring suitable protective groups. Moreover, once deprotected the molecules were not soluble any more in organic solvents due to their high polarity (ribityl chain and lactam of the uracil). We therefore decided to set-up a second medicinal chemistry strategy aiming to obtain a prodrug of the precursor of MAIT cell antigens namely 5-A-RU.

III. Prodrug strategy and vectorization of 5-A-RU

A. Introduction and rationale

Prodrugs are inactive substance that must be converted into the pharmacologically active agent by metabolic or physico-chemical transformation⁸⁴. They are widely used to overcome pharmacokinetic issues, chemical instability or to avoid/limit side effects of drugs (especially for cytotoxic drugs).

Since highly active antigens derived from the riboflavin biosynthesis pathway are known and suffer from chemical instability, a good strategy would be to make a stable prodrug of one of these products. Making a prodrug of 5-OP-RU seemed challenging in practice because it would have implied to protect the chemically unstable α -iminocarbonyl moiety susceptible both to cyclization and hydrolysis. The alternative option was to make a prodrug of its precursor 5-A-RU. 5-A-RU can react *in situ* with endogenous methylglyoxal (of bacteria or animal cells) to give 5-OP-RU and we showed through our previous biological evaluation that 5-A-RU induced a significant activation of murine MAIT cells *in vitro*, most likely by generating 5-OP-RU *in situ*. Making a prodrug of 5-A-RU is a good option because the molecule is even more unstable than 5-OP-RU in a water environment (quick autooxidation of the primary aromatic amine already discussed earlier). The conjugation of this precise amine to a cleavable linker would form a strategic anchoring point, especially because this amine has a good nucleophilicity, much better than the secondary amine of the ribityl chain⁵⁸.

All these arguments motivated us to design and synthesize a new prodrug of 5-A-RU. We will provide the chemical structure of the prodrug in the next section, before detailing its chemical synthesis and biological assessment.

B. Design, synthesis and biological evaluation of a new prodrug of 5-A-RU

1. Design of an enzymatically cleavable prodrug of 5-A-RU

To get an effective prodrug able to induce an immune response, we must ensure that it can be internalized inside APCs to be correctly processed. Thus, we have to use a carrier capable of inducing phagocytosis/endocytosis to activate APCs. Polystyrene latex beads are a good choice for this purpose since they have been largely used and validated in phagocytosis assays⁸⁵. Latex beads are insoluble polymer commercially available with different diameter of particles. Diameters typically around 1 μ M are optimal for phagocytosis because of the similar size to most bacteria⁸⁶. This carrier can mimic the phagocytosis of bacteria by APCs and activate them. Latex beads are also available with diverse

functional groups at their surface (carboxylate, amine or aldehyde/sulfate) allowing the chemical coupling of proteins or small molecules to the polymer (either by adsorption on beads or through covalent coupling). Thus, both the 5-A-RU conjugate and other antigens could be loaded on the beads. Latex beads would therefore constitute a good tool for studying the use of MAIT cells as a vaccine therapeutic target. Once the model validated using latex beads as carrier, we could next think of using a more physiologically compatible polymer (soluble polymer like polyethylene glycol or dextran).

Next, we have to find a linker that could be cleaved inside APCs after phagocytosis. We decided to use a dipeptide linker sensitive to enzymatic cathepsin cleavage. APCs are known to express several types of cathepsins that are notably involved in antigen processing (Cat L, Cat B, Cat S, Cat D...) ⁸⁷. We chose to use the phenylalanine-arginine dipeptide (Phe-Arg) because it is recognized by numerous types of cathepsins (Cat B, Cat L, Cat S) ⁸⁸⁻⁹⁰. Thus, the non-specific cleavage of the dipeptide by different cathepsins would maximize the chances of releasing 5-A-RU inside APCs. Furthermore, this linker has been extensively used in fluorogenic probes able to release 7-amino-4-methylcoumarin (AMC) by cathepsin cleavage ⁹¹. The use of a PEG spacer was envisioned to add distance between the dipeptide and the bulky latex bead polymer to favor the release of the substrate. The design of the 5-A-RU prodrug is displayed in Figure 35.

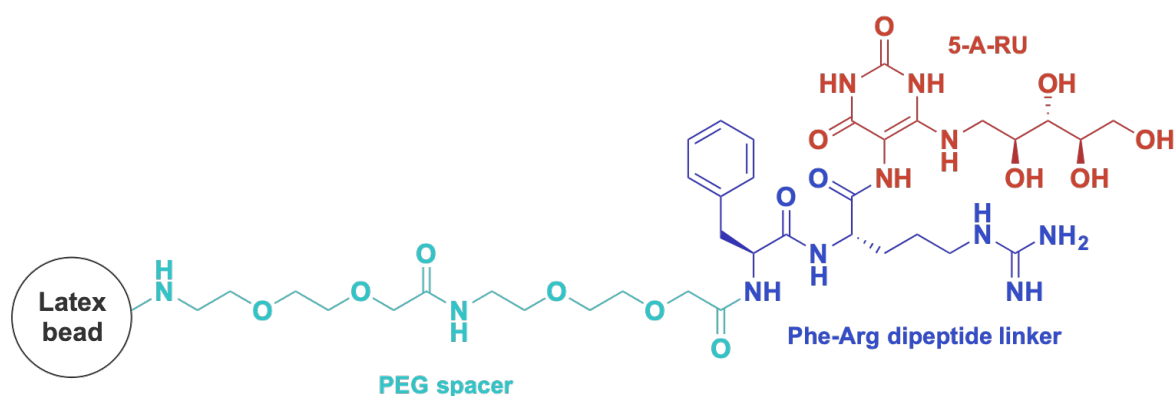


Figure 35: Design of the 5-A-RU prodrug

2. Chemical synthesis

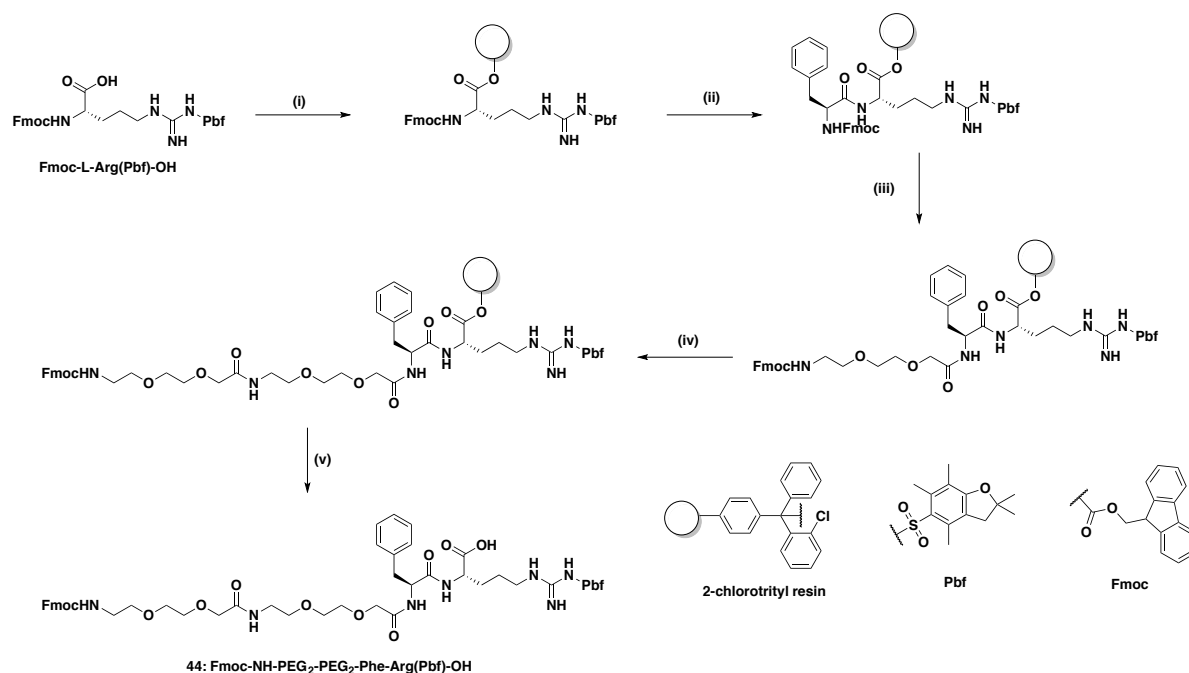
The chemical synthesis and biochemical evaluation of the prodrug was done by Mélinna Dantec, a second year master student working in our team during 6 months under my supervision.

a) *Linker synthesis by solid-phase peptide synthesis (SPPS)*

The linker was synthesized by SPPS supported on 2-chlorotrityl resin. Commercial Fmoc-NH-Phe-OH, Fmoc-NH-Arg(Pbf)-OH and Fmoc-NH-PEG₂-OH were used for the synthesis. The use of Fmoc

protective group allowed us to easily deprotect the reactive amino group under basic conditions without detaching the molecule from the support since the resin was not sensitive to such basic conditions. Protection of the reactive guanidine moiety of arginine was also required to avoid side reactions. Pbf group (2,2,4,6,7-pentamethyldihydrobenzofuran-5-sulfonyl) was used for this purpose. This sulfonamide protective group is not sensitive to basic conditions required to deprotect Fmoc group. Furthermore, Pbf deprotection requires stronger acidic conditions for its removal than the one needed for the detachment of the linker from the resin. Thus, the linker could be obtained with Fmoc and Pbf protection at the end, and with the free carboxylic acid that will react with 5-A-RU.

Fmoc-NH-Arg(Pbf)-OH was first coupled to the 2-chlorotrityl resin with DIEA in DCM (Scheme 15). The Fmoc group was removed with a 20% piperidine in DMF solution and the free amine was coupled to Fmoc-NH-Phe-OH using benzotriazol-1-yl-oxytripyrrolidinophosphonium hexafluorophosphate (PyBOP) coupling agent and DIEA as a base. The two PEG moieties were sequentially added by Fmoc deprotection and peptide coupling using the same conditions (PyBOP and DIEA as reagents). Finally, the linker was detached from the resin with a mixture of trifluoroethanol/acetic acid/water (TFE/AcOH/H₂O) and the product was precipitated from cold diethyl ether to give the pure linker **44**.



Scheme 15: Solid phase peptide synthesis of 44. Conditions and reagents: (i) 2-chlorotrityl chloride resin, DIEA in DCM; (ii) 1) 20% piperidine in DMF, 2) Fmoc-NH-Phe-OH, DIEA, PyBOP in DMF; (iii) 1) 20% piperidine in DMF, 2) Fmoc-NH-PEG₂-OH, DIEA, PyBOP in DMF; (iv) 1) 20% piperidine in DMF, 2) Fmoc-NH-PEG₂-OH, DIEA, PyBOP in DMF; (v) TFA/AcOH/H₂O (7/1/2); Total yield: 47%

b) *Coupling of 44 to 7-amino-4-methylcoumarin (AMC)*

The second part of the prodrug synthesis was the coupling of the small molecules to the linker. This step turned out to be the most challenging. 7-amino-4-methylcoumarin (AMC) was conjugated to the peptide **44** in a first time in order to optimize the conditions of reaction. This coumarin derivative was chosen for its chemical properties. Indeed, like 5-A-RU, AMC presents an aromatic primary amine. Contrary to 5-A-RU, which is difficult and long to synthesize (need to prepare each time a fresh batch of 5-A-RU by hydrogenation of **4**), AMC is a cheap molecule that is commercially available. Moreover, the use of this molecule was considered to validate the efficiency of the vector and the cleavage by cathepsins by exploiting its fluorogenic properties. All the attempts to get the product are summarized in Table 2. First tries with common coupling reagents PyBOP and HATU failed to give the desired product (Entry 1 to 3 of Table 2). Therefore, we decided to investigate the reactivity of the different reagents to explain the lack of reactivity and to find the best conditions for the coupling reaction.

Table 2 : Attempts for the chemical coupling of AMC with 44 (all reactions were done under inert atmosphere of argon and monitored by UPLC-MS)

| Entry | R | Reagents | Solvent | Conditions | Results |
|-------|----------------|--|----------|---------------|--|
| 1 | AMC | PyBOP 2 eq, DIEA 4 eq | DMF | rt, 48h | No product formed |
| 2 | AMC | HATU 2 eq, DIEA 4 eq | DMF | rt, 48h | No product formed |
| 3 | AMC | PyBOP 2eq, DIEA 4 eq | DMF | MW, 50°C, 1h | Degradation of the starting material; Traces of the desired product |
| 4 | Propargylamine | HATU 2 eq, DIEA 4 eq | DMF | rt, 48h | Formation of the desired conjugate |
| 5 | AMC | POCl ₃ | Pyridine | 0°C to rt, ON | Degradation of the starting material |
| 6 | AMC | SOCl ₂ | DMF | rt, 1h | Degradation of the starting material |
| 7 | AMC | EDC 2 eq, HOBT 2 eq, DIEA 4 eq | DMF | rt, 3 days | Degradation of the starting material |
| 8 | AMC | BTFH 2 eq, DIEA 4 eq | DCM | rt, ON | Degradation of the starting material |
| 9 | AMC | TCFH 2 eq, DIEA 4 eq | DCM | rt, ON | Formation of the desired product; Epimerization |
| 10 | AMC | TFFH 2 eq, DIEA 4 eq | DCM | rt, ON | Formation of the desired product; Epimerization |
| 11 | AMC | TCFH 2 eq, HOBT 2 eq, NMI 4 eq | DCM | rt, ON | Formation of the desired product; Epimerization |
| 12 | AMC | TCFH 2 eq, CuCl ₂ 0.5 eq, DIEA 4 eq | DCM | rt, ON | Formation of the desired product along with impurities; No epimerization |
| 13 | AMC | TCFH 2 eq, Oxyma 0.5 eq, DIEA 4 eq | DCM | rt, ON | Formation of the desired product along with impurities; No epimerization |

i) Influence of the structure of the linker

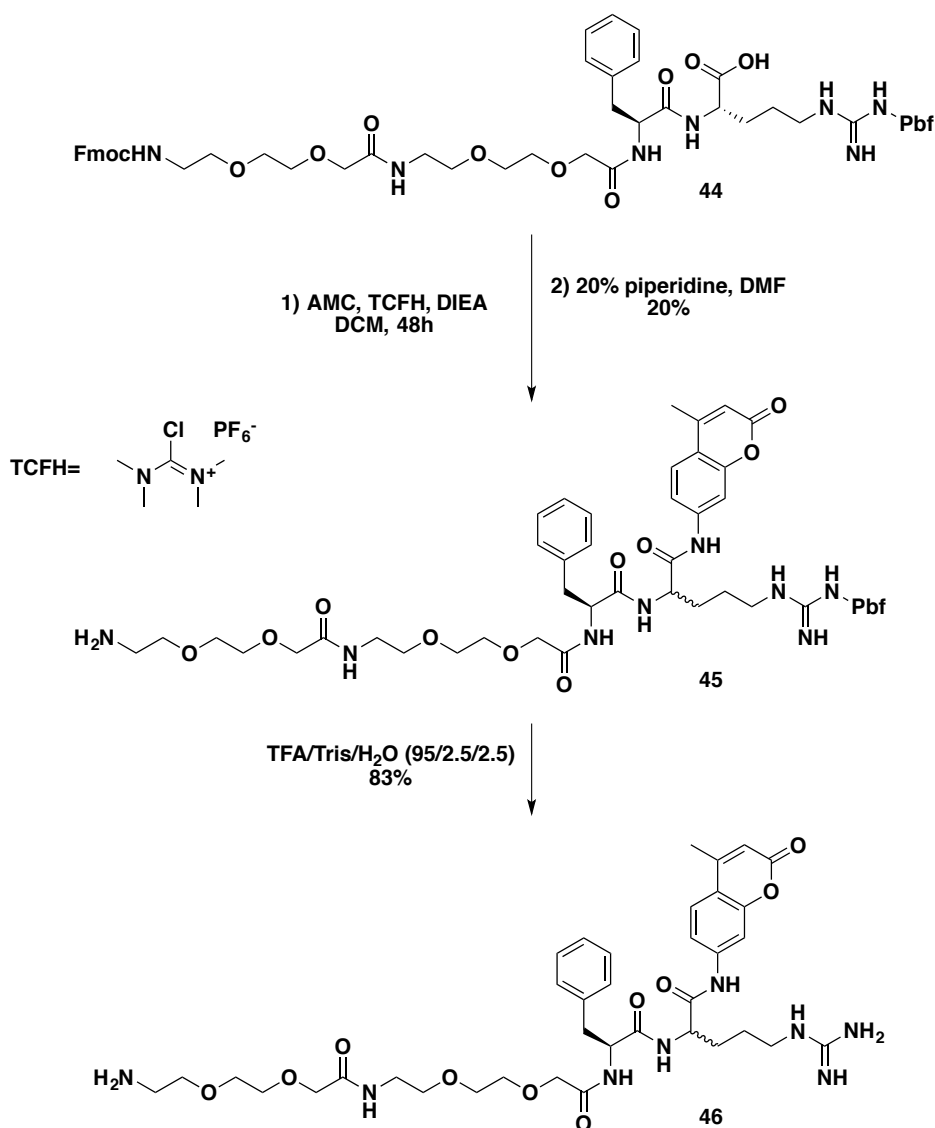
We initially thought that the structure of **44** could be responsible for the lack of reactivity because of a steric hindrance notably due to the PEG spacer. Thus, we tried the coupling between less hindered and fully protected L-arginine (Fmoc-L-Arg(Pbf)-OH) and AMC with HATU and DIEA reagents. The reaction worked but many impurities were formed. This experiment showed that protected arginine was sufficiently reactive but the conditions still needed to be optimized. Then, we synthesized by SPPS the dipeptide analogue of **44** lacking the PEG spacer. Fmoc-NH-Phe-Arg(Pbf)-OH was synthesized using the same protocol as described before (Scheme 15). This time, the reaction with AMC did not work and only degradation of the starting material was observed. These results confirmed that the steric hindrance of the linker could be in part responsible for the reactivity issue.

ii) Influence of the reactivity of the primary amine

We then tested the reactivity of the primary amine. To do so, we tried to couple **44** with propargylamine (aliphatic primary amine) using HATU and DIEA reagents (Entry 4 of Table 2). The desired product was formed suggesting that the poor reactivity of the primary amine of AMC was an important limiting factor of the coupling reaction. Indeed, the amino group of AMC is poorly reactive because of its conjugation with the aromatic ring. We concluded that more powerful and less bulky coupling agents must be used to improve our chances to get the desired product.

iii) Influence of the coupling agent

Following the previous idea, POCl₃ and SOCl₂ (in pyridine) were used to form more reactive acyl chlorides intermediates but only degradation products were obtained during the reactions (Entry 5-6 of Table 2). Then, other reactive coupling agents were tried (EDC with HOBt and BTFFH) with DIEA but it resulted in degradation of the starting material (Entry 7-8 of Table 2). Finally, TCFH (Chloro-*N,N,N',N'*-tetramethylformamidinium hexafluorophosphate) was used because it was described as one of the most powerful and not too bulky coupling reagent in the literature⁹². The reagent was added to the peptide for a pre-activation during 15 min followed by addition of AMC. Fortunately, the desired product was observed and no degradation of the starting material occurred (Entry 9 of Table 2). However, the conversion was not complete and some amount of activated peptide still remained in the mixture after 3 days of reaction (monitored by UPLC-MS). Still, compound **45** was obtained after direct removal of the Fmoc protective group and preparative HPLC purification.



Scheme 16: Synthesis of 46 (44-AMC conjugate)

Another issue of the coupling reaction was an epimerization of the asymmetric carbon of arginine (two products with similar m/z peaks were observed in UPLC-MS) (Figure 36a). Epimerization should best be avoided because the non-natural peptide formed cannot be recognized by cathepsins. However, the epimerized product could be used as a negative control for the cathepsin cleavage test. Other conditions were tried to avoid/limit epimerization. First, TFFH (fluorinated analogue of TCFH that is described to limit epimerization⁹³) and TCFH/HOBt were used as coupling systems with NMI. Both conditions were successful to give **45** but epimerization still occurred (Entry 10-11 of Table 2). Then, couples TCFH/CuCl₂ and TCFH/OxyMa were tried with DIEA (Entry 12-13 of Table 2)^{94,95}. It prevented the epimerization but major side products were formed in both cases (Figure 36b). We finally decided to maintain the reaction with TCFH and DIEA in DCM even if some amount of epimerized product was isolated along with the desired product. Final deprotection of the Pbf group under acidic conditions afforded **46** (Scheme 16).

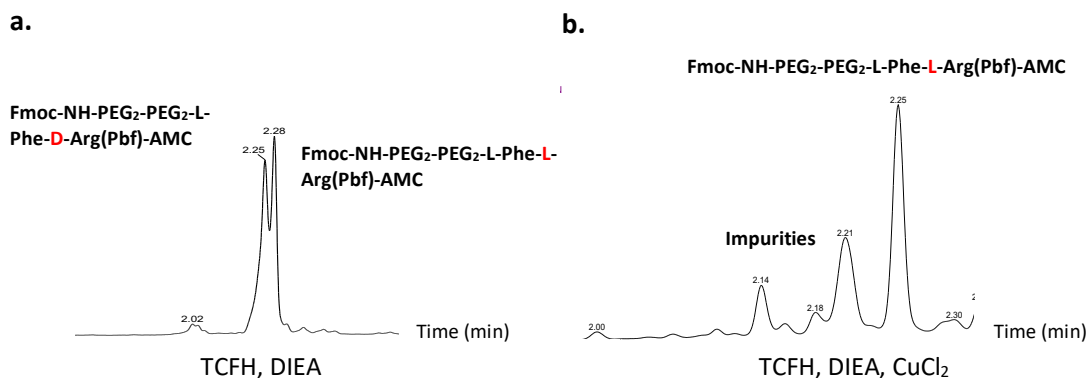


Figure 36: UPLC-MS analysis of the coupling reaction between **44 and AMC. a. Use of TCFH with DIEA led to epimerization; b. Addition of CuCl₂ avoided the epimerization but led to the formation of many impurities**

c) *Coupling of **44** to 5-A-RU and ethynyl-5-A-RU (**72**)*

The same steps were repeated to couple 5-A-RU to **44**. 5-A-RU was synthesized by reducing **4** and it was directly used after work-up for the reaction. However, no conversion of the starting material was observed with 5-A-RU, most likely due to a complete insolubility in DCM (Entry 1 of Table 3). Other more polar solvents were tried with the same reagents (TCFH and DIEA). 5-A-RU is highly soluble in DMSO so we tried to do the reaction in this solvent. Unfortunately, no activation of the peptide occurred in DMSO and for this reason the coupling to 5-A-RU failed (Entry 2 of Table 3). We also tried to activate the peptide in acetonitrile before adding a 5-A-RU solution in DMSO but again no desired product was formed even if the peptide was well activated this time (Entry 3 of Table 3). A DCM/water emulsion was then tried in presence of TBAB (tert-butyl ammonium bromide), a phase agent transfer, but only degradation of the starting material was observed (Entry 4 of Table 3).

Table 3: Attempts for the chemical coupling of 5-A-RU and 72 to 44 (all reactions were done under inert atmosphere of argon and monitored by UPLC-MS)

| Entry | R | Reagents | Solvent | Conditions | Results |
|-------|-------|----------------------------|----------------------|--------------|---|
| 1 | 5-ARU | TCFH 2 eq, DIEA 4 eq | DCM | rt, 48h | No reaction |
| 2 | 5-ARU | TCFH 2 eq, DIEA 4 eq | DMSO | rt, 48h | No activation of the peptide |
| 3 | 5-ARU | TCFH 2 eq, DIEA 4 eq | ACN/DMSO | rt, 48h | Activation of the peptide but no coupling reaction |
| 4 | 5-ARU | TCFH 2 eq, DIEA 4 eq, TBAB | DCM/H ₂ O | TBAB, rt, ON | Degradation of the starting material |
| 5 | 72 | TCFH 2eq, DIEA 4 eq | DCM | rt, 48h | Degradation of starting material; Traces of the desired product |
| 6 | 72 | TCFH 2 eq, DIEA 4 eq | Pyridine | rt, 3 days | Degradation of starting material; Traces of the desired product |
| 7 | 72 | TCFH 2 eq, DIEA 4 eq | DCM/MeOH | rt, ON | Formation of the desired product along with impurities |
| 8 | 72 | TCFH 2 eq, NMI 4 eq | DCM/MeOH | rt, ON | Formation of the desired product along with impurities |

We then tried to couple **44** with more soluble ethinyl-5-A-RU **72** that was already synthesized (detailed in the last chapter of the thesis). **72** is an analogue of 5-A-RU bearing a terminal alkyne at the extremity of the ribityl chain (5' position) and it was isolated as hydrochloride salts. Reaction of **72** with methylglyoxal gave **73** (ethinyl-5-OP-RU), which showed a similar biological activity as 5-OP-RU. We found that ethinyl-5-A-RU was more soluble than 5-A-RU in polar solvent like methanol. The conjugation reaction between **72** and **44** was tried with TCFH and DIEA in different solvents. No reaction occurred in DCM while only traces of the desired product were observed in pyridine (limited solubility of **72** in this solvent) (Entry 5-6 of Table 3).

Finally, a mixture of DCM/MeOH was tested (Entry 7 of Table 3). **44** was activated in DCM before adding a solution of **72** in methanol. This time, the desired product was formed but other undesired reactions occurred: reaction of MeOH with activated peptide to give a methyl ester derivative (pink frame in Figure 37), reaction of the peptide linker on the secondary amine of the ethinyl-5-ARU (red frame in Figure 37) and epimerization of all these products.

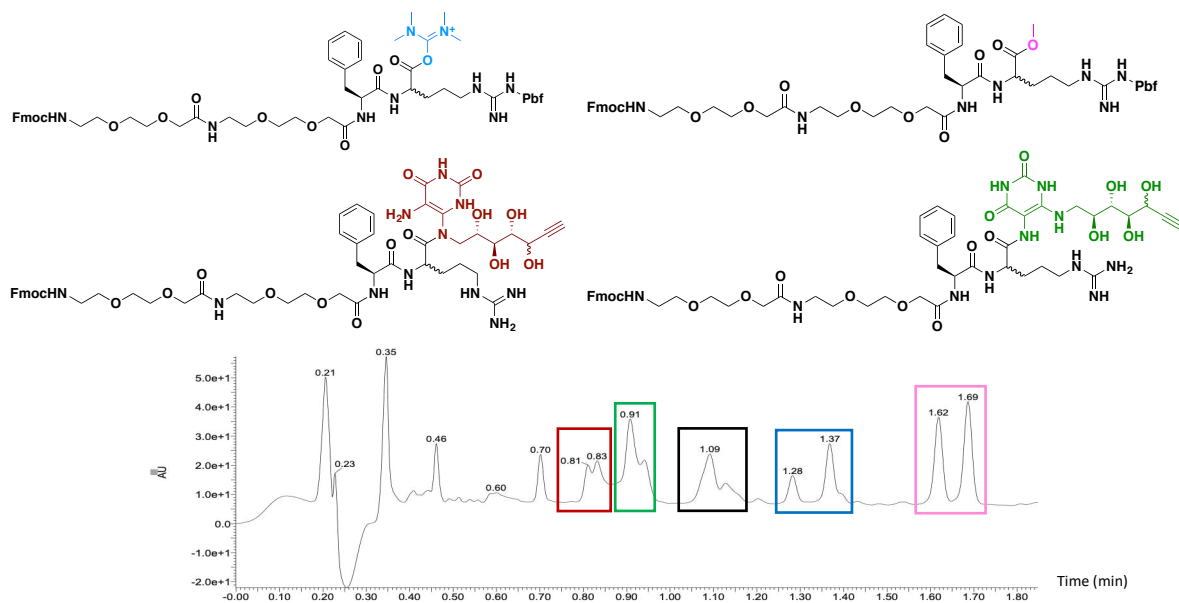
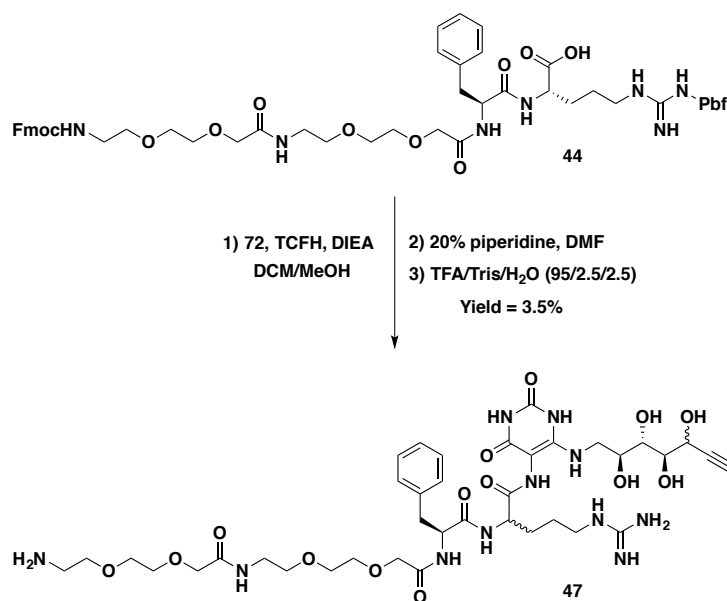


Figure 37: UPLC-MS analysis of the reaction between 44 and ethynyl-5-A-RU 72. red: conjugation with the secondary amine of 72; green: desired product; black: peptide 44; blue: activated peptide; pink: methyl ester derivative

After deprotection of the Fmoc group with a solution of piperidine in DMF, purification was done by preparative RP-HPLC to isolate the desired intermediates (green frame in Figure 37). The purification allowed to recover an enriched fraction containing the desired epimer but we could not completely remove the other one. Finally, the Pbf group was removed under acidic conditions (TFA/Tris/H₂O 95/5/5) and the product was precipitated from cold diethyl ether to give **47** (isolated as a mixture of two epimers) (Scheme 17).



Scheme 17: Synthesis of 47 (44-ethynyl-5-A-RU conjugate)

^1H NMR analysis of **47** allowed to validate that it was the result of to the coupling of N8H to the linker (and not N7H secondary amine). Indeed, the analysis showed a complete disappearance of the primary amine (N8H) peak, consequence of the reaction with the carboxylic acid of **44** (Figure 38).

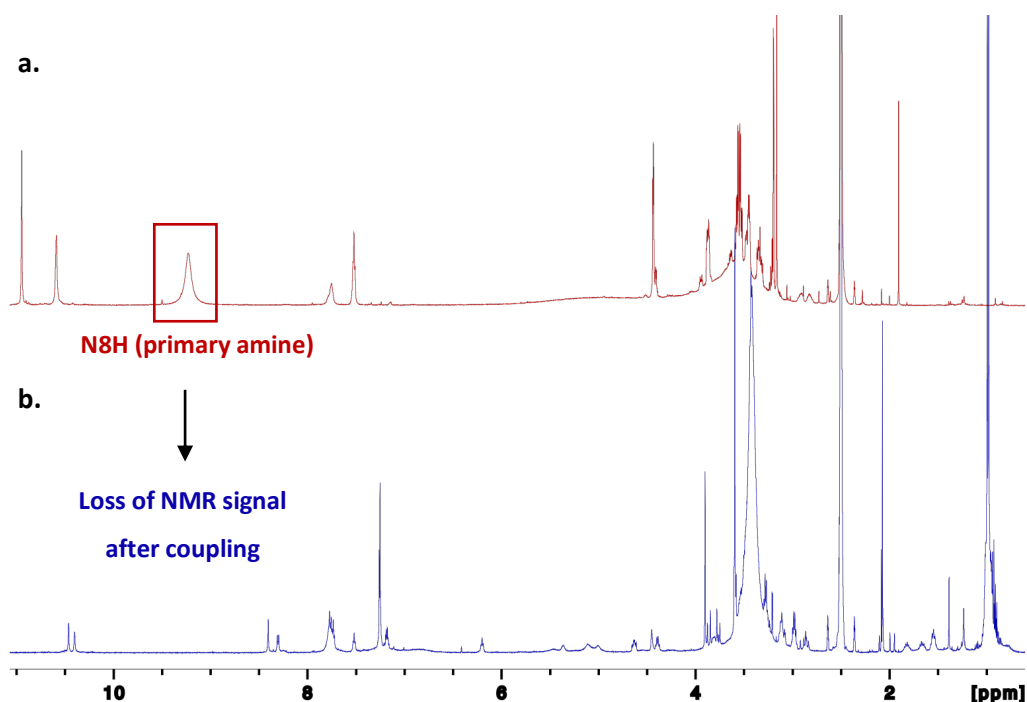
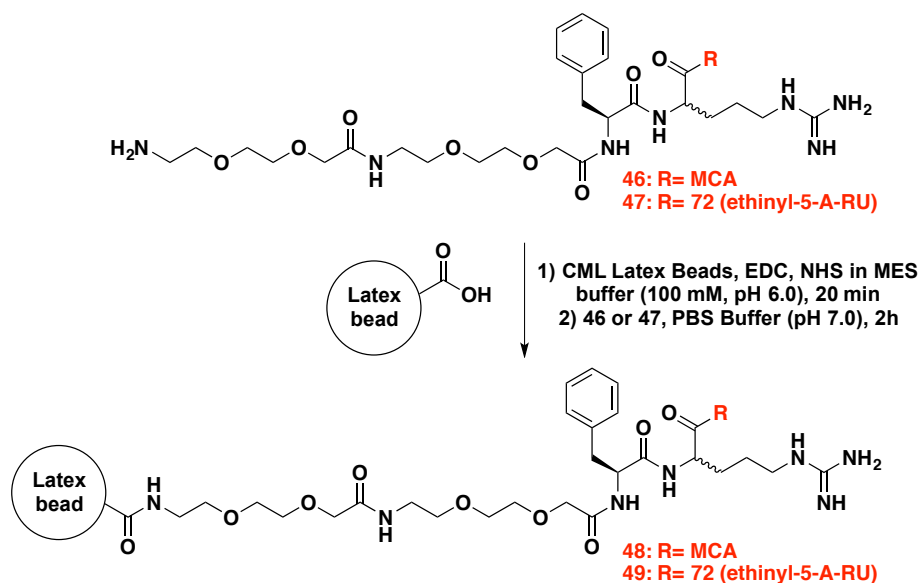


Figure 38: ^1H NMR analysis of a. **72**; b. conjugate **47**

d) *Conjugation of **46** and **47** to carboxylate-modified latex beads (CML)*

Latex bead conjugation was done by adapting a protocol from the literature⁹⁶. Commercial CML particles of 1 μm were chosen to form an amide bond with the free terminal amino group of the PEG moiety. The two-step coupling began with the formation of an activated N-hydroxysuccinimide (NHS) ester with EDC in MES buffer followed by the addition of **46** and **47** in PBS buffer giving **48** and **49**, respectively (Scheme 18). Finally, glycine was added to cap uncoupled activated esters in order to limit undesirable coupling in biological media (as recommended by the supplier).



Scheme 18: Synthesis of CML bead conjugates 48 and 49

Analysis of **48** under UV light (354 nm) confirmed that the coupling reaction worked (Figure 39a). A click reaction was done between **49** and AF₄₈₈-azide fluorophore for the same purpose. At 354 nm, fluorescence signal was observed for **49** with AF₄₈₈-azide whereas no fluorescence was detected for **49** alone and latex beads with AF₄₈₈-azide (negative controls) (Figure 39b).

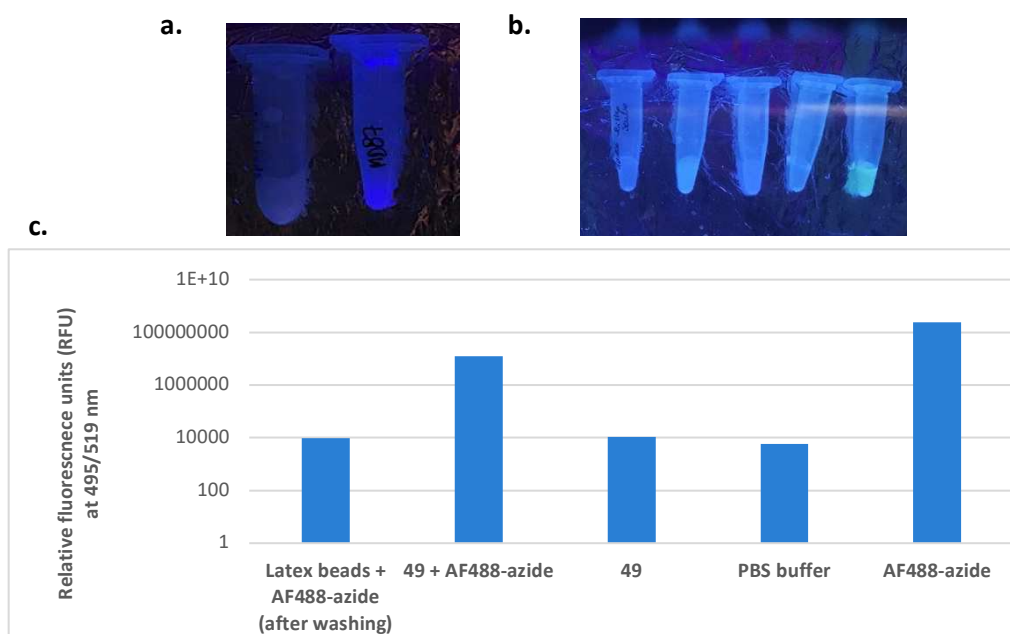


Figure 39: Analysis of the coupling reactions to CML beads; a. fluorescence at 354 nm (from left to right): CML beads, 48; b) fluorescence at 354 nm (from left to right): CML beads + AF₄₈₈-azide (after washing of the beads), 49 + AF₄₈₈-azide, 49, PBS buffer, AF₄₈₈-azide; c) Measurements of fluorescence of the click reaction at 495/519 nm ($\lambda_{exc}/\lambda_{emi}$)

Quantitative measurements of fluorescence at 495/519 nm ($\lambda_{exc}/\lambda_{emi}$) by spectrofluorimetry confirmed the results obtained at 354 nm (Figure 39c).

3. Biochemical and biological evaluation of the prodrugs

a) *Biochemical evaluation*

Biochemical evaluation of AMC conjugates (**46** without latex beads and **48** with latex beads) was done to ensure their efficient cleavage to release AMC and the free peptide linker in the presence of cathepsins. We used cathepsin L for the test as Phe-Arg dipeptide is a well-known substrate of this enzyme. The cleavage was monitored by fluorescence spectroscopy at 380/460 nm ($\lambda_{exc}/\lambda_{emi}$) with an incubation in a 96-well plate at 37°C during 2 hours (Figure 40). AMC release was observed with **46** and **48** in the presence of cathepsin L whereas no fluorescence at all was detected without cathepsin L (negative control). AMC release was faster with **46** and it reached a plateau faster when compared to **48**. This can probably be explained by the steric hindrance caused by the latex beads that would limit the access of the enzyme to the cleavable moiety.

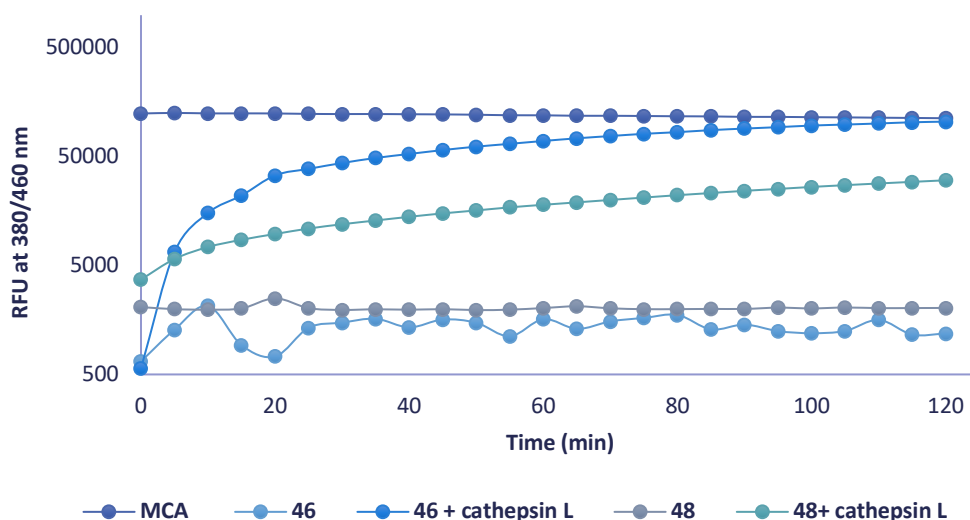


Figure 40: Cathepsin L cleavage assay of 46 and 48. The cleavage was evaluated by measuring the fluorescence intensity at 380/460 nm ($\lambda_{exc}/\lambda_{emi}$) due to the release of AMC in the media

After 2 hours incubation, the supernatant from the well containing **46** and cathepsin L was injected in UPLC-MS (Figure 41). The analysis confirmed the cleavage of the conjugate to release both AMC and the free linker ($H_2N-PEG_2-PEG_2-Phe-Arg-OH$). As expected, the small amount of D-arginine epimer formed during the coupling reaction was not cleaved. Altogether, these data confirmed the efficient and cathepsin L specific cleavage of both **46** and **48**.

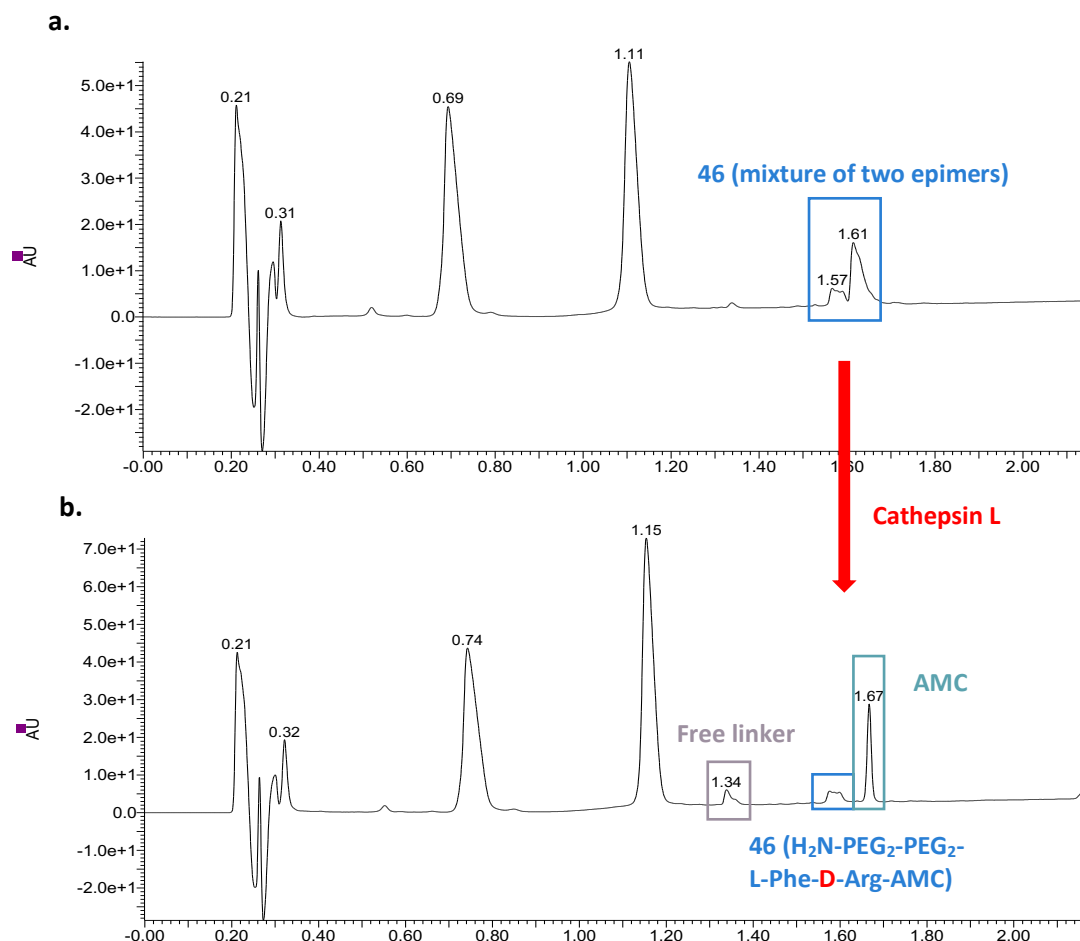


Figure 41: UPLC-MS analysis of Cathepsin L cleavage of 46. a. analysis of 46 without cathepsin L; b. analysis of 46 after incubation with cathepsin L

The same cleavage experiment was done with **47**, under the same experimental conditions. Unfortunately, UPLC-MS analysis did not reveal any cleavage of the conjugate by cathepsin L (the molecule remained unchanged even after 24h incubation). We first hypothesized that the PEG linker might be too bulky to allow the cathepsin to access to the dipeptide. We therefore tested the cleavage of the same linker without PEG groups (H₂N-Phe-Arg-**72**) but again no cleavage was observed. It finally seemed that the chemical structure of **72** was responsible for the lack of reactivity towards cathepsin L. In comparison with AMC, **72** and 5-A-RU are much more hydrophilic and polar (hydroxyl groups of the ribityl chain and lactam groups of the uracil ring). These two molecules are also less planar than AMC because of the ribityl chain. All these divergent properties might be responsible for the non-recognition of cathepsin L.

b) *Biological evaluation on murine MAIT cells*

Even if biochemical evaluation of **47** failed, we still wanted to test the prodrug in biological assays with the idea that it could be recognized by other cathepsins. We used murine bone marrow dendritic cells (BMDCs) as APCs for the biological evaluation. Unlike WT3-m cells, BMDCs are able to induce phagocytosis and trafficking through endolysosomal compartment where cathepsins are abundant. Products **47** and **49** were incubated with BMDCs and murine MAIT cells (from the spleen of $iV\alpha 19 V\beta 8^+$ double transgenic mice) with and without addition of exogenous methylglyoxal (Figure 42).

5-OP-RU (**12a**), ethinyl-5-A-RU (**72**) and ethinyl-5-OP-RU (**73**) were used as positive controls. These compounds induced an activation of MAIT cells with the same range of activity as usual. **47** slightly activated MAIT cells at high concentration (10 μ M) and this was more pronounced in the presence of exogenous methylglyoxal (almost as active as **72**). In contrast, CML conjugate **49** did not induce MAIT cell activation even with methylglyoxal addition. These results showed that **47** could be cleaved in cells in contrast with the results obtained from the biochemical evaluation with cathepsin L. Therefore, the cleavage was likely mediated by other cathepsins than cathepsin L. However, the poor activity obtained may be the consequence of a partial cleavage of the prodrug. It is also important to recall that **47** was isolated and further used in biology as a mixture of two epimers with the minor one being insensitive to cathepsin cleavage (non-natural peptide derivative). This could also partly explain the low activity of **47** compared to **72**.

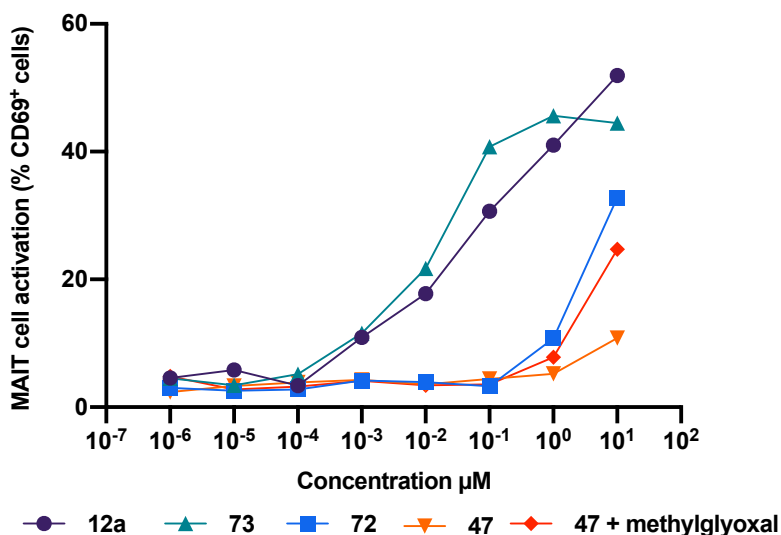


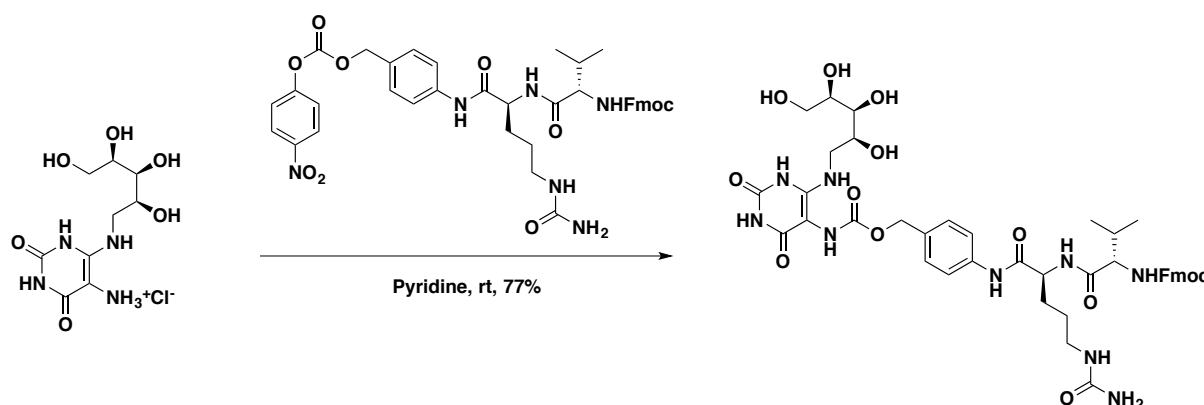
Figure 42: Biological evaluation of **47** and **49** on MAIT cells

C. Design, synthesis and biological evaluation of a self-immolative prodrug of 5-A-RU

1. Rationale and bibliography

During our work, another research group developed prodrugs of 5-A-RU aiming to design adjuvants for cancer vaccine⁷⁰. They used a similar strategy to design new drug conjugates with a cathepsin cleavable dipeptide linker. They chose the well-known cathepsin B sensitive valine-citrulline (Val-Cit) dipeptide along with the *para*-aminobenzylalcohol (PAB) self-immolative unit between 5-A-RU and the dipeptide. Thus, they formed a carbamate linkage instead of a peptide bond. The Val-Cit-PAB linker has been widely used in targeted antitumoral agents called antibody-drug conjugates (ADC) with several of them already on the drug market (AdcetrisTM, PolivyTM) and others under clinical evaluation⁹⁷.

The synthesis of the conjugate required activation of the linker through the formation of a *para*-nitrophenyl (PNP) ester, which could then react with 5-A-RU in pyridine to form the desired product (Scheme 19). The authors reported a high chemical stability of the conjugate in water (at ambient temperature) without any degradation occurring after weeks.



Scheme 19: Chemical structure and synthesis of Fmoc-NH-Val-Cit-PAB-5-A-RU conjugate

Biological assessment of the molecule showed a higher *in vitro* activity than 5-A-RU on human peripheral blood mononuclear cells (PBMCs), meaning that the cleavage by cathepsins was effective and that it was consistent with a higher chemical stability of the prodrug (Figure 43). However, the activation was lower than for 5-OP-RU (5-A-RU + exogenous methylglyoxal). Interestingly, no targeting moiety that would have driven internalization inside APCs to trigger antigen processing was needed. This likely means that the conjugate alone was able to get into the cell and to traffic through the endolysosomal compartment. Some investigation was made about the antigen processing of the prodrug. The results supported a loading of the conjugates on MR1 in endolysosomal compartment

(recycling pathway of MR1) instead of in the ER. Finally, *in vivo* evaluation was conducted on mice with intravenous injection of either 5-A-RU or the prodrug. After 18h, both molecules induced a strong activation of MAIT cells (increased expression of CD69 and CD25 at the cell membrane surface) from lungs at high dose (180 nmol) whereas only the prodrug activated MAIT cells at the lower dose (5 nmol).

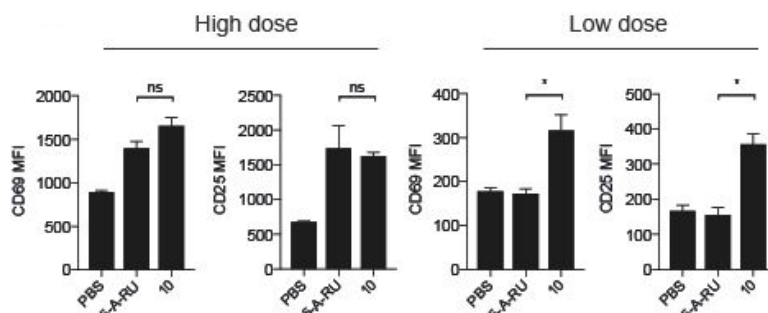


Figure 43: In vivo MAIT cell activation in mice with 5-A-RU and 5-A-RU prodrug (10)

The same research group patented some analogues of this prodrug including **CI-072**, which is additionally conjugated to ovalbumin protein to induce an adaptive immune response (Figure 44)⁹⁸. They used a cyclooctyne ring and strain promoted azide-alkyne cycloaddition (SPAAC) to introduce the protein.

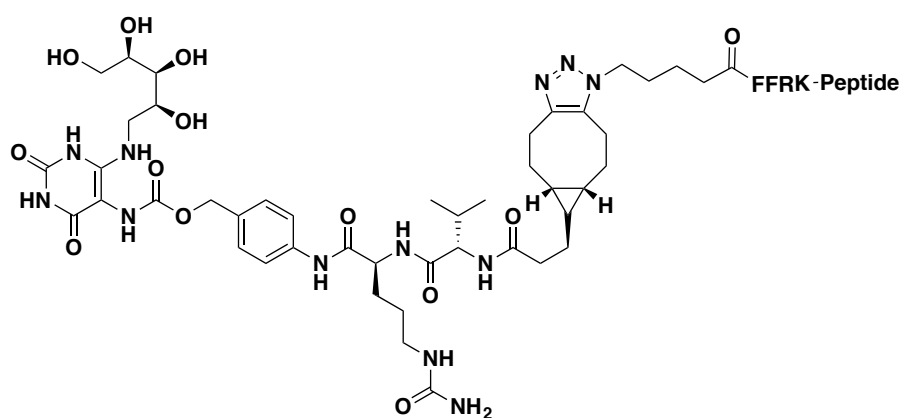


Figure 44: Chemical structure of CI-072

CI-072 was able to activate human MAIT cells *in vitro* and *in vivo* with higher potency than 5-A-RU. Moreover, the conjugate was able to induce OVA peptide cross-presentation to CD8⁺ T cells and the cells displayed more pronounced cytotoxic effects than with 5-A-RU alone. **CI-072** was also able to induce some anti-tumor activity on B16-OVA cells (mouse model for human melanoma) resulting in a delay in tumor growth contrary to 5-A-RU. This effect was dependent on the presence of 5-A-RU in the conjugate since the same linker without 5-A-RU did not induce significant anti-tumor activity.

Altogether, these results suggest that the prodrug of 5-A-RU could be used as a therapeutic anti-tumor vaccine and they support the adjuvant quality of 5-A-RU in such vaccine. However, the molecule has only been studied for its anti-tumor activity and not as antimicrobial vaccine. Therefore and since this was our objective, we decided to continue our research project by designing an analogous prodrug of the first one we synthesized to study and assess its potential utilization as antimicrobial vaccine.

2. Design of the self-immolative prodrug

We aimed to design a prodrug constituted of the effective Val-Cit-PAB linker bound to 5-A-RU (Figure 45). Like the other prodrug that we synthesized, we planned to couple this linker to CML beads separated by a PEG spacer.

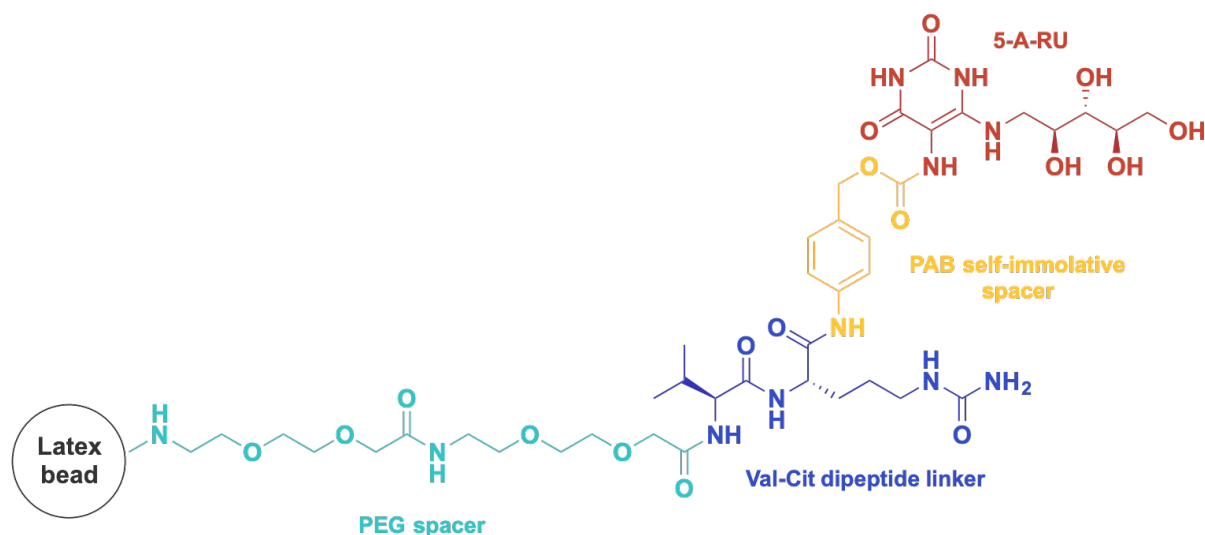
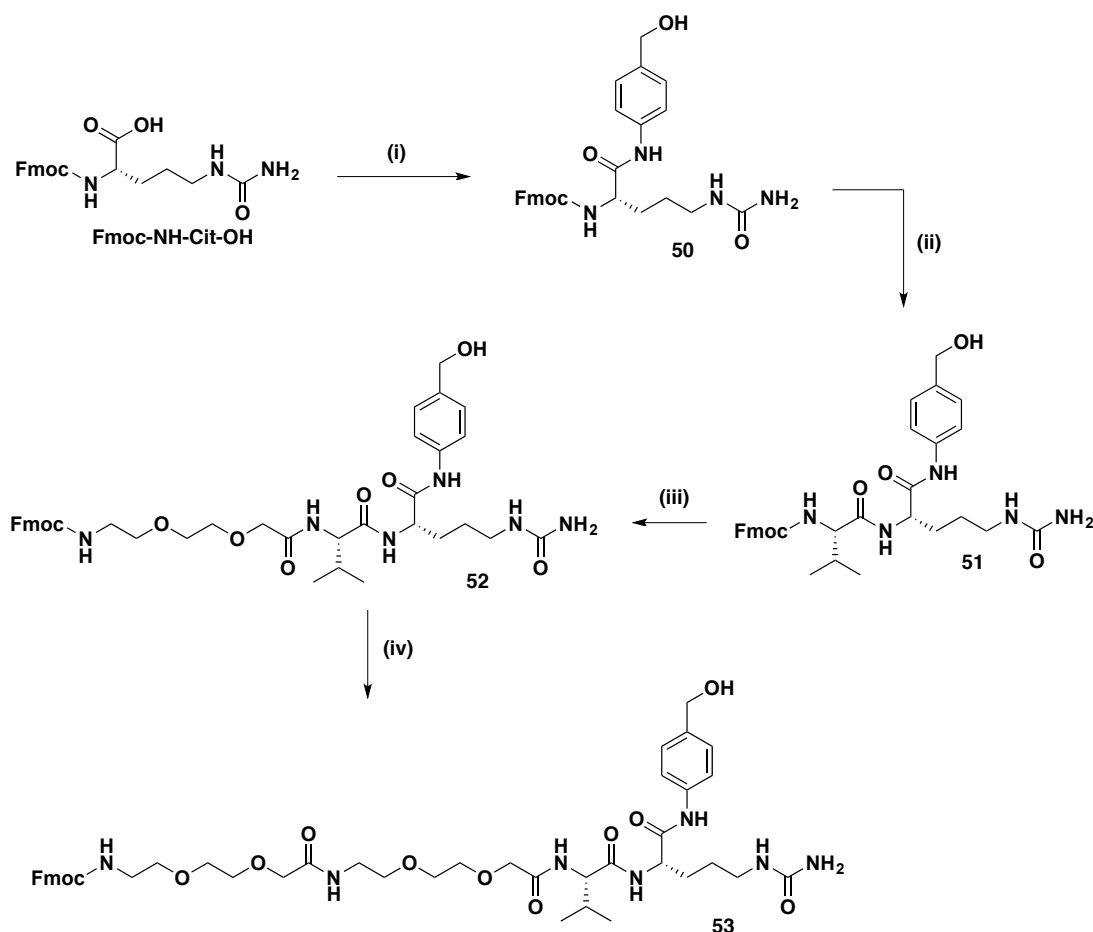


Figure 45: Chemical structure of the self-immolative prodrug of 5-A-RU

3. Chemical synthesis of the prodrug

a) *Linker synthesis*

This time, the linker was synthesized in solution following a described procedure⁹⁹. Fmoc-protected amino acid and PEG derivatives were used. The synthesis started by the reaction between Fmoc-NH-Cit-OH and 4-aminobenzyl alcohol with HATU coupling reagent and DIEA as a base to give **50** (Scheme 20). Fmoc deprotection by a 20% piperidine in DMF solution followed by reaction with Fmoc-NH-Val-OSu (NHS-ester of Fmoc-protected L-valine was synthesized in the lab and directly used without purification) afforded **51**. Product **52** was obtained after removal of the Fmoc group of **51** and coupling with Fmoc-NH-PEG₂-OSu. The latter two steps were repeated a second time to give **53**.



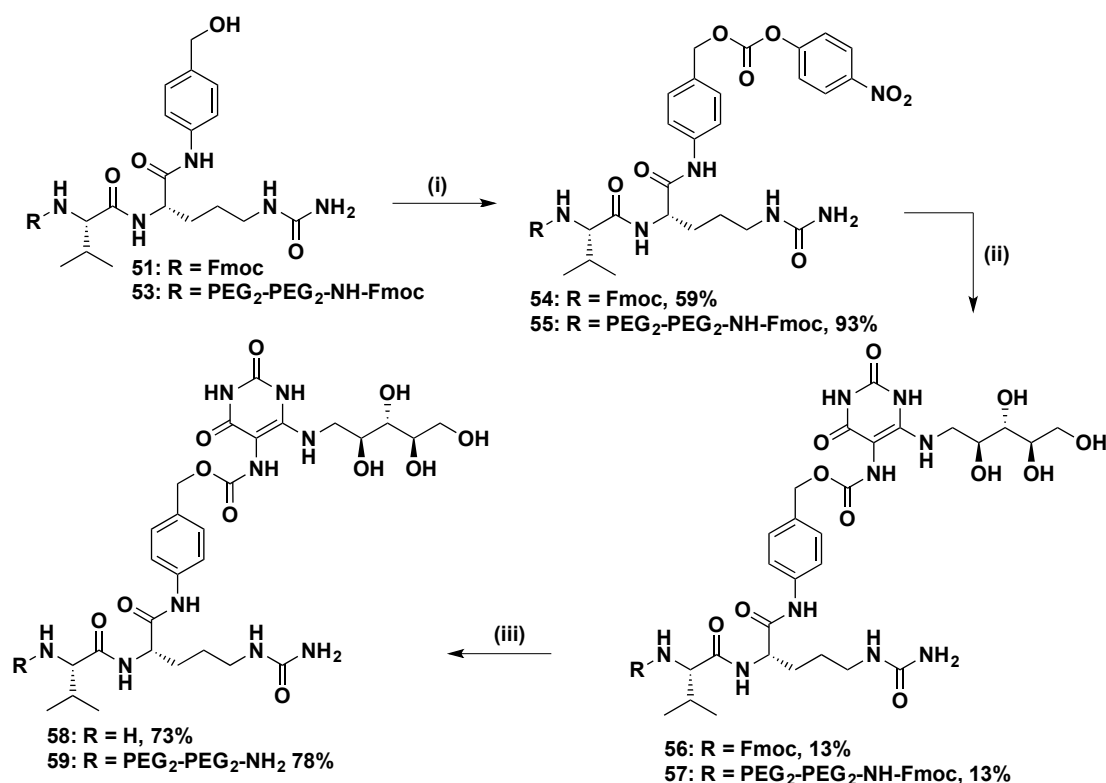
Scheme 20: Synthesis of prodrug linkers **51 and **53**.** Reagents and conditions: (i) 4-aminobenzyl alcohol, HATU, DIEA in DMF, 87%; (ii) 1) 20% piperidine in DMF, 2) Fmoc-NH-Val-O-Su in DMF, 56%; (iii) 20% piperidine in DMF, 2) Fmoc-NH-PEG₂-O-Su in DMF, 47%; (iv) 20% piperidine in DMF, 2) Fmoc-NH-PEG₂-O-Su in DMF, 47%

b) *Coupling of **51** and **53** to 5-A-RU*

The coupling of 5-A-RU to **51** (giving the previously described product⁷⁰) and **53** was planned. Reaction of molecules **51** and **53** with bis(4-nitrophenyl)carbonate gave the PNP carbonate analogues **54** and **55** (Scheme 21). First attempts to couple these compounds to neutral 5-A-RU reduced from 5-N-RU (**4**) failed (no reaction happened). This was most likely correlated with the insolubility of 5-A-RU in pyridine that was already found during the synthesis of **47**. On the contrary, when we used hydrochloride salts of 5-A-RU (**5**), slow solubilization and neutralization of the product occurred allowing the conversion of the starting materials to give the desired compounds **56** and **57**. This unexpected difference of reactivity between 5-A-RU and its hydrochloride salts may be explained by the formation of pyridinium hydrochloride salts with 5-A-RU.HCl. It would form a pseudo-ionic liquid with hydrogen bond donor pyridinium. Since 5-A-RU is highly polar and can make a lot of hydrogen bonds, it could explain the solubilization in this solvent upon deprotonation of 5-A-RU salts. In contrast,

neutral 5-A-RU was completely insoluble in pyridine probably because of the insufficient polarity of pyridine and because it could not form such hydrogen bonds with 5-A-RU. This result also explains why the formation of **47** worked (use of **72** as hydrochloride salts) while it failed with neutral 5-A-RU.

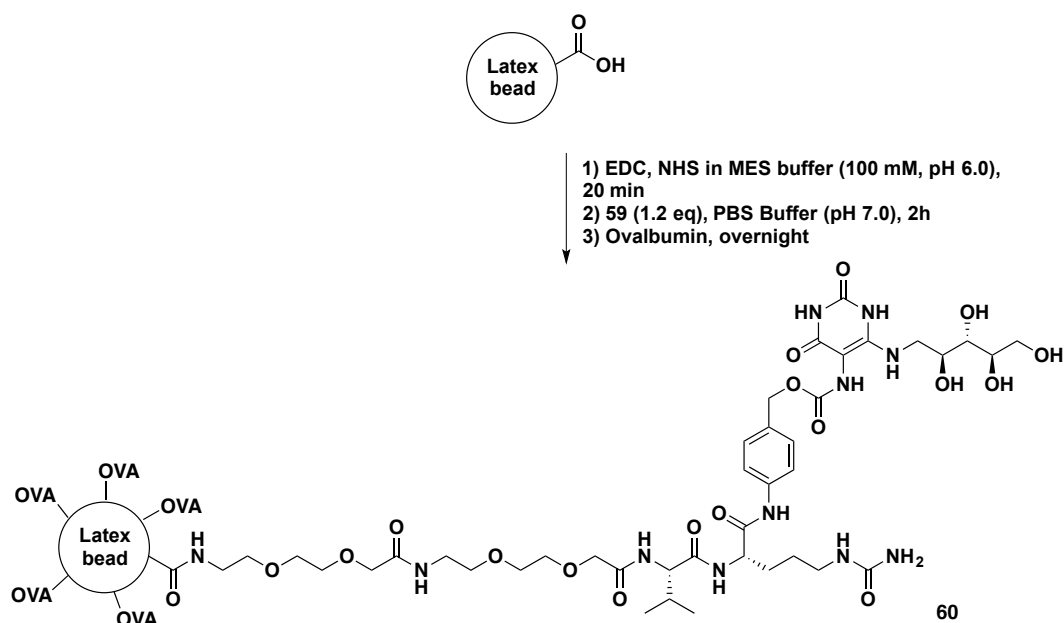
Nevertheless, only approximately half of the starting material was consumed during the reaction (monitoring by UPLC-MS) and several side products were formed (degradation of **54** and **55** under basic conditions). These issues were associated with difficulties to purify the resulting products (preparative HPLC was required) and low reaction yields (always below 20% yield). We repeated the reaction several times to get enough product to finish the synthesis. Finally, Fmoc protecting groups were removed more easily with piperidine in DMF to give the final products **58** and **59**.



Scheme 21: Synthesis of 5-A-RU prodrugs 58 and 59. Reagents and conditions: (i) bis-4-nitrophenyl carbonate, DIPEA in DMF overnight; (ii) 5-A-RU in pyridine, 2h; (iii) piperidine in DMF, 15 min

c) *Coupling of 59 and ovalbumin to CML beads*

59 conjugate was coupled to CML beads using the same conditions as for the synthesis of **49**. NHS-activated esters were formed on CML beads with EDC coupling reagent in MES buffer (pH 6.0), followed by the coupling to **59** in PBS buffer (pH 7.4) (Scheme 22).



Scheme 22: Synthesis of CML bead conjugate 60

To quantify the amount of conjugate bound to latex beads, we kept the washing media after reaction containing the residual product. A calibration curve was obtained with UPLC-MS by measuring the area of UV absorbance peaks at different concentrations of **59**. We calculated that 43% of the mass of **59** was consumed during the reaction (coupled to latex beads) meaning that approximately 35% of the carboxylate sites were linked to the conjugate (calculations were done in accordance with supplier specifications).

Endotoxin free ovalbumin was finally added to the beads for an overnight mechanical stirring. Ovalbumin could either covalently bind with the remaining activated NHS esters or could bind by passive adsorption at the surface of CML beads.

4. Biological evaluation

Murine MAIT cell activation with **60** as well as **58** and **59** was assessed using BMDCs as antigen presenting cells (Figure 46). Previous conjugates **47** and **49** (with Phe-Arg linker) were tested to compare the potency of the different prodrugs and 5-A-RU and 5-OP-RU were used as positive controls. Unfortunately, no activation was detected with all latex bead conjugates, even with the addition of exogenous methylglyoxal in the media. However, a better potency was detected with the two prodrugs **58** and **59** compared to 5-A-RU (approximately a 10-fold increased potency). This suggests an efficient release of 5-A-RU in cells leading to MAIT cell activation after the formation of 5-OP-RU *in situ* (even if the activation was lower than the one observed with exogenous 5-OP-RU). Finally, first prodrug **47** was still able to activate MAIT cells but it was less potent than **58** and **59**.

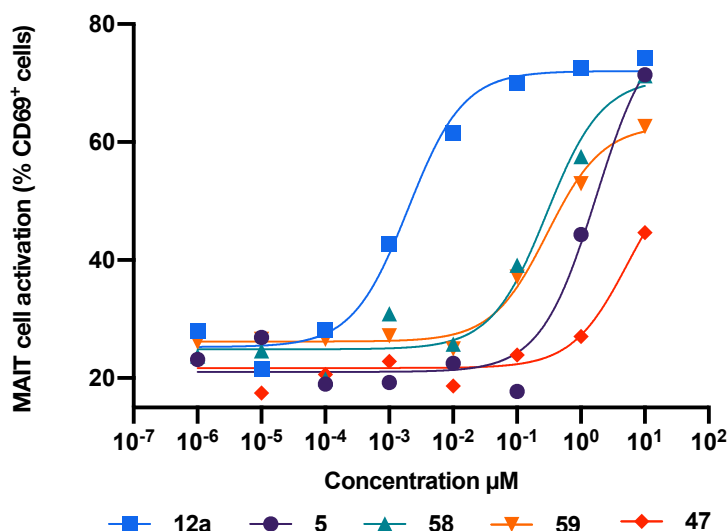


Figure 46: Biological evaluation of the different prodrugs on murine MAIT cells

D. Summary and conclusion

In this work, we designed two different cathepsin cleavable prodrugs, one of 5-A-RU and the other of potent analogue **72**. Synthesis of the first prodrug **47** was tedious, especially regarding the coupling between the linker and **72**. The peptide bond was indeed very difficult to build and required the use of strong activating agent (TCFH). The choice of reaction solvent (DCM/MeOH) was essential to get a solubilization of **72**, allowing the reaction to proceed. Unfortunately, epimerization of arginine stereocenter occurred giving some minor amount of D-epimer that could not be cleaved by cathepsins. The mixture of prodrugs obtained was stable in water environment over days, showing the success of the strategy to stabilize highly unstable **72** (and therefore 5-A-RU). Then, the biological assessment showed a small potency of the prodrug at activating MAIT cells meaning that some cleavage of the prodrug occurred in cells. However, the latex bead conjugate **49** failed at activating MAIT cells, presumably because of too much bulkiness blocking the access of the cathepsins to the cleavable site. Still, all this work gave us some encouraging starting results but a more reactive linker was required to increase the release of 5-A-RU. This is why we chose to design a second prodrug bearing an effective and already validated linker with a self-immolative spacer between the cleavable peptide and 5-A-RU⁷⁰. The synthesis of the second prodrug was easier than the previous one and the resulting conjugate without latex beads (**59**) was more potent than 5-A-RU at activating MAIT cells. However, the CML bead conjugate **60** was not able to activate MAIT cells like **49**. Therefore, the use of another more biocompatible carrier should be envisioned.

IV. Design and synthesis of a new chemical probe for the study of MAIT cell biology

A. Introduction

1. Rationale and goals

As previously discussed, a lot of questions are still to be addressed to get a better understanding of the diverse immune roles of MAIT cells and importantly to determine whether they could be used as therapeutic targets of innovative immunotherapies (such as mucosal vaccines). For this purpose, we decided to design a new chemical probe, analogue of 5-OP-RU, that would allow us to track and visualize MAIT cell antigens bound to MR1 complex, inside tissues and cells. Chemical probes are by definition selective small-molecule modulators of a protein's function allowing the user to ask mechanistic and phenotypic questions about its molecular target(s) in biochemical, cell-based or animal studies¹⁰⁰. They have been widely used tools both for the exploration of fundamental research biology and for drug discovery (target identification and validation)¹⁰¹.

The use of this Chemical Biology tool would help to determine the frequency and localization of MAIT cell ligands and their target MR1 in cells first (*in vitro*), and then in animal models (*in vivo* study in mice) under different physiological or pathogenic contexts. Such a tool could also provide insight about the nature of immune cells that are able to present antigens to MAIT cells. Moreover, it could also help to explain the mechanisms of a recent observation that 5-OP-RU can travel from the skin of mice to their thymus to mediate positive selection of MAIT cells¹⁰.

Our strategy was to design a chemical analogue of 5-OP-RU bearing an additional terminal alkyne, enabling the molecule to react with a fluorophore (functionalized with an azide) through bio-orthogonal CuAAC (copper(I)-catalyzed azide-alkyne cycloaddition), also commonly referred as “click chemistry”.

2. Bio-orthogonal chemistry

a) *Definition and different classes*

Bio-orthogonal reactions have become a key tool for chemical biologists, allowing them to explore biomolecules' localization and functions inside living systems (both *in vitro* and *in vivo*). By definition, bio-orthogonal reactions are rapid and selective chemical reactions that are compatible with biological system under physiological conditions. They basically rely on a two-step process with first the incorporation of a chemical handle (or reporter group) in the biomolecule of interest, followed

by the addition of a reactive probe for bio-orthogonal labelling, enabling the detection of the reporter-biomolecule complex (by fluorescence microscopy, SDS-PAGE analysis, mass spectrometry...) (Figure 47).



Figure 47: Bio-orthogonal reactions¹⁰²

Bio-orthogonal reactions must respect the following criteria: (i) the reactions must work in aqueous media with high selectivity (without interfering with biomolecules), (ii) they must proceed efficiently with fast enough kinetic at low concentrations, (iii) the reagents must be biocompatible and non-toxic, (iv) the functional groups must be as small as possible to limit disturbances of the labeled biomolecules.

Different bio-orthogonal reactions following these rules have been developed (Figure 48). Some polar reactions between ketone/aldehyde and aminoxy/hydrazide compounds were initially used but the products of condensation obtained were too sensitive to hydrolysis in aqueous media¹⁰³. Staudinger ligation was then developed using a functionalized triarylphosphine responsible for the reduction of an azide to an amine leading to the coupling through amide bond formation. This reaction is still used today because of its high selectivity and biocompatibility but it often displays a slow kinetic of reaction limiting its applications as well as oxidation issues for the triarylphosphine moiety.

The most powerful bio-orthogonal reactions rely on cycloaddition reactions. 1,3-dipolar cycloaddition are the most widely used bio-orthogonal reactions, especially the copper(I)-catalyzed azide-alkyne cycloaddition (CuAAC). This reaction relies on the ligation of two bio-orthogonal moieties carrying respectively an azide and an alkyne groups assisted by Cu(I) catalysis (see details in the next section). Strain-promoted azide-alkyne cycloaddition (Cu-free cycloaddition) was more recently developed to get rid of the use of cytotoxic Cu(I) salts. However, the kinetic of reaction is slower by at least ten times than for CuAAC.

Inverse electron-demand Diels-Alder reaction (IED-DA) is another powerful bio-orthogonal reaction displaying the fastest kinetic (even better than CuAAC). Most of these reactions involve a *trans*-cyclooctene (TCO) derivative and an electron-deficient tetrazine analogue. However, the two components of the reaction often lack chemical stability under physiological conditions. Indeed, TCO

can undergo *trans* to *cis* isomerization resulting in a non-active moiety, while most electron deficient tetrazines used for IED-DA readily hydrolyze in water.

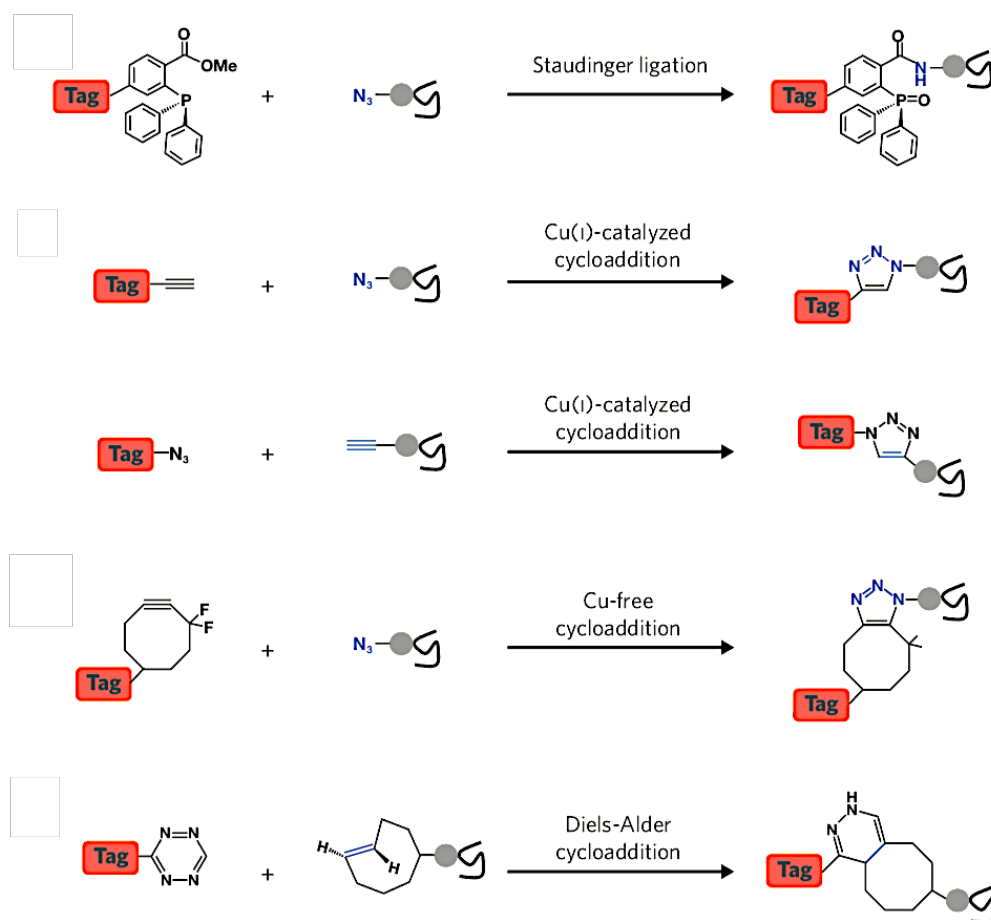


Figure 48: Most efficient and commonly used bio-orthogonal reactions¹⁰⁴

The choice of the bio-orthogonal reaction for a Chemical Biology study is not trivial and it depends on the biological application for which it is intended. All the reactions discussed above possess their own advantages and limitations and the chemical biologist must find the best fit by taking into account the biocompatibility and the required rate of the reaction. After careful consideration, we chose to design a chemical probe able to react through CuAAC for the study of MAIT cell biology. Our choice was strongly motivated by the small size of alkyne and azide moieties that are used for the reaction. Indeed, available crystallographic data from the literature showed that the binding pocket formed by MR1 and the MAIT cell TCR is narrow and modification of the structure of 5-OP-RU done in the studies described before was often deleterious for biological activity. Thus, it appeared that CuAAC was the more relevant option as alkyne and azide are the smallest bio-orthogonal reagents known.

b) *Copper(I)-catalyzed azide-alkyne cycloaddition (CuAAC)*

CuAAC reactions rely on 1,3-dipolar cycloaddition between an azide and an alkyne with the use of copper(I) as catalyst. Uncatalyzed 1,3-dipolar cycloaddition was pioneered by Huisgen in the early 1960s but the reactions required elevated temperature or high pressure to proceed and also resulted in a poor regioselectivity (mixture of 1,4- and 1,5-regioisomers)¹⁰⁵. Thus, it did not fulfill the requirements of bio-orthogonal chemistry depicted above. In 2002, Sharpless and Meldal research groups improved the reaction by using Cu(I) salts as catalysts of the reaction^{106,107}. Not only did the reaction become highly regioselective with only the synthesis of the desired 1,4-regioisomer, but it also considerably improved the kinetic of reaction. The reaction could therefore proceed at room temperature with high efficiency. This improvement allowed the use of CuAAC click chemistry for bio-orthogonal reactions and it is still today the most frequently used bio-orthogonal reaction. This is explained mostly by high kinetic and efficiency, the small size and highly selective reactivity of alkyne and azide moieties (inert towards surrounding biological entities).

The mechanism of the reaction has been largely investigated. It is a stepwise process proceeding first by the formation of a π -complex between the alkyne group and Cu(I) salts (bound to its ligands) **I** leading to a copper-acetylide complex **II**¹⁰⁸ (Figure 49). Then a complex with the azide derivative is formed (**III**) leading to a nucleophilic attack of the azide on the alkyne and the formation of a six-membered ring intermediate **IV**. A second C-N bond is formed to give the 1,2,3-triazole product **V** which generates at the end only the 1,4-regioisomer **VI**.

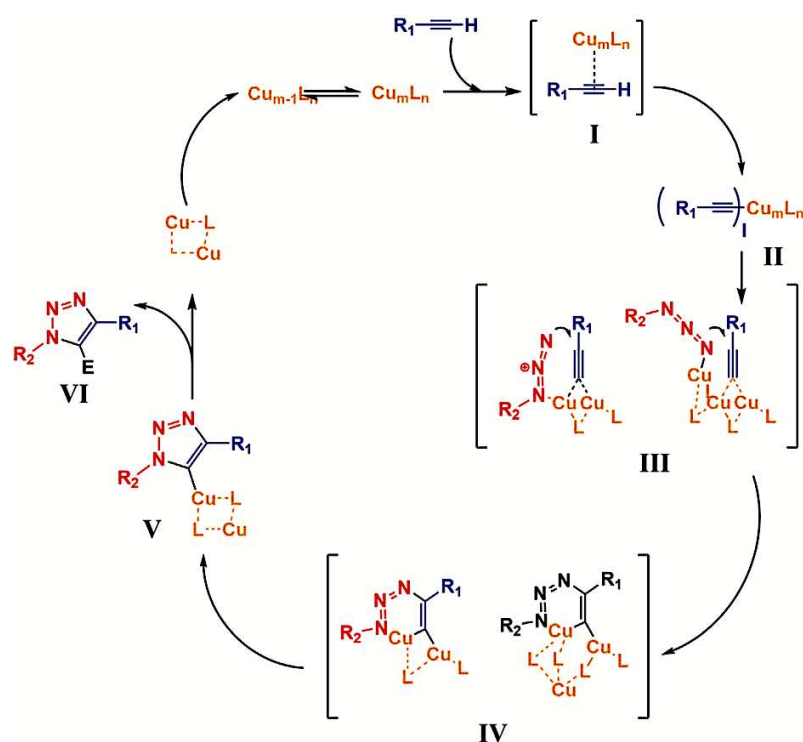


Figure 49: Detailed mechanism of CuAAC reaction¹⁰⁸

CuAAC reactions have been widely used to label and visualize a wide range of biomolecules including proteins, glycans, nucleic acids and lipids mostly *in vitro*^{102,109}. The transition to *in vivo* CuAAC was slower and more difficult because of several limitations, with the most important one being the toxicity of Cu(I). Biocompatible ligands bearing a polytriazole core stabilizing Cu(I) oxidation state were developed to overcome these issues¹¹⁰. The first molecule TBTA was introduced by the Fokin group and several improvements to its structure gave some more powerful and biocompatible ligands like THPTA and BTTES (Figure 50)¹⁰⁹.

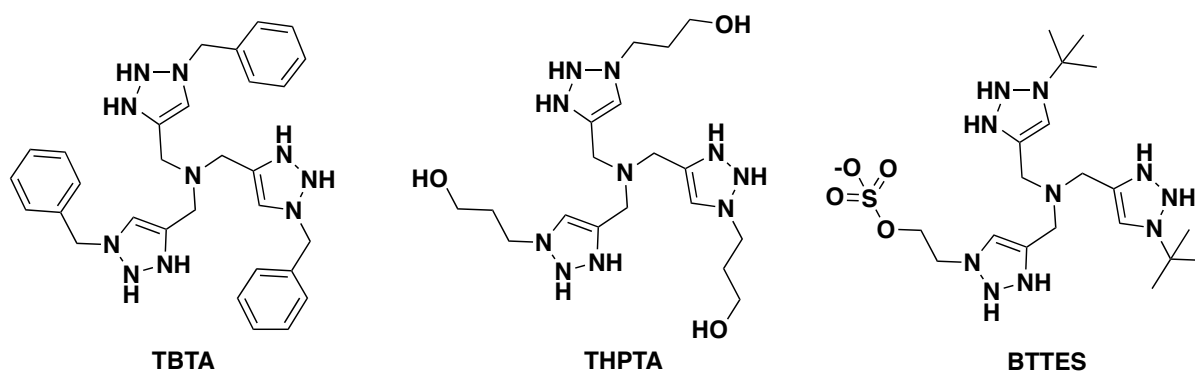


Figure 50: Chemical structure of CuAAC ligands

3. Design of the chemical probe

The position for the introduction of the ethynyl moiety was essential. The first priority was to maintain the interaction between the ligand and MR1. We thus decided to introduce the functional group on the ribityl part of the molecule, far from the α -iminocarbonyl group interacting with Lys43 of MR1. Relying on structural data from the literature, two options were considered: introducing the ethynyl group through chemical bonding to 4'-OH or 2'-OH hydroxyl groups or by carbon-carbon bonding to the 5' position of the ribityl moiety (as neighboring 5'-OH and 4'-OH were described as less-essential for the binding to the TCR⁶⁰) (Figure 51). We were aware that the latter chemical modification would create a new stereocenter giving two diastereomers.

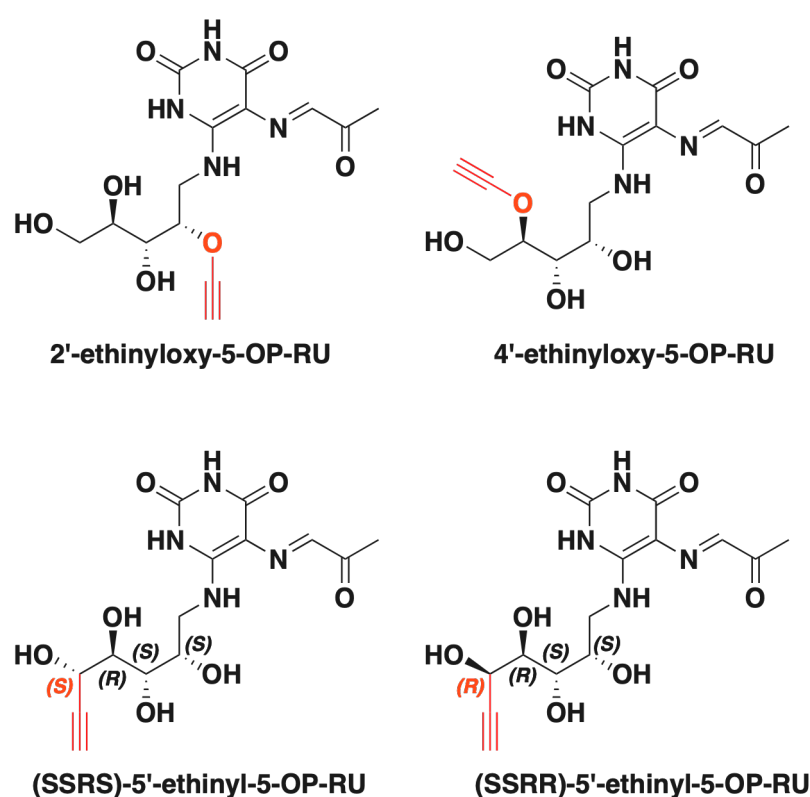


Figure 51: Chemical structure of envisioned ethynyl-functionalized analogues of 5-OP-RU

In silico studies were done to help choose the best chemical probe to synthesize. All the modelling data were generated by Anke Steinmetz from Sanofi. Derivatization of ribityl hydroxyl groups by an ethynyl function as well as 5'-ethinylation were evaluated by molecular docking. 4'-ethinyloxy-5-A-RU, 2'-ethinyloxy-5-A-RU, SSRR, and SSRS diastereomers of 5'-ethynyl-5-A-RU docked well to the MR1/TCR model prepared from the crystal structure of the ternary complex of 7-hydroxy-6-methyl-8-D-ribyllumazine/MR1/TCR (PDB entry 4L4V¹¹¹). Comparison to the ternary complex of 5-OE-RU with MR1/TCR (PDB entry 4NQE⁶) showed perfect conservation of the 5-OE-RU binding mode by uracil and ribityl moieties of 4'-, 2'-ethinyloxy-derivatives and SSRR-5'-ethynyl-5-A-RU in one of the three retained

poses (Appendix C). SSRS-5'-ethinyl-5-A-RU also conserved the binding mode of the uracil moiety, however the ribityl chain adapted its conformation to accommodate the rigid ethinyl group. The conformations of the three retained poses proposed different solutions to optimize hydrogen bonding to the protein. The conformation closest to the one of 5-OE-RU and forming a hydrogen bond by 3'-OH to the hydroxyl group of TCR Y95^G was retained for further studies (Figure 52). 5'-ethinyl and 4'-ethinyloxy derivatives pointed the ethinyl group to a solvent channel leading to bulk solvent while 5'R-ethinylation presented the advantage of preserving the entire potential of hydrogen bond formation of all hydroxyl groups in terms of donor or acceptor. Both 5'R- and 5'S-ethinyl ligand permitted excellent fitting of the reacted fluorophore probe to the solvent channel (*vide infra*). Thus, chemical synthesis of 5'-ethinyl derivatives was undertaken.

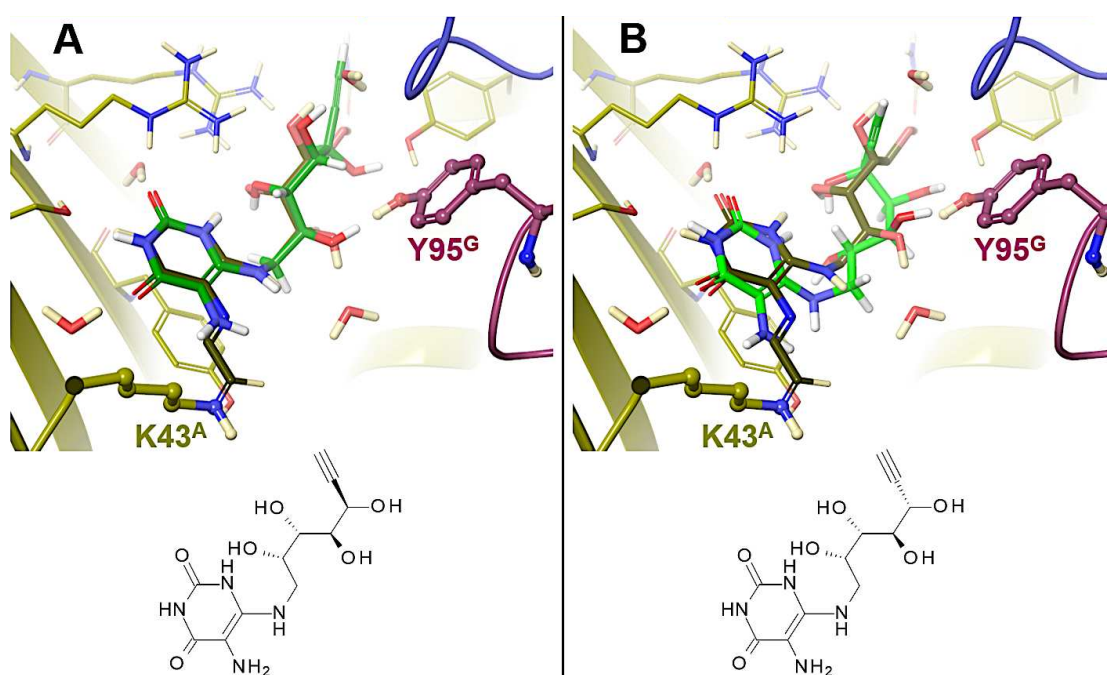
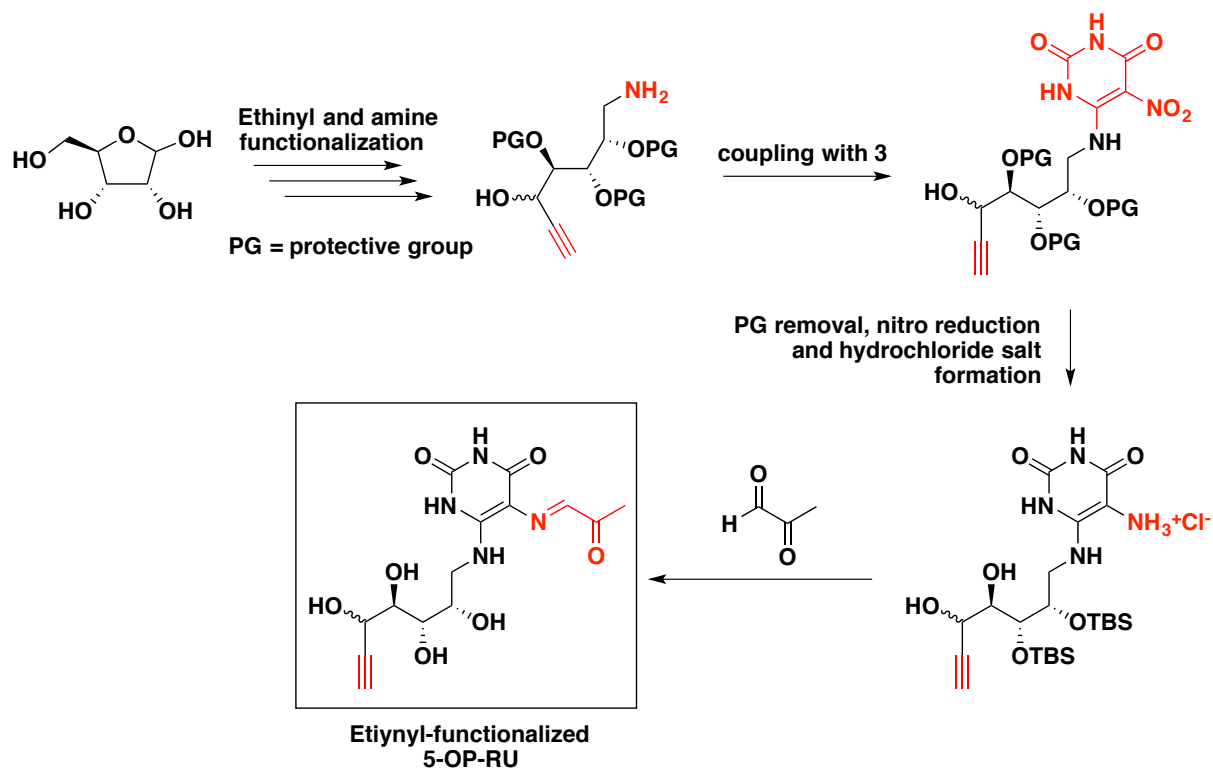


Figure 52: Poses of ethinyl-5-A-RU docked to MR1/TCR complex in comparison to the crystal structure of the ternary complex of 5-OE-RU; Top: close-ups of the ligand-binding site with 5'R and 5'S diastereomers in A and B, respectively. Protein is depicted by ribbon diagrams with MR1 chain A, TCR chains G and H colored in olive, plum, and blue, respectively. Selected amino acids and ligands are represented as ball-and-sticks or tubes. Carbon atoms of 5-OE-RU, 5'R- and 5'S-ethinylated ligands are depicted in dark green, green, and bright green, oxygen, nitrogen, and hydrogen atoms in red, blue, and white, respectively. Bottom: 2-dimensional sketches of the chemical structure of ethinyl-5-A-RU

B. Synthesis of the chemical probe

1. Synthesis strategy

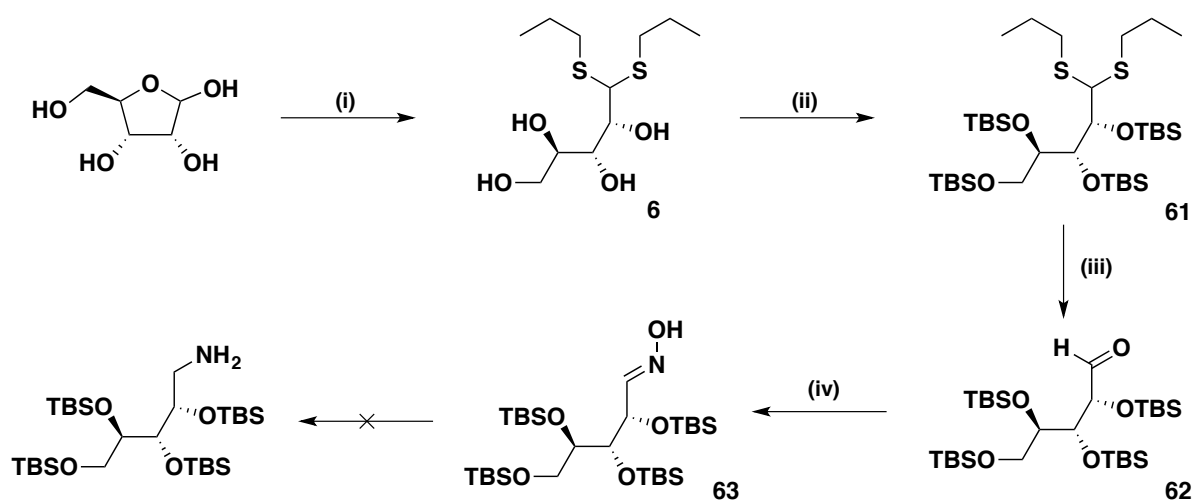
We decided to synthesize the ribityl moiety separately from the uracil ring. We aimed to functionalize it both by ethynyl and amino groups before coupling it to the uracil core (Scheme 23). One of the main challenges of the synthesis was the choice of the protective groups. They were very important for purification purposes and for the selective introduction of the alkyne function. We thought of using TBS protective groups as they would highly decrease the polarity of the intermediates of synthesis, thus making purification much easier. Furthermore, several conditions were described in the literature for selective deprotection of primary alcohol over secondary alcohol protected by TBS groups¹¹². This would allow the ethynyl-functionalization on the terminal carbon of the ribityl tail. Another crucial step was the coupling of the ribityl chain to the uracil ring. We envisioned to use the nitro precursor **3** for this purpose. Removal of the protective groups after coupling and nitro reduction to an amine would give ethynyl-5-A-RU. We were aware that this product would probably be unstable (sensitive to oxidation) like 5-A-RU⁷³. To overcome this issue, we planned to synthesize the hydrochloride salt analogue. Finally, reaction with methylglyoxal in DMSO (with the same conditions as for **12a**) would afford a stable solution of the desired ethynyl-functionalized analogue of 5-OP-RU.



Scheme 23: Ethynyl-5-OP-RU chemical synthesis strategy

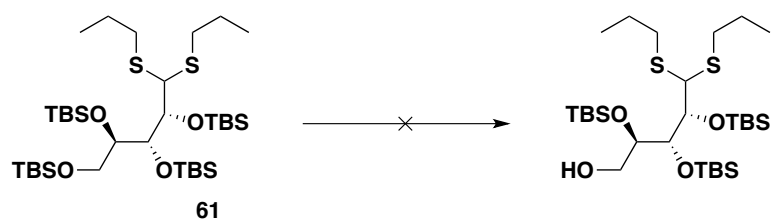
2. Initial synthesis route with attempts to functionalize D-ribose by an amine and an alkyne

The synthesis of ethynyl-functionalized 5-OP-RU started from commercial D-ribose (Scheme 24). Thioketal protection of the aldehyde followed by protection of the four hydroxyl groups with TBS triflate gave fully protected molecule **61**. Removal of the thioketal groups under oxidative conditions gave aldehyde **62** and reaction with hydroxylamine afforded oxime **63**. Surprisingly, attempts to reduce the oxime by LiAlH_4 (under the same conditions as for **10**) failed to give the corresponding amine (no reaction occurred).



Scheme 24: Initial synthesis of ethynyl-D-ribitylamine. Reagents and conditions: (i) *n*-propanethiol in 37% HCl 0°C to rt, 87%; (ii) TBS-OTf, 2,6-lutidine in CH_2Cl_2 , rt, 54%; (iii) I_2 , NaHCO_3 in acetone/water, 83%; (iv) $\text{NH}_2\text{OH}\cdot\text{HCl}$, NaHCO_3 in EtOH/ H_2O , 71%

While running this synthesis, we also tried different conditions from the literature to selectively deprotect the TBS protecting group of the primary alcohol of **61** but unfortunately none of them worked¹¹² (Scheme 25). A problem of reactivity was suspected due to the presence of the thioketal groups that motivated us to move towards a second synthesis strategy.

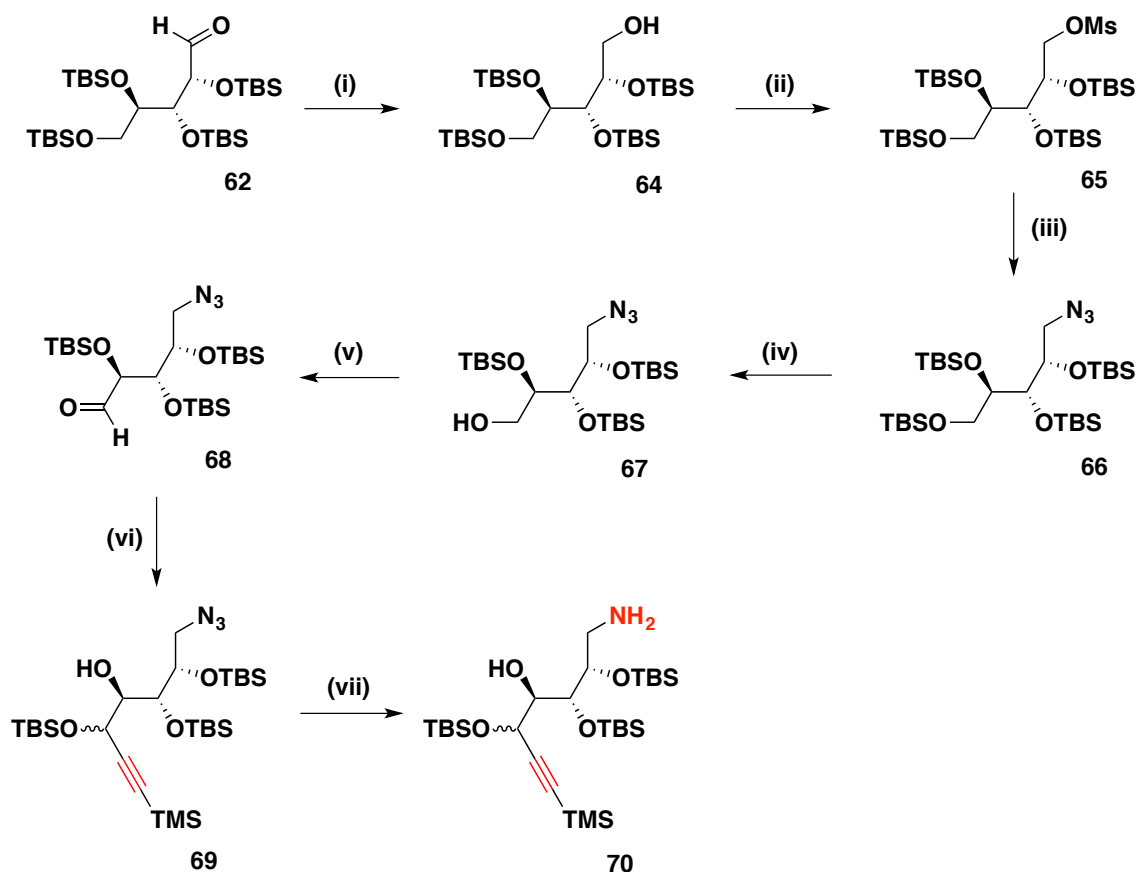


Scheme 25: Attempts to selectively deprotect the primary alcohol of 61

| Reagents | Conditions | Results |
|--------------------------------|------------------------------------|----------------------------|
| 1R-(-)-camphorsulfonic acid | 0.3 eq, DCM/MeOH 1/1, 0°C to rt | no reaction |
| <i>p</i> -toluenesulfonic acid | 0.1 eq, DCM/MeOH 1/1, 0°C to rt | degradation of the product |
| TFA/H ₂ O 1/1 | 50 eq TFA, DCM/MeOH 1/1, 0°C to rt | degradation of the product |
| TBAF | 1.2 eq, DCM/MeOH 1/1, 0°C to rt | no reaction |

3. Second strategy: synthesis of an azido precursor of protected D-ribitylamine

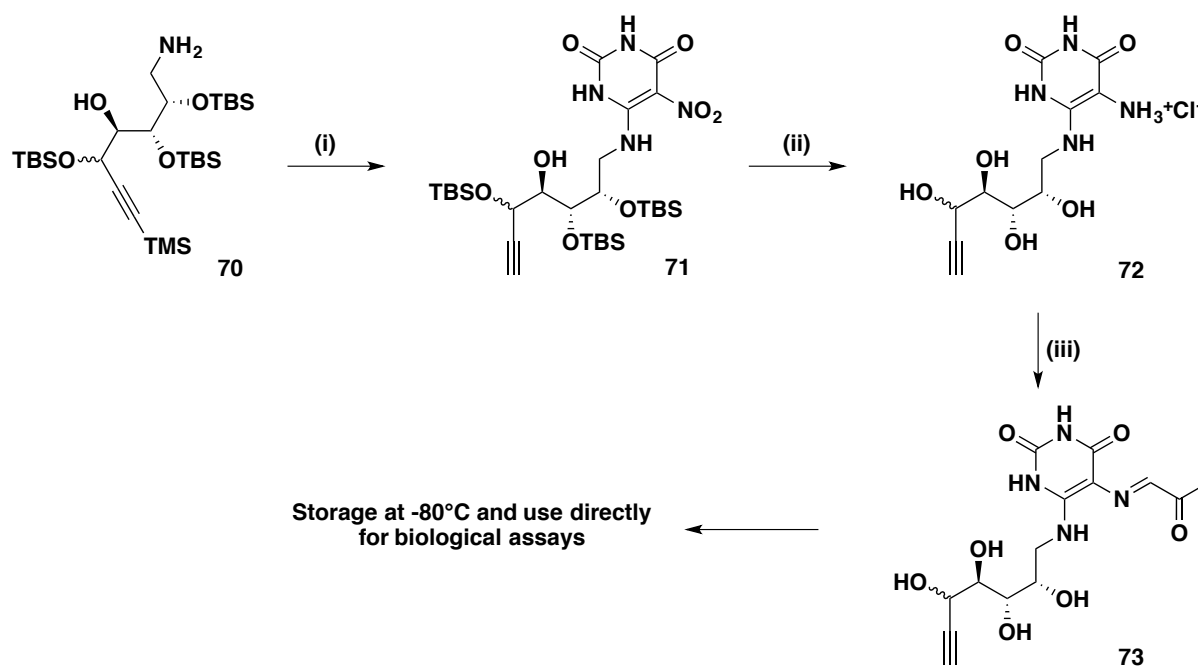
The second synthetic strategy of synthesis relied on the introduction of an azido group as a stable precursor for an amine, prior to alkyne functionalization (Scheme 26). **62** was reduced to the corresponding alcohol **64** by sodium borohydride. Activation of the hydroxyl group by mesylation (**65**) and reaction with sodium azide gave azido precursor **66** in high yield. This time, selective deprotection of the primary alcohol was effective using camphorsulfonic acid to obtain **67** in 19% yield, together with the starting material which could be recovered. The resulting alcohol was quantitatively oxidized using Dess-Martin periodinane (DMP) reagent to give **68**. TMS-acetylene addition on **68** was done with *n*-butyllithium leading to an expected mixture of two diastereomers of **69**, but with an unexpected migration of the neighbor TBS position (detailed in the next section). The synthesis was pursued with the mixture of the two diastereomers. Finally, the azide group of **69** was reduced by Staudinger reaction to give the fully functionalized amine **70**.



Scheme 26: Synthesis of ethinyl-D-ribitylamine. Reagents and conditions: (i) NaBH₄ in MeOH, 0°C to rt, 90% (ii) MsCl in pyridine, rt, 95%; (iii) NaN₃ in DMF, 120°C, 99%; (iv) (1R)-(-)-camphorsulfonic acid in MeOH/CH₂Cl₂, rt, 19%; (v) DMP reagent in CH₂Cl₂, 0°C to rt, 71%; (vi) TMS-acetylene, n-BuLi in THF -78°C to rt, 45%; (vii) PPh₃ in THF/H₂O, 75%

4. Synthesis of ethinyl-5-A-RU and ethinyl-5-OP-RU

70 was coupled to **3** (6-chloro-5-nitropyrimidine-2,4(1H,3H)-dione) with mild heating and TMS group was then removed using potassium methanolate to afford **71** (Scheme 27). This time, reduction of the nitro group was not possible by hydrogenation due to the presence of the alkyne. Instead, we used sodium dithionite reagent that allowed a clean and selective reduction of the aromatic nitro to the corresponding amine, directly followed by acid deprotection of the three remaining TBS groups by 37% HCl in methanol to afford **72** (also called ethinyl-5-A-RU). The mixture of diastereomers was isolated as desired as hydrochloride salts, which were found to be stable over several weeks upon storage at -20°C under argon atmosphere. In the presence of water, the salts were rapidly hydrolyzed leading to a fast degradation, comparable to the one observed with 5-A-RU. Finally, compound **73** was obtained like **12a** from condensation reaction between **72** and methylglyoxal in DMSO during 48h (reaction monitored by UPLC-MS). The solution was kept at -80°C and each time used in biology assays immediately after dilution in cell culture media because of its instability.



Scheme 27: Synthesis of ethinyl-5-OP-RU 73. Conditions and reagents: (i) 1) 6-chloro-5-nitrouracil, Et₃N in DMF, 50°C; 2) K₂CO₃ in MeOH, rt, 71%; (ii) 1) Na₂S₂O₄ in MeOH/H₂O, 90°C; 2) 37% HCl in MeOH, 0°C to rt, 58% ; (iii) methylglyoxal in DMSO, 48h (product not isolated)

5. Diastereomers **71a** and **71b** separation and identification

Intermediate **71** was obtained as a mixture of two diastereomers with a ratio of 95/5 according to UPLC-MS analysis. This stereoselectivity was likely due to the presence of lithium ion during the TMS-acetylene addition (giving **69**) that could be chelated by the aldehyde and the neighboring TBS-protected alcohol. Using a Cram chelation model, we could predict the absolute configuration of the two diastereomers. Thus, the major epimer should have a 5'R configuration and the minor a 5'S configuration. To prove this hypothesis, we first managed to separate the two diastereomers **71a** (major diastereomer) and **71b** (minor diastereomer) by preparative RP-HPLC (Figure 53).

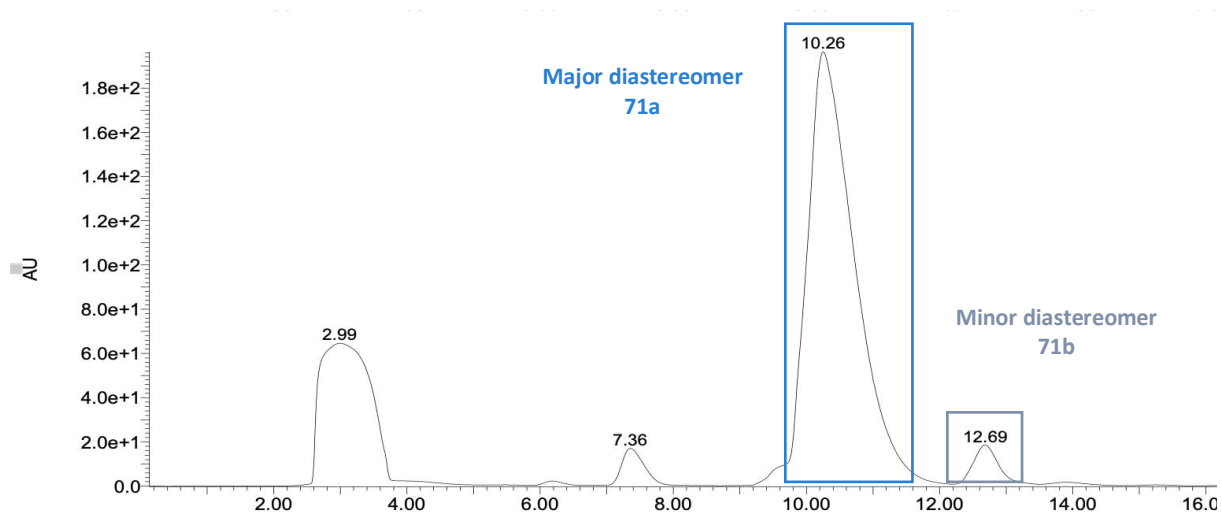


Figure 53: Preparative HPLC chromatogram of 71 (separation of the two diastereomers) : 10.26 min : major diastereomer 71a; 12.69: minor diastereomer 71b

Then, we tried to use Mosher ester method to determine the stereochemistry of the compounds but no reaction occurred with Mosher's acid chloride derivatives, probably due to the bulkiness of the TBS groups. Finally, we managed to obtain crystals of **71a** in a mixture of acetonitrile/water (small needles were formed after slow evaporation of the solvent).

X-ray crystallography analysis of **71a** was done by Pascal Retailleau (laboratoire de cristallographie structurale at Institut de Chimie des Substances Naturelles) (see Appendix D for additional experimental details). The data confirmed our initial hypothesis that the major diastereomer was 5'R (Figure 54). Unexpectedly, we also found that one TBS group had migrated from the 4'-OH to the 5'-OH during TMS-acetylene addition. To determine if the same migration had occurred with **71b**, we acetylated the free hydroxyl group (reaction with acetic anhydride with pyridine in DCM) and ran ^1H NMR analysis that confirmed the same migration of the TBS position (unambiguous increase of the chemical shift for the $\text{H}_{4'}$ NMR signal from 3.91 ppm to 5.13 ppm). This TBS migration did not change the synthetic scheme as all TBS groups were removed later.

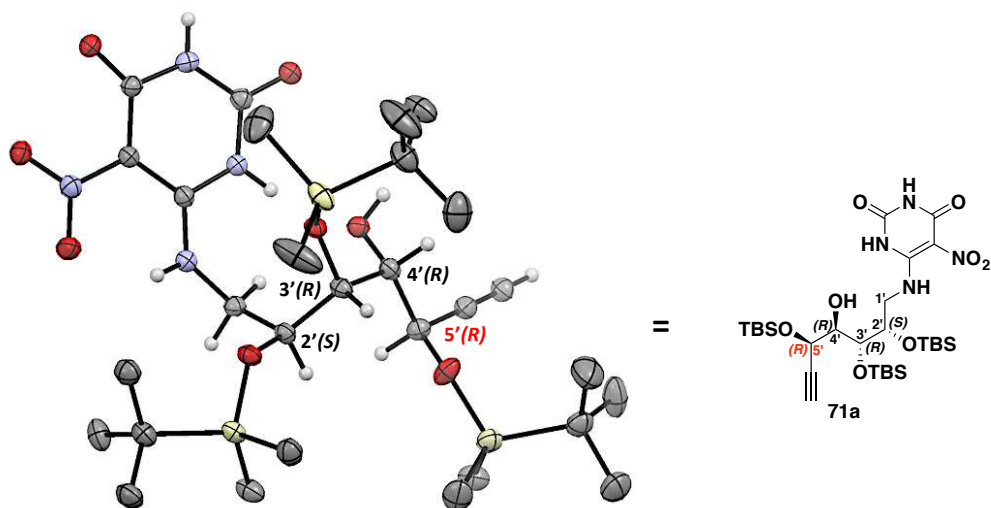


Figure 54: ORTEP view of one conformer of compound **71a** with absolute configuration of the ribityl chain stereocenters. The thermal ellipsoids are drawn at the level of 30% probability

C. Biological evaluation and validation of the chemical probes

1. Rationale and goals

To further use the ligands as chemical probes, we must validate several essential criteria. The probes should be biologically active, therefore able to up-regulate MR1 (and hopefully to activate MAIT cells). Next, we had to verify that the click reaction works efficiently *in vitro*. To do so, we planned to do a CuAAC bio-orthogonal reaction using an azide-functionalized fluorophore, enabling the visualization of the ligands inside cells (WT3-m cells overexpressing MR1 in a first time). Finally, we had to demonstrate the specificity of binding to MR1 to ensure that the fluorescent signal truly corresponds to the ligand bound to MR1 instead of other biomolecules. For this purpose, we decided to do the click reaction in wild-type WT3 cells (WT3-WT) that poorly express MR1 in addition to WT3-m cells and then to compare the fluorescent signals obtained with those cell strains.

2. Biological evaluation of the diastereomeric mixture **73**

The diastereomeric mixture **73** was tested both for its capacity to up-regulate MR1 and to activate MAIT cells (Figure 55). **73** strongly up-regulated MR1 with higher potency compared to 5-OP-RU. **73** was also able to activate MAIT cells from double transgenic mice (even if 5-OP-RU was slightly more active). All these results were very encouraging but we wanted to evaluate each diastereomer separately as they could have different biological activity.

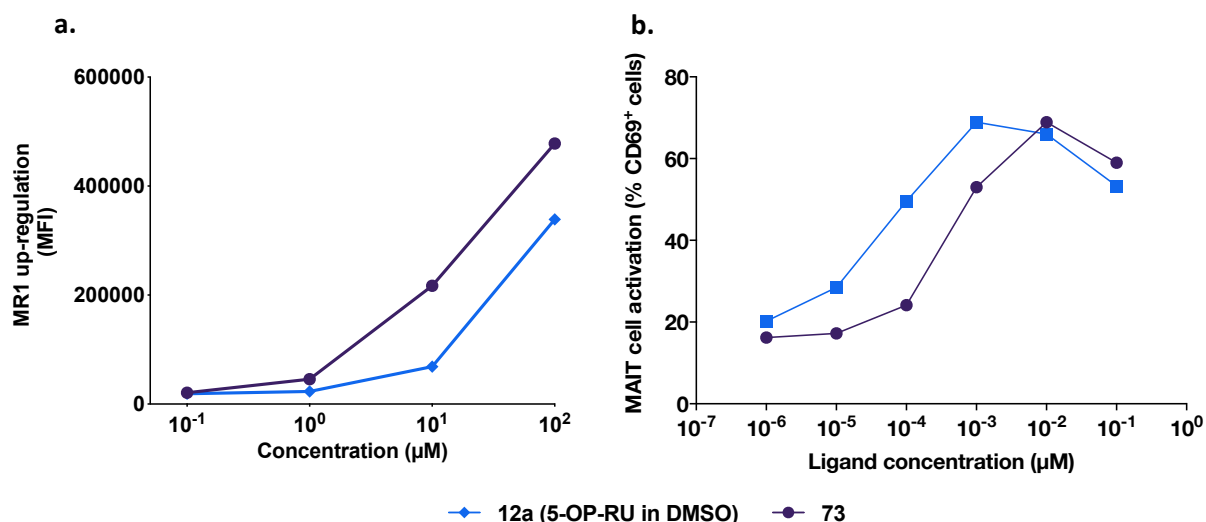


Figure 55: Biological evaluation of the diastereomeric mixture 73. a. MR1 up-regulation assay; b. MAIT cell activation assay; MFI: mean fluorescence intensity of PE-conjugated antibody anti-MR1 signal

3. Biological evaluation of the two diastereomers 73a and 73b

a) *MR1 up-regulation assay*

The capacity of the two ethynyl-functionalized analogues of 5-OP-RU (**73a** and **73b**) to up-regulate MR1 at the cell surface of WT3-m cells was assessed. Data are depicted both as a percentage of MR1 positive cells (

Figure 56a) and corresponding mean fluorescence intensity of PE-conjugated antibody anti-MR1 (

Figure 56b). The two diastereomers were responsible for a strong and similar MR1 up-regulation after 2 hours incubation. The up-regulation was more pronounced than the one obtained with positive control 5-OP-RU (consistent with the results obtained with **73**). As reported with the other analogues of 5-OP-RU synthesized, these data suggest that the chemical modification of the ribityl chain is not deleterious to the binding and up-regulation of MR1. Most importantly, these results validate the mandatory pre-requisite high affinity binding of the ligands to MR1 for the further validation of the probes.

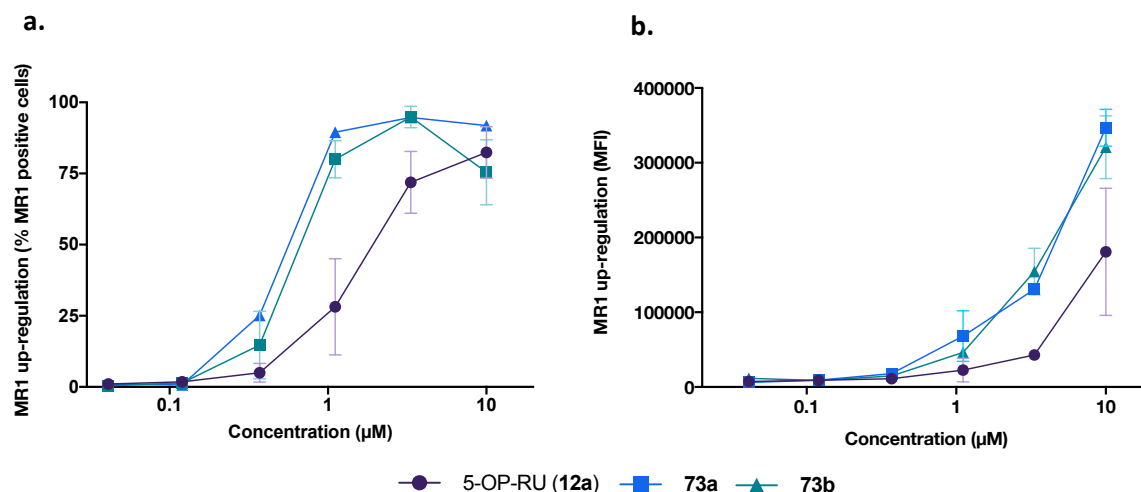


Figure 56: MR1 up-regulation in the presence of 12a, 73a or 73b. A: percentage of MR1 positive cells; B: MFI: mean fluorescence intensity of PE-conjugated antibody anti-MR1 signal; Data displayed on the graphs are means \pm SD of technical duplicates.

b) MAIT cell activation

The two diastereomers **73a** and **73b** were then tested for their ability to activate murine MAIT cells. **12a** was again used as positive control. WT3-m cells were used as antigen presenting cells. MAIT cells were obtained from enriched T cell populations of spleen of either $i\alpha 19$ single transgenic or $i\alpha 19V\beta 8$ double transgenic mice. The two clickable ligands activated MAIT cells of double transgenic mice with an activity close to 5-OP-RU (

Figure 57a). In contrast, no biological activity was detected with MAIT cells from single transgenic mice with **73a** and **73b** whereas 5-OP-RU strongly activated MAIT cells (

Figure 57b). These data suggest that activation of MAIT cells by compounds **73a** and **73b** is strongly dependent on the nature of the TCR β chain expressed by MAIT cells. An analogous specificity was previously described by Keller *et al.* with the diclofenac (DCF) and its metabolites (see previous section). DCF was responsible for a weak activation of Jurkat.MAIT A-F7 cell line expressing TCR that uses TRBV6-1 but it did not activate Jurkat.MAIT-#6 and Jurkat.MAIT-C-F7 expressing TCR with TRBV6-4 and TRBV20, respectively⁵⁹. In contrast, the absolute configuration of C6' stereocenter does not seem to have any influence over the biological activity of the two molecules.

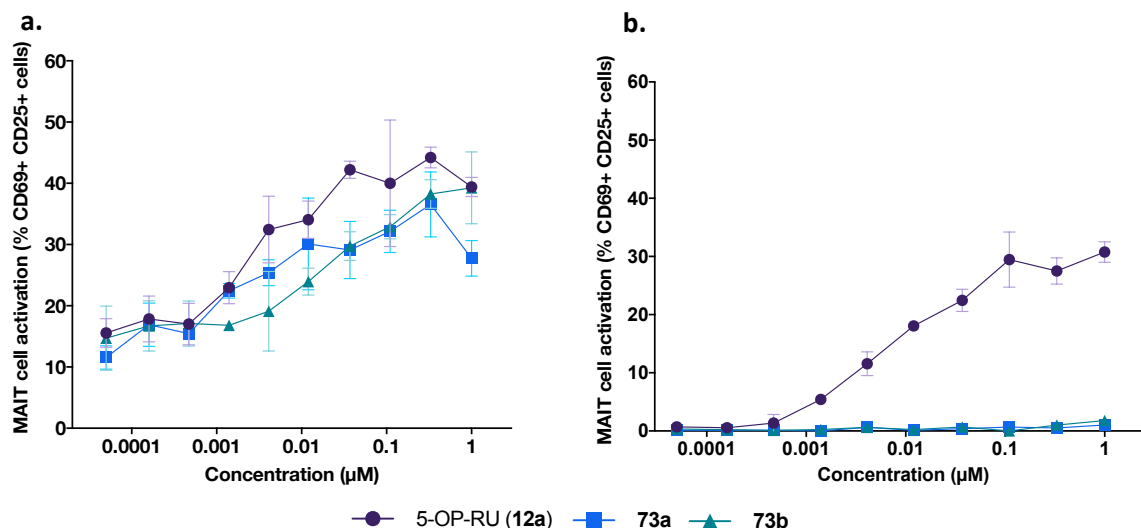


Figure 57: MAIT cell activation by 12a, 73a and 73b. A: *iVα19 Vβ8* double transgenic mice; B: *iVα19* simple transgenic mice; Data displayed on the graphs are means \pm SD of technical duplicates.

4. In vitro validation of the use of **73** as a chemical probe for the study of MAIT cell biology

We finally performed *in vitro* CuAAC experiments to confirm the efficient and selective bioconjugation of the ligand to MR1 in cells. Since the two diastereomers showed similar biological activity, we used mixture **73** for these experiments. The cells were incubated for 1 hour with **73** (10 μM) before fixation, permeabilization and click reaction with a dye (AF₄₈₈ functionalized as an azide). WT3 wild type cells (WT3-WT) were used as negative control as they express low endogenous level of MR1⁸¹. The cells were finally analyzed by epifluorescence microscopy. The images we obtained showed a strong fluorescence at a perinuclear localization (likely in the Golgi apparatus) in WT3-m cells (Figure 58). In contrast, almost no fluorescence signals were observed with WT3-WT cells in accordance with lower expression of MR1 in these cells. These results strongly support a specific binding of **73** to MR1 and tend to validate our CuAAC strategy *in vitro* to reveal the presence and localization of MR1 inside cells.

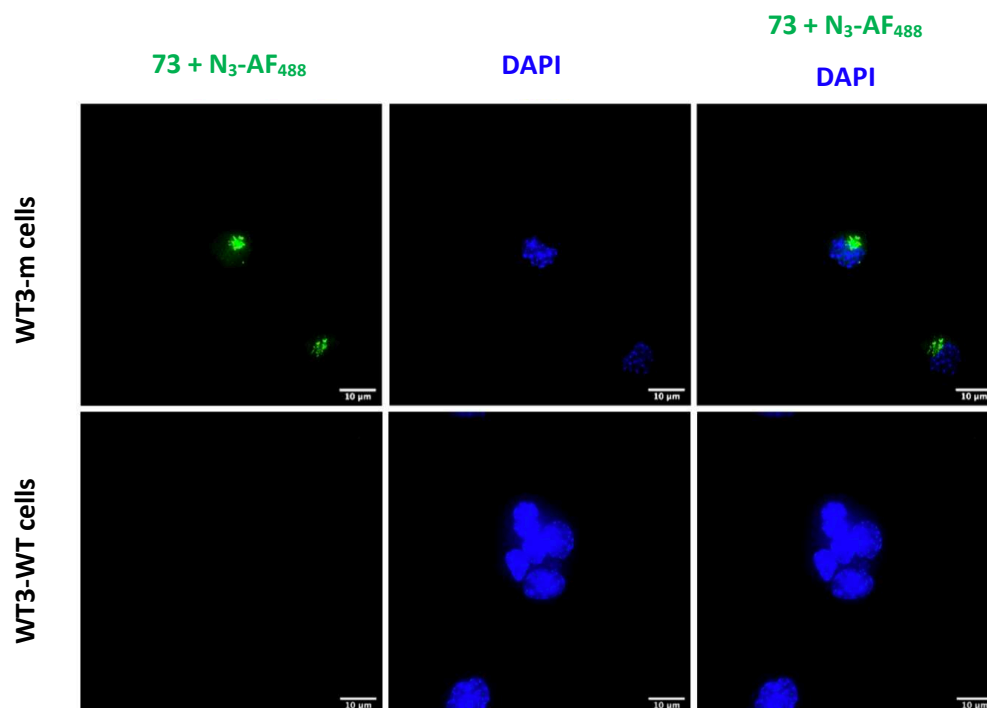


Figure 58: Epifluorescence microscopy images showing **73** conjugated to azide- AF_{488} fluorophore (green) and DAPI (blue) in WT3-m cells or WT3-WT cells

D. Summary and conclusion

In this work, we described the synthesis of the first clickable MAIT cell agonists for its use through bio-orthogonal reactions. We managed to obtain a radiocrystallographic structure permitting to assign unambiguously the stereochemistry of the generated stereocenters and to discover an unexpected migration of one TBS protecting group. The biological activity of the two molecules was confirmed with a strong MR1 up-regulation induced by both diastereomers reflecting a high affinity of the ligands for this protein. *In situ* click chemistry reaction in cells successfully revealed under fluorescence microscopy the clickable ligands selectively bound to MR1. Thus, we validated our CuAAC click chemistry strategy *in vitro*.

Interestingly, the two isolated diastereomers of **73** strongly activated double $\alpha\beta$ TCR transgenic mice, similarly to 5-OP-RU but no activation was detected with MAIT cells from single $iV\alpha 19$ transgenic mice. These results suggest a structural specificity of the potent molecules towards the MAIT cell TCR. This discovery could provide additional information about the yet poorly understood basis of interaction to the TCR β chain necessary for the recognition of vitamin B2 derivative antigens.

V. General conclusion and perspectives

All the research work done aimed to design new stable analogues of MAIT cell potent antigens that could be used to give information about MAIT cell biology and especially to determine if such cells could be used as therapeutic targets for the development of new immunotherapies (mostly new vaccines). Our first medicinal chemistry approach was to synthesize stable analogues of 5-OP-RU. Few molecules were synthesized in collaboration with a research team from Sanofi and the molecules were evaluated in biology at Institut Curie. All this collaborative work gave interesting structure-activity relationships information helping us to better understand the basis of recognition of the MAIT cell TCR and MR1. These data combined with the one obtained from structural biology studies provide more accurate fundamental knowledge about the basis of interaction of the ligands with their targets. However, we still lack highly potent stable analogues of 5-OP-RU since all the pharmacomodulation performed led to a significant decrease of MAIT cell activation. Finally, it seems very difficult to modify the chemical structure of 5-OP-RU without drastically losing potency. Still, several other pharmacomodulations of 5-OP-RU structure could be envisioned such as the one displayed in Figure 59.

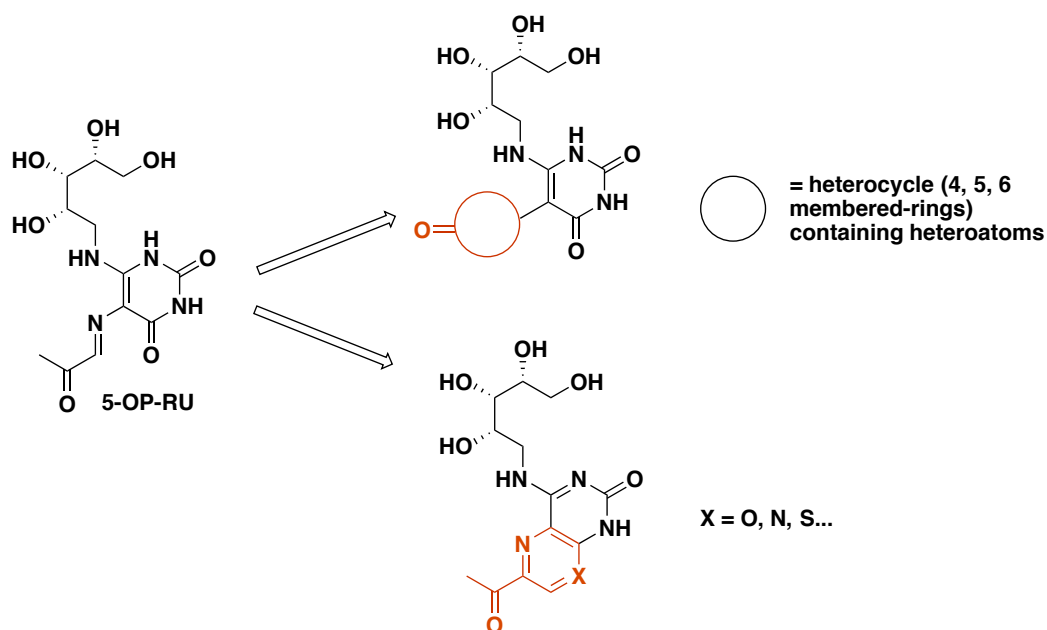


Figure 59: Other possible pharmacomodulations of 5-OP-RU

In a second time, we developed prodrugs of 5-A-RU, the chemical precursor of 5-OP-RU. Two different prodrugs with different cleavable linkers were produced. Chemical synthesis of the prodrugs was highly challenging especially because of the non-favorable physico-chemical properties of 5-A-RU and its insolubility in organic solvents. Still, we managed to obtain the prodrugs after many attempts, and biological evaluation of the molecules confirmed the efficiency of the prodrug strategy,

as simple conjugates without carriers were able to activate MAIT cells. However, the strategy to use CML beads as immunogenic carriers failed. The use of a longer PEG chain spacer could be envisioned to avoid this issue and the use of another more biocompatible carrier should be considered. Nevertheless, the chemical stability of the prodrugs and especially the biological results that we described along with data from the literature with the Val-Cit-PAB linker are truly encouraging. They tend to underline the potential use of 5-A-RU prodrugs as antimicrobial vaccine adjuvants though more careful biological studies are required to confirm its efficacy and safety of use.

Finally, we synthesized new chemical probes, clickable analogues of 5-OP-RU that can allow us to track and visualize MAIT cell ligands in cells. The probes were validated *in vitro* and the next steps will be to validate their use *in vivo*. For this purpose, we plan to inject the clickable ligand to mice followed by tissue harvest and bio-orthogonal reaction as it was previously successfully done in other applications^{113,114}. The use of ligand-assisted CuAAC could be considered to get a more efficient click reaction. These interesting new tools clearly open new avenues for the study of MAIT cell biology.

Experimental part

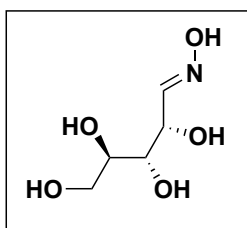
I. Chemistry

A. General aspects

All materials were obtained from commercial suppliers and used without further purification. Anhydrous solvents were obtained with PureSolve™ solvent purification system (DCM, Et₂O, toluene, THF). All reactions were monitored by Thin Layer Chromatography (TLC) using Merck Silicagel 60F-254 thin layer plates and by Ultra Performance Liquid Chromatography coupled to Mass Spectrometry (UPLC-MS) with Waters Acquity UPLC BEH apparatus (C18 1.7 μm VanGuard pre-column 3/Pk 2.1 x 5 mm column) and mass spectra were recorded using electrospray ionization method with Waters ZQ 2000 spectrometer. Column chromatography was carried out on silicagel Merck 60 (0.040-0.063 μm diameter). High resolution mass spectrometry (HR-MS) analyses were done on a Thermo Scientific Q Exactive™ Plus spectrometer with electron spray ionization method. ¹H and ¹³C NMR analyses were performed in deuterated solvents (CDCl₃, CD₃OD, DMSO-d₆, CD₂Cl₂, D₂O) with Bruker AVANCE 400 MHz or 500 MHz. Chemical shifts are reported as δ values in parts per million (ppm) relative to tetramethylsilane as internal standard and coupling constants (J) are given in hertz (Hz). The following abbreviations are used to describe peak patterns when appropriate: s (singlet), brs (broad singlet), d (doublet), t (triplet), brt (broad triplet), q (quartet), m (multiplet), dd (doublet of doublet), ddd (doublet of doublet of doublet), td (triplet of doublet).

B. Protocol and product characterizations

(2S,3S,4R,E)-2,3,4,5-tetrahydroxypentanal oxime (1)⁷¹



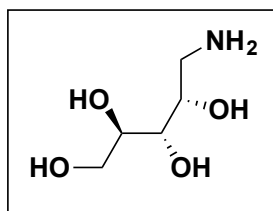
| Raw formula | Molecular mass | Aspect | Yield |
|--|----------------------------|-------------|-------|
| C ₅ H ₁₁ NO ₅ | 165.06 g.mol ⁻¹ | White solid | 78% |

To a suspension of NH₂OH.HCl (2.31 g, 2.5 eq, 33 mmol) in EtOH (12mL) was added dropwise a solution of NaOMe (1.4 g, 2.0 eq, 26 mmol) in EtOH (12 mL). After 15 min, the suspension was filtered and the filtrate was heated to 70°C. D-ribose (2.0 g, 1.0 eq, 13 mmol) was added slowly until all the material was dissolved. The mixture was stirred at 70°C during 30 min and then cooled to room temperature and left standing overnight. The precipitate was filtered and washed with EtOH to give **1** (Z/E mixture) as a white solid.

¹H NMR (400 MHz, D₂O) δ: Z-isomer (minor): 6.94 (d, 1H, J= 6.3 Hz), 5.11 (dd, 1H, J= 6.3, 3.7 Hz), 3.92-3.77 (m, 3H), 3.77-3.60 (m, 3H). E isomer (major): 7.57 (d, 1H, J= 6.8 Hz), 4.47 (dd, 1H, J= 6.8, 4.6 Hz), 3.92-3.77 (m, 3H), 3.77-3.60 (m, 3H)

¹³C NMR (101 MHz, D₂O) δ: Z-isomer (minor): 151.5, 72.7, 71.0, 65.3, 62.6. E-isomer (major): 151.1, 73.0, 71.4, 69.4, 65.31, 62.5

(2R,3S,4S)-5-aminopentane-1,2,3,4-tetraol (2)⁷¹



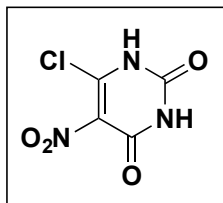
| Raw formula | Molecular mass | Aspect | Yield |
|--|----------------------------|-----------|-------|
| C ₅ H ₁₃ NO ₄ | 151.08 g.mol ⁻¹ | Brown oil | 103 % |

1 (1.6 g, 1.0 eq, 9.7 mmol) was solubilized in AcOH (15 mL) and PtO₂ (0.44 g, 0.02 eq, 0.19 mmol) was added. The slurry was stirred under H₂ atmosphere at room temperature for 2 days (complete solubilization of the product). The mixture was dried under vacuum and the product was purified on ion exchange resin (Amberlite IR120 Hydrogen Form) using 3N NH₄OH as eluent. Compound **2** was isolated (along with a minor impurity) as a brown oil.

¹H NMR (400 MHz, D₂O) δ: 3.84-3.66 (m, 3H), 3.66-3.58 (m, 2H), 2.86 (dd, 1H, J= 13.5, 3.1 Hz), 2.67 (dd, 1H, J= 13.5, 8.3 Hz)

¹³C NMR (101 MHz, D₂O) δ: 73.1, 72.5, 72.0, 62.4, 42.2

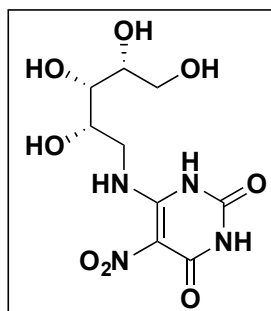
6-chloro-5-nitropyrimidine-2,4(1H,3H)-dione (3)⁷¹



| Raw formula | Molecular mass | Aspect | Yield |
|---|----------------------------|--------------|-------|
| C ₄ H ₂ ClN ₃ O ₄ | 190.97 g.mol ⁻¹ | Yellow solid | 73 % |

6-chlorouracil (6.82 mmol, 1.0 eq, 1.0 g) was added portionwise to sulfuric acid (3.23 mL) at 15°C. The mixture was cooled to 0°C and fuming nitric acid (1.08 mL) was added dropwise. The mixture was allowed to react at 10°C for 30 minutes. Then cold water was added and the product was extracted by EtOAc. The organic layer was dried over MgSO₄ and deeply dried under vacuum to give **3** as a light-yellow solid.

5-nitro-6-(((2S,3S,4R)-2,3,4,5-tetrahydroxypentyl)amino)pyrimidine-2,4(1H,3H)-dione (5-N-RU, 4)⁷¹



| Raw formula | Molecular mass | Aspect | Yield |
|--|----------------------------|--------------|-------|
| C ₉ H ₁₄ N ₄ O ₈ | 306.08 g.mol ⁻¹ | Yellow solid | 45 % |

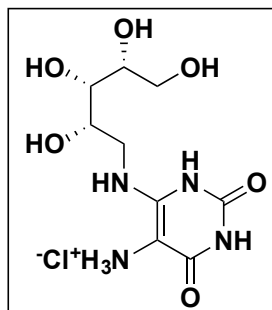
To a solution of **3** (430 mg, 1.0 eq, 2.25 mmol) in EtOH (2mL) was added a solution of **2** (680 mg, 2.0 eq, 4.49 mmol) in H₂O (3 mL). The mixture was stirred and 2N KOH (2mL) was added dropwise. The mixture was stirred for 3h and the formed precipitate was filtered and washed by few volumes of EtOH. The precipitate was solubilized in H₂O (10 mL) and excess acetone was added. The formed precipitate was filtered and washed by acetone. The product was finally solubilized in water and lyophilized to give **4** as a yellow solid.

MS (ESI), *m/z*: 307.3 [M+H]⁺

¹H NMR (400 MHz, D₂O) δ : 4.02 (td, 1H, J= 6.7, 3.4 Hz), 3.92-3.79 (m, 3H), 3.72-3.62 (m, 3H)

¹³C NMR (101 MHz, D₂O) δ : 161.9, 160.6, 157.7, 111.1, 72.6, 72.1, 70.2, 62.4, 43.2

2,4-dioxo-6-(((2S,3S,4R)-2,3,4,5-tetrahydroxypentyl)amino)-1,2,3,4-tetrahydropyrimidin-5-aminium chloride (5-A-RU.HCl, 5)



| Raw formula | Molecular mass | Aspect | Yield |
|--|--|------------|-------|
| C ₉ H ₁₇ ClN ₄ O ₆ | 312.08 g.mol ⁻¹ (neutral form: 276.11 g.mol ⁻¹) | Pink solid | 72 % |

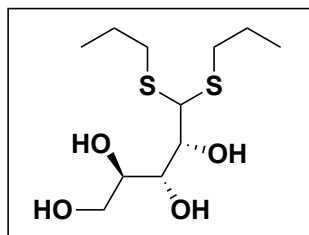
To a solution of **4** (70 mg, 1.0 eq, 0.23 mmol) in water was added Pd/C 10% (7 mg). The mixture was allowed to react at room temperature under H₂ atmosphere overnight. The product was then carefully filtered on celite to avoid as much as possible contact with air and washed with few volumes of water. 1N HCl (0.3 mL) was added to the filtrate and the product was dried under vacuum to give **5** as a pink solid.

HR-MS (ESI), *m/z* 277.1 [M+H]⁺

¹H NMR (400 MHz, D₂O) δ: 4.01 (ddd, 1H, J= 7.5, 6.0, 2.8 Hz), 3.87–3.77 (m, 2H), 3.76–3.71 (m, 1H), 3.71–3.64 (m, 2H), 3.56 (dd, 1H, J= 14.7, 7.5 Hz)

¹³C NMR (101 MHz, D₂O) δ: 160.9, 150.8, 150.4, 82.6, 72.2, 72.0, 70.3, 62.3, 44.5

(2R,3R,4R)-5,5-bis(propylthio)pentane-1,2,3,4-tetraol (6)⁷²



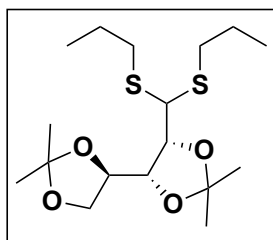
| Raw formula | Molecular mass | Aspect | Yield |
|---|----------------------------|-------------|-------|
| C ₁₁ H ₂₄ O ₄ S ₂ | 284.11 g.mol ⁻¹ | White solid | 47% |

n-propanethiol (14 mL, 2.2 eq, 0.15 mol) was added to a solution of D-ribose (10 g, 1.0 eq, 0.067 mol) in 37% HCl (10 mL) at 0°C. The solution was stirred at room temperature for 1h30. Then, water (80 mL) was added and the solution was stirred for few minutes until a white precipitate appeared. The precipitate was filtrated and washed by water (3 x 50 mL) and hexane (3 x 50 mL). The product was dried under vacuum and **6** was obtained as a white solid.

¹H NMR (400 MHz, CDCl₃) δ: 4.20-4.19 (m, 1H), 3.98-3.85 (m, 5H), 3.52 (s, 4H), 2.75-2.61 (m, 4H), 1.68-1.59 (m, 4H), 1.00 (td, 6H, J= 7.3 Hz, 1.3 Hz)

¹³C NMR (101 MHz, CDCl₃) δ: 74.7, 73.3, 72.7, 63.3, 55.7, 33.9, 33.8, 23.1, 22.9, 13.7, 13.6

(4*R*,4'*R*,5*R*)-5-(bis(propylthio)methyl)-2,2,2',2'-tetramethyl-4,4'-bi(1,3-dioxolane) (7)⁷²



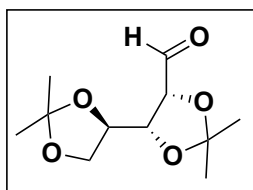
| Raw formula | Molecular mass | Aspect | Yield |
|---|----------------------------|---------------|-------|
| C ₁₇ H ₃₂ O ₄ S ₂ | 364.17 g.mol ⁻¹ | Colorless oil | 53 % |

6 (5.0 g, 1.0 eq, 18 mmol) was dissolved in acetone (50 mL) and 2,2-dimethoxypropane (43.11 mL, 20 eq, 352 mmol) and *p*-toluenesulfonic acid (670 mg, 0.2 eq, 3.52 mmol) were added. The mixture was stirred at room temperature for 2h30. Aqueous 5% Na₂CO₃ was added and the product was extracted with DCM. The organic layer was dried over MgSO₄ and concentrated under vacuum. The product was purified by column chromatography (hexane/TBME 10/1) afforded **7** as a colorless oil.

¹H NMR (500 MHz, CDCl₃) δ: 4.63-4.59 (m, 1H), 4.52 (dd, 1H, J= 6.5 Hz, 4.2 Hz), 4.23-4.22 (d, 1H, J= 4.3 Hz), 4.13-4.06 (m, 2H), 3.88 (dd, 1H, J= 8.7 Hz, 5.7 Hz), 2.78-2.57 (m, 4H), 1.71-1.47 (m, 4H), 1.47 (s, 3H), 1.39 (s, 3H), 1.31 (s, 6H), 0.98 (td, 6H, J= 7.3 Hz, 0.5 Hz)

¹³C NMR (126 MHz, CDCl₃) δ: 109.8, 109.2, 81.5, 79.1, 73.3, 68.4, 51.0, 33.4, 32.9, 26.9, 26.7, 25.5, 24.9, 22.9, 22.5, 13.9, 13.8

(4*R*,4'*R*,5*R*)-2,2,2',2'-tetramethyl-[4,4'-bi(1,3-dioxolane)]-5-carbaldehyde (8)⁷²



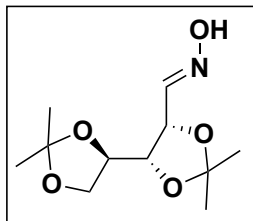
| Raw formula | Molecular mass | Aspect | Yield |
|--|----------------------------|---------------|-------|
| C ₁₁ H ₁₈ O ₅ | 230.12 g.mol ⁻¹ | Colorless oil | 76 % |

To **7** (2.60 g, 1.0 eq, 7.13 mmol) in a 10/1 mixture of acetone/H₂O (20/2 mL) was added at 0°C NaHCO₃ (2.70 g, 4.5 eq, 32 mmol) and iodine (3.62 g, 2 eq, 14.3 mmol). The solution was stirred at room temperature overnight. Additional amounts of iodine (1.81 g, 1.0 eq, 7.13 mmol) and NaHCO₃ (0.60 g, 1.0 eq, 7.13 mmol) were added to the mixture to reach complete conversion of **7**. After 4h stirring, aqueous 30% Na₂S₂O₃ was added and the mixture was stirred for 5 minutes. The product was then extracted with EtOAc and the organic layer was dried over MgSO₄ and concentrated under vacuum. The compound was purified by column chromatography (hexane/ EtOAc 20%) and **8** was obtained as a colorless oil.

¹H NMR (500 MHz, CDCl₃) δ: 9.71 (d, 1H, J= 2.0 Hz), 4.60 (dd, 1H, J= 6.8 Hz, 2.0 Hz), 4.32-4.27 (m, 1H), 4.11-4.07 (m, 2H), 3.92-3.88 (m, 1H), 1.53 (s, 3H), 1.40 (s, 3H), 1.37 (s, 3H), 1.30 (s, 3H)

¹³C NMR (126 MHz, CDCl₃) δ: 197.8, 111.4, 110.3, 81.9, 78.9, 73.7, 67.6, 27.5, 26.8, 25.6, 25.2

(E)-2,2,2',2'-tetramethyl-[4,4'-bi(1,3-dioxolane)]-5-carbaldehyde oxime (9)⁷²



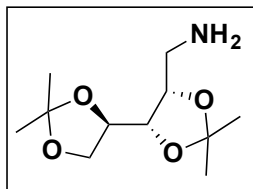
| Raw formula | Molecular mass | Aspect | Yield |
|---|----------------------------|---------------|-------|
| C ₁₁ H ₁₉ NO ₅ | 245.13 g.mol ⁻¹ | Colorless oil | 77 % |

NH₂OH.HCl (4.07 g, 4.5 eq, 0.59 mol) was added in EtOH/H₂O (40/4 mL). NaHCO₃ was added (4.37 g, 4.0 eq, 0.52 mol) and the mixture was stirred at room temperature for 30 min. The resulting solution was directly added to **8** (3.0 g, 1.0 eq, 0.13 mol) and the mixture was stirred 2h at room temperature. Excess solvent was removed under vacuum, water was added to the mixture and the product was extracted by Et₂O. The organic layer was dried over MgSO₄ and concentrated under vacuum. The product was purified by column chromatography (hexane/EtOAc 30%) to give **9** as a colorless oil.

¹H NMR (400 MHz, CDCl₃) δ: major stereoisomer E: 8.20 (brs, 1H), 7.47 (d, 1H, J= 7.0 Hz), 4.77 (dd, 1H, J= 7.0 Hz, 5.9 Hz), 4.11-4.07 (m, 3H), 3.95-3.88 (m, 1H), 1.47 (s, 3H), 1.40 (s, 3H), 1.37 (s, 3H), 1.32 (s, 3H)

¹³C NMR (101 MHz, CDCl₃) δ: major stereoisomer E: 147.9, 110.2, 110.1, 78.7, 75.3, 73.6, 67.6, 27.8, 26.9, 25.5, 25.4

((4*S*,4'*R*,5*S*)-2,2,2',2'-tetramethyl-[4,4'-bi(1,3-dioxolan)]-5-yl)methanamine (10)⁷²



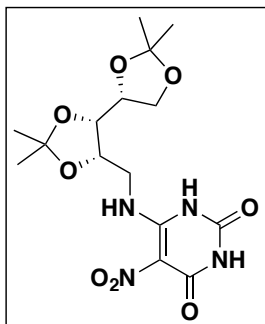
| Raw formula | Molecular mass | Aspect | Yield |
|---|----------------------------|-----------|-------|
| C ₁₁ H ₂₁ NO ₄ | 231.15 g.mol ⁻¹ | Brown oil | 76 % |

To **9** (1.70 g, 1.0 eq, 6.93 mmol) in dry THF (35 mL) was added LiAlH₄ (1.32 g, 5.0 eq, 34.7 mmol). The solution was heated at reflux for 4h. After cooling in ice bath, MgSO₄·7H₂O (30 g) was slowly added and the suspension was stirred during 1h. The mixture was filtered on MgSO₄, washed by MTBE and concentrated under vacuum to give **10** as a colorless oil.

¹H NMR (500 MHz, CDCl₃) δ: 4.25-4.22 (m, 1H), 4.12-4.04 (m, 2H), 4.01-3.99 (m, 1H), 3.90 (dd, 1H, J= 8.1 Hz, 5.2 Hz), 3.07 (dd, 1H, J= 13.2 Hz, J= 5.2 Hz), 2.94 (dd, 1H, J= 13.2 Hz, 7.8 Hz), 2.51 (brs, 2H), 1.40-1.39 (m, 6H), 1.33 (m, 6H)

¹³C NMR (126 MHz, CDCl₃) δ: 109.9, 108.5, 79.8, 78.4, 73.3, 68.2, 41.6, 28.2, 26.9, 25.6 (2C)

5-nitro-6-(((4*S*,4'*R*,5*S*)-2,2,2',2'-tetramethyl-[4,4'-bi(1,3-dioxolan)]-5-yl)methyl)amino)pyrimidine-2,4(1*H*,3*H*)-dione (11)



| Raw formula | Molecular mass | Aspect | Yield |
|---|----------------------------|--------------|-------|
| C ₁₅ H ₂₂ N ₄ O ₈ | 386.14 g.mol ⁻¹ | Yellow solid | 93 % |

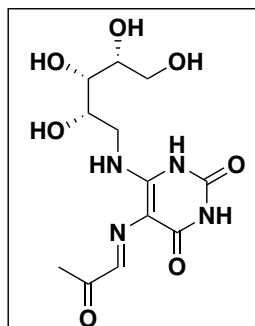
A solution of **10** (95 mg, 1.2 eq, 0.496 mmol) and triethylamine (70 μ L, 1.2 eq, 0.496 mmol) in anhydrous DCM (1 mL) was added to a solution of **3** (96 mg, 1.0 eq, 0.413 mmol) in anhydrous DCM (1 mL). The mixture was stirred at room temperature (under argon) during 12h. The solvent was removed under vacuum and the product was purified by column chromatography (DCM/MeOH 8%) to give **11** as a yellow solid.

MS (ESI), m/z : 387.1 [M+H]⁺

¹H NMR (400 MHz, CDCl₃) δ : 11.12 (brs, 1H), 9.75 (brt, 1H, J= 5.8 Hz), 9.68 (brs, 1H), 4.38-4.34 (m, 1H), 4.14-4.05 (m, 3H), 4.02-3.99 (m, 1H), 3.90-3.86 (m, 1H), 3.69-3.64 (m, 1H), 1.42 (s, 3H), 1.39 (s, 3H), 1.36 (s, 3H), 1.29 (s, 3H)

¹³C NMR (101 MHz, CDCl₃) δ : 161.5, 160.8, 158.1, 111.6, 110.4, 108.7, 78.8, 75.4, 73.2, 68.2, 40.2, 28.1, 26.6, 25.8, 25.6

5-(((E)-2-oxopropylidene)amino)-6-(((2S,3S,4R)-2,3,4,5-tetrahydroxypentyl)amino)pyrimidine-2,4(1H,3H)-dione (12 or 5-OP-RU)

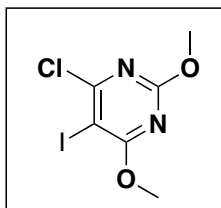


| Raw formula | Molecular mass | Aspect |
|---|----------------------------|------------------------|
| C ₁₂ H ₁₈ N ₄ O ₇ | 330.12 g.mol ⁻¹ | Brown solution in DMSO |

12a: 5-OP-RU was synthesized from **5** without purification and isolation because of its chemical instability. A stock solution (1 mL) of freshly synthesized **5** was prepared at 10 mM in DMSO. Methylglyoxal solution (40% in H₂O) was diluted in DMSO to obtain a solution at 50 mM and 1 mL of this solution was added to 1 mL of 10 mM solution of **5**. The mixture was allowed to react at room temperature for 48h to give a stock solution of **12a** at 5 mM. The conversion of **5** to **12a** was monitored by UPLC-MS by analyzing aliquots. The solution of **12a** was aliquoted (5µL aliquots) and freezed at -80°C for further utilization in biological assays. For each use of these aliquots, **12a** was quickly diluted to the desired concentrations and rapidly added on cells to limit as much as possible degradation of the molecule.

12b: 5-OP-RU was synthesized from **5** without purification and isolation because of its chemical instability. Stock solution (1 mL) of freshly synthesized **5** was prepared at 10 mM in water. The solution of **5** was aliquoted (5µL aliquots) and freezed at -80°C for further utilization in biological assays. Methylglyoxal solution (40% in H₂O) was diluted in water to obtain a solution at 50 mM and 5 µL of this solution was added to 5 µL aliquot of 10 mM solution of **5**. The solution was diluted to desired concentrations and quickly added on cells to avoid as much as possible degradation of the compound.

4-chloro-5-iodo-2,6-dimethoxypyrimidine (14)⁷⁸



| Raw formula | Molecular mass | Aspect | Yield |
|--|----------------------------|----------------|-------|
| C ₆ H ₆ ClIN ₂ O ₂ | 299,92 g.mol ⁻¹ | Poudre blanche | 63% |

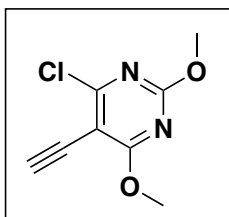
To a solution of 6-chloro-2,4-dimethoxypyrimidine (0.600 g, 1.0 eq, 3.44 mmol) in acetonitrile (30 ml) was added N-iodosuccinimide (0.929 g, 1.2 eq, 4.13 mmol) followed by 5 mL of acetic acid and 1 mL of acetic anhydride. The mixture was heated under reflux overnight. After cooling to room temperature, the mixture was neutralized by adding aqueous 5% Na₂CO₃ and the product was extracted by DCM. The organic layer was dried over MgSO₄, filtered and concentrated under vacuum. The product was purified by column chromatography (hexane/EtOAc 10%) to obtain **14** as a white solid.

MS (ESI), m/z (%): 300.98 [M+H]⁺, 302.91 [M+H+2]⁺

¹H NMR (400 MHz, CDCl₃) δ: 4.04 (s, 3H), 3.99 (s, 3H)

¹³C NMR (101 MHz, CDCl₃) δ: 171.0, 164.9, 164.8, 70.6, 56.1, 55.8

4-chloro-5-ethynyl-2,6-dimethoxypyrimidine (15)



| Raw formula | Molecular mass | Aspect | Yield |
|---|----------------------------|-------------|-------|
| C ₈ H ₇ ClN ₂ O ₂ | 198.02 g.mol ⁻¹ | Beige solid | 57% |

The synthesis was adapted from a described protocol of a different molecule¹¹⁵

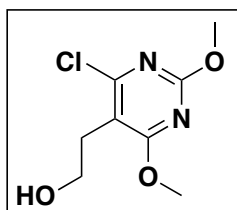
To **14** (1.96 g, 1.0 eq, 6.54 mmol) in a 1:1 mixture of diisopropylethylamine (4mL) and THF (4mL) was added under argon atmosphere Cu(I) iodide (1,24 g, 1.0 eq, 6.54 mmol), bis(triphenylphosphine)palladium dichloride (0.46 g, 0.1 eq, 0.65 mmol) and ethynyltrimethylsilane (2.79 mL, 3.0 eq, 19.6 mmol). The tube was sealed and the reaction stirred at 70°C overnight. After completion, the mixture was filtered on celite and washed with DCM. Water was added and the product was extracted by DCM. The organic layer was washed by saturated aqueous NH₄Cl, dried over MgSO₄ and concentrated under vacuum to give a brown oil (1.12 g of crude product was obtained). TMS removal was done by dissolving the crude intermediate (1.12 g, 1.0 eq, 4.1 mmol) in MeOH (5 mL) followed by K₂CO₃ addition (0.63 g, 1.1 eq, 4.55 mmol) at 0°C. The mixture was stirred at room temperature during 15 min. Water was added to the mixture and the product was extracted by DCM. The organic layer was dried over MgSO₄ and concentrated under vacuum The product was purified by column chromatography (hexane/EtOAc 10%) to get **15** as a beige solid.

MS (ESI), m/z (%): 198.8 [M+H]⁺, 201.2 [M+H+2]⁺

¹H NMR (400 MHz, CDCl₃) δ: 4.06 (s, 3H), 4.02 (s, 3H), 3.59 (s, 1H)

¹³C NMR (101 MHz, CDCl₃) δ: 172.3, 163.5, 162.9, 98.2, 87.7, 73.7, 55.9, 55.6

2-(4-chloro-2,6-dimethoxypyrimidin-5-yl)ethan-1-ol (16)



| Raw formula | Molecular mass | Aspect | Yield |
|--|----------------------------|---------------|-------|
| C ₈ H ₁₁ ClN ₂ O ₃ | 218.05 g.mol ⁻¹ | Colorless oil | 52% |

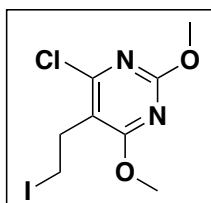
Bis(pinacolato)diboron (76 mg, 3.0 eq, 0.30 mmol) was introduced in a sealed tube with cesium carbonate (131 mg, 4.0 eq, 0.4 mmol) under argon atmosphere. Dry acetonitrile (1 mL) was added followed by a **15** (20 mg, 1.0 eq, 0.10 mmol) solution in acetonitrile (1 mL) and MeOH (20 μ L, 5.0 eq, 0.5 mmol). The tube was sealed and the reaction was heated at 100°C overnight. After cooling, the solvent was removed under vacuum and the product was diluted in 5 mL of MeOH. 3M sodium hydroxide (1 mL) and hydrogen peroxide (30% w/w in H₂O; 1 mL) were added to the mixture. The reaction was stirred for 2h at room temperature. Then, H₂O/DCM extraction was done and the organic layer was dried over MgSO₄ and concentrated under vacuum. The small amount of aldehyde formed was reduced using excess sodium borohydride in MeOH (5 mL). The mixture was quenched by saturated aqueous NH₄Cl and the product was extracted by DCM. The organic layer was dried over MgSO₄ and concentrated under vacuum. The product was purified by column chromatography (hexane/EtOAc 50%) to give **16** as a colorless oil.

MS (ESI), *m/z* (%): 219.0 [M+H]⁺, 221.0 [M+H+2]⁺

¹H NMR (400 MHz, CDCl₃) δ : 3.99 (s, 3H), 3.96 (s, 3H), 3.78 (t, 2H, J = 6.9 Hz), 2.91 (t, 2H, J = 6.9 Hz), 1.69 (brs, 1H)

¹³C NMR (101 MHz, CDCl₃) δ : 170.6, 162.9, 160.6, 109.5, 61.0, 55.0, 53.3, 29.3

4-chloro-5-(2-iodoethyl)-2,6-dimethoxypyrimidine (17)



| Raw formula | Molecular mass | Aspect | Yield |
|---|----------------------------|-------------|-------|
| C ₈ H ₁₀ ClIN ₂ O ₂ | 327.95 g.mol ⁻¹ | White solid | 74% |

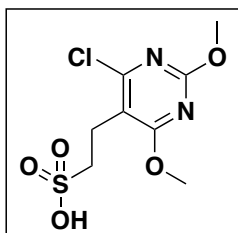
To **16** (97 mg, 1.0 eq, 0.45 mmol) in dry THF (3 mL) was added triphenylphosphine (175 mg, 1.5 eq, 0.67 mmol) and imidazole (60 mg, 2.0 eq, 0.89 mmol). Iodine solution (169 mg, 1.5 eq, 0.67 mmol) in THF (3 mL) was added dropwise. Completion of the reaction was obtained after 30 min of stirring at room temperature. THF was evaporated under vacuum and the mixture was quenched with water. The product was extracted by DCM and the organic layer was dried over MgSO₄ and concentrated under vacuum. The product was purified by column chromatography (hexane/EtOAc 10/1) to get **17** as a white solid.

MS (ESI), *m/z* (%): 329.0 [M+H]⁺, 331.0 [M+H+2]⁺

¹H NMR (400 MHz, CDCl₃) δ : 4.00 (s, 3H), 3.98 (s, 3H), 3.26-3.17 (m, 4H)

¹³C NMR (101 MHz, CDCl₃) δ : 170.1, 163.0, 160.3, 112.0, 55.4, 55.1, 30.2, 0.7

2-(4-chloro-2,6-dimethoxypyrimidin-5-yl)ethane-1-sulfonic acid (18)



| Raw formula | Molecular mass | Aspect | Yield |
|--|----------------------------|-------------|-------|
| C ₈ H ₁₁ ClN ₂ O ₂ S | 282.01 g.mol ⁻¹ | White solid | 88% |

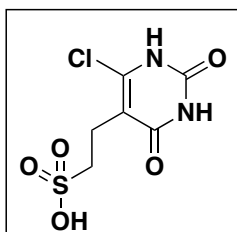
To **17** (95 mg, 1.0 eq, 0.29 mmol) in a 1/1 mixture of acetone/water (3/3 mL) was added excess sodium thiosulfate. The reaction was heated under reflux for 4h. Acetone was removed under vacuum and the resulting mixture was partially solubilized in MeOH. The remaining salts were filtered and washed with few volumes of MeOH. The filtrate was concentrated under vacuum to give **18** as a white solid.

MS (ESI), *m/z*: 283.1 [M+H]⁺, 285.1 [M+H+2]⁺

¹H NMR (500 MHz, CD₃OD) δ : 4.04 (s, 3H), 3.97 (s, 3H), 3.14-3.10 (m, 2H), 2.94-2.91 (m, 2H)

¹³C NMR (126 MHz, CD₃OD) δ : 171.7, 164.3, 161.0, 111.6, 55.7, 55.5, 50.0, 22.7

2-(6-chloro-2,4-dioxo-1,2,3,4-tetrahydropyrimidin-5-yl)ethane-1-sulfonic acid (19)



| Raw formula | Molecular mass | Aspect | Yield |
|---|----------------------------|-------------|-------|
| C ₆ H ₇ ClN ₂ O ₅ S | 253.98 g.mol ⁻¹ | White solid | 65% |

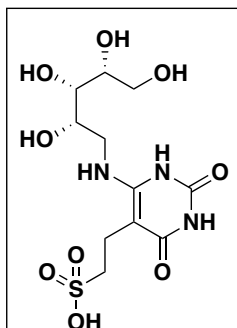
18 (50 mg, 1.0 eq, 0.18 mmol) was dissolved in a 1/1 mixture of 37% HCl/AcOH (1 mL of each) and the mixture was heated at reflux during 2.5h. The mixture was concentrated under vacuum, dissolved in few volumes of MeOH and precipitated from excess Et₂O. The precipitate was filtered, washed three times by Et₂O and dried under vacuum to give **19** as a white solid.

MS (ESI), m/z (%): 255.0 [M+H]⁺, 257.0 [M+H+2]⁺

¹H NMR (500 MHz, D₂O) δ: 3.06 (m, 2H), 2.90 (m, 2H)

¹³C NMR (126 MHz, D₂O) δ: 164.7, 151.2, 143.8, 109.1, 48.0, 20.9

2-(2,4-dioxo-6-(((2S,3S,4R)-2,3,4,5-tetrahydroxypropyl)amino)-1,2,3,4-tetrahydropyrimidin-5-yl)ethane-1-sulfonic acid (13)



| Raw formula | Molecular mass | Aspect | Yield |
|---|------------------------------|-------------|-------|
| C ₁₁ H ₁₉ ClN ₃ O ₉ S | 369.0842 g.mol ⁻¹ | White solid | 22% |

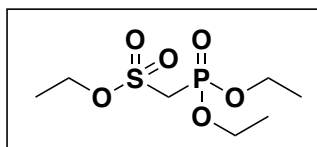
To **19** (20 mg, 1.0 eq, 0.71 mmol) in EtOH (4mL) was added **12** (110 mg, 7.0 eq, 0.48 mmol). The tube was sealed and the mixture heated at 130°C for 48h. The solvent was removed under vacuum and the product was solubilized in few volumes of MeOH and precipitated by adding excess Et₂O. The precipitate was filtered, washed with Et₂O and the resulting beige powder was dried under vacuum before adding a 10/1 mixture of TFA/H₂O (1/0.1 mL). The mixture was allowed to react at room temperature overnight. The mixture was concentrated under vacuum and directly purified by preparative C18 RP-HPLC using the following conditions: Solvent A: H₂O + 0.1% formic acid; Solvent B: ACN + 0.1% formic acid. Gradient of 25 min starting with 100% A for 5 min, then 5% B for 5 min and then gradual increase of B to reach 100% B at 20 min followed by 5 min with 100% B. The product was lyophilized to give **13** as a white solid.

HR-MS (ESI), *m/z* (%): 370.0921 [M+H]⁺

¹H NMR (500 MHz, D₂O) δ : 3.99-3.96 (m, 1H), 3.87-3.80 (m, 2H), 3.73 (t, 1H, J= 6.3 Hz), 3.67 (dd, 1H, J= 11.7 Hz, 6.7 Hz), 3.63 (dd, 1H, J= 14.9 Hz, 2.9 Hz), 3.51 (dd, 1H, J= 14.9 Hz, 7.3 Hz), 3.0-2.87 (m, 2H), 2.74-2.71 (m, 2H)

¹³C NMR (126 MHz, D₂O) δ : 164.84, 151.4, 144.2, 109.0, 72.8, 71.8, 67.8, 62.5, 48.0, 41.0, 20.9

Ethyl (diethoxyphosphoryl)methanesulfonate (20)



| Raw formula | Molecular mass | Aspect | Yield |
|--|----------------------------|------------|-------|
| C ₇ H ₁₇ O ₆ PS | 260.05 g.mol ⁻¹ | Yellow oil | 63% |

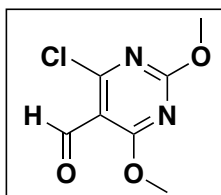
To a solution of ethyl methanesulfonate (1.30 g, 1.8 eq, 10 mmol) in dry THF (13 ml) was added at -78°C, *n*-butyllithium (2.5 M in hexane, 6.4 mL, 1.1 eq, 11.6 mmol) and the mixture was stirred at the same temperature for 30 min. Diethyl chlorophosphate was added (0.84 mL, 1.0 eq 5.79 mmol) dropwise. The mixture was stirred for 30 minutes at -78°C and then at -50°C for 1h. The mixture was quenched by saturated aqueous NH₄Cl and the product was extracted by DCM. The organic layer was dried over MgSO₄ and concentrated under vacuum. The product was purified by column chromatography (hexane/EtOAc 60%) to give **20** as a yellow oil.

MS (ESI), *m/z* (%): 260.6 [M+H]⁺, 259.2 [M-H]⁻

¹H NMR (400 MHz, CDCl₃) δ : 4.39 (q, 2H, J= 7.1 Hz), 4.25-4.18 (m, 4H), 3.70 (d, 2H, J= 17.2 Hz), 1.41 (t, 3H, J= 7.1 Hz), 1.35, (td, 6H, J= 7.0 Hz, 0.6 Hz)

¹³C NMR (101 MHz, CDCl₃) δ : 68.5, 63.9, 63.8, 48.0 (d, J = 140.2 Hz), 16.4, 16.3, 15.1

4-chloro-2,6-dimethoxypyrimidine-5-carbaldehyde (21**)**¹¹⁶



| Raw formula | Molecular mass | Aspect | Yield |
|---|----------------------------|--------------|-------|
| C ₇ H ₇ ClN ₂ O ₃ | 202.01 g.mol ⁻¹ | Yellow solid | 64 % |

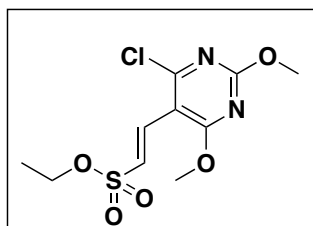
6-chloro-2,4-dimethoxypyrimidine (3.0 g, 1.0 eq, 170 mmol) was dissolved in dry THF (30 mL) and the solution was cooled to -78°C. *n*-butyllithium (2.5 M in hexane, 8.25 mL, 1.2 eq, 206 mmol) was added and the reaction was stirred during 30 min. DMF (3.16 mL, 2.4 eq, 408 mmol) was added and the mixture was stirred for 2h at -78°C. 2N HCl (50 mL) was added to quench the mixture and the mixture was allowed to warm up while stirring for 15 min. The product was extracted by Et₂O and the organic layer was dried over MgSO₄ and concentrated under vacuum. The compound was purified by column chromatography (hexane/EtOAc 20%) to afford **21** as a yellow solid.

MS (ESI), *m/z* (%): 203.1 [M+H]⁺, 205.2 [M+H+2]⁺

¹H NMR (400 MHz, CDCl₃) δ : 10.30 (brs, 1H), 4.12 (s, 3H), 4.08 (s, 3H)

¹³C NMR (101 MHz, CDCl₃) δ : 185.5, 171.9, 165.3, 165.2, 109.2, 56.3, 55.7

Ethyl-(E)-2-(4-chloro-2,6-dimethoxypyrimidin-5-yl)ethene-1-sulfonate (22)



| Raw formula | Molecular mass | Aspect | Yield |
|---|----------------------------|-------------|-------|
| C ₁₀ H ₁₃ ClN ₂ O ₅ S | 308.02 g.mol ⁻¹ | White solid | 69% |

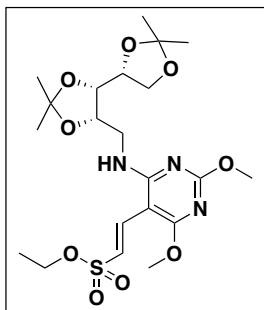
20 (403 mg, 1.2 eq, 1.55 mmol) was dissolved in dry THF (3 mL) and *t*-BuOK (174 mg, 1.2 eq, 1.55 mmol) was added. The mixture was stirred for 30 minutes at room temperature. It was then cooled to 0°C and a solution of **21** (260 mg, 1.0 eq, 1.29 mmol) in THF (3 mL) was added dropwise. The mixture was stirred during 30 minutes. EtOAc was added and the organic layer was washed three times by saturated aqueous NaCl. The product was purified by column chromatography (hexane/EtOAc 20%) and **22** was obtained as a white solid.

MS (ESI), *m/z* (%): 309.2 [M+H]⁺, 311.2 [M+H+2]⁺

¹H NMR (400 MHz, CDCl₃) δ: 7.78 (d, 1H, J= 15.6 Hz), 7.15 (d, 1H, J= 15.6 Hz), 4.22 (q, 2H, J= 7.1 Hz), 4.13 (s, 3H), 4.05 (s, 3H), 1.40 (t, 3H, J= 7.1 Hz)

¹³C NMR (101 MHz, CDCl₃) δ: 170.2, 163.9, 163.4, 133.6, 125.5, 106.0, 67.0, 56.1, 55.8, 15.0

Ethyl-(E)-2-(2,4-dimethoxy-6-(((4*S*,4'*R*,5*S*)-2,2,2',2'-tetramethyl-[4,4'-bi(1,3-dioxolan)]-5-yl)methyl)amino)pyrimidin-5-yl)ethene-1-sulfonate (23**)**



| Raw formula | Molecular mass | Aspect | Yield |
|---|----------------------------|-------------|-------|
| C ₂₁ H ₃₃ N ₃ O ₉ S | 503.19 g.mol ⁻¹ | Brown paste | 66% |

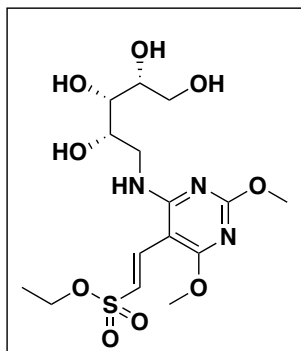
To **22** (200 mg, 1.0 eq, 0.65 mmol) in dry toluene (4 mL) was added under argon atmosphere Pd(dba)₃ (59 mg, 0.1 eq, 0.06 mmol), xantphos (38 mg, 0.1 eq, 0.06 mmol), Cs₂CO₃ (423 mg, 2.0 eq, 1.30 mmol) and **12** (300 mg, 2.0 eq, 1.30 mmol). The solution was stirred at room temperature overnight. Toluene was removed under vacuum and H₂O/DCM extraction was performed. The organic layer was dried over MgSO₄ and concentrated under vacuum. The product was purified by column chromatography (hexane/AcOEt gradient 20% to 30% EtOAc) and it was obtained as a brown paste.

MS (ESI), *m/z* (%): 504.4 [M+H]⁺, 502.5 [M-H]⁻

¹H NMR (400 MHz, CDCl₃) δ: 7.33 (d, 1H, J= 15.2 Hz), 6.87 (d, 1H, J= 15.2 Hz), 5.91 (brt, 1H, J= 5.7 Hz), 4.43-4.38 (m, 1H), 4.25-3.91 (m, 13H), 3.69-3.63 (m, 1H), 1.45 (s, 3H), 1.41-1.40 (m, 6H), 1.37 (t, 3H, J= 7.1 Hz), 1.32 (s, 3H)

¹³C NMR (101 MHz, CDCl₃) δ: 170.4, 165.0, 163.1, 132.7, 119.4, 110.8, 109.0, 88.9, 78.5, 75.3, 73.3, 68.2, 66.2, 54.9, 54.6, 41.0, 28.1, 26.7, 25.6, 25.5, 15.0

Ethyl-(E)-2-(2,4-dimethoxy-6-(((2S,3S,4R)-2,3,4,5-tetrahydroxypentyl)amino)pyrimidin-5-yl)ethene-1-sulfonate (24)



| Raw formula | Molecular mass | Aspect | Yield |
|---|----------------------------|-------------|-------|
| C ₁₅ H ₂₅ N ₃ O ₉ S | 423.13 g.mol ⁻¹ | Brown paste | 47% |

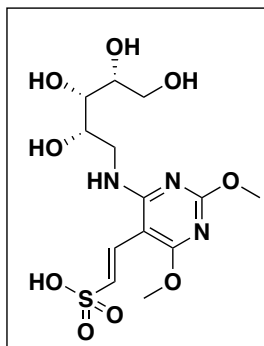
23 (138 mg, 1.0 eq, 0.27 mmol) was dissolved in acetonitrile (3 mL) and a 10/1 mixture of TFA/H₂O (3/0.3 mL) was added at 0°C. The solution was stirred at room temperature for 2h. 5% aqueous Na₂CO₃ was added and the product was extracted by DCM. The organic layer was dried over MgSO₄ and concentrated under vacuum. The product was purified by column chromatography (DCM/MeOH gradient from 5% to 10% MeOH) to give **24** as a brown paste.

MS (ESI), m/z (%): 424.2 [M+H]⁺

¹H NMR (400 MHz, CD₃OD) δ: 7.56 (d, 1H, J= 15.2 Hz), 6.89 (d, 1H, J= 15.2 Hz), 4.17 (q, 2H, J= 7.1 Hz), 4.04 (s, 3H), 3.96-3.92 (m, 4H), 3.86-3.78 (m, 3H), 3.71-3.58 (m, 3H), 1.35 (t, 3H, J= 7.1 Hz)

¹³C NMR (101 MHz, CD₃OD) δ: 171.5, 166.2, 165.0, 134.7, 120.1, 89.7, 74.3, 73.9, 72.8, 67.7, 64.2, 55.3, 55.0, 45.6, 15.2

(E)-2-(2,4-dimethoxy-6-(((2S,3S,4R)-2,3,4,5-tetrahydroxypentyl)amino)pyrimidin-5-yl)ethene-1-sulfonic acid (25)



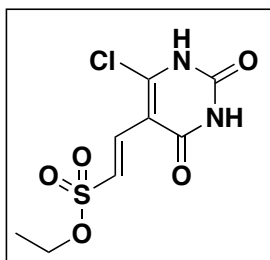
| Raw formula | Molecular mass | Aspect | Yield |
|---|----------------------------|--------------|-------|
| C ₁₃ H ₂₁ N ₃ O ₉ S | 395.10 g.mol ⁻¹ | Purple solid | 40% |

To **24** (22 mg, 1.0 eq, 0.052 mmol) in acetone was added potassium iodide (10 mg, 1.2 eq, 0.062 mmol) and the mixture was stirred at reflux for 6h. The solvent was removed under vacuum and the product was dissolved in a few volumes of MeOH and precipitated from Et₂O. The precipitate was filtered and washed several times by Et₂O. **25** was obtained as a purple solid after drying under vacuum.

MS (ESI), *m/z* (%): 395.8 [M+H]⁺

¹H NMR (400 MHz, CD₃OD) δ : 7.10 (d, 1H, J= 15.5 Hz), 6.94 (d, 1H, J= 15.4 Hz), 4.00-3.96 (m, 1H), 3.90 (s, 3H), 3.88 (s, 3H), 3.85-3.73 (m, 3H), 3.68-3.60 (m, 2H), 3.55-3.49 (s, 1H)

Ethyl-(E)-2-(6-chloro-2,4-dioxo-1,2,3,4-tetrahydropyrimidin-5-yl)ethene-1-sulfonate (26)



| Raw formula | Molecular mass | Aspect | Yield |
|---|----------------------------|--------------------|-------|
| C ₈ H ₉ ClN ₂ O ₅ S | 279.99 g.mol ⁻¹ | Light yellow solid | 66% |

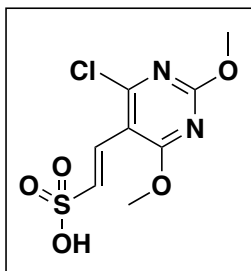
To **22** (100 mg, 1.0 eq, 0.33 mmol) in acetonitrile (5 mL) was added sodium iodide (487 mg, 10 eq, 3.25 mmol) and trimethylsilyl chloride (0.41 mL, 10 eq, 3.25 mmol). The mixture was stirred at room temperature for 30 minutes. Water was added to quench the reaction and the product was extracted by EtOAc. The organic layer was dried over MgSO₄ and concentrated under vacuum. The product was purified by column chromatography (DCM/MeOH 10%) to give **26** as a light yellow solid.

MS (ESI), *m/z*: 279.4 [M-H]⁻

¹H NMR (400 MHz, CD₃OD) δ: 7.65 (d, 1H, J= 14.9 Hz), 7.36 (d, 1H, J= 14.9 Hz), 4.12 (q, 2H, J= 7.1 Hz), 1.34 (t, 3H, J= 7.1 Hz)

¹³C NMR (101 MHz, CD₃OD) δ: 165.6, 164.2, 158.0, 139.1, 117.5, 101.9, 67.4, 15.2

(E)-2-(4-chloro-2,6-dimethoxypyrimidin-5-yl)ethene-1-sulfonic acid (27)



| Raw formula | Molecular mass | Aspect | Yield |
|---|----------------------------|-------------|--------------|
| C ₈ H ₉ ClN ₂ O ₅ S | 279.99 g.mol ⁻¹ | White solid | Quantitative |

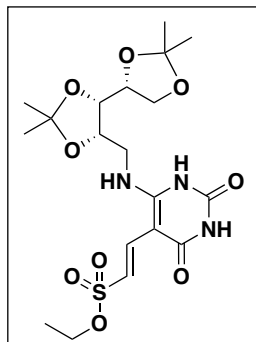
To **22** (200 mg, 1.0 eq, 0.65 mmol) in acetone (5 mL) was added potassium iodide (323 mg, 3.0 eq, 1.95 mmol) and the mixture was stirred at reflux for 3h. The formed precipitate was filtered and washed several times by acetone before being dried under vacuum to give **27** as a white solid.

MS (ESI), *m/z*: 281.2 [M+H]⁺

¹H NMR (400 MHz, D₂O) δ : 7.34 (d, 1H, J= 15.8 Hz), 7.27 (d, 1H, J= 15.8 Hz), 4.09 (s, 3H), 4.01 (s, 3H)

¹³C NMR (101 MHz, D₂O) δ : 169.7, 162.8, 160.8, 132.5, 125.4, 106.5, 55.8, 55.6

ethyl-(E)-2-(2,4-dioxo-6-(((4*S*,4'*R*,5*S*)-2,2,2',2'-tetramethyl-[4,4'-bi(1,3-dioxolan)]-5-yl)methyl)amino)-1,2,3,4-tetrahydropyrimidin-5-yl)ethene-1-sulfonate (28)



| Raw formula | Molecular mass | Aspect | Yield |
|---|----------------------------|-------------|-------|
| C ₁₉ H ₂₉ N ₃ O ₉ S | 475.16 g.mol ⁻¹ | Brown paste | 15% |

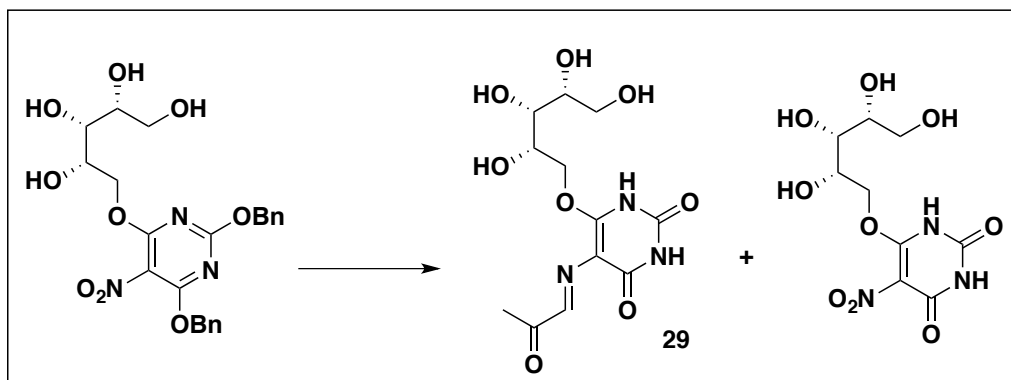
To **26** (50 mg, 1.0 eq, 0.18 mmol) in dry DMF was added **12** (83 mg, 2.0 eq, 0.36 mmol) and triethylamine (50 μ L, 2.0 eq, 0.36 mmol). The mixture was heated at 80°C for 3h. DMF was removed under vacuum and the product was directly purified by column chromatography (DCM/MeOH 2% to 10% gradient). Compound **28** was obtained as a brown paste.

MS (ESI), m/z : 476.6 [M+H]⁺

¹H NMR (400 MHz, CDCl₃) δ : 8.83 (brs, 1H), 7.45 (d, 1H, J= 14.5 Hz), 7.29 (d, 1H, J= 14.5 Hz), 6.70 (brt, 1H, J= 6.1 Hz), 4.43-4.39 (m, 1H), 4.19-4.11 (m, 5H), 3.98-3.88 (m, 2H), 3.72-3.65 (m, 1H), 1.51 (s, 3H), 1.45 (s, 3H), 1.39-1.33 (m, 9H)

¹³C NMR (101 MHz, CDCl₃) δ : 162.0, 154.8, 149.4, 133.3, 116.2, 110.9, 110.3, 84.6, 78.0, 76.6, 73.3, 68.1, 66.4, 43.4, 27.8, 26.8, 25.4, 25.3, 15.0

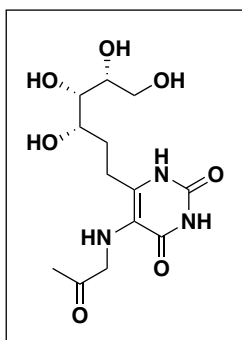
5-(((E)-2-oxopropylidene)amino)-6-(((2S,3R,4R)-2,3,4,5-tetrahydroxy)oxy)pyrimidine-2,4(1H,3H)-dione (29)⁸⁰



| Raw formula | Molecular mass | Aspect |
|---|----------------------------|-----------------------|
| C ₁₂ H ₁₇ N ₃ O ₈ | 331.10 g.mol ⁻¹ | Red solution in water |

Nitro precursor of **29** with uracil protected by benzyl groups was furnished by Sanofi. This precursor (45 mg, 1.0 eq, 0.08 mmol) was dissolved in a MeOH/EtOAc mixture (3/1 mL) and 10% Pd/C was added (4.5 mg, 0.1 eq). The solution was allowed to react at room temperature under H₂ atmosphere overnight to give the desired amino derivative along with a nitro analogue impurity (according to UPLC-MS analysis). The mixture was carefully filtered on celite to avoid as much as possible contact with air and washed with a few volumes of MeOH. The solvent was removed under vacuum and a solution at 10 mM concentration in water was directly prepared and frozen at -80°C (the amino intermediate was not isolated because of its chemical instability). Product **29** was prepared right before addition on cells by adding methylglyoxal to aliquots of the stock solution (same protocol as for **12b**)

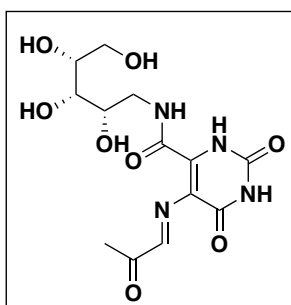
5-((2-oxopropyl)amino)-6-((3S,4S,5R)-3,4,5,6-tetrahydroxyhexyl)pyrimidine-2,4(1H,3H)-dione (31)



| Raw formula | Molecular mass | Aspect |
|---|----------------------------|-----------------------------|
| C ₁₃ H ₂₁ N ₃ O ₇ | 331.14 g.mol ⁻¹ | Colorless solution in water |

31 was synthesized following the same protocol as for **12b**. Briefly, a stock solution of the amino precursor (hydrochloride salts) furnished by Sanofi was diluted to a 10 mM concentration and it was frozen at -80°C. Aliquots of 5 µL were made and 5 µL of 50 mM methylglyoxal was added followed by 15 minutes reaction. The product was then directly added on cells for biological evaluation.

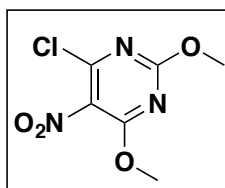
2,6-dioxo-5-(((E)-2-oxopropylidene)amino)-N-((2S,3S,4R)-2,3,4,5-tetrahydroxypentyl)-1,2,3,6-tetrahydropyrimidine-4-carboxamide (32)



| Raw formula | Molecular mass | Aspect |
|---|----------------------------|-----------------------------|
| C ₁₃ H ₁₈ N ₄ O ₈ | 358.11 g.mol ⁻¹ | Colorless solution in water |

32 was synthesized following the same protocol as for **12b**. Briefly, a stock solution of the amino precursor furnished by Sanofi was diluted to a 10 mM concentration and it was frozen at -80°C. Aliquots of 5 µL were made and 5 µL of 50 mM methylglyoxal was added followed by 15 minutes reaction. The product was then directly added on cells for biological evaluation.

4-chloro-2,6-dimethoxy-5-nitropyrimidine (33)¹¹⁷



| Raw formula | Molecular mass | Aspect | Yield |
|---|----------------------------|--------------|-------|
| C ₆ H ₆ ClN ₃ O ₄ | 219.00 g.mol ⁻¹ | Yellow solid | 56% |

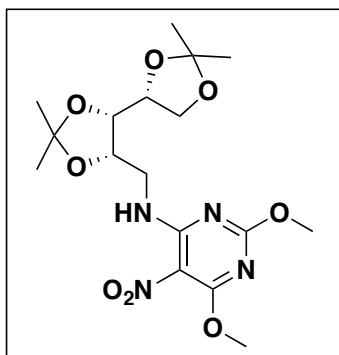
Sulfuric acid (0.75 mL) was added dropwise to fuming nitric acid ($\geq 90\%$, 1.25 mL) at 0°C followed by 6-chloro-2,4-dimethoxypyrimidine (50 mg, 1.0 eq, 0.29 mmol). The reaction mixture was stirred at 85°C for 2h30, then cooled to room temperature, poured into ice-water, and stirred for 20 min. The resulting solid was filtered, washed three times with ice-water, and dried under vacuum to give **33** as a yellow solid.

MS (ESI), m/z : 220.0 [M+H]⁺, 222.1 [M+H+2]⁺

¹H NMR (400 MHz, CDCl₃) δ : 4.10 (s, 3H), 4.07 (s, 3H)

¹³C NMR (101 MHz, CDCl₃) δ : 163.9, 162.7, 153.7, 77.4, 56.6, 56.3

2,6-dimethoxy-5-nitro-N-(((4S,4'R,5S)-2,2,2',2'-tetramethyl-[4,4'-bi(1,3-dioxolan)]-5-yl)methyl)pyrimidin-4-amine (34)¹¹⁷



| Raw formula | Molecular mass | Aspect | Yield |
|---|----------------------------|---------------|-------|
| C ₁₇ H ₂₆ N ₄ O ₈ | 414.18 g.mol ⁻¹ | Yellow powder | 75% |

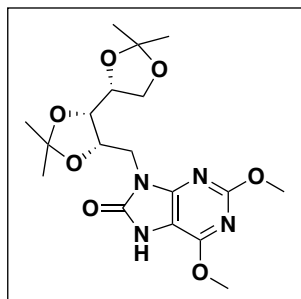
To **33** (0.65 g, 1.0 eq, 2.97 mmol) in DMF (5 ml) was added **12** (1.25 g, 2.2 eq, 6.53 mmol). The mixture was stirred at room temperature for 19h. Then, DMF was evaporated under vacuum and water/DCM extraction was performed. The organic layer was dried over MgSO₄ and concentrated under vacuum. The product was purified by column chromatography (hexane/EtOAc 30%) to give **34** as a yellow solid.

MS (ESI), m/z (%): 415.3 [M+H]⁺

¹H NMR (400 MHz, CDCl₃) δ: 4.41-4.37 (m, 1H), 4.21-4.12 (m, 3H), 4.08 (s, 3H), 4.05-4.00 (m, 4H), 3.93-3.91 (m, 1H), 3.80-3.74 (m, 1H), 1.70 (brs, 1H), 1.45 (s, 3H), 1.43 (s, 3H), 1.38 (s, 3H), 1.37 (s, 3H)

¹³C NMR (101 MHz, CDCl₃) δ: 167.4, 163.7, 159.1, 112.8, 110.6, 109.2, 78.7, 75.3, 73.3, 68.3, 55.6, 55.5, 40.8, 28.0, 26.6, 25.7, 25.5

2,6-dimethoxy-9-(((4*S*,4'*R*,5*S*)-2,2,2',2'-tetramethyl-[4,4'-bi(1,3-dioxolan)]-5-yl)methyl)-7,9-dihydro-8*H*-purin-8-one (35)



| Raw formula | Molecular mass | Aspect | Yield |
|---|----------------------------|--------------|-------|
| C ₁₈ H ₂₆ N ₄ O ₇ | 410.18 g.mol ⁻¹ | Yellow solid | 71% |

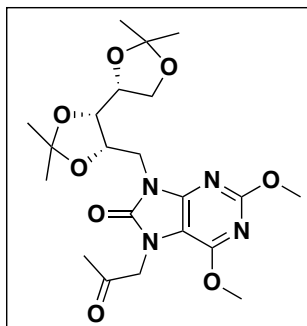
34 (623 mg, 1.0 eq, 1.50 mmol) was dissolved in MeOH (6 mL) and 10% Pd/C (160 mg, 0.1 eq) was added. The reaction mixture was stirred at room temperature under H₂ atmosphere for 24h. The mixture was filtered on celite, rinsed by MeOH and DCM, and the solvents were removed under vacuum. The crude intermediate (630 mg, 1.0 eq, 1.63 mmol) was dissolved in DCM (60 mL). Triethylamine (2.29 mL, 10 eq, 16.3 mmol) and triphosgene (193 mg, 0.4 eq, 0.65 mmol) were sequentially added at 0°C, under argon atmosphere. The mixture was slowly warmed up to room temperature and stirred for 30 minutes. After completion, water was added and the product was extracted by DCM. The organic layer was washed by saturated aqueous NaHCO₃, dried over MgSO₄ and concentrated under vacuum. The product was purified by column chromatography (hexane/EtOAc 50%) to give **35** as a yellow powder.

MS (ESI), *m/z* (%): 411.3 [M+H]⁺, 409.3 [M-H]⁻

¹H NMR (500 MHz, CDCl₃) δ: 4.93-4.89 (m, 1H), 4.27-4.08 (m, 5H), 4.04 (s, 3H), 3.98-3.93 (m, 4H), 1.78 (s, 1H), 1.47 (s, 3H), 1.39 (s, 3H), 1.29 (s, 3H), 1.28 (s, 3H)

¹³C NMR (126 MHz, CDCl₃) δ: 160.5, 153.9, 153.6, 152.1, 110.0, 109.7, 100.8, 78.1, 73.9, 73.2, 68.4, 55.0, 54.1, 41.1, 28.1, 26.9, 25.8, 25.3

2,6-dimethoxy-7-(2-oxopropyl)-9-(((4*S*,4'*R*,5*S*)-2,2,2',2'-tetramethyl-[4,4'-bi(1,3-dioxolan)]-5-yl)methyl)-7,9-dihydro-8*H*-purin-8-one (36)



| Raw formula | Molecular mass | Aspect | Yield |
|---|----------------------------|--------------|-------|
| C ₂₁ H ₃₀ N ₄ O ₈ | 466.21 g.mol ⁻¹ | Yellow paste | 94% |

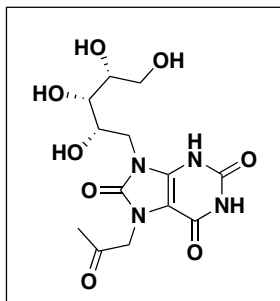
To **35** (100 mg, 1.0 eq, 0.24 mmol) in DMF (5 mL) was added sodium hydride (60% dispersion in mineral oil, 59 mg, 10 eq, 2.4 mmol) at 0°C. The mixture was stirred at the same temperature until gas released ceased (approximately 30 min). Then, chloroacetone (0.98 mL, 5.0 eq, 1.22 mmol) was added and the reaction was stirred at room temperature during 1h. Water was added to the mixture and the product was extracted by DCM. The organic layer was dried over MgSO₄ and dried under vacuum. The crude product was purified by column chromatography (hexane/AcOEt 50%) to give **36** as a yellow paste.

MS (ESI), *m/z* (%): 476.4 [M+H]⁺, 489.4 [M+H+Na]⁺

¹H NMR (400 MHz, CDCl₃) δ: 4.88-4.83 (m, 1H), 4.70 (s, 2H), 4.25-4.02 (m, 5H), 3.96-3.90 (m, 7H), 2.20 (s, 3H), 1.44 (s, 3H), 1.38 (s, 3H), 1.28 (s, 3H), 1.25 (s, 3H),

¹³C NMR (101 MHz, CDCl₃) δ: 201.6, 160.3, 153.7, 153.3, 151.4, 110.0, 109.7, 102.4, 78.0, 74.0, 73.2, 68.4, 55.0, 54.2, 51.7, 41.5, 28.1, 26.9 (2C), 25.8, 25.3

7-(2-oxopropyl)-9-((2S,3S,4R)-2,3,4,5-tetrahydroxypentyl)-7,9-dihydro-1H-purine-2,6,8(3H)-trione
(37)



| Raw formula | Molecular mass | Aspect | Yield |
|---|------------------------------|-------------|-------|
| C ₁₃ H ₁₈ N ₄ O ₈ | 358.1125 g.mol ⁻¹ | White solid | 84% |

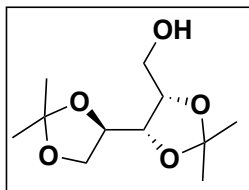
36 (107 mg, 1.0 eq, 0.23 mmol) was dissolved in a 1:1 mixture of 37% HCl/MeOH (2 mL of each) and the mixture was heated under reflux for 3h. The solvent was removed under vacuum and the product was purified by preparative C18 RP-HPLC using the following conditions: Solvent A: Water + 0.1% formic acid; Solvent B: ACN + 0.1% formic acid; 25 min run with a gradient starting from 100% A for 5 min, then 5% B for 5 min and then gradual increase of B to reach 100% B at 20 min followed by 5 min with 100% B. After lyophilization, the product was recovered as a white solid.

HR-MS (ESI), *m/z* (%): 359.1195 [M+H]⁺

¹H NMR (500 MHz, D₂O) δ : 4.95 (s, 2H), 4.15-4.08 (m, 2H), 4.03-3.97 (m, 1H), 3.87 (td, 1H, J= 6.8 Hz, 3.1 Hz), 3.81 (dd, 1H, J= 11.9 Hz, 3.1 Hz), 3.76-3.74 (m, 1H), 3.68 (dd, 1H, J= 11.9 Hz, 6.8 Hz), 2.34 (s, 3H)

¹³C NMR (126 MHz, D₂O) δ : 207.1, 155.1, 152.4, 151.9, 139.6, 98.0, 72.6, 72.0, 69.2, 62.4, 51.2, 44.3, 26.3

((4*S*,4'*R*,5*S*)-2,2,2',2'-tetramethyl-[4,4'-bi(1,3-dioxolan)]-5-yl)methanol (38)



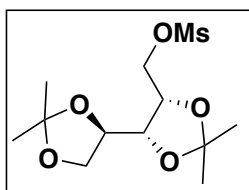
| Raw formula | Molecular mass | Aspect | Yield |
|--|----------------------------|---------------|-------|
| C ₁₁ H ₂₀ O ₅ | 232.13 g.mol ⁻¹ | Colorless oil | 48 % |

8 (140 mg, 1.0 eq, 0.61 mmol) was dissolved in MeOH (2 mL) and sodium borohydride was slowly added at 0°C. The reaction was stirred at room temperature for 30 min. A saturated aqueous NH₄Cl was added and the product was extracted by DCM. The organic layer was dried over MgSO₄ and concentrated under vacuum. The product was purified by column chromatography (hexane/AcOEt 20%) to give **38** as a colorless oil.

¹H NMR (400 MHz, CDCl₃) δ: 4.37-4.32 (m, 1H), 4.18-4.12 (m, 2H), 4.08-4.03 (m, 1H), 3.99-3.92 (m, 1H), 3.89-3.78 (m, 2H), 2.68 (brs, 1H), 1.41 (s, 3H), 1.40 (s, 3H), 1.35 (s, 3H), 1.34 (s, 3H)

¹³C NMR (101 MHz, CDCl₃) δ: 110.2, 108.9, 78.3, 77.5, 73.5, 68.2, 60.8, 27.9, 26.8, 25.5, 25.3

((4R,4'R,5S)-2,2,2',2'-tetramethyl-[4,4'-bi(1,3-dioxolan)]-5-yl)methyl methanesulfonate (39)



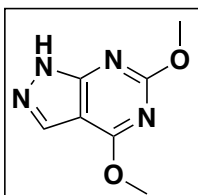
| Raw formula | Molecular mass | Aspect | Yield |
|--|----------------------------|------------|-------|
| C ₁₂ H ₂₂ O ₇ S | 310.11 g.mol ⁻¹ | Yellow oil | 89 % |

To **38** (231 mg, 1.0 eq, 1.0 mmol) in pyridine (5 mL) was added at 0°C methanesulfonyl chloride (0.09 mL, 1.2 eq, 1.19 mmol). The mixture was stirred 3h at room temperature. Pyridine was then removed under vacuum and water/DCM extraction was performed. The organic layer was dried over MgSO₄ and concentrated under vacuum. The product was purified by column chromatography (hexane/AcOEt 50%) to give **39** as a yellow oil.

¹H NMR (400 MHz, CDCl₃) δ: 4.60 (dd, 1H, J= 11.0 Hz, 2.7 Hz), 4.47-4.44 (m, 1H), 4.34 (dd, 1H, J= 11.0 Hz, 8.2 Hz), 4.13-4.10 (m, 1H), 4.03-4.00 (m, 2H), 3.92-3.90 (m, 1H), 3.08 (s, 3H), 1.45 (s, 3H), 1.39 (s, 3H), 1.35 (s, 3H), 1.32 (s, 3H)

¹³C NMR (101 MHz, CDCl₃) δ: 110.2, 109.9, 77.7, 75.6, 73.2, 68.6, 68.1, 37.9, 27.9, 27.0, 25.4 (2C)

4,6-dimethoxy-1H-pyrazolo[3,4-d]pyrimidine (40)



| Raw formula | Molecular mass | Aspect | Yield |
|---|----------------------------|-------------|-------|
| C ₇ H ₈ N ₄ O ₂ | 180.06 g.mol ⁻¹ | White solid | 59 % |

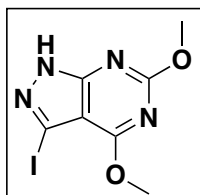
21 (2.23 g, 1.0 eq, 11.0 mmol) was dissolved in MeOH (30 mL) and hydrazine monohydrate was added (0.58 mL, 1.2 eq, 12 mmol). The reaction was stirred at reflux for 3h. MeOH was removed under vacuum and water/DCM extraction was done. The organic layer was dried over MgSO₄ and concentrated under vacuum. The product was purified by column chromatography (hexane/AcOEt 50%) to give **40** as a white solid.

HR-MS (ESI), *m/z* (%): 181.3 [M+H]⁺

¹H NMR (400 MHz, DMSO-d₆) δ : 13.59 (brs, 1H), 8.04 (s, 1H), 4.03 (s, 3H), 3.92 (s, 3H)

¹³C NMR (101 MHz, DMSO-d₆) δ : 164.5, 164.0, 157.8, 131.9, 97.9, 54.6, 54.0

3-iodo-4,6-dimethoxy-1H-pyrazolo[3,4-d]pyrimidine (41)



| Raw formula | Molecular mass | Aspect | Yield |
|--|----------------------------|-------------|-------|
| C ₇ H ₇ IN ₄ O ₂ | 305.96 g.mol ⁻¹ | White solid | 46 % |

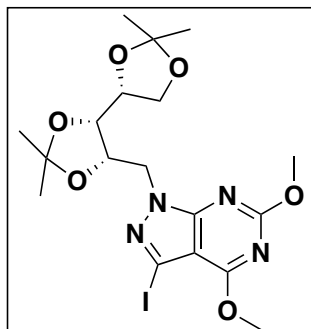
To **40** (384 mg, 1.0 eq, 2.13 mmol) in DMF (10 mL) was added N-iodosuccinimide (578 mg, 1.2 eq, 2.56 mmol). The mixture was heated at reflux for 7h. After cooling, water/DCM extraction was performed. The organic layer was dried over MgSO₄ and concentrated under vacuum. The product was purified by column chromatography (hexane/EtOAc 50%) to give **41** as a white solid.

HR-MS (ESI), *m/z* (%): 307.0 [M+H]⁺

¹H NMR (400 MHz, DMSO-d₆) δ : 13.88 (brs, 1H), 4.04 (s, 3H), 3.91 (s, 3H)

¹³C NMR (101 MHz, DMSO-d₆) δ : 164.3, 163.9, 158.0, 101.9, 89.7, 54.8, 54.3

3-iodo-4,6-dimethoxy-1-(((4*S*,4'*R*,5*S*)-2,2,2',2'-tetramethyl-[4,4'-bi(1,3-dioxolan)]-5-yl)methyl)-1*H*-pyrazolo[3,4-*d*]pyrimidine (42)



| Raw formula | Molecular mass | Aspect | Yield |
|--|----------------------------|-------------|-------|
| C ₁₈ H ₂₅ IN ₄ O ₆ | 520.08 g.mol ⁻¹ | White solid | 39 % |

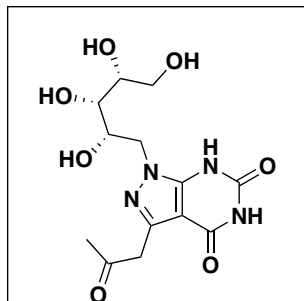
To **41** (200 mg, 1.0 eq, 0.65 mmol) in DMF (3 mL) was added potassium carbonate (270 mg, 3.0 eq, 1.96 mmol) and a **38** (608 mg, 2.0 eq, 1.96 mmol) solution in DMF (2 mL). The mixture was heated at reflux for 24h. After completion, water was added and the product was extracted by DCM. The organic layer was dried over MgSO₄ and concentrated under vacuum. The product was purified by column chromatography (hexane/EtOAc 20%) to give **42** as a colorless oil that solidified upon standing to a white solid.

HR-MS (ESI), *m/z* (%): 520.9 [M+H]⁺

¹H NMR (500 MHz, CDCl₃) δ: 4.89-4.85 (m, 1H), 4.60 (dd, 1H, *J* = 13.9 Hz, *J* = 9.9 Hz), 4.50 (dd, 1H, *J* = 13.9 Hz, 3.4 Hz), 4.22-4.16 (m, 2H), 4.13-4.09 (m, 4H), 4.02 (s, 3H), 3.98-3.93 (m, 1H), 1.46 (s, 3H), 1.38 (s, 3H), 1.28 (s, 3H), 1.27 (s, 3H)

¹³C NMR (126 MHz, CDCl₃) δ: 165.1, 164.4, 157.6, 110.0, 109.8, 103.5, 87.5, 78.0, 75.9, 73.3, 68.4, 55.2, 54.6, 47.8, 28.2, 26.9, 25.8, 25.4

1-(4,6-dimethoxy-1-(((4*S*,4'*R*,5*S*)-2,2,2',2'-tetramethyl-[4,4'-bi(1,3-dioxolan)]-5-yl)methyl)-1*H*-pyrazolo[3,4-*d*]pyrimidin-3-yl)propan-2-one (43)



| Raw formula | Molecular mass | Aspect | Yield |
|---|----------------------------|--------|--------|
| C ₁₃ H ₁₈ N ₄ O ₇ | 342.12 g.mol ⁻¹ | - | Traces |

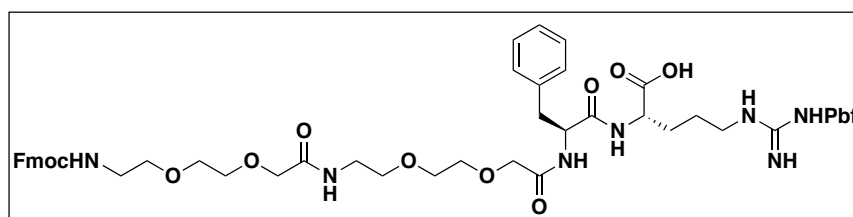
Isopropenyl acetate (3 μ L, 1.25 eq, 24 μ mol) and tributyltin methoxide (6 μ L, 1.25 eq, 24 μ mol) were dissolved in dry toluene (0.5 mL) and the solution was heated at 50°C for 1h under argon atmosphere. The solution was added to **42** (10 mg, 1.0 eq, 19 μ mol), tri(*o*-tolyl)phosphine (3 mg, 0.5 eq, 9.6 μ mol) and PdCl₂(MeCN)₂ (1.0 mg, 0.1 eq, 1.9 μ mol) beforehand dissolved in dry toluene (0.5 mL). The tube was sealed and the mixture was stirred at 130°C overnight. Solvent was removed under vacuum, water was added and the product was extracted by EtOAc. The organic layer was dried over MgSO₄ and concentrated under vacuum. The product was purified by column chromatography (hexane/EtOAc 30%) to give a mixture of products that were directly used for reaction. The mixture was dissolved in MeOH (0.5 mL) and 37% HCl was added (0.5 mL). The mixture was stirred at reflux for 2h. The solvent was removed under vacuum and the product was directly purified by preparative C18 RP-HPLC using the following conditions: Solvent A: Water + 0.1% formic acid; Solvent B: ACN + 0.1% formic acid. 25 min run with a gradient starting from 100% A for 5 min, then 5% B for 5 min and then gradual increase of B to reach 100% B at 20 min followed by 5 min with 100% B. After freeze drying, the product was recovered as a white solid.

MS (ESI), *m/z* (%): 343.5 [M+H]⁺

Solid phase synthesis procedure:

Manual SPPS method was used for the peptide synthesis with 2-Chlorotrityl chloride resin. All amino-acids used were protected by Fmoc NH-protecting group removable using a 20% piperidine in DMF solution. PyBOP was used as coupling reagent and DIEA as base. Washes were done with DCM and DMF after each step of deprotection and coupling. pH was controlled during the reactions. Each coupling reaction was monitored by 2,4,6-Trinitrobenzenesulfonic acid (TNBS) test. Briefly, two drops of DIEA and two drops of TNBS 0.1% were added to one sample of the resin. After 3 minutes, coupled beads remained yellow while uncoupled beads displayed an orange color. Loading of the resin was quantified by analysis of Fmoc-protecting group (in the washing media) using UV spectrophotometry. Absorbance was measured at 301 nm wavelength.

Fmoc-NH-PEG₂-PEG₂-Phe-Arg(Pbf)-OH (44)



| Raw formula | Molecular mass | Aspect | Yield |
|--|-----------------------------|-------------|-------|
| C ₅₅ H ₇₁ N ₇ O ₁₄ S | 1085.48 g.mol ⁻¹ | White solid | 46 % |

Fmoc-NH-Arg(Pbf)-OH (1.09 g, 2.0 eq, 1.68 mmol) was coupled to 2-chlorotrityl chloride resin (1.0 g, 1 eq) with DIEA (0.585 mL, 4 eq, 3.36 mmol) in DMF (10 mL) within 30 min. The resin was capped with a solution of DCM/MeOH/DIEA (10 mL, 17/2/1) during 15 min (10 + 5 min). A solution of 20% piperidine in DMF (10 mL) was added for the deprotection of Fmoc-protecting group for 5 min and then 10 min (twice). After washes, Fmoc-NH-Phe-OH (0.650 g, 2.0 eq, 1.68 mmol), DIEA (585 μ L, 4 eq, 3.36 mmol) and PyBOP (0.877 g, 2.0 eq, 1.68 mmol) were added to the resin in suspension in DMF (10 mL) and the solution was stirred for 30 min. TNBS test was done with a small sample of resin beads to check the completion of the coupling reaction. The same steps of deprotection and coupling were done two times for the coupling of Fmoc-NH-PEG₂-OH (0.65 g, 2.0 eq, 1.68 mmol) using the same conditions. Then, a solution of TFE/AcOH/DCM (2/1/7, 10 mL) was added to and the mixture was stirred for 2h. The beads were washed with DCM and the solution was concentrated under vacuum. A second

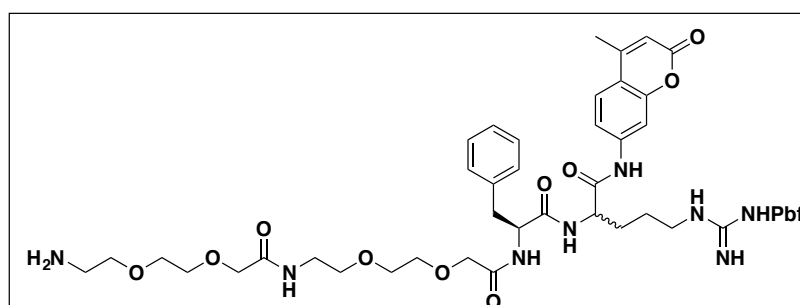
cleavage was done using the same conditions and following the same steps. The peptide was then precipitated from cold EtO₂ and the precipitate was washed with diethyl ether and dried under vacuum to give **44** as a white solid.

HR-MS (ESI), *m/z* (%): 1086.3 [M+H]⁺

¹H NMR (500 MHz, CD₂Cl₂) δ: 7.77 (d, 2H, J= 7.5 Hz), 7.59 (d, 2H, J= 7.5 Hz), 7.42-7.37 (m, 3H), 7.33-7.27 (m, 3H), 7.23-7.15 (m, 5H), 6.35 (brs, 2H), 6.19 (brs, 1H), 5.67 (brt, 1H, J= 5.5 Hz), 4.77-4.73 (m, 1H), 4.48-4.38 (m, 3H), 4.24-4.18 (m, 1H), 3.96-3.80 (m, 4H), 3.62-3.30 (m, 16H), 3.19-3.15 (m, 3H), 3.00-2.92 (m, 3H), 2.54 (s, 3H), 2.47 (s, 3H), 2.05-2.02 (m, 4H), 1.91-1.85 (m, 1H), 1.73-1.67 (m, 1H), 1.54-1.46 (m, 2H), 1.42 (s, 6H)

¹³C NMR (126 MHz, CD₂Cl₂) δ: 174.2, 173.8, 171.6, 171.1, 171.0, 159.0, 157.0, 156.9, 144.5, 141.8, 138.6, 137.0, 133.5, 132.7, 129.7, 128.9, 128.1, 127.4, 127.3, 125.4, 125.2, 120.3, 117.8, 86.8, 71.3, 70.7-70.2, 66.8, 54.5, 52.7, 47.7, 43.5, 41.3, 40.9, 39.1, 38.2, 29.5, 28.7, 25.4, 20.7, 19.4, 18.1, 12.6

H₂N-PEG₂-PEG₂-Phe-Arg(Pbf)-AMC (45)



| Raw formula | Molecular mass | Aspect | Yield |
|--|-----------------------------|--------------|-------|
| C ₅₀ H ₆₈ N ₈ O ₁₃ S | 1020.46 g.mol ⁻¹ | Yellow solid | 20 % |

44 (200 mg, 1.0 eq, 0.18 mmol), TCFH (101 mg, 2.0 eq, 0.36 mmol) and DIEA (80 μL, 4.0 eq, 0.72 mmol) were dissolved in anhydrous DCM at 0°C under argon atmosphere. The solution was stirred for 20 min at room temperature. 7-amino-4-methylcoumarin (39 mg, 1.2 eq, 0.22 mmol) was added at 0°C and the solution was stirred for 20 min at 0°C and overnight at room temperature. The solution was washed

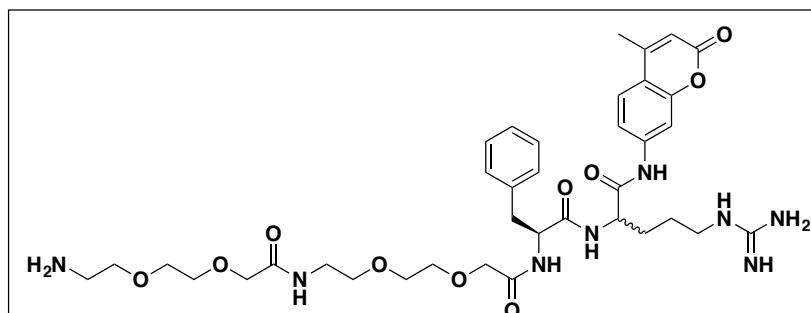
by saturated NaCl_(aq) and 5% Na₂CO_{3(aq)}. The organic layer was dried over MgSO₄ and evaporated under vacuum. The intermediate Fmoc-NH-PEG₂-PEG₂-Phe-Arg(Pbf)-AMC was stirred in a 20% piperidine in DMF (5mL) solution during 1h at room temperature. The solvent was evaporated under vacuum and the product was purified by preparative C18 RP-HPLC using the following gradient: 5% ACN (0.1% formic acid)/95% H₂O (0.1% formic acid) to 70/30% ACN/H₂O over 25 minutes. The fractions containing the product were freeze dried to give **45** as a yellow powder (mixture of two epimers).

HR-MS (ESI), *m/z* (%): 1021.1 [M+H]⁺

¹H NMR (500 MHz, CD₂Cl₂) δ: 10.21 (brs, 1H), 8.66 (s, 1H), 8.26-8.23 (m, 1H), 7.77-7.71 (m, 2H), 7.51-7.38 (m, 3H), 7.24-7.10 (m, 5H), 7.02 (brs, 1H), 6.63 (brs, 2H), 6.10 (d, 1H, J= 7.3 Hz), 4.77-4.76 (m, 1H), 4.64-4.60 (m, 1H), 4.56-4.51 (m, 1H), 4.02-3.91 (m, 4H), 3.70-3.33 (m, 14H), 3.23-2.90 (m, 8H), 2.55 (d, 3H, J= 8.4 Hz), 2.48 (d, 3H, J= 6.3 Hz), 2.35 (d, 3H, J= 10.2 Hz), 2.05 (d, 3H, J= 6.2 Hz), 1.95-1.75 (m, 2H), 1.74-1.53 (m, 2H), 1.43 (s, 6H)

¹³C NMR (126 MHz, CD₂Cl₂) δ: 172.0, 170.9, 170.4, 169.2, 161.1, 158.7, 156.9, 154.1, 152.8, 142.0, 138.2, 136.7, 133.0, 132.3, 129.3, 128.6, 127.0, 125.1, 124.9, 117.5, 116.0, 115.9, 113.0, 107.1, 86.6, 70.7, 70.2, 70.1, 69.9, 67.7, 54.8, 54.6, 43.1, 40.0, 38.7, 38.1, 37.9, 29.2, 28.3, 25.5, 19.2, 18.4, 17.9, 12.2

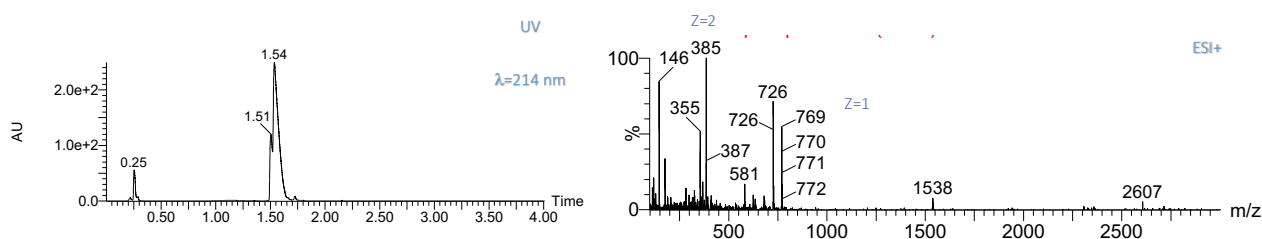
H₂N-PEG₂-PEG₂-Phe-Arg-AMC (46)



| Raw formula | Molecular mass | Aspect | Yield |
|--|----------------------------|--------------|-------|
| C ₃₇ H ₅₂ N ₈ O ₁₀ | 768.38 g.mol ⁻¹ | Yellow solid | 83 % |

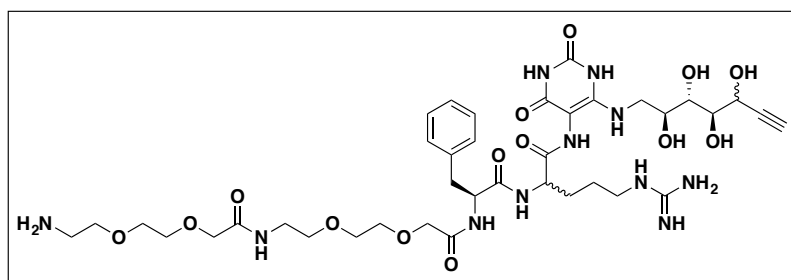
45 (15 mg, 1.0 eq, 0.10 mmol) was dissolved in a mixture of TFA/Tris/H₂O (95/2.5/2.5, 2mL) and stirred during 2h at room temperature. Cold Et₂O was added and the precipitate was filtered and washed with Et₂O. After drying under vacuum, **46** was obtained as a yellow powder (mixture of two epimers).

HR-MS (ESI), m/z (%): 769.9 [M+H]⁺



¹H NMR (500 MHz, DMSO-d₆) δ : 10.58 (s, 1H), 10.42 (s, 1H), 8.65-8.57 (m, 2H), 7.86-7.67 (m, 5H), 7.58-7.51 (m, 2H), 7.29-7.14 (m, 6H), 6.30-6.28 (m, 1H), 5.75 (s, 1H), 4.69-4.66 (m, 1H), 4.48-4.43 (m, 1H), 4.38-4.34 (m, 1H), 3.92-3.75 (m, 4H), 3.60-3.56 (m, 4H), 3.52-3.340 (m, 5H), 3.29-3.25 (m, 2H), 3.16-2.87 (m, 4H), 2.41 (dd, 2H, J= 4.4 Hz, J= 1.3 Hz), 1.85-1.63 (m, 3H), 1.62-1.41 (m, 3H), 1.38-1.20 (m, 4H)

H₂N-PEG₂-PEG₂-Phe-Arg-72 (47)

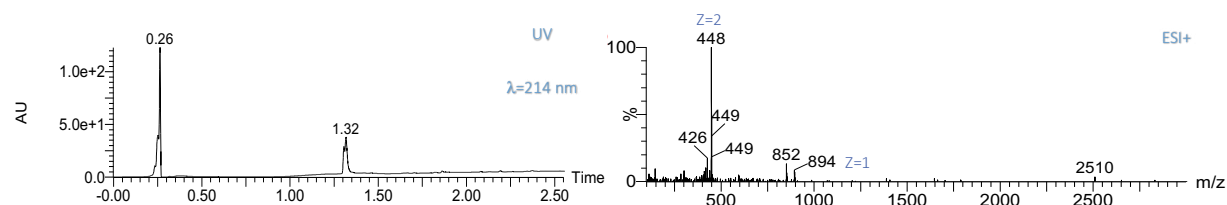


| Raw formula | Molecular mass | Aspect | Yield |
|---|----------------------------|--------------|-------|
| C ₃₈ H ₅₉ N ₁₁ O ₁₄ | 893.42 g.mol ⁻¹ | Yellow solid | 3.5 % |

44 (109 mg, 1.0 eq, 0.10 mmol), TCFH (56 mg, 2.0 eq, 0.2 mmol) and DIEA (40 μ L, 4.0 eq, 0.4 mmol) were dissolved in anhydrous DCM at 0°C under argon atmosphere. The solution was stirred for 20 min at room temperature. **72** (60 mg, 2.0 eq, 0.2 mmol) was dissolved in few volumes of anhydrous MeOH and it was added to the mixture at 0°C. The solution was stirred for 20 min at 0°C and then overnight at room temperature. The solvent was removed under vacuum and the intermediate was stirred in a 20% piperidine in DMF (5mL) solution during 1h at room temperature. The solvent was evaporated under vacuum. The product was purified by preparative C18 RP-HPLC with a 20% to 50% ACN elution

gradient over 15 minutes. The fractions containing the product were freeze dried. Then, the product was solubilized in a mixture of TFA/Tris/H₂O (95/2.5/2.5, 2mL) and stirred during 2h at room temperature. Cold Et₂O was added and the precipitate was filtered and washed with Et₂O (10 mL). After drying under vacuum, **47** was obtained as a yellow powder (mixture of two epimers).

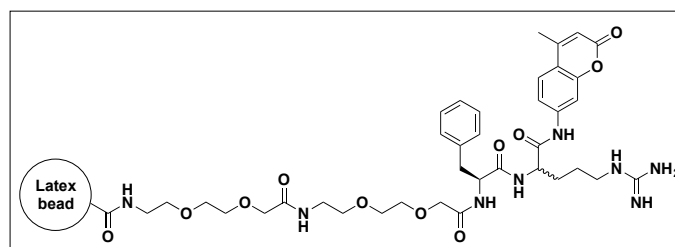
HR-MS (ESI), *m/z* (%): 894.1 [M+H]⁺



¹H NMR (500 MHz, DMSO-*d*₆) δ : 10.46 (s, 1H), 10.40 (s, 1H), 8.40 (s, 1H), 8.31 (d, 1H, *J* = 7.1 Hz), 7.78-7.84-7.70 (m, 4H), 7.52 (brt, 1H, *J* = 5.4 Hz), 7.26-7.16 (m, 4H), 6.90 (brs, 1H), 6.21 (brt, 1H, *J* = 5.8 Hz), 5.46-5.00 (m, 4H), 4.65-4.60 (m, 1H), 4.93-4.37 (m, 2H), 3.90-3.74 (m, 6H), 3.60-3.61-3.57 (m, 6H), 3.56-3.30 (4H hidden by water peak), 3.29-3.25 (m, 2H), 3.21 (d, 1H, *J* = 2.2 Hz), 3.14-3.07 (m, 4H), 3.00-2.95 (m, 2H), 2.92-2.83 (m, 2H), 2.08-2.07 (m, 3H), 1.84-1.74 (m, 1H), 1.73-1.60 (m, 1H), 1.57-1.52 (m, 2H), 1.38 (s, 1H), 1.23 (s, 1H)

¹³C NMR (101 MHz, DMSO-*d*₆) δ : 171.8, 171.2, 169.4, 169.3, 160.8, 158.0, 157.7, 156.7, 152.16, 150.0, 137.6, 135.5, 129.2, 128.1, 126.3, 86.3, 83.9, 75.6, 74.6, 72.5, 71.16, 70.0, 69.8, 69.6, 69.4, 69.3, 68.9, 66.6, 63.2, 59.5, 53.4, 52.4, 43.9, 40.5, 38.6, 38.0, 37.2, 30.7, 29.0, 24.4

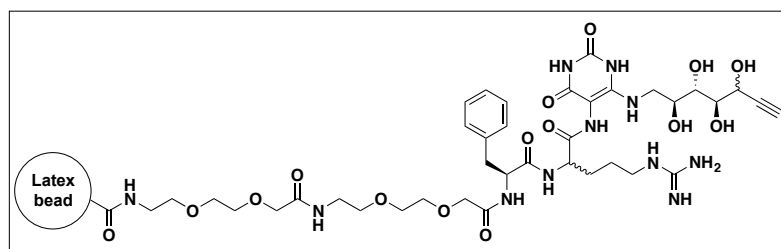
LB-NH-PEG₂-PEG₂-Phe-Arg-AMC (**48**)



1 mL of the stock suspension of carboxylate-modified latex beads (CML beads, 4% w/v, 1 μ m diameter) was introduced in a 1.5 mL Eppendorf vial. The beads were washed three times with MES Buffer (100 mM, pH 6.0) and the supernatant was discarded after centrifugation (10 min, 15000 rpm). A solution of EDC (40 mg/mL) and NHS (12 mg/mL) in MES buffer was added and the beads were stirred on rotator

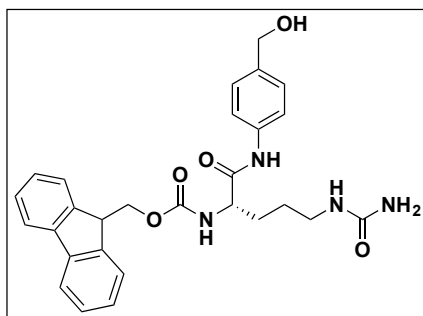
(20 min, 750 rpm). Activated beads were washed three times with MES Buffer. They were re-suspended in PBS Buffer and a solution of **46** (2 mg/mL in PBS) was added. The mixture was then stirred on rotator (2h, 750 rpm). The conjugated beads were washed three times and re-suspended in a glycine Buffer (750 µg/mL). The tube was stirred on rotator (1h, 750 rpm) and washed again with PBS buffer. The conjugated beads were stocked at 4°C in PBS Buffer and protected from light.

LB-NH-PEG₂-PEG₂-Phe-Arg-72 (**49**)



1 mL of the stock suspension of carboxylate-modified latex beads (CML beads, 4% w/v, 1 µm diameter) was introduced in a 1.5 mL Eppendorf vial. The beads were washed three times with MES Buffer (100 mM, pH 6.0) and the supernatant was discarded after centrifugation (10 min, 15000 rpm). A solution of EDC (40 mg/mL) and NHS (12 mg/mL) in MES buffer was added and the beads were stirred on rotator (20 min, 750 rpm). Activated beads were washed three times with MES Buffer. They were re-suspended in PBS Buffer and a solution of **47** (2 mg/mL in PBS) was added. The mixture was stirred on rotator (2h, 750 rpm). The conjugated beads were washed three times and re-suspended in glycine Buffer (750 µg/mL). The tube was stirred on rotator (1h, 750 rpm) and washed again with PBS buffer. The conjugated beads were stocked at 4°C in PBS Buffer and protected from light. A small sample of the conjugated beads was analyzed by fluorometric Click reaction test using Click-iT® EdU Imaging Kit from InVitrogen. Beads were incubated with Alexa Fluor Azide 488™, ascorbate and CuSO₄ in Click-iT EdU Buffer. After 1h, the fluorescence was measured using SpectraMax ID3 spectrophotometer at 495/519 nm wavelengths.

Fmoc-NH-Cit-PAB-OH (50)



| Raw formula | Molecular mass | Aspect | Yield |
|---|----------------------------|-------------|-------|
| C ₂₈ H ₃₀ N ₄ O ₅ | 502.22 g.mol ⁻¹ | White solid | 87% |

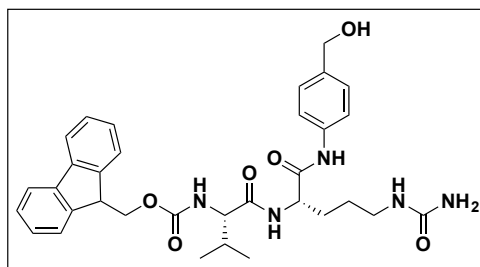
To a solution of Fmoc-NH-Cit-OH (1.45 g, 1.0 eq, 3.66 mmol) in dry DMF (10 mL) was added 4-aminobenzyl alcohol (1.35 g, 3.0 eq, 11 mmol) followed by DIPEA (0.5 mL, 1.0 eq, 3.66 mmol). The solution was stirred for 15 minutes and HATU was added (1.53 g, 1.1 eq, 4.03 mmol). The mixture was stirred overnight. The product was concentrated under vacuum and purified by column chromatography (DCM/MeOH 2% to 5%) and **50** was obtained as a white solid.

MS (ESI), *m/z* (%): 503.3 [M+H]⁺

¹H NMR (500 MHz, DMSO-*d*₆) δ : 9.98 (s, 1H), 7.89 (d, 2H, *J* = 7.6 Hz), 7.75 (t, 2H, *J* = 6.5 Hz), 7.66 (d, 1H, *J* = 8.1 Hz), 7.56 (d, 2H, *J* = 8.4 Hz), 7.43-7.40 (m, 2H), 7.35-7.31 (m, 2H), 7.24 (d, 2H, *J* = 8.4 Hz), 5.99 (brt, 1H, *J* = 5.6 Hz), 5.43 (s, 2H), 5.09 (t, 1H, *J* = 5.7 Hz), 4.43 (d, 2H, *J* = 5.6 Hz), 4.28-4.15 (m, 4H), 3.08-3.01 (m, 1H), 2.99-2.92 (m, 1H), 1.70-1.58 (m, 2H), 1.52-1.35 (m, 2H)

¹³C NMR (126 MHz, DMSO-*d*₆) δ : 171.0, 158.9, 156.1, 143.9, 143.8, 140.7, 137.6, 137.4, 127.6, 127.0, 126.9, 125.4, 120.1, 118.9, 65.7, 62.6, 55.0, 46.7, 40.4, 29.3, 26.9

Fmoc-NH-Val-Cit-PAB-OH (51)



| Raw formula | Molecular mass | Aspect | Yield |
|---|----------------------------|--------------|-------|
| C ₃₃ H ₃₉ N ₅ O ₆ | 601.29 g.mol ⁻¹ | Yellow solid | 56 % |

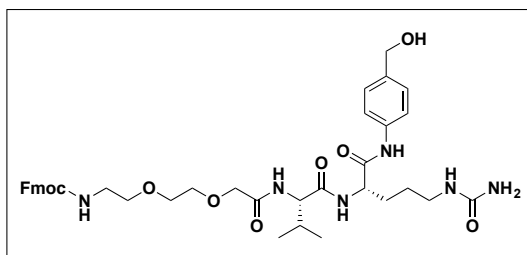
50 (1.0 g, 1.0 eq, 1.99 mmol) was stirred in a 20% piperidine in DMF solution (8 mL) for 30 min. The solvent was removed under vacuum and the product was precipitated from cold Et₂O and washed with the same solvent to remove residual amounts of piperidine. After deep drying under vacuum, the intermediate was dissolved in dry DMF (8 mL) and Fmoc-NH-Val-OSu was added (1.05 g, 1.2 eq, 2.4 mmol). The mixture was stirred at room temperature for 3h. The solvent was removed under vacuum and the product was purified by flash chromatography (DCM/MeOH 3% to 12%) to give **51** as a yellow solid.

MS (ESI), *m/z* (%): 602.4 [M+H]⁺

¹H NMR (500 MHz, DMSO-*d*₆) δ: 9.98 (brs, 1H), 8.11 (d, 1H, *J*= 7.6 Hz), 7.89 (d, 2H, *J*= 7.6 Hz), 7.74 (t, 2H, *J*= 7.9 Hz), 7.56-7.54 (m, 2H), 7.45-7.39 (m, 3H), 7.32 (td, 2H, *J*= 7.4 Hz, 0.9 Hz), 7.24-7.22 (m, 2H), 5.99 (brt, 1H, *J*= 5.6 Hz), 5.40 (s, 2H), 5.10 (brt, 1H, *J*= 5.4 Hz), 4.44-4.43 (m, 3H), 4.34-4.20 (m, 3H), 3.93 (dd, 1H, *J*= 8.9 Hz, 7.1 Hz), 3.05-2.88 (m, 2H), 2.05-1.96 (m, 1H), 1.75-1.55 (m, 2H), 1.50-1.33 (m, 2H), 0.89-0.85 (m, 6H)

¹³C NMR (126 MHz, DMSO-*d*₆) δ: 171.2, 170.4, 158.9, 156.1, 143.9, 143.8, 140.7, 137.5, 137.4, 127.6, 127.1, 126.9, 125.4, 120.1, 118.9, 65.7, 62.6, 60.1, 53.1, 46.7, 30.4, 29.5, 26.8, 19.2, 18.3

Fmoc-NH-PEG₂-Val-Cit-PAB-OH (52)



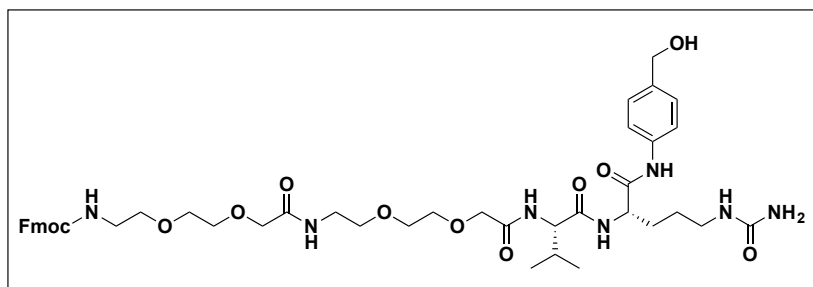
| Raw formula | Molecular mass | Aspect | Yield |
|---|----------------------------|-------------|-------|
| C ₃₉ H ₅₀ N ₆ O ₉ | 746.36 g.mol ⁻¹ | White solid | 47 % |

51 (1.0 g, 1.0 eq, 1.66 mmol) was stirred in a 20% piperidine in DMF solution (8 mL) for 30 min. Then, the solvent was removed under vacuum and the product was precipitated from cold Et₂O and washed with the same solvent to remove residual amounts of piperidine. After deep drying under vacuum, the intermediate was dissolved in dry DMF (8 mL) and Fmoc-NH-PEG₂-OSu was added (0.962 g, 1.2 eq, 2.00 mmol). The mixture was stirred at room temperature for 3h. The solvent was removed under vacuum and the crude was purified by flash chromatography (DCM/MeOH 0% to 15%) to give **52** as a yellow solid.

MS (ESI), m/z (%): 747.5 [M+H]⁺

¹H NMR (500 MHz, DMSO-d₆) δ: 9.96 (brs, 1H), 8.34 (d, 1H, J= 7.5 Hz), 7.88 (d, 2H, J= 7.5 Hz), 7.68 (d, 2H, J= 7.4 Hz), 7.56-7.54 (m, 2H), 7.48 (d, 1H, J= 9.0 Hz), 7.40 (t, 2H, J= 7.4 Hz), 7.34-7.30 (m, 3H), 7.23-7.22 (m, 2H), 6.00 (brt, 1H, J= 5.7 Hz), 5.42 (s, 2H), 5.09 (brs, 1H), 4.43-4.38 (m, 3H), 4.34-4.27 (m, 3H), 4.20 (t, 1H, J= 6.9 Hz), 3.95 (s, 2H), 3.64-3.55 (m, 4H), 3.45-3.40 (m, 2H), 3.19-3.13 (m, 2H), 3.04-2.93 (m, 2H), 2.04-1.96 (m, 1H), 1.73-1.56 (m, 2H), 1.48-1.32 (m, 2H), 0.88 (d, 3H, J= 6.8 Hz), 0.82 (d, 3H, J= 6.8 Hz)

¹³C NMR (126 MHz, DMSO-d₆) δ: 170.7, 170.3, 169.0, 158.9, 156.2, 143.9, 140.7, 137.5, 137.4, 128.9, 127.6, 127.3, 127.0, 126.9, 125.2, 121.1, 120.1, 119.0, 118.9, 70.3, 69.7, 69.3, 69.2, 65.3, 62.6, 56.6, 53.2, 46.7, 38.6, 31.1, 29.4, 26.9, 25.2, 19.2, 18.0

Fmoc-NH-PEG₂-PEG₂-Val-Cit-PAB-OH (53)

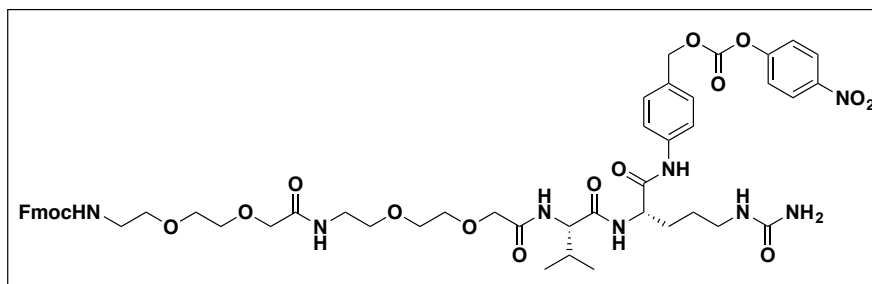
| Raw formula | Molecular mass | Aspect | Yield |
|--|----------------------------|-------------|-------|
| C ₄₅ H ₆₁ N ₇ O ₁₂ | 891.44 g.mol ⁻¹ | White solid | 61 % |

52 (150 mg, 1.0 eq, 0.20 mmol) was stirred in a 20% piperidine in DMF solution (1 mL) for 30 min. Then, the solvent was removed under vacuum and the product was precipitated from cold diethyl ether and washed with the same solvent to remove residual amounts of piperidine. After deep drying under vacuum, the intermediate was dissolved in dry DMF (1 mL) and Fmoc-NH-PEG₂-OSu was added (124 mg, 1.2 eq, 0.26 mmol). The mixture was stirred at room temperature for 3h. The solvent was removed under vacuum and the crude was purified by flash chromatography (DCM/MeOH 0% to 15%) to give **53** as a white solid.

MS (ESI), m/z (%): 892.5 [M+H]⁺

¹H NMR (400 MHz, DMSO-d₆) δ: 9.99 (brs, 1H), 8.39-8.34 (m, 1H), 7.89-7.83 (m, 3H), 7.67-7.65 (m, 1H), 7.56-7.50 (m, 3H), 7.43-7.32 (m, 4H), 7.24-7.22 (m, 2H), 6.61 (brm, 1H), 6.28 (s, 2H), 6.02 (brm, 1H), 5.43 (s, 2H), 4.43-4.30 (m, 4H), 3.95-3.86 (m, 4H), 4.61-3.53 (m, 11H), 3.46 (brt, 2H, J= 6.0 Hz), 3.40 (brt, 2H, J= 6.0 Hz), 3.29 (q, 2H, J= 11.5 Hz, 5.6 Hz), 3.1-2.89 (m, 4H), 2.05-1.96 (m, 1H), 1.72-1.55 (m, 2H), 1.48-1.38 (m, 2H), 0.89-0.82 (m, 6H)

¹³C NMR (101 MHz, DMSO-d₆) δ: 170.7, 170.3, 169.3, 169.0, 158.9, 142.6, 139.4, 137.5, 137.4, 128.9, 127.3, 126.9, 124.9, 121.4, 120.0, 118.8, 109.7, 70.2, 70.1, 69.9, 69.7, 69.4, 69.3, 69.0, 67.0, 62.6, 56.7, 53.2, 38.5, 37.9, 31.1, 30.4, 29.3, 26.8, 25.1, 19.2, 18.0

Fmoc-NH-PEG₂-PEG₂-Val-Cit-PAB-PNP (55)

| Raw formula | Molecular mass | Aspect | Yield |
|--|-----------------------------|-------------|-------|
| C ₅₂ H ₆₄ N ₈ O ₁₆ | 1056.44 g.mol ⁻¹ | White solid | 93 % |

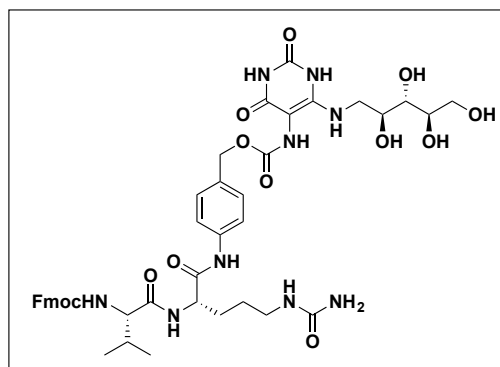
53 (50 mg, 1.0 eq, 0.056 mmol) was dissolved in DMF (1 mL). Bis(4-nitrophenyl)carbonate (34 mg, 2.0 eq, 0.11 mmol) and DIEA (11 μ L, 1.5 eq, 0.084 mmol) were added and the mixture was stirred at room temperature overnight. DMF was removed under vacuum and the product was purified by column chromatography (DCM/MeOH 5% to 10%) to give **55** as a white solid.

MS (ESI), *m/z* (%): 1057.9 [M+H]⁺

¹H NMR (500 MHz, DMSO-*d*₆) δ : 10.11 (s, 1H), 8.36 (d, 1H, *J* = 7.4 Hz), 8.32-8.30 (m, 2H), 7.88 (d, 1H, *J* = 7.5 Hz), 7.69-7.64 (m, 5H), 7.57-7.55 (m, 2H), 7.46 (d, 1H, *J* = 9.0 Hz), 7.42-7.38 (m, 4H), 7.33-7.30 (m, 3H), 5.98 (brt, 1H, *J* = 5.6 Hz), 5.42 (s, 2H), 5.24 (s, 2H), 4.42-4.38 (m, 1H), 4.34-4.28 (m, 3H), 4.20 (t, 1H, *J* = 6.7 Hz), 3.93 (s, 2H), 3.86 (s, 2H), 3.62-3.50 (m, 8H), 3.47-3.40 (m, 4H), 3.29-3.25 (m, 2H), 3.14 (dd, 2H, *J* = 11.6 Hz, 5.8 Hz), 3.97-2.92 (m, 2H), 2.03-1.96 (m, 1H), 1.74-1.56 (m, 2H), 1.49-1.33 (m, 2H), 1.23 (s, 1H), 0.88 (d, 3H, *J* = 6.8 Hz), 0.82 (d, 3H, *J* = 6.8 Hz)

¹³C NMR (126 MHz, DMSO-*d*₆) δ : 170.8, 170.6, 169.2, 169.0, 158.9, 156.2, 155.3, 151.9, 145.2, 143.9, 140.7, 139.4, 129.5, 129.3, 127.6, 127.0, 125.4, 125.1, 122.6, 120.1, 119.0, 70.2, 70.1, 69.9, 69.7, 69.3, 69.1, 69.0, 65.3, 59.7, 56.6, 53.2, 46.7, 38.5, 37.9, 31.0, 29.2, 26.9, 19.2, 17.9

Fmoc-NH-Val-Cit-PAB-5-A-RU (56)



| Raw formula | Molecular mass | Aspect | Yield |
|--|----------------------------|-------------|-------|
| C ₄₃ H ₅₃ N ₉ O ₁₃ | 903.38 g.mol ⁻¹ | White solid | 13 % |

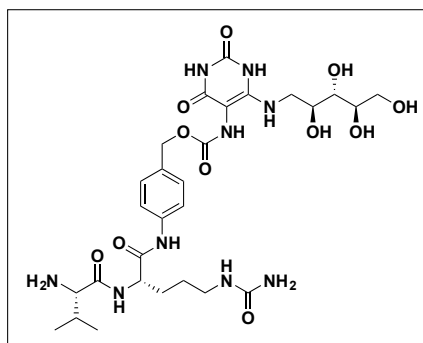
To **54** (20 mg, 1.0 eq, 0.026 mmol) was added **5** (24 mg, 3.0 eq, 0.078 mmol) followed by pyridine (0.3 mL). The mixture was stirred at room temperature during 2h. Pyridine was removed under vacuum and the product was purified by preparative C18 RP-HPLC using the following gradient: 30% ACN (0.1% formic acid)/70% H₂O (0.1% formic acid) to 50% ACN over 20 minutes and 100% ACN over 5 minutes. The product was freeze dried to give **56** as a white solid.

MS (ESI), *m/z* (%): 904.4 [M+H]⁺

¹H NMR (500 MHz, DMSO-*d*₆) δ : 10.24 (brs, 1H), 10.06-10.01 (brm, 1H), 8.12 (d, 1H, *J* = 7.2 Hz), 7.89 (d, 2H, *J* = 7.8 Hz), 7.76-7.73 (m, 2H), 7.60-7.52 (m, 3H), 7.43-7.40 (m, 3H), 7.34-7.22 (m, 4H), 6.50-6.43 (brm, 1H), 5.97 (brs, 1H), 5.40 (s, 2H), 4.97 (s, 2H), 4.44-4.40 (m, 1H), 4.33-4.29 (m, 1H), 4.25-4.23 (m, 2H), 3.95-3.92 (m, 1H), 3.69-3.64 (m, 1H), 3.58 (dd, 1H, *J* = 10.8 Hz, 3.3 Hz), 3.53-3.50 (m, 1H), 3.45-3.39 (m, 3H), 3.27-3.24 (m, 1H), 3.04-2.99 (m, 1H), 2.97-2.91 (m, 1H), 2.02-1.96 (m, 1H), 1.73-1.56 (m, 2H), 1.49-1.33 (m, 2H), 1.12 (s, 1H), 0.88 (d, 3H, *J* = 6.7 Hz), 0.85 (d, 3H, *J* = 6.7 Hz)

¹³C NMR (126 MHz, DMSO-*d*₆) δ : 171.2, 170.5, 161.2, 158.8, 156.2, 156.1, 152.9, 150.4, 143.9, 143.7, 140.6, 138.5, 131.6, 128.5, 127.6, 127.0, 125.3, 120.1, 118.9, 86.9, 72.7, 72.5, 71.6, 65.6, 65.4, 63.1, 60.0, 53.1, 46.7, 44.4, 30.4, 29.5, 26.7, 19.2, 18.2

H₂N-Val-Cit-PAB-5-A-RU (58)



| Raw formula | Molecular mass | Aspect | Yield |
|--|----------------------------|-------------|-------|
| C ₂₈ H ₄₃ N ₉ O ₁₁ | 681.31 g.mol ⁻¹ | White solid | 73 % |

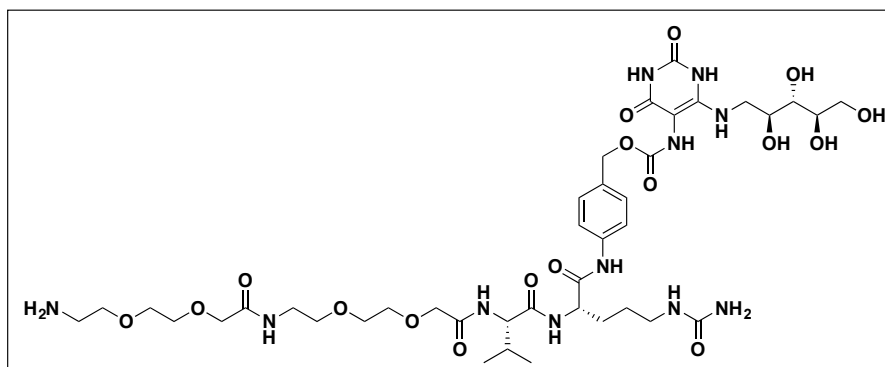
56 (6 mg, 1.0 eq, 6.64 μmol), was dissolved in DMF (0.3 mL) and piperidine was added (3 μL, 5.0 eq, 33.2 μmol). The mixture was stirred at room temperature for 10 min. The solvent was removed under vacuum and the product was purified by preparative C18 RP-HPLC using the following conditions: Solvent A: Water + 0.1% formic acid; Solvent B: ACN + 0.1% formic acid. Gradient of 25 min starting with 100% A for 5 min, then 5% B for 5 min and then gradual increase of B to reach 100% B at 20 min followed by 5 min with 100% B. After lyophilization, the product was recovered as a white solid.

MS (ESI), m/z (%): 682.3 [M+H]⁺

¹H NMR (500 MHz, DMSO-d₆) δ: 10.32 (brs, 1H), 10.15 (brs, 1H), 8.26-8.24 (m, 2H), 7.62-7.53 (m, 3H), 7.35-7.22 (m, 2H), 6.56-6.46 (m, 1H), 6.02-5.99 (m, 1H), 5.42 (brs, 2H), 4.97-4.95 (m, 2H), 4.45 (brs, 1H), 3.70-3.67 (m, 1H), 3.58 (dd, 1H, J = 11.0 Hz, 3.4 Hz), 3.53-3.49 (m, 1H), 3.46-3.39 (m, 4H), 3.29-3.21 (m, 2H), 3.16 (d, 1H, J = 5.0 Hz), 3.06-2.99 (m, 1H), 2.97-2.91 (m, 1H), 2.0-1.93 (m, 1H), 1.74-1.67 (m, 1H), 1.63-1.56 (m, 1H), 1.45-1.34 (m, 2H), 0.90 (d, 3H, J = 6.8 Hz), 0.82 (d, 3H, J = 6.8 Hz)

¹³C NMR (126 MHz, DMSO-d₆) δ: 173.0, 170.6, 163.9, 161.2, 158.9, 156.2, 153.0, 150.1, 138.5, 131.7, 128.6, 119.0, 86.9, 72.6, 71.4, 65.5, 63.1, 59.1, 52.6, 44.4, 38.6, 31.0, 29.9, 26.7, 19.3, 17.1

H₂N-PEG₂-PEG₂-Val-Cit-PAB-5-A-RU (59)



| Raw formula | Molecular mass | Aspect | Yield |
|---|------------------------------|-------------|-------|
| C ₄₀ H ₆₅ N ₁₁ O ₁₇ | 971.4560 g.mol ⁻¹ | White solid | 61 % |

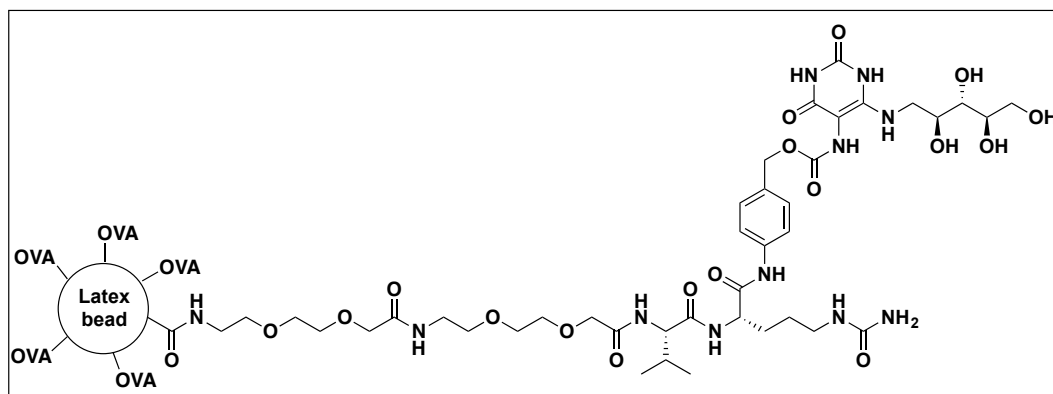
57 (6.0 mg, 1.0 eq, 6.64 μmol), was dissolved in DMF (0.3 mL) and piperidine was added (3 μL, 5.0 eq, 33.2 μmol). The mixture was stirred at room temperature for 10 min. The solvent was removed under vacuum and the product was purified by preparative C18 RP-HPLC using the following conditions: Solvent A: Water + 0.1% formic acid; Solvent B: ACN + 0.1% formic acid. Gradient of 25 min starting with 100% A for 5 min, then 5% B for 5 min and then gradual increase of B to reach 100% B at 20 min followed by 5 min with 100% B. After lyophilization, the product was recovered as a white solid.

MS (ESI), m/z (%): 972.6 [M+H]⁺

¹H NMR (500 MHz, DMSO-d₆) δ: 10.13 (brs, 1H), 8.44-8.39 (m, 2H), 7.73 (t, 1H, J= 5.9 Hz), 7.61-7.50 (m, 3H), 7.34-7.22 (m, 2H), 6.45-6.40 (m, 1H), 6.12-6.06 (m, 1H), 5.45 (s, 2H), 4.97 (s, 2H), 4.41-4.37 (m, 1H), 4.32 (dd, 1H, J= 8.8 Hz, 6.6 Hz), 3.95 (s, 2H), 3.88 (s, 2H), 3.67-3.24 (m, 24H), 3.03-2.91 (m, 2H), 2.89-2.82 (m, 2H), 2.04-1.97 (m, 1H), 1.76-1.55 (m, 2H), 1.49-1.31 (m, 2H), 0.88 (d, 3H, J= 6.7 Hz), 0.83 (d, 3H, J= 6.7 Hz)

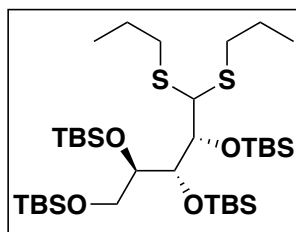
¹³C NMR (126 MHz, DMSO-d₆) δ: 170.8, 170.5, 169.3, 169.0, 166.6, 165.2, 161.3, 158.9, 156.2, 153.9, 150.8, 138.6, 131.6, 128.5, 127.4, 118.9, 86.9, 72.8, 72.5, 71.7, 70.3, 70.0, 69.9, 69.7, 69.4, 69.3, 69.0, 68.8, 65.5, 63.1, 56.6, 53.2, 44.4, 38.5, 38.0, 31.1, 29.2, 26.8, 19.2, 18.0

LB-HN-PEG₂-PEG₂-Val-Cit-PAB-5-A-RU (60)



0.25 mL of the stock suspension of carboxylate-modified latex beads (CML beads, 4% w/v, 1 μ m diameter) was introduced in a 1.5 mL Eppendorf vial. The beads were washed three times with MES Buffer (100 mM, pH 6.0) and the supernatant was discarded after centrifugation (10 min, 15000 rpm). A solution of EDC (40 mg/mL) and NHS (12 mg/mL) in MES buffer was added and the beads were stirred on rotator (20 min, 750 rpm). Activated beads were then washed with MES Buffer three times. They were re-suspended in PBS Buffer and a solution of **59** (2 mg/mL in PBS) was added. The tube was placed on rotator (2h, 750 rpm) for stirring. The conjugated beads were washed three times and the supernatant was kept to determine the average loading on beads. The conjugate was re-suspended in PBS Buffer and ovalbumin solution (2 mg/mL of EndoFit endotoxin free ovalbumin from InVivoGen) was added. The tube was stirred in rotator (overnight, 750 rpm) and washed again with PBS buffer. The conjugated beads were stocked at 4°C in PBS Buffer (250 μ L) and protected from light.

(5R,6R,7R)-5-(bis(propylthio)methyl)-6,7-bis((tert-butyl dimethylsilyl)oxy)-2,2,3,3,10,10,11,11-octamethyl-4,9-dioxa-3,10-disiladodecane (61)



| Raw formula | Molecular mass | Aspect | Yield |
|---|------------------------------|-------------|-------|
| C ₃₅ H ₈₀ O ₄ S ₂ Si ₄ | 740.4575 g.mol ⁻¹ | White solid | 54% |

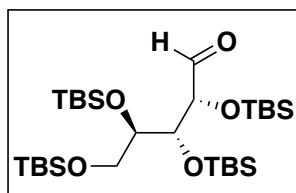
To **6** (1.0 g, 1.0 eq, 3.51 mmol) in DCM (8 mL) was added dry 2,6-lutidine (2.58 mL, 5.0 eq, 17.6 mmol) and TBDMS triflate (3.63 mL, 4.5 eq, 16.0 mmol) dropwise at 0°C. The mixture was stirred at 0°C for 30 minutes and then at room temperature for 3h. After completion, water was added and the product was extracted with DCM. The organic layer was washed by 10% aqueous CuSO₄ to remove residual 2,6-lutidine. It was then dried over MgSO₄ and concentrated under vacuum. The product was purified by column chromatography (hexane 100%) to give **61** as a colorless oil that solidified upon standing as a white powder.

HR-MS (ESI), *m/z* (%): 775.4279 [M+Cl]⁻

¹H NMR (400 MHz, CDCl₃) δ: 4.19 (ddd, 1H, J= 7.4 Hz, 3.9 Hz, 1.0 Hz), 4.10 (d, 1H, J= 1.4 Hz), 4.07 (dd, 1H, J= 8.5 Hz, 1.0 Hz), 3.90 (dd, 1H, J= 8.5 Hz, 1.4 Hz), 3.69 (dd, 1H, J= 10.5 Hz, 3.9 Hz), 3.58 (dd, 1H, J= 10.5 Hz, 7.4 Hz), 2.76-2.70 (m, 1H), 2.63-2.55 (m, 1H), 2.53-2.44 (m, 2H), 1.66-1.56 (m, 4H), 1.01-0.89 (m, 42H), 0.28 (s, 3H), 0.21 (s, 3H), 0.17 (s, 3H), 0.14 (s, 3H), 0.12 (s, 3H), 0.10 (s, 3H), 0.05 (s, 6H)

¹³C NMR (101 MHz, CDCl₃) δ: 78.40, 77.96, 73.79, 64.26, 57.24, 35.23, 33.84, 26.60-26.31 (12C), 23.38, 22.98, 18.93, 18.70, 18.57, 18.51, 13.96, 13.76, -2.80, -3.27, -3.42, -4.12, -4.16, -5.14, -5.20 (2C)

(2R,3R,4R)-2,3,4,5-tetrakis((tert-butyldimethylsilyl)oxy)pentanal (62)



| Raw formula | Molecular mass | Aspect | Yield |
|--|----------------------------|-------------|-------|
| C ₂₉ H ₆₆ O ₅ Si ₄ | 606.40 g.mol ⁻¹ | White solid | 83% |

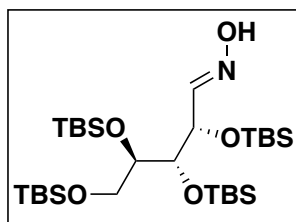
To **61** (1.0 g, 1.0 eq, 1.35 mmol) in a mixture of acetone/water (5/0.5 mL) was added NaHCO₃ (0.51 g, 4.5 eq, 6.08 mmol) and iodine (0.69 g, 2.0 eq, 2.70 mmol) at 0°C. The mixture was stirred at room temperature for 16h. Additional amounts of NaHCO₃ (0.11 g, 1.0 eq, 1.35 mmol) and iodine (0.34 g, 1.0 eq, 1.35 mmol) were added and the mixture was further stirred for 4h. 10% aqueous Na₂S₂O₃ was added to quench excess iodine and the product was extracted by DCM. The organic layer was dried over MgSO₄ and concentrated under vacuum. The product was purified by column chromatography (elution gradient hexane 100% to hexane/EtOAc 10/1) to get **62** as a colorless oil.

MS (ESI), *m/z*: 631.3 [M+Na]⁺

¹H NMR (400 MHz, CDCl₃) δ : 9.64 (d, 1H, *J* = 1.6 Hz), 4.31 (dd, 1H, *J* = 3.4 Hz, 1.6 Hz), 4.01-4.00 (m, 1H), 3.89-3.85 (m, 1H), 3.71 (dd, 1H, *J* = 10.4 Hz, 5.4 Hz), 3.55 (dd, 1H, *J* = 10.4 Hz, 5.6 Hz), 0.91-0.86 (m, 36H), 0.10-0.05 (m, 24H)

¹³C NMR (101 MHz, CDCl₃) δ : 202.25, 78.13, 77.82, 75.44, 64.81, 26.16-26.04 (12C), 18.49 (2C), 18.33 (2C), -4.13, -4.37 (4C), -4.80, -5.11, -5.18.

(2S,3S,4R,E)-2,3,4,5-tetrakis((tert-butyldimethylsilyl)oxy)pentanal oxime (63)



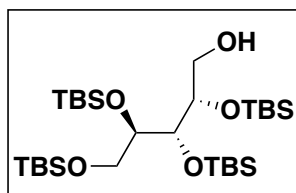
| Raw formula | Molecular mass | Aspect | Yield |
|---|----------------------------|---------------|-------|
| C ₂₉ H ₆₇ NO ₅ Si ₄ | 621.41 g.mol ⁻¹ | colorless oil | 90% |

NaHCO₃ (28 mg, 4.0 eq, 0.33 mmol) was added to a solution of NH₂OH.HCl (26 mg, 4.5 eq, 0.37 mmol) in EtOH/H₂O (3/0.3 mL) and the suspension was stirred for 30 min at room temperature. **62** (50 mg, 1.0 eq, 0.08 mmol) was added and the mixture was stirred overnight. Water was added and the product was extracted by DCM. The organic layer was dried over MgSO₄ and concentrated under vacuum. The product was purified by column chromatography (hexane/EtOAc 10%) to give **63** as a colorless oil.

¹H NMR (400 MHz, CDCl₃) δ: 7.28 (m, 1H), 4.39 (dd, 1H, J = 7.8 Hz, 6.4 Hz), 3.90-3.87 (m, 1H), 3.82-3.76 (m, 2H), 3.55 (dd, 1H, J = 10.3 Hz, 6.4 Hz), 1.27 (brs, 1H), 0.91-0.88 (m, 36H), 0.12-0.06 (m, 24H)

¹³C NMR (101 MHz, CDCl₃) δ: 152.4, 78.0, 75.1, 71.3, 64.9, 26.2-26.0 (12C), 18.6, 18.4 (2C), 18.3, -4.0 (2C), -4.2, -4.5, -4.5 (2C), -5.2, -5.3

(2S,3S,4R)-2,3,4,5-tetrakis((tert-butyl)dimethylsilyloxy)pentan-1-ol (64)



| Raw formula | Molecular mass | Aspect | Yield |
|--|----------------------------|-------------|-------|
| C ₂₉ H ₆₈ O ₅ Si ₄ | 609.41 g.mol ⁻¹ | White solid | 90% |

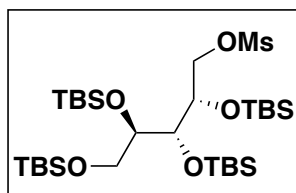
To **63** (290 mg, 1.0 eq, 0.48 mmol) in MeOH (5 mL) was added NaBH₄ (27 mg, 1.5 eq, 0.48 mmol) at 0°C. The mixture was then stirred at room temperature for 3h. The reaction was quenched by a saturated aqueous NH₄Cl. The product was extracted by DCM and the organic layer was dried over MgSO₄ and concentrated under vacuum. The product was purified by column chromatography (hexane/EtOAc 10/1) and **64** was obtained as a colorless oil.

MS (ESI), *m/z*: 609.9 [M+H]⁺

¹H NMR (400 MHz, CDCl₃) δ : 3.90-3.83 (m, 3H), 3.72-3.66 (m, 3H), 3.57-3.53 (m, 1H), 2.04 (brs, 1H), 0.92-0.90 (m, 36H), 0.12-0.05 (m, 24H)

¹³C NMR (101 MHz, CDCl₃) δ : 77.01, 75.73, 73.04, 64.72, 63.37, 26.21-26.11 (12C), 18.53, 18.46, 18.36, 18.26, -3.87, -4.17, -4.25, -4.42 (2C), -4.73, -5.16, -5.25.

(2S,3R,4R)-2,3,4,5-tetrakis((tert-butyldimethylsilyl)oxy)pentyl methanesulfonate (65)



| Raw formula | Molecular mass | Aspect | Yield |
|---|----------------------------|---------------|-------|
| C ₃₀ H ₇₀ O ₇ SSi ₄ | 686.39 g.mol ⁻¹ | Colorless oil | 75% |

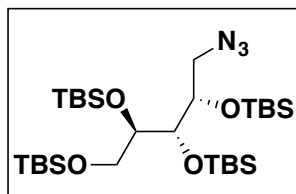
To **64** (1.28 g, 1.0 eq, 2.1 mmol) in pyridine (5 mL) was added at 0°C methanesulfonyl chloride (0.2 mL, 1.2 eq, 2.5 mmol) dropwise. The mixture was then stirred at room temperature for 3h. After completion, pyridine was removed under vacuum. Water was added and the product was extracted by DCM. The organic layer was dried over MgSO₄ and concentrated under vacuum. The product was purified by column chromatography (hexane/EtOAc 10/0.5) and **65** was isolated as a colorless oil.

MS (ESI), *m/z*: 709.7 [M+Na]⁺

¹H NMR (400 MHz, CDCl₃) δ : 4.50-4.46 (m, 1H), 4.17-4.13 (m, 2H), 3.92 (m, 1H), 3.74-3.70 (m, 1H), 3.62 (dd, 1H, *J* = 10.5 Hz, 6.0 Hz), 3.56 (dd, 1H, *J* = 10.5 Hz, 5.4 Hz), 2.96 (s, 3H), 0.91-0.89 (m, 36H), 0.14-0.05 (m, 24H)

¹³C NMR (101 MHz, CDCl₃) δ : 77.16 (signal under solvent peak), 75.80, 72.40, 71.11, 64.46, 37.20, 26.17-26.09 (12C), 18.46-18.27 (4C), -4.17 to -4.44 (6C), -5.11 to -5.22 (2C)

(5S,6S,7R)-5-(azidomethyl)-6,7-bis((tert-butyldimethylsilyl)oxy)-2,2,3,3,10,10,11,11-octamethyl-4,9-dioxa-3,10-disiladodecane (66)



| Raw formula | Molecular mass | Aspect | Yield |
|---|------------------------------|---------------|-------|
| C ₂₉ H ₆₇ N ₃ O ₄ Si ₄ | 633.4209 g.mol ⁻¹ | Colorless oil | 99% |

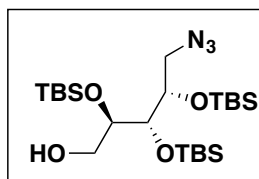
To **65** (1.0 g, 1.0 eq, 1.46 mmol) in dry DMF (5 mL) was added sodium azide (0.14 g, 1.5 eq, 2.2 mmol) and the reaction was heated under reflux for 2h. DMF was then removed under vacuum. Water was added and the product was extracted by DCM. The organic layer was dried over MgSO₄ and concentrated under vacuum. The product was purified by column chromatography (hexane 100%) to give **66** as a colorless oil.

HR-MS (ESI), *m/z*: 634.4285 [M+H]⁺

¹H NMR (400 MHz, CDCl₃) δ : 3.98-3.93 (m, 1H), 3.88-3.86 (m, 1H), 3.78-3.74 (m, 1H), 3.64 (dd, 1H, J= 10.4 Hz, 5.2 Hz), 3.55 (dd, 1H, J= 10.4 Hz, 5.6 Hz), 3.49 (dd, 1H, J= 12.8 Hz, 2.5 Hz), 3.34 (dd, 1H, J= 12.8 Hz, 6.3 Hz), 0.93-0.89 (m, 36H), 0.14-0.05 (m, 24H)

¹³C NMR (101 MHz, CDCl₃) δ : 77.09, 75.46, 72.44, 64.58, 54.36, 26.22-26.17 (12C), 18.51, 18.47, 18.30, 18.21, -4.12, -4.17, -4.20, -4.36, -4.42, -4.45, -5.11, -5.23.

(2R,3S,4S)-5-azido-2,3,4-tris((tert-butyldimethylsilyl)oxy)pentan-1-ol (67)



| Raw formula | Molecular mass | Aspect | Yield |
|---|----------------------------|------------------|-------|
| C ₂₃ H ₅₃ N ₃ O ₄ Si ₃ | 519.33 g.mol ⁻¹ | Light yellow oil | 19% |

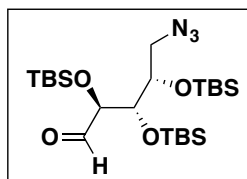
To **66** (367 mg, 1.0 eq, 0.58 mmol) in a 1/1 mixture of DCM/MeOH (4/4 mL) was added (1R)-(-)-10-camphorsulfonic acid (13 mg, 0.1 eq, 0.06 mmol). The mixture was stirred at room temperature during 6h, then quenched with 5% aqueous Na₂CO₃ and extracted by DCM. The combined organic layers were dried over MgSO₄ and concentrated under vacuum. The product was purified by chromatography (hexane/EtOAc 5%). The purification allowed to recover all the starting material that did not react in addition to **67** obtained as a light yellow oil.

MS (ESI), *m/z*: 542.4 [M+Na]⁺

¹H NMR (400 MHz, CDCl₃) δ : 3.96-3.93 (m, 1H), 3.85 (dd, 1H, *J* = 5.9 Hz, 3.3 Hz), 3.73-3.70 (m, 2H), 3.62-3.58 (m, 1H), 3.42 (dd, 1H, *J* = 12.8 Hz, 3.6 Hz), 3.32 (dd, 1H, *J* = 12.8 Hz, 6.4 Hz), 1.76 (brs, 1H), 0.92-0.89 (m, 27H), 0.16-0.12 (m, 18H)

¹³C NMR (101 MHz, CDCl₃) δ : 76.59, 73.42, 72.87, 63.15, 53.63, 26.20-26.05 (9C), 18.47, 18.25, 18.22, -4.02, -4.28, -4.30, -4.37, -4.43, -4.73

(2S,3S,4S)-5-azido-2,3,4-tris((tert-butyldimethylsilyl)oxy)pentanal (68)



| Raw formula | Molecular mass | Aspect | Yield |
|---|------------------------------|---------------|-------|
| C ₂₃ H ₅₁ N ₃ O ₄ Si ₃ | 517.3187 g.mol ⁻¹ | colorless oil | 71% |

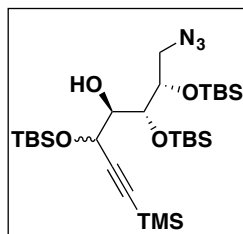
To **67** (58 mg, 1.0 eq, 0.11 mmol) in dry DCM (1.5 mL) was added NaHCO₃ (37 mg, 4.0 eq, 0.45 mmol) and Dess-Martin periodinane reagent (95 mg, 2.0 eq, 0.22 mmol) at 0°C. The reaction was stirred at room temperature for 30 min. Then, 10% aqueous Na₂S₂O₃ and 5% aqueous Na₂CO₃ were added to quench the reaction. The product was extracted by DCM and the organic layer was dried over MgSO₄ and concentrated under vacuum. The crude product was purified by chromatography (hexane/EtOAc 10/0.5) and obtained as a colorless oil.

HR-MS (ESI), *m/z*: 535.3540 [M+NH₄]⁺

¹H NMR (400 MHz, CDCl₃) δ : 9.61 (d, 1H, J= 1.5 Hz), 4.21-4.20 (m, 1H), 3.96-3.95 (m, 2H), 3.51-3.47 (m, 1H), 3.40-3.36 (m, 1H), 0.93-0.86 (m, 27H), 0.16-0.10 (m, 18H)

¹³C NMR (101 MHz, CDCl₃) δ : 203.67, 78.64, 77.55, 71.72, 53.29, 26.10-26.01 (9C), 18.47, 18.36, 18.14, -4.03, -4.07, -4.32, -4.41, -4.67, -4.88

(6R,7R,8S)-8-(azidomethyl)-7-((tert-butyldimethylsilyloxy)-2,2,3,3,10,10,11,11-octamethyl-5-((trimethylsilyl)ethynyl)-4,9-dioxo-3,10-disiladodecan-6-ol (69)



| Raw formula | Molecular mass | Aspect | Yield |
|---|----------------------------|---------------|-------|
| C ₂₈ H ₆₁ N ₃ O ₄ Si ₄ | 615.37 g.mol ⁻¹ | colorless oil | 45% |

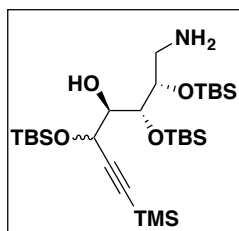
TMS-acetylene (0.049 mL, 3.0 eq, 0.58 mmol) was dissolved in dry THF (2 mL). The mixture was cooled at -78°C and *n*-butyllithium (2.5 M in hexane solution, 0.23 mL, 3.0 eq, 0.58 mmol) was added. The mixture was gradually warmed up to 0°C and further stirred for an additional 1h. The reaction mixture was again cooled to -78°C and a **68** (0.100 g, 1.0 eq, 0.19 mmol) solution in THF (2 mL) was added dropwise. The mixture was gradually warmed-up to room temperature and stirred for 3h. After completion, the mixture was quenched by saturated aqueous NH₄Cl and the product was extracted by DCM. The organic layer was dried over MgSO₄ and concentrated under vacuum. The product was purified by column chromatography (hexane/EtOAc 10/0.5) and it was isolated as a mixture of two diastereomers (a fraction of the major diastereomer was isolated for NMR analysis). A light yellow oil was obtained.

MS (ESI), *m/z*: 638.6 [M+Na]⁺

¹H NMR (400 MHz, CDCl₃) (major diastereomer) δ : 4.55 (d, 1H, J= 3.7 Hz), 4.16-4.12 (m, 1H), 3.90 (dd, 1H, J= 6.6 Hz, 2.9 Hz), 3.75 (dd, 1H, J= 6.6 Hz, 3.8 Hz), 3.41 (dd, 1H, J= 12.8 Hz, 3.6 Hz), 3.34 (dd, 1H, J= 12.8 Hz, 6.9 Hz), 2.09 (brs, 1H), 0.95-0.88 (m, 27H), 0.18-0.12 (m, 27H)

¹³C NMR (101 MHz, CDCl₃) (major diastereomer) δ : 103.73, 91.90, 78.00, 76.21, 72.37, 65.90, 53.33, 26.21-26.15 (9C), 18.52, 18.44, 18.31, -0.08 (3C), -3.73, (2C), -4.05, -4.17, -4.57, -4.70

(4R,5S,6S)-7-amino-4,5,6-tris((tert-butyldimethylsilyl)oxy)-1-(trimethylsilyl)hept-1-yn-3-ol (70)



| Raw formula | Molecular mass | Aspect | Yield |
|---|------------------------------|---------------|-------|
| C ₂₈ H ₆₃ NO ₄ Si ₄ | 589.3834 g.mol ⁻¹ | colorless oil | 75% |

To **69** (0.280 mg, 1.0 eq, 0.46 mmol) in a 5/1 mixture of THF/H₂O (2.5 mL/0.5 mL) was added triphenylphosphine (1.19 g, 10 eq, 4.55 mmol). The mixture was heated under reflux during 2h. THF was removed under vacuum and water/DCM extraction was performed. The organic layer was dried over MgSO₄ and concentrated under vacuum. The product was purified by column chromatography (hexane/EtOAc 10/0.5 followed by hexane/EtOAc 5/5) and isolated as a mixture of two diastereomers (a fraction of the major diastereomer was isolated for NMR analysis). A colorless oil was obtained.

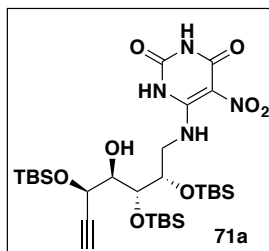
HR-MS (ESI), *m/z*: 590.3912 [M+H]⁺

¹H NMR (400 MHz, CDCl₃) (major diastereomer) δ : 4.61 (d, 1H, J= 3.4 Hz), 4.12 (t, 1H, J= 5.8 Hz), 4.06 (dd, 1H, J= 7.0 Hz), 3.58 (dd, 1H, J= 7.0 Hz, 3.4 Hz), 2.90 (d, 2H, J= 13.1 Hz, 5.8 Hz), 2.78 (dd, 1H, J= 13.1 Hz, 5.8 Hz), 2.42 (s, 2H), 0.92-0.89 (m, 27H), 0.16-0.11 (m, 27H)

¹³C NMR (101 MHz, CDCl₃) (major diastereomer) δ : 103.99, 91.71, 77.56, 75.86, 74.75, 66.49, 42.73, 26.22-25.97 (9C), 18.46-18.37 (3C), -0.09 (3C), -3.52, -3.87, -4.50, -4.56, -4.74, -4.81

5-nitro-6-(((2S,3S,4R,5R)-2,3,4-tris((tert-butyldimethylsilyl)oxy)-5-hydroxyhept-6-yn-1-yl)amino)pyrimidine-2,4(1H,3H)-dione (71a) and 5-nitro-6-(((2S,3S,4R,5S)-2,3,4-tris((tert-butyldimethylsilyl)oxy)-5-hydroxyhept-6-yn-1-yl)amino)pyrimidine-2,4(1H,3H)-dione (71b)

To **70** (237 mg, 1.0 eq, 0.40 mmol) in dry DMF (3 mL) was added 6-chloro-5-nitouracil (92 mg, 1.2 eq, 0.48 mmol) and triethylamine (0.28 mL, 5.0 eq, 2.0 mmol). The mixture was heated at 50°C for 3h. DMF was removed under vacuum, water was added and the product was extracted by EtOAc. The organic layer was dried over MgSO₄ and concentrated under vacuum. TMS removal was directly done without further purification (120 mg of crude intermediate were obtained). The intermediate was dissolved in MeOH (2 mL) and K₂CO₃ (72 mg, 3.0 eq, 0.54 mmol) was added. The mixture was stirred at room temperature for 2h. Water was added to the mixture and the product was extracted by EtOAc. The organic layer was dried over MgSO₄ and concentrated under vacuum. The crude residue was purified by preparative C18 RP-HPLC using a gradient ACN/water 0.1% formic acid as following: 85% ACN/15% H₂O for 1 min followed by gradual increase to 100% ACN after 20 min and 2 minutes more of 100% ACN. The two diastereomers were isolated separately as light yellow powders (108 mg for the major one and 2.4 mg for the minor one).

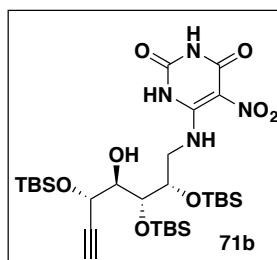


| Raw formula | Molecular mass | Aspect | Yield |
|---|----------------------------|---------------|-------|
| C ₂₉ H ₅₆ N ₄ O ₈ Si ₃ | 672.37 g.mol ⁻¹ | Yellow powder | 41% |

MS (ESI), *m/z*: 673.9 [M+H]⁺

¹H NMR (400 MHz, CDCl₃) 71a δ : 11.08 (s, 1H), 10.24 (brt, 1H, J= 6.8 Hz), 9.41 (s, 1H), 5.07 (s, 1H), 4.68 (dd, 1H, J= 3.6 Hz, 2.2 Hz), 4.39-4.37 (m, 1H), 4.21 (d, 1H, J= 4.9 Hz), 3.98 (t, 1H, J= 4.1 Hz), 3.88-3.81 (m, 1H), 3.75-3.69 (m, 1H), 2.52 (d, 1H, J= 2.2 Hz), 0.93-0.83 (m, 27H), 0.16-0.08 (m, 18H)

¹³C NMR (101 MHz, CDCl₃) 71a δ: 157.18, 153.98, 147.73, 109.59, 81.59, 77.58, 75.68, 75.34, 71.84, 61.19, 46.97, 26.04-25.85 (9C), 18.39, 18.20 (2C), -3.99, -4.01, -4.80, -4.83, -4.93, -4.96

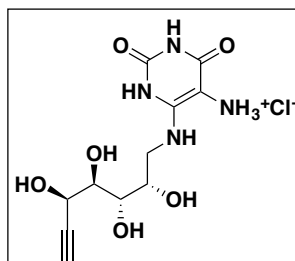


MS (ESI), *m/z*: 673.5 [M+H]⁺

¹H NMR (400 MHz, CDCl₃) 71b δ: 10.48 (s, 1H), 10.30 (brt, 1H, *J* = 6.8 Hz), 8.51 (s, 1H), 4.52 (s, 1H), 4.40 (dd, 1H, *J* = 7.5 Hz, 1.5 Hz), 4.20-4.17 (m, 2H), 3.92-3.85 (m, 2H), 3.70-3.65 (m, 1H), 2.54 (d, 1H, *J* = 1.9 Hz), 0.92-0.88 (m, 27H), 0.19 (s, 3H), 0.17 (s, 3H), 0.12-0.10 (m, 9H), 0.05 (s, 3H)

¹³C NMR (101 MHz, CDCl₃) 71b δ: 156.33, 153.77, 147.07, 109.47, 82.11, 79.46, 76.06, 75.14, 72.06, 63.82, 47.75, 25.92-25.81 (9C), 18.27, 18.23, 18.10, -4.12, -4.28, -4.49, -4.79 (2C), -4.98.

5-amino-6-(((2S,3S,4R,5R)-2,3,4,5-tetrahydrohept-6-yn-1-yl)amino)pyrimidine-2,4(1H,3H)-dione
(72a)



| Raw formula | Molecular mass | Aspect | Yield |
|---|------------------------------|--------------------|-------|
| C ₁₁ H ₁₇ ClN ₄ O ₆ | 336.0837 g.mol ⁻¹ | Pink to red powder | 53% |

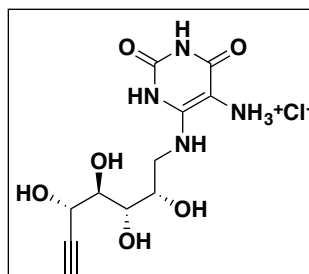
71a (26 mg, 1.0 eq, 0.41 mmol) was heated to 90°C in a 10/1 mixture of MeOH/H₂O (3/0.3 mL). Then Na₂S₂O₄ (58 mg, 8.0 eq, 0.33 mmol) was quickly added and the mixture was stirred under reflux for 15 minutes. Excess MeOH was removed under vacuum and the product was extracted by EtOAc. The organic layer was dried over MgSO₄ and concentrated under vacuum. The crude intermediate was dissolved in MeOH (1 mL) and cooled to 0°C prior to addition of 37% HCl (1 mL). The mixture was then stirred at room temperature for 3 hours. The product was concentrated under vacuum, dissolved in a few volumes of MeOH and precipitated from EtOAc. The precipitate was filtered and washed several times with EtOAc. After deep drying under vacuum, **72a** was obtained as pink to red powder corresponding to the amine hydrochloride salts.

HR-MS (ESI), *m/z*: 335.0770 [M+H]⁺

¹H NMR (500 MHz, CD₃OD) δ: 4.61 (dd, 1H, J= 4.1 Hz, 2.2 Hz), 4.05-4.02 (m, 1H), 3.81 (dd, 1H, J= 7.5 Hz, 5.0 Hz), 3.70 (dd, 1H, J= 7.5 Hz, 4.1 Hz), 3.65-3.61 (m, 1H), 3.56 (dd, 1H, J= 14.7 Hz, 7.2 Hz), 2.86 (d, 1H, J= 2.2 Hz).

¹³C NMR (126 MHz, CD₃OD) δ: 161.89, 151.65, 151.31, 83.45, 82.96, 76.46, 75.67, 73.61, 72.96, 64.97, 46.24

5-amino-6-(((2S,3S,4R,5S)-2,3,4,5-tetrahydroxyhept-6-yn-1-yl)amino)pyrimidine-2,4(1H,3H)-dione
(72b)



| Raw formula | Molecular mass | Aspect | Yield |
|---|------------------------------|------------|-------|
| C ₁₁ H ₁₇ ClN ₄ O ₆ | 336.0837 g.mol ⁻¹ | Red powder | 75% |

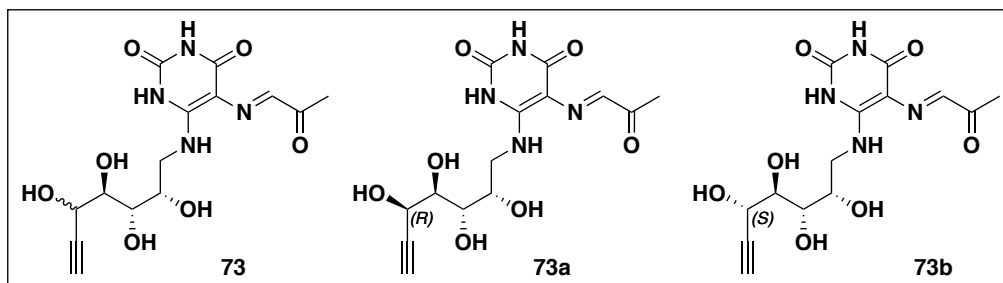
71b (7 mg, 1.0 eq, 0.011 mmol) was heated to 90°C in a 10/1 mixture of MeOH/H₂O (1/0.1 mL). Then Na₂S₂O₄ (15 mg, 8.0 eq, 0.09 mmol) was quickly added and the mixture was stirred under reflux for 15 minutes. Excess MeOH was removed under vacuum and the product was extracted by EtOAc. The organic layer was dried over MgSO₄ and concentrated under vacuum. The crude intermediate was dissolved in MeOH (1 mL) and cooled to 0°C prior to addition of 37% HCl (1 mL). The mixture was then stirred at room temperature for 3 hours. The product was concentrated under vacuum, dissolved in a few volumes of MeOH and precipitated from EtOAc. The precipitate was filtered and washed with EtOAc. After deep drying under vacuum, **72b** was obtained as pink-red powder corresponding to the amine hydrochloride salts.

HR-MS (ESI), *m/z*: 335.0770 [M+H]⁺

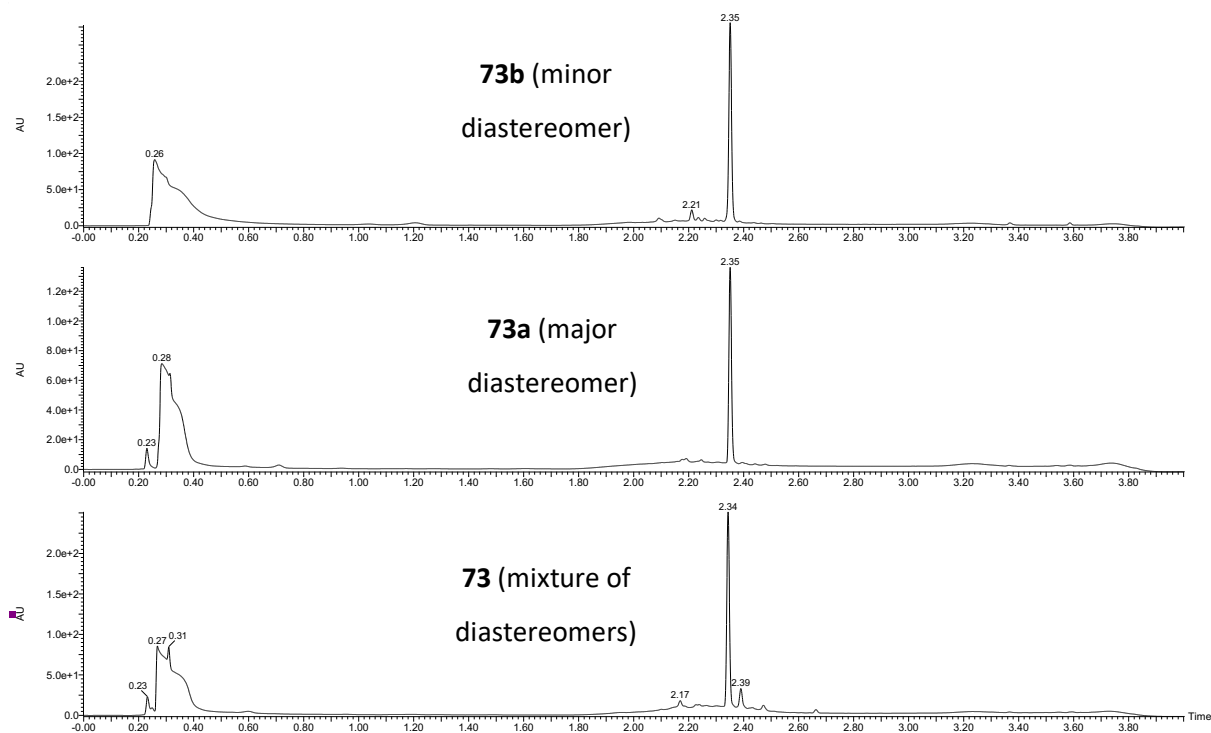
¹H NMR (500 MHz, CD₃OD) δ: 4.58 (dd, 1H, J = 3.3 Hz, 2.3 Hz), 4.03-4.00 (m, 1H), 3.83 (dd, 1H, J = 7.3 Hz, 5.4 Hz), 3.75 (dd, 1H, J = 7.3 Hz, 3.4 Hz), 3.60-3.55 (m, 2H), 2.86 (d, 1H, J = 2.3 Hz)

¹³C NMR (126 MHz, CD₃OD) δ: 161.88, 151.64, 151.30, 84.22, 83.43, 76.77, 74.84, 73.11, 72.53, 63.52, 46.46

5-(((*E*)-2-oxopropylidene)amino)-6-(((2*S*,3*S*,4*R*)-2,3,4,5-tetrahydroxyhept-6-yn-1-yl)amino)pyrimidine-2,4(1*H*,3*H*)-dione (73**, **73a** and **73b**)**



Stock solution (1 mL) of freshly synthesized **72**, **72a** and **72b** were prepared at 10 mM concentration in DMSO. Methylglyoxal solution (40% in H₂O) was diluted in DMSO to obtain a solution at 50 mM concentration and 1 mL of this solution was added to 1 mL of each 10 mM stock solution. The mixtures were allowed to react at room temperature for 48h to give 5 mM solutions of **73**, **73a** and **73b** that were aliquoted and frozen at -80°C. Completion of the reactions was controlled by UPLC-MS analysis of an aliquot using the following gradient conditions: A: water + 0.1% formic acid, B: CH₃CN + 0.1% formic acid; gradient: 100% A to 100% B over 4 min. Corresponding UPLC-MS chromatograms are displayed below:



C. Molecular modelling

All the work of molecular modelling was done by Anke Steinmetz. Experimental conditions used to generate the molecular modelling data are depicted below (see Appendix C for additional details).

Molecular modeling was carried out using Drug Discovery Suite by Schrödinger Inc. in versions 2016.u3 or 2020.u1 for model visualization, ligand design and preparation, protein structure preparation, homology modeling and loop refinement, energy minimizations, molecular dynamics simulations and analyses. More specifically the programs and tools Maestro, Protein Preparation Wizard, Ligprep, Epik, Glide, PRIME, Macromodel, and Desmond were used applying standard settings and procedures unless specified otherwise. Implicit or explicit SPC water models were applied with force field parameters OPLS3.

PDB entries 4L4V and 4NQE were prepared in the Protein Preparation Wizard by replacing missing side chains, commitment of alternative side chain conformations by visual inspection, optimization of hydrogen bonding networks with pK_a calculation by Epik, and minimization of hydrogen atoms only. Missing loops were not modeled at this stage as these regions were at a distance of at least 24 Å from the ligand binding site. The MR1/TCR complex formed by chains A, B, G, and H of 4LV4 was prepared for docking by Glide. All water molecules were deleted prior to grid calculation by Glide. The coordinates of the grid center were visually optimized in the ligand binding site. Outer box dimensions were increased to 36 Å each and all relevant or potentially interesting hydrogen bond donors or acceptors were indicated for grid calculations. Subsets of anchoring points by hydrogen bonding were selected during subsequent standard precision docking. Models of both, **72a** and **72b** stereoisomers were prepared by ligprep for docking. 25 poses per ligand were retained for post-docking energy minimization and 3 final poses per ligand saved. Poses were selected by visual inspection that compared to ligand binding observed in 4NQE. Notably hydrogen bonding to Tyr95^G by 2'- or 3'-OH was an important criterium.

D. X-ray crystallography

Crystals of **71a** were made at Institut Curie and all the X-ray crystallography analysis was done by Pascal Retailleau (laboratoire de cristallographie structurale at Institut de Chimie des Substances Naturelles).

71a was dissolved at room temperature in a 80/20 mixture of acetonitrile/water and was left at room temperature for solvent evaporation. After 2 days, small needles were formed but necessarily brought to PROXIMA 2A (PX2A) beamline at the SOLEIL Synchrotron, Gif-sur-Yvette, Paris, France, for complete data collection at T = 100K. Crystal data, data collection and structure refinement details for **71a** crystal model are available in the Appendix D but are summarized below:

CCDC 1990644 contains the supplementary crystallographic data. These data can be obtained free of charge from the Cambridge Crystallographic Data Centre via www.ccdc.cam.ac.uk/data_request/cif.

Crystal data: $C_{29}H_{56}N_4O_8Si_3 \cdot 0.5 (H_2O)$, Mw = 682.34, monoclinic, $P2_1$, $a = 13.108(1)$, $b = 31.263(1)$, $c = 19.120(1)$ Å, $\beta = 90.008(6)^\circ$, $V = 7835.3(8)$ Å³, $Z = 8$, $\rho_{\text{calcd}} = 1.156$ g cm⁻³, $\mu = 0.169$ mm⁻¹, $F(000) = 2048$, colorless needles, $0.23 \times 0.05 \times 0.04$ mm³, $T = 100$ K, synchrotron PX2A radiation, $\lambda = 0.70848$ Å, 97118 reflections, 17140 unique Laue group reflections, (97.1%) with overall $R_{\text{sym}} = 0.090$, 32863 point group reflections, Pseudo-merohedral twin law ($\bar{1} 0 0, 0 \bar{1} 0, 0 0 1$), $BASF = 0.646$ (10), 1830 parameters, 218 restraints $GOF = 1.027$, $wR2 = 0.1541$, $R = 0.0572$ for 30820 reflections with $I > 2\sigma(I)$, Flack parameter $x = -0.08(6)$.

E. Biochemical assay

Mouse cathepsin L (CL) activity Assay Kit (Abcam ab65306) was used. 10-fold dilution of CL was done in CL Buffer. Ligands were prepared at 1 mM solution in CL Buffer. In a 96-well plate, 95 µL of CL Buffer, 2 µL of solution 1 mM of ligands and 1 µL DTT were added. 5 µL of CL solution was then added and the plate was incubated at 37°C. Supernatant was analyzed by UPLC/MS after 2 hours. For fluorescent ligands (positive control Ac-NH-Phe-Arg-AFC, **46** and **48**), the cleavage was monitored by fluorescence measurement at 380/460 nm and 400/505 nm wavelengths with SpectraMax ID3 spectrophotometer.

II. Biology

A. Cell culture

The different adherent cell lines (WT3-WT, WT3-m) were cultured in DMEM + GlutaMAX media supplemented with 10% FCS, penicillin and streptomycin, non-essential amino acids, HEPES, and sodium pyruvate (all from Gibco™). Incubation of the cells was done at 37°C (5% CO₂). Trypsine (from Gibco™) was used to detach the cells from the culture flasks at each passage. Cells were used in biological experiments when they reached approximately 80% confluence in culture flasks.

B. Bone marrow dendritic cells (BMDCs)

BMDCs from C57BL/6 mice were furnished by Francesca Lucibello (PhD student from Olivier Lantz's team). They were cultured 14 days before use. They were either activated by 4 µL LPS for evaluation of small molecules or not for the latex bead conjugates (activation induced by the phagocytosis of the beads).

C. Mice

The murine model used for the biological evaluation of the compounds were described previously⁸. Briefly, iV α 19-Tg animals were on a C α -deficient B6 background to avoid endogenous V α expression. All V β 8-Tg mice were generated on the C57BL/6 background, and iV α 19-Tg mice were backcrossed onto the C57BL/6 background for more than 10 generations. All mice were housed in our accredited specific pathogen-free colony and genotyped by PCR or FACS staining, as appropriate. Animal experiments were done in accordance with the guidelines of the French Veterinary Department and the ethical committee of Institut Curie.

D. MR1 up-regulation assay

A suspension of WT3-m cells was prepared and 100 000 cells were introduced into 96 well-plates. The cells were incubated 3h at 37°C (5% CO₂). The ligands to be tested were diluted to the desired concentrations in culture media and added into the wells. The plates were incubated for 2h at 37°C (5% CO₂). Cells were detached using Versene solution (EDTA solution) on ice for 10 minutes, centrifuged (4 min, 4°C, 1350 rpm) and further stained by PE-conjugated anti-MR1 antibody at 4°C and in the dark. The cells were centrifuged (4 min, 4°C, 1350 rpm) and re-suspended in FACS buffer (10 mM EDTA in PBS) containing DAPI (1/10 000 dilution) to exclude dead cells. The cells were analyzed using CytoFLEX flow cytometer (Beckman Coulter).

E. MAIT cell activation assay

MAIT cell activation assay was performed following a published procedure⁸². A suspension of WT3-m cells was prepared and 100 000 cells were introduced into 96 well-plates. The cells were incubated 3h at 37°C (5% CO₂). The ligands to be tested were diluted to the desired concentrations in culture media and added into the wells. The cells were incubated for 2h at 37°C (5% CO₂) for APC activation. Enriched MAIT cell suspension was obtained by mechanical disruption of splenocytes of transgenic mice (iV α 19 simple transgenic or iV α 19 V β 8 double transgenic mice) on cell strainers. Cells were centrifuged (5 min, 1350 rpm) and red blood cells were lysed using a red blood lysis buffer. After centrifugation (5 min, 1350 rpm), cells were re-suspended in culture media and 160 000 cells of the suspension were added into the wells for overnight incubation (16 hours). Cells were subsequently washed, centrifuged (4 min, 4°C, 1350 rpm) and stained at 4°C and in the dark by the following conjugated antibodies: Ab anti-TCR β -APC, Ab anti-V β 6-FITC, Ab anti-V β 8-FITC, Ab anti-CD4-BV785, Ab anti-CD8-Alexa fluor 700, Ab anti-CD25-PE Texas red, Ab anti-CD69-PC7. Cells were washed, centrifuged (4 min, 4°C, 1350 rpm) and finally re-suspended in FACS buffer (10 mM EDTA in PBS) containing DAPI (1/10 000 dilution) to

exclude dead cells. The cells were analyzed on CytoFLEX flow cytometer (Beckman Coulter). Activation of MAIT cells ($V\beta 6^+/V\beta 8^+$, $CD4^-$, $CD8^{+/-}$ cells) was determined by the detection of an up-regulation of CD69 (and CD25) activation markers.

F. Competition assay

MAIT cell suspension was prepared following the above described protocol for MAIT cell activation. The competitive ligands to be tested were diluted to the desired concentrations in culture media and added into the wells. After 1h incubation, 5-OP-RU was added (with various concentrations) and the plates were incubated overnight. MAIT cell activation read-out was done as described above with antibody staining and analysis by flow cytometry.

G. MR1 tetramer staining assay

MR1 preparation and staining assay was done in collaboration with Yara El Morr (PhD student from Olivier Lantz's team).

1. MR1 tetramer preparation

Biotinylated monomers of MR1 were engineered and refolded with ligands at the recombinant protein platform of Institut Curie by Ahmed El Marjou. Tetramers were then produced following NIH protocol. Briefly, 10 μ g of monomers of MR1 bound to either **12** (5-OP-RU) or **13** was added in Eppendorf vials. Streptavidin fluorescent bead suspension (0.5 mg/mL concentration) was added sequentially. 13 μ L were first added and the suspension was incubated in the dark at room temperature for 10 min followed by 10 μ L with the same incubation and finally 5.5 μ L and identical incubation. Tetramers were stored at 4°C.

2. Tetramer staining assay

Enriched MAIT cell suspension was obtained by mechanical disruption of splenocytes of transgenic mice (iV α 19 simple transgenic or iV α 19 V β 8 double transgenic mice) on cell strainers. After centrifugation (5 min, 1350 rpm), red blood cells were lysed using a red blood lysis buffer. The cells were centrifugated (5 min, 1350 rpm) and re-suspended in FACS buffer and put into FACS tubes. Tetramer solutions were centrifugated (10 min, 4°C, 1350 rpm) and 50 μ L of the supernatants were added on cells followed by 30 min staining in the dark at room temperature. The cells were then washed and centrifuged (4 min, 4°C, 1350 rpm). Antibody staining was done with Ab anti-TCR β -PE-Cy5

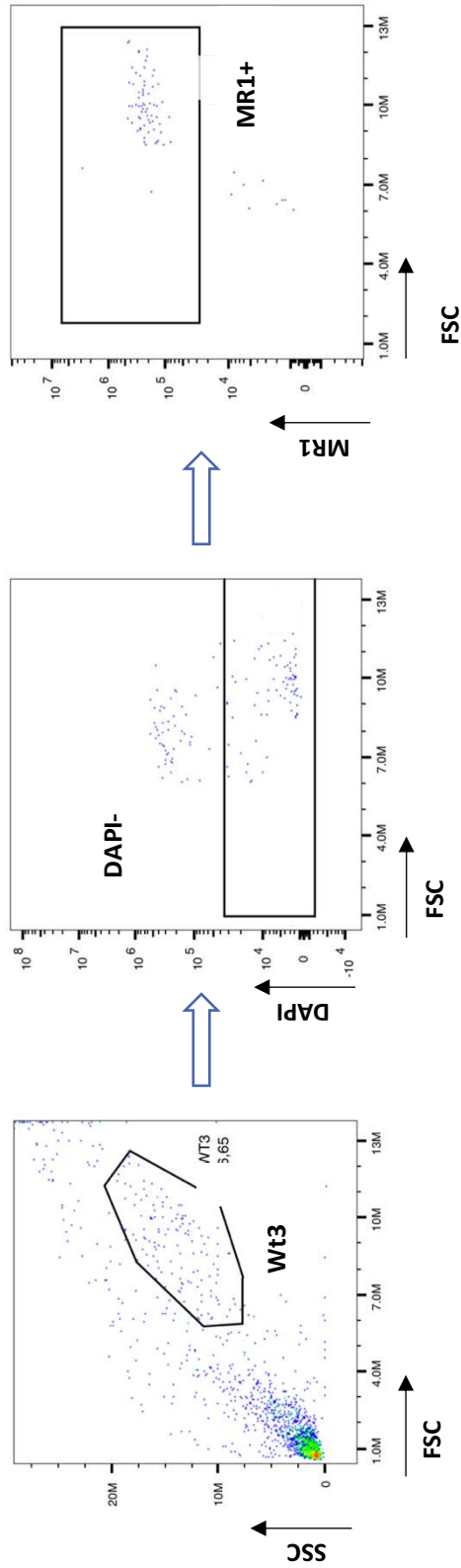
(1/200^e dilution) and Ab anti-CD19-AF700 (1/200^e dilution) during 20 minutes on ice and in the dark. After washing, the cells were centrifuged (4 min, 4°C, 1350 rpm) and re-suspended in FACS buffer. Read-out was done by flow cytometer LSRII.

H. Click chemistry experiments

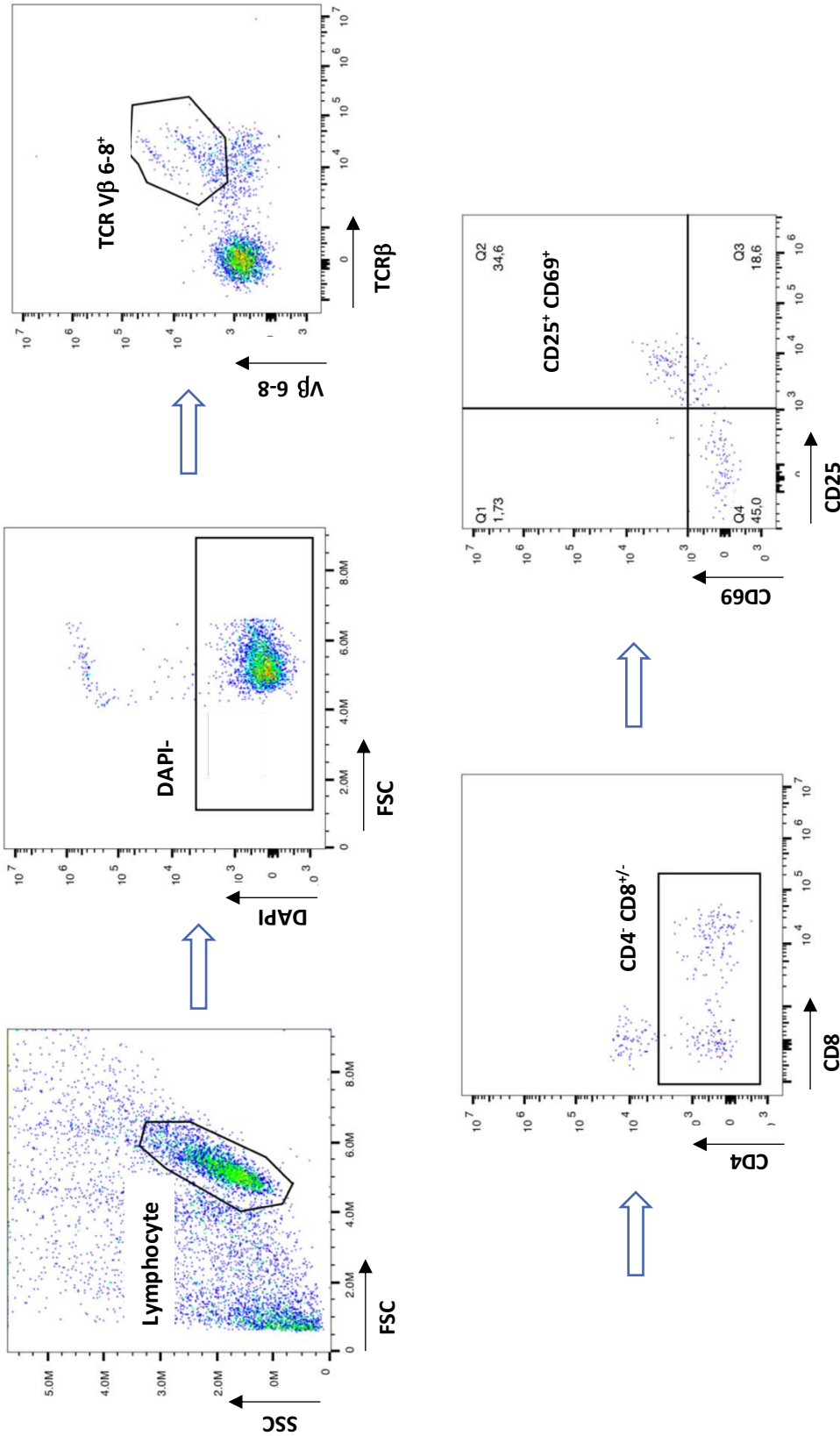
Coverslips (12 mm diameter) were incubated with a mixture of collagen (15 µg/mL, 100 µL) and fibronectine (1 µg/mL, 20 µL) in PBS (20 mL) for 1h at 37°C. Coverslips were transferred into 4-well plates and 100 000 cells were added on the adherent coverslips (1 mL of the suspension per well). The cells were incubated 16 hours at 37°C (5% CO₂). They were subsequently treated with **73** or EdU positive control (10 µM final concentration for each product, 1h incubation at 37°C, 5% CO₂). Coverslips were washed with PBS and the cells were fixed using paraformaldehyde 2% in PBS (1 mL per well) during 12 minutes. Cells were washed thrice with PBS and they were permeabilized using Triton X100 0.1% for 5 minutes (1 mL per well). Coverslips were again washed thrice by PBS. Click chemistry reaction was done following the supplier procedure (Click-it™ EdU cell proliferation kit for imaging Alexa Fluor™ 488 dye supplied from ThermoFisher Scientific) with the following solution: PBS (supplied at 10X concentration and diluted to 1X in nuclease free water, 40 µL), AF₄₈₈-azide (2.5 µL) and ascorbic acid (100 µL). Drops of the solution (50 µL) were deposited on parafilm and coverslips were added on the drops and incubated at room temperature for 30 minutes. Then, coverslips were deposited on PBS drops for 5 min washing. The same operation was repeated two more times. Coverslips were finally washed by MilliQ water, dried on Kimtech paper and mounted on slides with Vectashield® antifade mounting medium containing DAPI (Vector laboratories). Fluorescent microscopy analysis was performed with DeltaVision RT epifluorescence microscope. Images were acquired as z-stacks and deconvolution was done with SoftWorx software. Images were analyzed with ImageJ software (NIH).

Appendices

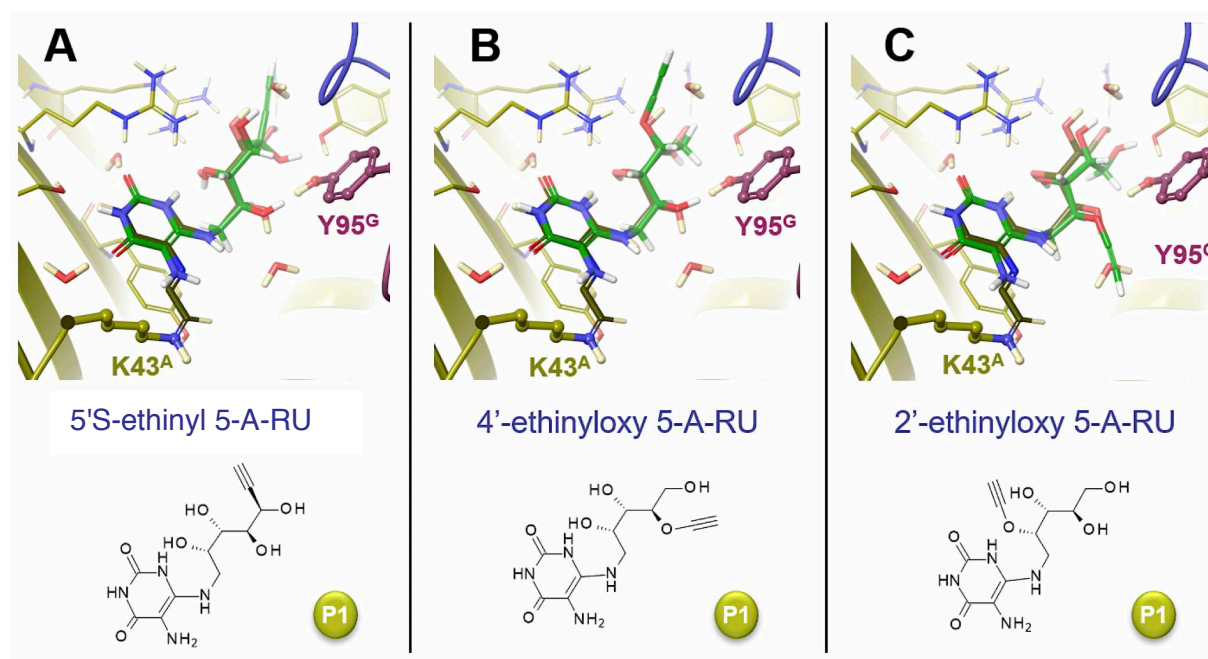
Appendix A : Flow cytometry gating strategy for MR1 up-regulation assay



Appendix B : Flow cytometry gating strategy for MAIT cell activation assay



Appendix C: Molecular modelling of clickable analogues of 5-A-RU



Appendix C figure : Derivatization points for fluorescent probes. Poses of derivatized 5-A-RU docked to MR1/TCR complex in comparison to the crystal structure of the ternary complex of 5-OE-RU;

Top: close-ups of the ligand-binding site with 5'R-ethinylated, 4'O-, and 2'O-ethinyloxy derivatized 5-A-RU in A, B, and C, respectively. All three possibilities of introducing an ethinyl group were given priority 1 by docking compared to further, not revealed designs. Protein is depicted by ribbon diagrams with MR1 chain A, TCR chains G and H colored in olive, plum, and blue, respectively. Selected amino acids and ligands are represented as ball-and-sticks or tubes. Carbon atoms of 5-OE-RU and derivatized ligands are depicted in dark green and green, oxygen, nitrogen, and hydrogen atoms in red, blue, and white, respectively. Bottom: 2-dimensional sketches of the chemical structure of the docked ligands.

Appendix D : Crystallographic data of compound 71a

Compound **71a** was dissolved at room temperature in a 80/20 mixture of acetonitrile/water and was let at room temperature for solvent evaporation. After 2 days, small needles were obtained and were then transferred into Paratone[®] oil upon a microscope slide, to be isolated under a binocular and mounted on a MiTiGen cryoloop to be cryocooled using LN₂. X-ray diffraction data were necessarily collected on the PROXIMA 2A (PX2A) beamline at the SOLEIL Synchrotron, Gif-sur-Yvette, Paris, France, ($\lambda = 0.70848 \text{ \AA}$) up to a resolution of $(\sin \theta/\lambda)_{\max} = 0.58 \text{ \AA}^{-1}$ at $T = 100\text{K}$. They were indexed, integrated with *XDS*^[1] and scaled with *AIMLESS*,^[2,3] as implemented within the *autoProc* toolbox.^[4] The structure was solved by intrinsic phasing methods (*SHELXT* program),^[5] then refined by full-matrix least-squares methods on F^2 using *SHELXL-L*.^[6] The Sohncke $P2_1$ unit cell contains eight molecules of **71a**, and four copies were refined independently altogether with 2 waters in the asymmetric unit. All non-hydrogen atoms improved by anisotropic refinement. Most of the H atoms were identified in difference maps nevertheless they were essentially positioned geometrically using a riding model with U_{iso} set to xU_{eq} (parent atom) and x equal to 1.5 when parent atoms are methyl carbons, or water or hydroxyl oxygens, and 1.2 for nitrogen atoms and the rest of the carbons tertiary CH, secondary CH₂, and acetylenic ones. Except a couple of methyl groups of one disordered silyl ether group, methyl H atoms were idealized and included as rigid groups allowed to rotate but not tip (AFIX 137 vs 33). Unlike the amide hydrogens (AFIX 43), the position of the amine ones was refined using distance restraints. Angle and bond distances were also restrained in the case of the water molecule that bridges the two compounds present in the asymmetric unit and which is also tweezed by the two hydroxyl H atoms from each compound, that were also allowed to rotate (AFIX 147). One out of four conformers shows some disorder at the level of two *tert*-butyldimethylsilyl (TBDMS) groups, which was handled by refining their position parameters over two sets of sites for each TBDMS group with occupancy factors 0.653 (11) and 0.698 (11) for the major ones, respectively. Restraints on displacement parameters (SAME, RIGU, ISOR) were applied to these sets of disordered groups. Using its TwinRotMat routine, *PLATON*^[7] suggested a twofold rotation axis around the c crystallographic axis as twin element with the matrix ($\bar{1} \ 0 \ 0, 0 \ \bar{1} \ 0, 0 \ 0 \ 1$). Therefore, the initial data set was kept with the final refinement performed using the *HKL5* file as constructed from all observations involving domain 1 only with *PLATON*. The final BASF parameter as indication of the two crystal domains ratio was 0.646 (10). Statistics are reported in Table 1. Furthermore the absolute configuration of the diastereomers could be ascertained by the exploitation of the anomalous dispersion mainly brought by Si atoms leading to a meaningful Flack parameter value of -0.08(6) determined using 12895 quotients $[(I+) - (I-)] / [(I+) + (I-)]$.^[8] This confirmed the expected chiral centers **2'S**, **3'S**, **4'R**, and therefore established the chirality for **5'R**.

CCDC 1990644 contains the supplementary crystallographic data for this paper. These data can be obtained free of charge from the Cambridge Crystallographic Data Centre via www.ccdc.cam.ac.uk/data_request/cif.

References

- 1 Kabsch, W. (2010). XDS. *Acta Cryst.* D66, 125-132.
- 2 Evans, P.R. and Murshudov, G.N. (2013). *Acta Cryst.* D69, 1204-1214.
- 3 Winn, M.D., Ballard, C.C., Cowtan, K.D. Dodson, E.J., Emsley, P., Evans, P.R., Keegan, R.M., Krissinel, E.B., Leslie, A.G.W., McCoy, A., McNicholas, S.J., Murshudov, G.N., Pannu, N.S., Potterton, E.A., Powell, H.R., Read, R.J., Vagin, A. and Wilson, K.S. (2011). *Acta. Cryst.* D67, 235-242.
- 4 Vonrhein, C., Flensburg, C., Keller, P., Sharff, A., Smart, O., Paciorek, W., Womack, T. and Bricogne, G. (2011). *Acta Cryst.* D67, 293-302.
- 5 Sheldrick, G. M. (2015). *Acta Crystallogr.*, C71, 3-8.
- 6 Sheldrick, G. M. (2015). *Acta Crystallogr.*, A71, 3-8.
- 7 Spek, A.L. (2009) *Acta Crystallogr.*, D65, 148–155.
- 8 Parsons, S. Flack, H.D. and Wagner, T. (2013) *Acta Crystallogr.*, B69 249-259

| Table 1 Crystal data and structure refinement for 71a . | |
|---|--|
| Identification code | 5-nitro-6-(((2S,3S,4R,5R)-2,3,5-tris((tert-butyldimethylsilyl)oxy)-4-hydroxyhept-6-yn-1-yl)amino)pyrimidine-2,4(1H,3H)-dione |
| Empirical formula | C ₂₉ H ₅₆ N ₄ O ₈ Si ₃ , 0.5 (H ₂ O) |
| Formula weight | 682.34 |
| Temperature/K | 100(2) |
| Crystal system | monoclinic |
| Space group | P2 ₁ |
| a/Å | 13.108(1) |
| b/Å | 31.263(1) |
| c/Å | 19.120(1) |
| α/° | 90 |
| β/° | 90.008(6) |
| γ/° | 90 |
| Volume/Å ³ | 7835.3(8) |
| Z | 8 |

| | |
|--|---|
| $\rho_{\text{calc}}/\text{g}/\text{cm}^3$ | 1.156 |
| μ/mm^{-1} | 0.169 |
| F(000) | 2952.0 |
| Crystal size/ mm^3 | $0.23 \times 0.05 \times 0.04$ |
| Radiation | synchrotron ($\lambda = 0.70848$) |
| 2θ range for data collection/ $^\circ$ | 2.124 to 54.066 |
| Index ranges | $-16 \leq h \leq 16, -40 \leq k \leq 40, -24 \leq l \leq 0$ |
| Reflections collected | 97118 |
| Independent reflections | 32863 [$R_{\text{sigma}} = 0.0795$] |
| Data/restraints/parameters | 32863/218/1830 |
| Goodness-of-fit on F^2 | 1.026 |
| Final R indexes [$I \geq 2\sigma(I)$] | $R_1 = 0.0572, wR_2 = 0.1541$ |
| Final R indexes [all data] | $R_1 = 0.0597, wR_2 = 0.1593$ |
| Largest diff. peak/hole / $e \text{ \AA}^{-3}$ | 0.42/-0.44 |
| Flack parameter | -0.08(6) |

Bibliography

- (1) Downey, A. M.; Kapłonek, P.; Seeberger, P. H. MAIT Cells as Attractive Vaccine Targets. *FEBS Lett.* **2019**, *593* (13), 1627–1640. <https://doi.org/10.1002/1873-3468.13488>.
- (2) Porcelli, S.; Yockey, C. E.; Brenner, M. B.; Balk, S. P. Analysis of T Cell Antigen Receptor (TCR) Expression by Human Peripheral Blood CD4-8- Alpha/Beta T Cells Demonstrates Preferential Use of Several V Beta Genes and an Invariant TCR Alpha Chain. *J. Exp. Med.* **1993**, *178* (1), 1–16. <https://doi.org/10.1084/jem.178.1.1>.
- (3) Tilloy, F.; Treiner, E.; Park, S. H.; Garcia, C.; Lemonnier, F.; de la Salle, H.; Bendelac, A.; Bonneville, M.; Lantz, O. An Invariant T Cell Receptor Alpha Chain Defines a Novel TAP-Independent Major Histocompatibility Complex Class Ib-Restricted Alpha/Beta T Cell Subpopulation in Mammals. *J. Exp. Med.* **1999**, *189* (12), 1907–1921. <https://doi.org/10.1084/jem.189.12.1907>.
- (4) Treiner, E.; Duban, L.; Bahram, S.; Radosavljevic, M.; Wanner, V.; Tilloy, F.; Affaticati, P.; Gilfillan, S.; Lantz, O. Selection of Evolutionarily Conserved Mucosal-Associated Invariant T Cells by MR1. *Nature* **2003**, *422* (6928), 164–169. <https://doi.org/10.1038/nature01433>.
- (5) Hashimoto, K.; Hirai, M.; Kurosawa, Y. A Gene Outside the Human MHC Related to Classical HLA Class I Genes. *Science* **1995**, *269* (5224), 693–695. <https://doi.org/10.1126/science.7624800>.
- (6) Corbett, A. J.; Eckle, S. B. G.; Birkinshaw, R. W.; Liu, L.; Patel, O.; Mahony, J.; Chen, Z.; Reantragoon, R.; Meehan, B.; Cao, H.; Williamson, N. A.; Strugnell, R. A.; Sinderen, D. V.; Mak, J. Y. W.; Fairlie, D. P.; Kjer-Nielsen, L.; Rossjohn, J.; McCluskey, J. T-Cell Activation by Transitory Neo-Antigens Derived from Distinct Microbial Pathways. *Nature* **2014**, *509* (7500), 361–365. <https://doi.org/10.1038/nature13160>.
- (7) Seach, N.; Guerri, L.; Le Bourhis, L.; Mburu, Y.; Cui, Y.; Bessoles, S.; Soudais, C.; Lantz, O. Double-Positive Thymocytes Select Mucosal-Associated Invariant T Cells. *J. Immunol. Baltim. Md 1950* **2013**, *191* (12), 6002–6009. <https://doi.org/10.4049/jimmunol.1301212>.
- (8) Martin, E.; Treiner, E.; Duban, L.; Guerri, L.; Laude, H.; Toly, C.; Premel, V.; Devys, A.; Moura, I. C.; Tilloy, F.; Cherif, S.; Vera, G.; Latour, S.; Soudais, C.; Lantz, O. Stepwise Development of MAIT Cells in Mouse and Human. *PLOS Biol.* **2009**, *7* (3), e1000054. <https://doi.org/10.1371/journal.pbio.1000054>.
- (9) Koay, H.-F.; Gherardin, N. A.; Enders, A.; Loh, L.; Mackay, L. K.; Almeida, C. F.; Russ, B. E.; Nold-Petry, C. A.; Nold, M. F.; Bedoui, S.; Chen, Z.; Corbett, A. J.; Eckle, S. B. G.; Meehan, B.; d’Udekem, Y.; Konstantinov, I. E.; Lappas, M.; Liu, L.; Goodnow, C. C.; Fairlie, D. P.; Rossjohn, J.; Chong, M. M.;

Kedzierska, K.; Berzins, S. P.; Belz, G. T.; McCluskey, J.; Uldrich, A. P.; Godfrey, D. I.; Pellicci, D. G. A Three-Stage Intrathymic Development Pathway for the Mucosal-Associated Invariant T Cell Lineage. *Nat. Immunol.* **2016**, *17* (11), 1300–1311. <https://doi.org/10.1038/ni.3565>.

(10) Legoux, F.; Bellet, D.; Daviaud, C.; Morr, Y. E.; Darbois, A.; Niort, K.; Procopio, E.; Salou, M.; Gilet, J.; Ryffel, B.; Balvay, A.; Foussier, A.; Sarkis, M.; Marjou, A. E.; Schmidt, F.; Rabot, S.; Lantz, O. Microbial Metabolites Control the Thymic Development of Mucosal-Associated Invariant T Cells. *Science* **2019**, *366* (6464), 494–499. <https://doi.org/10.1126/science.aaw2719>.

(11) Legoux, F.; Salou, M.; Lantz, O. Unconventional or Preset A β T Cells: Evolutionarily Conserved Tissue-Resident T Cells Recognizing Nonpeptidic Ligands. *Annu. Rev. Cell Dev. Biol.* **2017**, *33* (1), 511–535. <https://doi.org/10.1146/annurev-cellbio-100616-060725>.

(12) Reantragoon, R.; Corbett, A. J.; Sakala, I. G.; Gherardin, N. A.; Furness, J. B.; Chen, Z.; Eckle, S. B. G.; Uldrich, A. P.; Birkinshaw, R. W.; Patel, O.; Kostenko, L.; Meehan, B.; Kedzierska, K.; Liu, L.; Fairlie, D. P.; Hansen, T. H.; Godfrey, D. I.; Rossjohn, J.; McCluskey, J.; Kjer-Nielsen, L. Antigen-Loaded MR1 Tetramers Define T Cell Receptor Heterogeneity in Mucosal-Associated Invariant T Cells. *J. Exp. Med.* **2013**, *210* (11), 2305–2320. <https://doi.org/10.1084/jem.20130958>.

(13) Martin, E.; Treiner, E.; Duban, L.; Guerri, L.; Laude, H.; Toly, C.; Premel, V.; Devys, A.; Moura, I. C.; Tilloy, F.; Cherif, S.; Vera, G.; Latour, S.; Soudais, C.; Lantz, O. Stepwise Development of MAIT Cells in Mouse and Human. *PLOS Biol.* **2009**, *7* (3), e1000054. <https://doi.org/10.1371/journal.pbio.1000054>.

(14) Franciszkiewicz, K.; Salou, M.; Legoux, F.; Zhou, Q.; Cui, Y.; Bessoles, S.; Lantz, O. MHC Class I-Related Molecule, MR1, and Mucosal-Associated Invariant T Cells. *Immunol. Rev.* **2016**, *272* (1), 120–138. <https://doi.org/10.1111/imr.12423>.

(15) Cui, Y. Biologie Des Cellules MAIT Chez La Souris. thesis, Sorbonne Paris Cité, 2015.

(16) Kurioka, A.; Walker, L. J.; Klenerman, P.; Willberg, C. B. MAIT Cells: New Guardians of the Liver. *Clin. Transl. Immunol.* **2016**, *5* (8), e98. <https://doi.org/10.1038/cti.2016.51>.

(17) Kurioka, A.; Ussher, J. E.; Cosgrove, C.; Clough, C.; Fergusson, J. R.; Smith, K.; Kang, Y.-H.; Walker, L. J.; Hansen, T. H.; Willberg, C. B.; Klenerman, P. MAIT Cells Are Licensed through Granzyme Exchange to Kill Bacterially Sensitized Targets. *Mucosal Immunol.* **2015**, *8* (2), 429–440. <https://doi.org/10.1038/mi.2014.81>.

(18) Bourhis, L. L.; Dusseaux, M.; Bohineust, A.; Bessoles, S.; Martin, E.; Premel, V.; Coré, M.; Sleurs, D.; Serriari, N.-E.; Treiner, E.; Hivroz, C.; Sansonetti, P.; Gougeon, M.-L.; Soudais, C.; Lantz, O. MAIT Cells Detect and Efficiently Lyse Bacterially-Infected Epithelial Cells. *PLOS Pathog.* **2013**, *9* (10),

e1003681. <https://doi.org/10.1371/journal.ppat.1003681>.

- (19) Salio, M.; Gasser, O.; Gonzalez-Lopez, C.; Martens, A.; Veerapen, N.; Gileadi, U.; Verter, J. G.; Napolitani, G.; Anderson, R.; Painter, G.; Besra, G. S.; Hermans, I. F.; Cerundolo, V. Activation of Human Mucosal-Associated Invariant T Cells Induces CD40L-Dependent Maturation of Monocyte-Derived and Primary Dendritic Cells. *J. Immunol.* **2017**. <https://doi.org/10.4049/jimmunol.1700615>.
- (20) Wieczorek, M.; Abualrous, E. T.; Sticht, J.; Álvaro-Benito, M.; Stolzenberg, S.; Noé, F.; Freund, C. Major Histocompatibility Complex (MHC) Class I and MHC Class II Proteins: Conformational Plasticity in Antigen Presentation. *Front. Immunol.* **2017**, *8*, 292. <https://doi.org/10.3389/fimmu.2017.00292>.
- (21) Young, M. H.; Gapin, L. Mucosal Associated Invariant T Cells: Don't Forget Your Vitamins. *Cell Res.* **2013**, *23* (4), 460–462. <https://doi.org/10.1038/cr.2012.168>.
- (22) Karamooz, E.; Harriff, M. J.; Lewinsohn, D. M. MR1-Dependent Antigen Presentation. *Semin. Cell Dev. Biol.* **2018**, *84*, 58–64. <https://doi.org/10.1016/j.semcdb.2017.11.028>.
- (23) Bourhis, L. L.; Martin, E.; Péguillet, I.; Guihot, A.; Froux, N.; Coré, M.; Lévy, E.; Dusseaux, M.; Meyssonier, V.; Premel, V.; Ngo, C.; Riteau, B.; Duban, L.; Robert, D.; Huang, S.; Rottman, M.; Soudais, C.; Lantz, O. Antimicrobial Activity of Mucosal-Associated Invariant T Cells. *Nat. Immunol.* **2010**, *11* (8), 701–708. <https://doi.org/10.1038/ni.1890>.
- (24) Gold, M. C.; Cerri, S.; Smyk-Pearson, S.; Cansler, M. E.; Vogt, T. M.; Delepine, J.; Winata, E.; Swarbrick, G. M.; Chua, W.-J.; Yu, Y. Y. L.; Lantz, O.; Cook, M. S.; Null, M. D.; Jacoby, D. B.; Harriff, M. J.; Lewinsohn, D. A.; Hansen, T. H.; Lewinsohn, D. M. Human Mucosal Associated Invariant T Cells Detect Bacterially Infected Cells. *PLOS Biol.* **2010**, *8* (6), e1000407. <https://doi.org/10.1371/journal.pbio.1000407>.
- (25) Kjer-Nielsen, L.; Patel, O.; Corbett, A. J.; Nours, J. L.; Meehan, B.; Liu, L.; Bhati, M.; Chen, Z.; Kostenko, L.; Reantragoon, R.; Williamson, N. A.; Purcell, A. W.; Dudek, N. L.; McConville, M. J.; O'Hair, R. A. J.; Khairallah, G. N.; Godfrey, D. I.; Fairlie, D. P.; Rossjohn, J.; McCluskey, J. MR1 Presents Microbial Vitamin B Metabolites to MAIT Cells. *Nature* **2012**, *491* (7426), 717–723. <https://doi.org/10.1038/nature11605>.
- (26) Kjer-Nielsen, L.; Corbett, A. J.; Chen, Z.; Liu, L.; Mak, J. Y.; Godfrey, D. I.; Rossjohn, J.; Fairlie, D. P.; McCluskey, J.; Eckle, S. B. An Overview on the Identification of MAIT Cell Antigens. *Immunol. Cell Biol.* **2018**, *96* (6), 573–587. <https://doi.org/10.1111/imcb.12057>.
- (27) Eckle, S. B. G.; Corbett, A. J.; Keller, A. N.; Chen, Z.; Godfrey, D. I.; Liu, L.; Mak, J. Y. W.; Fairlie, D. P.; Rossjohn, J.; McCluskey, J. Recognition of Vitamin B Precursors and Byproducts by Mucosal Associated Invariant T Cells. *J. Biol. Chem.* **2015**, *290* (51), 30204–30211.

<https://doi.org/10.1074/jbc.R115.685990>.

(28) McWilliam, H. E. G.; Eckle, S. B. G.; Theodossis, A.; Liu, L.; Chen, Z.; Wubben, J. M.; Fairlie, D. P.; Strugnell, R. A.; Mintern, J. D.; McCluskey, J.; Rossjohn, J.; Villadangos, J. A. The Intracellular Pathway for the Presentation of Vitamin B–Related Antigens by the Antigen-Presenting Molecule MR1. *Nat. Immunol.* **2016**, *17* (5), 531–537. <https://doi.org/10.1038/ni.3416>.

(29) Harriff, M. J.; Karamooz, E.; Burr, A.; Grant, W. F.; Canfield, E. T.; Sorensen, M. L.; Moita, L. F.; Lewinsohn, D. M. Endosomal MR1 Trafficking Plays a Key Role in Presentation of Mycobacterium Tuberculosis Ligands to MAIT Cells. *PLOS Pathog.* **2016**, *12* (3), e1005524. <https://doi.org/10.1371/journal.ppat.1005524>.

(30) McWilliam, H. E. G.; Villadangos, J. A. How MR1 Presents a Pathogen Metabolic Signature to Mucosal-Associated Invariant T (MAIT) Cells. *Trends Immunol.* **2017**, *38* (9), 679–689. <https://doi.org/10.1016/j.it.2017.06.005>.

(31) Ussher, J. E.; Willberg, C. B.; Klenerman, P. MAIT Cells and Viruses. *Immunol. Cell Biol.* **2018**, *96* (6), 630–641. <https://doi.org/10.1111/imcb.12008>.

(32) Mondot, S.; Boudinot, P.; Lantz, O. MAIT, MR1, Microbes and Riboflavin: A Paradigm for the Co-Evolution of Invariant TCRs and Restricting MHC-I-like Molecules? *Immunogenetics* **2016**, *68* (8), 537–548. <https://doi.org/10.1007/s00251-016-0927-9>.

(33) Harriff, M. J.; Cansler, M. E.; Toren, K. G.; Canfield, E. T.; Kwak, S.; Gold, M. C.; Lewinsohn, D. M. Human Lung Epithelial Cells Contain Mycobacterium Tuberculosis in a Late Endosomal Vacuole and Are Efficiently Recognized by CD8+ T Cells. *PLOS ONE* **2014**, *9* (5), e97515. <https://doi.org/10.1371/journal.pone.0097515>.

(34) Jiang, J.; Yang, B.; An, H.; Wang, X.; Liu, Y.; Cao, Z.; Zhai, F.; Wang, R.; Cao, Y.; Cheng, X. Mucosal-Associated Invariant T Cells from Patients with Tuberculosis Exhibit Impaired Immune Response. *J. Infect.* **2016**, *72* (3), 338–352. <https://doi.org/10.1016/j.jinf.2015.11.010>.

(35) Jiang, J.; Wang, X.; An, H.; Yang, B.; Cao, Z.; Liu, Y.; Su, J.; Zhai, F.; Wang, R.; Zhang, G.; Cheng, X. Mucosal-Associated Invariant T-Cell Function Is Modulated by Programmed Death-1 Signaling in Patients with Active Tuberculosis. *Am. J. Respir. Crit. Care Med.* **2014**, *190* (3), 329–339. <https://doi.org/10.1164/rccm.201401-0106OC>.

(36) Saeidi, A.; Tien Tien, V. L.; Al-Batran, R.; Al-Darraj, H. A.; Tan, H. Y.; Yong, Y. K.; Ponnampalavanar, S.; Barathan, M.; Rukumani, D. V.; Ansari, A. W.; Velu, V.; Kamarulzaman, A.; Larsson, M.; Shankar, E. M. Attrition of TCR Va7.2+CD161++ MAIT Cells in HIV-Tuberculosis Co-Infection Is Associated with Elevated Levels of PD-1 Expression. *PLoS ONE* **2015**, *10* (4), e0124659.

- (37) Yang, Q.; Xu, Q.; Chen, Q.; Li, J.; Zhang, M.; Cai, Y.; Liu, H.; Zhou, Y.; Deng, G.; Deng, Q.; Zhou, B.; Kornfeld, H.; Chen, X. Discriminating Active Tuberculosis from Latent Tuberculosis Infection by Flow Cytometric Measurement of CD161-Expressing T Cells. *Sci. Rep.* **2015**, *5* (1), 1–8. <https://doi.org/10.1038/srep17918>.
- (38) Smith, D. J.; Hill, G. R.; Bell, S. C.; Reid, D. W. Reduced Mucosal Associated Invariant T-Cells Are Associated with Increased Disease Severity and Pseudomonas Aeruginosa Infection in Cystic Fibrosis. *PLoS One* **2014**, *9* (10), e109891. <https://doi.org/10.1371/journal.pone.0109891>.
- (39) Leung, D. T.; Bhuiyan, T. R.; Nishat, N. S.; Hoq, M. R.; Aktar, A.; Rahman, M. A.; Uddin, T.; Khan, A. I.; Chowdhury, F.; Charles, R. C.; Harris, J. B.; Calderwood, S. B.; Qadri, F.; Ryan, E. T. Circulating Mucosal Associated Invariant T Cells Are Activated in Vibrio Cholerae O1 Infection and Associated with Lipopolysaccharide Antibody Responses. *PLoS Negl. Trop. Dis.* **2014**, *8* (8), e3076. <https://doi.org/10.1371/journal.pntd.0003076>.
- (40) Booth, J. S.; Salerno-Goncalves, R.; Blanchard, T. G.; Patil, S. A.; Kader, H. A.; Safta, A. M.; Morningstar, L. M.; Czinn, S. J.; Greenwald, B. D.; Szein, M. B. Mucosal-Associated Invariant T Cells in the Human Gastric Mucosa and Blood: Role in Helicobacter Pylori Infection. *Front. Immunol.* **2015**, *6*, 466. <https://doi.org/10.3389/fimmu.2015.00466>.
- (41) Grimaldi, D.; Le Bourhis, L.; Sauneuf, B.; Dechartres, A.; Rousseau, C.; Ouaz, F.; Milder, M.; Louis, D.; Chiche, J.-D.; Mira, J.-P.; Lantz, O.; Pène, F. Specific MAIT Cell Behaviour among Innate-like T Lymphocytes in Critically Ill Patients with Severe Infections. *Intensive Care Med.* **2014**, *40* (2), 192–201. <https://doi.org/10.1007/s00134-013-3163-x>.
- (42) Cui, Y.; Franciszkiewicz, K.; Mburu, Y. K.; Mondot, S.; Bourhis, L. L.; Premel, V.; Martin, E.; Kachaner, A.; Duban, L.; Ingersoll, M. A.; Rabot, S.; Jaubert, J.; Villartay, J.-P. D.; Soudais, C.; Lantz, O. Mucosal-Associated Invariant T Cell–Rich Congenic Mouse Strain Allows Functional Evaluation. *J. Clin. Invest.* **2015**, *125* (11), 4171–4185. <https://doi.org/10.1172/JCI82424>.
- (43) Chen, Z.; Wang, H.; D'Souza, C.; Sun, S.; Kostenko, L.; Eckle, S. B. G.; Meehan, B. S.; Jackson, D. C.; Strugnell, R. A.; Cao, H.; Wang, N.; Fairlie, D. P.; Liu, L.; Godfrey, D. I.; Rossjohn, J.; McCluskey, J.; Corbett, A. J. Mucosal-Associated Invariant T-Cell Activation and Accumulation after in Vivo Infection Depends on Microbial Riboflavin Synthesis and Co-Stimulatory Signals. *Mucosal Immunol.* **2017**, *10* (1), 58–68. <https://doi.org/10.1038/mi.2016.39>.
- (44) Meierovics, A.; Yankelevich, W.-J. C.; Cowley, S. C. MAIT Cells Are Critical for Optimal Mucosal Immune Responses during in Vivo Pulmonary Bacterial Infection. *Proc. Natl. Acad. Sci.* **2013**, *110* (33), E3119–E3128. <https://doi.org/10.1073/pnas.1302799110>.

- (45) Wang, H.; D'Souza, C.; Lim, X. Y.; Kostenko, L.; Pediongco, T. J.; Eckle, S. B. G.; Meehan, B. S.; Shi, M.; Wang, N.; Li, S.; Liu, L.; Mak, J. Y. W.; Fairlie, D. P.; Iwakura, Y.; Gunnarsen, J. M.; Stent, A. W.; Godfrey, D. I.; Rossjohn, J.; Westall, G. P.; Kjer-Nielsen, L.; Strugnell, R. A.; McCluskey, J.; Corbett, A. J.; Hinks, T. S. C.; Chen, Z. MAIT Cells Protect against Pulmonary *Legionella Longbeachae* Infection. *Nat. Commun.* **2018**, *9* (1), 1–15. <https://doi.org/10.1038/s41467-018-05202-8>.
- (46) Salou, M.; Franciszkiewicz, K.; Lantz, O. MAIT Cells in Infectious Diseases. *Curr. Opin. Immunol.* **2017**, *48*, 7–14. <https://doi.org/10.1016/j.coi.2017.07.009>.
- (47) Wilgenburg, B. van; Scherwitzl, I.; Hutchinson, E. C.; Leng, T.; Kurioka, A.; Kulicke, C.; Lara, C. de; Cole, S.; Vasanaawathana, S.; Limpitikul, W.; Malasit, P.; Young, D.; Denney, L.; Moore, M. D.; Fabris, P.; Giordani, M. T.; Oo, Y. H.; Laidlaw, S. M.; Dustin, L. B.; Ho, L.-P.; Thompson, F. M.; Ramamurthy, N.; Mongkolsapaya, J.; Willberg, C. B.; Screaton, G. R.; Klenerman, P. MAIT Cells Are Activated during Human Viral Infections. *Nat. Commun.* **2016**, *7* (1), 1–11. <https://doi.org/10.1038/ncomms11653>.
- (48) Loh, L.; Wang, Z.; Sant, S.; Koutsakos, M.; Jegaskanda, S.; Corbett, A. J.; Liu, L.; Fairlie, D. P.; Crowe, J.; Rossjohn, J.; Xu, J.; Doherty, P. C.; McCluskey, J.; Kedzierska, K. Human Mucosal-Associated Invariant T Cells Contribute to Antiviral Influenza Immunity via IL-18–Dependent Activation. *Proc. Natl. Acad. Sci.* **2016**, *113* (36), 10133–10138. <https://doi.org/10.1073/pnas.1610750113>.
- (49) Toubal, A.; Nel, I.; Lotersztajn, S.; Lehuen, A. Mucosal-Associated Invariant T Cells and Disease. *Nat. Rev. Immunol.* **2019**, *19* (10), 643–657. <https://doi.org/10.1038/s41577-019-0191-y>.
- (50) Cosgrove, C.; Ussher, J. E.; Rauch, A.; Gärtner, K.; Kurioka, A.; Hühn, M. H.; Adelman, K.; Kang, Y.-H.; Fergusson, J. R.; Simmonds, P.; Goulder, P.; Hansen, T. H.; Fox, J.; Günthard, H. F.; Khanna, N.; Powrie, F.; Steel, A.; Gazzard, B.; Phillips, R. E.; Frater, J.; Uhlig, H.; Klenerman, P. Early and Nonreversible Decrease of CD161⁺ /MAIT Cells in HIV Infection. *Blood* **2013**, *121* (6), 951–961. <https://doi.org/10.1182/blood-2012-06-436436>.
- (51) Leeansyah, E.; Ganesh, A.; Quigley, M. F.; Sönnnerborg, A.; Andersson, J.; Hunt, P. W.; Somsouk, M.; Deeks, S. G.; Martin, J. N.; Moll, M.; Shacklett, B. L.; Sandberg, J. K. Activation, Exhaustion, and Persistent Decline of the Antimicrobial MR1-Restricted MAIT-Cell Population in Chronic HIV-1 Infection. *Blood* **2013**, *121* (7), 1124–1135. <https://doi.org/10.1182/blood-2012-07-445429>.
- (52) Godfrey, D. I.; Koay, H.-F.; McCluskey, J.; Gherardin, N. A. The Biology and Functional Importance of MAIT Cells. *Nat. Immunol.* **2019**, *20* (9), 1110–1128. <https://doi.org/10.1038/s41590-019-0444-8>.
- (53) Lukasik, Z.; Elewaut, D.; Venken, K. MAIT Cells Come to the Rescue in Cancer Immunotherapy? *Cancers* **2020**, *12* (2). <https://doi.org/10.3390/cancers12020413>.

- (54) Yan, J.; Allen, S.; McDonald, E.; Das, I.; Mak, J. Y. W.; Liu, L.; Fairlie, D. P.; Meehan, B. S.; Chen, Z.; Corbett, A. J.; Varelias, A.; Smyth, M. J.; Teng, M. W. L. MAIT Cells Promote Tumor Initiation, Growth and Metastases via Tumor MR1. *Cancer Discov.* **2019**. <https://doi.org/10.1158/2159-8290.CD-19-0569>.
- (55) Godfrey, D. I.; Le Nours, J.; Andrews, D. M.; Uldrich, A. P.; Rossjohn, J. Unconventional T Cell Targets for Cancer Immunotherapy. *Immunity* **2018**, *48* (3), 453–473. <https://doi.org/10.1016/j.immuni.2018.03.009>.
- (56) Rj, N.; Ej, A.; Mc, G.; Dm, L. The Role of Mucosal Associated Invariant T Cells in Antimicrobial Immunity. *Front. Immunol.* **2015**, *6*, 344–344. <https://doi.org/10.3389/fimmu.2015.00344>.
- (57) Eckle, S. B. G.; Birkinshaw, R. W.; Kostenko, L.; Corbett, A. J.; McWilliam, H. E. G.; Reantragoon, R.; Chen, Z.; Gherardin, N. A.; Beddoe, T.; Liu, L.; Patel, O.; Meehan, B.; Fairlie, D. P.; Villadangos, J. A.; Godfrey, D. I.; Kjer-Nielsen, L.; McCluskey, J.; Rossjohn, J. A Molecular Basis Underpinning the T Cell Receptor Heterogeneity of Mucosal-Associated Invariant T Cells. *J. Exp. Med.* **2014**, *211* (8), 1585–1600. <https://doi.org/10.1084/jem.20140484>.
- (58) Mak, J. Y. W.; Xu, W.; Reid, R. C.; Corbett, A. J.; Meehan, B. S.; Wang, H.; Chen, Z.; Rossjohn, J.; McCluskey, J.; Liu, L.; Fairlie, D. P. Stabilizing Short-Lived Schiff Base Derivatives of 5-Aminouracils That Activate Mucosal-Associated Invariant T Cells. *Nat. Commun.* **2017**, *8* (1), 1–13. <https://doi.org/10.1038/ncomms14599>.
- (59) Keller, A. N.; Eckle, S. B. G.; Xu, W.; Liu, L.; Hughes, V. A.; Mak, J. Y. W.; Meehan, B. S.; Pediongco, T.; Birkinshaw, R. W.; Chen, Z.; Wang, H.; D'Souza, C.; Kjer-Nielsen, L.; Gherardin, N. A.; Godfrey, D. I.; Kostenko, L.; Corbett, A. J.; Purcell, A. W.; Fairlie, D. P.; McCluskey, J.; Rossjohn, J. Drugs and Drug-like Molecules Can Modulate the Function of Mucosal-Associated Invariant T Cells. *Nat. Immunol.* **2017**, *18* (4), 402–411. <https://doi.org/10.1038/ni.3679>.
- (60) Awad, W.; Ler, G. J. M.; Xu, W.; Keller, A. N.; Mak, J. Y. W.; Lim, X. Y.; Liu, L.; Eckle, S. B. G.; Nours, J. L.; McCluskey, J.; Corbett, A. J.; Fairlie, D. P.; Rossjohn, J. The Molecular Basis Underpinning the Potency and Specificity of MAIT Cell Antigens. *Nat. Immunol.* **2020**, 1–12. <https://doi.org/10.1038/s41590-020-0616-6>.
- (61) Ler, G. J. M.; Xu, W.; Mak, J. Y. W.; Liu, L.; Bernhardt, P. V.; Fairlie, D. P. Computer Modelling and Synthesis of Deoxy and Monohydroxy Analogues of a Ribitylaminouracil Bacterial Metabolite That Potently Activates Human T Cells. *Chem. – Eur. J.* **2019**, *25* (68), 15594–15608. <https://doi.org/10.1002/chem.201903732>.
- (62) Braganza, C. D.; Shibata, K.; Fujiwara, A.; Motozono, C.; Sonoda, K.-H.; Yamasaki, S.; Stocker,

- B. L.; Timmer, M. S. M. The Effect of MR1 Ligand Glyco-Analogues on Mucosal-Associated Invariant T (MAIT) Cell Activation. *Org. Biomol. Chem.* **2019**, *17* (40), 8992–9000. <https://doi.org/10.1039/C9OB01436E>.
- (63) Braganza, C. D.; Motozono, C.; Sonoda, K.-H.; Yamasaki, S.; Shibata, K.; Timmer, M. S. M.; Stocker, B. L. Agonistic or Antagonistic Mucosal-Associated Invariant T (MAIT) Cell Activity Is Determined by the 6-Alkylamino Substituent on Uracil MR1 Ligands. *Chem. Commun.* **2020**, *56* (39), 5291–5294. <https://doi.org/10.1039/D0CC00247J>.
- (64) Maley, G. F.; Plaut, G. W. The Isolation, Synthesis, and Metabolic Properties of 6, 7-Dimethyl-8-Ribityllumazine. *J. Biol. Chem.* **1959**, *234* (3), 641–647.
- (65) WINESTOCK, C. H.; PLAUT, G. W. E. Synthesis and Properties of Certain Substituted Lumazines_{1,2}. *J. Org. Chem.* **1961**, *26* (11), 4456–4462. <https://doi.org/10.1021/jo01069a063>.
- (66) Katagiri, H.; Takeda, I.; Imai, K. Synthesis of Riboflavin by Microorganisms. *J. Vitaminol. (Kyoto)* **1959**, *5* (4), 287–297. <https://doi.org/10.5925/jnsv1954.5.287>.
- (67) Cresswell, R. M.; Wood, H. C. S. 928. The Biosynthesis of Pteridines. Part I. The Synthesis of Riboflavin. *J. Chem. Soc. Resumed* **1960**, No. 0, 4768–4775. <https://doi.org/10.1039/JR9600004768>.
- (68) Rowan, T.; Wood, H. C. S. The Biosynthesis of Pteridines. Part V. The Synthesis of Riboflavin from Pteridine Precursors. *J. Chem. Soc. C Org.* **1968**, No. 0, 452–458. <https://doi.org/10.1039/J39680000452>.
- (69) Cushman, M.; Patrick, D. A.; Bacher, A.; Scheuring, J. Synthesis of Epimeric 6,7-Bis(Trifluoromethyl)-8-Ribityllumazine Hydrates. Stereoselective Interaction with the Light Riboflavin Synthase of *Bacillus Subtilis*. *J. Org. Chem.* **1991**, *56* (15), 4603–4608. <https://doi.org/10.1021/jo00015a009>.
- (70) Lange, J.; Anderson, R. J.; Marshall, A. J.; Chan, S. T. S.; Bilbrough, T. S.; Gasser, O.; Gonzalez-Lopez, C.; Salio, M.; Cerundolo, V.; Hermans, I. F.; Painter, G. F. The Chemical Synthesis, Stability, and Activity of MAIT Cell Prodrug Agonists That Access MR1 in Recycling Endosomes. *ACS Chem. Biol.* **2020**, *15* (2), 437–445. <https://doi.org/10.1021/acscchembio.9b00902>.
- (71) Li, K.; Vorkas, C. K.; Chaudhry, A.; Bell, D. L.; Willis, R. A.; Rudensky, A.; Altman, J. D.; Glickman, M. S.; Aubé, J. Synthesis, Stabilization, and Characterization of the MR1 Ligand Precursor 5-Amino-6-D-Ribitylaminouracil (5-A-RU). *PLOS ONE* **2018**, *13* (2), e0191837. <https://doi.org/10.1371/journal.pone.0191837>.
- (72) Bender, M.; Mouritsen, H.; Christoffers, J. A Robust Synthesis of 7,8-Didemethyl-8-Hydroxy-5-Deazariboflavin. *Beilstein J. Org. Chem.* **2016**, *12* (1), 912–917. <https://doi.org/10.3762/bjoc.12.89>.

- (73) Cushman, M.; Yang, D.; Kis, K.; Bacher, A. Design, Synthesis, and Evaluation of 9-d-Ribityl-1,3,7-Trihydro-2,6,8-Purinetriene, a Potent Inhibitor of Riboflavin Synthase and Lumazine Synthase. *J. Org. Chem.* **2001**, *66* (25), 8320–8327. <https://doi.org/10.1021/jo010706r>.
- (74) Procházková, E.; Jansa, P.; Březinová, A.; Cechová, L.; Mertlíková-Kaiserová, H.; Holý, A.; Dračínský, M. Compound Instability in Dimethyl Sulphoxide, Case Studies with 5-Aminopyrimidines and the Implications for Compound Storage and Screening. *Bioorg. Med. Chem. Lett.* **2012**, *22* (20), 6405–6409. <https://doi.org/10.1016/j.bmcl.2012.08.065>.
- (75) Zhang, Y.; Jin, G.; Illarionov, B.; Bacher, A.; Fischer, M.; Cushman, M. A New Series of 3-Alkyl Phosphate Derivatives of 4,5,6,7-Tetrahydro-1-d-Ribityl-1H-Pyrazolo[3,4-d]Pyrimidinedione as Inhibitors of Lumazine Synthase: Design, Synthesis, and Evaluation. *J. Org. Chem.* **2007**, *72* (19), 7176–7184. <https://doi.org/10.1021/jo070982r>.
- (76) Cushman, M.; Mihalic, J. T.; Kis, K.; Bacher, A. Design, Synthesis, and Biological Evaluation of Homologous Phosphonic Acids and Sulfonic Acids as Inhibitors of Lumazine Synthase. *J. Org. Chem.* **1999**, *64* (11), 3838–3845. <https://doi.org/10.1021/jo9821729>.
- (77) Poynder, T. B.; Savaliya, D. P.; Molino, A.; Wilson, D. J. D.; Dutton, J. L. Elimination of Ethene from 1,2-Diiodoethane Induced by N-Heterocyclic Carbene Halogen Bonding*. *Aust. J. Chem.* **2019**, *72* (8), 614–619. <https://doi.org/10.1071/CH19237>.
- (78) Das, B.; Kundu, N. G. An Efficient Method for the Iodination of C5-Position of Dialkoxy Pyrimidines and Uracil Bases^{1,2}. *Synth. Commun.* **1988**, *18* (8), 855–867. <https://doi.org/10.1080/00397918808057855>.
- (79) Otrubova, K.; Cravatt, B. F.; Boger, D. L. Design, Synthesis, and Characterization of α -Ketoheterocycles That Additionally Target the Cytosolic Port Cys269 of Fatty Acid Amide Hydrolase. *J. Med. Chem.* **2014**, *57* (3), 1079–1089. <https://doi.org/10.1021/jm401820q>.
- (80) Talukdar, A.; Zhao, Y.; Lv, W.; Bacher, A.; Illarionov, B.; Fischer, M.; Cushman, M. O-Nucleoside, S-Nucleoside, and N-Nucleoside Probes of Lumazine Synthase and Riboflavin Synthase. *J. Org. Chem.* **2012**, *77* (14), 6239–6261. <https://doi.org/10.1021/jo3010364>.
- (81) Huang, S.; Martin, E.; Kim, S.; Yu, L.; Soudais, C.; Fremont, D. H.; Lantz, O.; Hansen, T. H. MR1 Antigen Presentation to Mucosal-Associated Invariant T Cells Was Highly Conserved in Evolution. *Proc. Natl. Acad. Sci. U. S. A.* **2009**, *106* (20), 8290–8295. <https://doi.org/10.1073/pnas.0903196106>.
- (82) Soudais, C.; Samassa, F.; Sarkis, M.; Bourhis, L. L.; Bessoles, S.; Blanot, D.; Hervé, M.; Schmidt, F.; Mengin-Lecreulx, D.; Lantz, O. In Vitro and In Vivo Analysis of the Gram-Negative Bacteria-Derived Riboflavin Precursor Derivatives Activating Mouse MAIT Cells. *J. Immunol.* **2015**, *194* (10), 4641–4649.

<https://doi.org/10.4049/jimmunol.1403224>.

(83) Choi, A.; Miller, S. C. Reductively-Labile Sulfonate Ester Protecting Groups That Are Rapidly Cleaved by Physiological Glutathione. *Org. Biomol. Chem.* **2017**, *15* (6), 1346–1349. <https://doi.org/10.1039/C7OB00063D>.

(84) Wu, K.-M. A New Classification of Prodrugs: Regulatory Perspectives. *Pharmaceuticals* **2009**, *2* (3), 77–81. <https://doi.org/10.3390/ph2030077>.

(85) Hoffmann, E.; Kotsias, F.; Visentin, G.; Bruhns, P.; Savina, A.; Amigorena, S. Autonomous Phagosomal Degradation and Antigen Presentation in Dendritic Cells. *Proc. Natl. Acad. Sci. U. S. A.* **2012**, *109* (36), 14556–14561. <https://doi.org/10.1073/pnas.1203912109>.

(86) Colino, J.; Duke, L.; Snapper, C. M. Non-Covalent Association of Protein and Capsular Polysaccharide on Bacteria-Sized Latex Beads as a Model for Polysaccharide-Specific Humoral Immunity to Intact Gram-Positive Extracellular Bacteria. *J. Immunol. Baltim. Md 1950* **2013**, *191* (6), 3254–3263. <https://doi.org/10.4049/jimmunol.1300722>.

(87) Matthews, S. P.; Werber, I.; Deussing, J.; Peters, C.; Reinheckel, T.; Watts, C. Distinct Protease Requirements for Antigen Presentation In Vitro and In Vivo. *J. Immunol.* **2010**, *184* (5), 2423–2431. <https://doi.org/10.4049/jimmunol.0901486>.

(88) Tchoupe, J. R.; Moreau, T.; Gauthier, F.; Bieth, J. G. Photometric or Fluorometric Assay of Cathepsin B, L and H and Papain Using Substrates with an Aminotrifluoromethylcoumarin Leaving Group. *Biochim. Biophys. Acta* **1991**, *1076* (1), 149–151. [https://doi.org/10.1016/0167-4838\(91\)90232-o](https://doi.org/10.1016/0167-4838(91)90232-o).

(89) Werle, B.; Staib, A.; Jülke, B.; Ebert, W.; Zladoidsky, P.; Sekirnik, A.; Kos, J.; Spiess, E. Fluorometric Microassays for the Determination of Cathepsin L and Cathepsin S Activities in Tissue Extracts. *Biol. Chem.* **1999**, *380* (9), 1109–1116. <https://doi.org/10.1515/BC.1999.138>.

(90) Kamboj, R. C.; Pal, S.; Raghav, N.; Singh, H. A Selective Colorimetric Assay for Cathepsin L Using Z-Phe-Arg-4-Methoxy- β -Naphthylamide. *Biochimie* **1993**, *75* (10), 873–878. [https://doi.org/10.1016/0300-9084\(93\)90042-Q](https://doi.org/10.1016/0300-9084(93)90042-Q).

(91) Lützner, N.; Kalbacher, H. Quantifying Cathepsin S Activity in Antigen Presenting Cells Using a Novel Specific Substrate. *J. Biol. Chem.* **2008**, *283* (52), 36185–36194. <https://doi.org/10.1074/jbc.M806500200>.

(92) Beutner, G. L.; Young, I. S.; Davies, M. L.; Hickey, M. R.; Park, H.; Stevens, J. M.; Ye, Q. TCFH–NMI: Direct Access to N-Acyl Imidazoliums for Challenging Amide Bond Formations. *Org. Lett.* **2018**, *20* (14), 4218–4222. <https://doi.org/10.1021/acs.orglett.8b01591>.

- (93) Al-Warhi, T. I.; Al-Hazimi, H. M. A.; El-Faham, A. Recent Development in Peptide Coupling Reagents. *J. Saudi Chem. Soc.* **2012**, *16* (2), 97–116. <https://doi.org/10.1016/j.jscs.2010.12.006>.
- (94) Miyazawa, T.; Otomatsu, T.; Fukui, Y.; Yamada, T.; Kuwata, S. Effect of Copper(II) Chloride on Suppression of Racemization in Peptide Synthesis by the Carbodiimide Method. *Int. J. Pept. Protein Res.* **1992**, *39* (3), 237–244. <https://doi.org/10.1111/j.1399-3011.1992.tb00795.x>.
- (95) Jad, Y. E.; Khattab, S. N.; Torre, B. G. de la; Govender, T.; Kruger, H. G.; El-Faham, A.; Albericio, F. Oxyma-B, an Excellent Racemization Suppressor for Peptide Synthesis. *Org. Biomol. Chem.* **2014**, *12* (42), 8379–8385. <https://doi.org/10.1039/C4OB01612B>.
- (96) Ghonge, T.; Ganguli, A.; Valera, E.; Saadah, M.; Damhorst, G. L.; Berger, J.; Pagan Diaz, G.; Hassan, U.; Chheda, M.; Haidry, Z.; Liu, S.; Hwu, C.; Bashir, R. A Microfluidic Technique to Estimate Antigen Expression on Particles. *APL Bioeng.* **2017**, *1* (1), 016103. <https://doi.org/10.1063/1.4989380>.
- (97) Dal Corso, A.; Pignataro, L.; Belvisi, L.; Gennari, C. Innovative Linker Strategies for Tumor-Targeted Drug Conjugates. *Chem. – Eur. J.* **2019**, *25* (65), 14740–14757. <https://doi.org/10.1002/chem.201903127>.
- (98) Anderson, R. J.; Painter, G. F.; Hermans, I. F.; Gasser, O. S.; Weinkove, R. Mait Cell Agonists. WO2019058289 (A1).
- (99) Mondal, D.; Ford, J.; Pinney, K. G. Improved Methodology for the Synthesis of a Cathepsin B Cleavable Dipeptide Linker, Widely Used in Antibody-Drug Conjugate Research. *Tetrahedron Lett.* **2018**, *59* (40), 3594–3599. <https://doi.org/10.1016/j.tetlet.2018.08.021>.
- (100) Arrowsmith, C. H.; Audia, J. E.; Austin, C.; Baell, J.; Bennett, J.; Blagg, J.; Bountra, C.; Brennan, P. E.; Brown, P. J.; Bunnage, M. E.; Buser-Doepner, C.; Campbell, R. M.; Carter, A. J.; Cohen, P.; Copeland, R. A.; Cravatt, B.; Dahlin, J. L.; Dhanak, D.; Edwards, A. M.; Frederiksen, M.; Frye, S. V.; Gray, N.; Grimshaw, C. E.; Hepworth, D.; Howe, T.; Huber, K. V. M.; Jin, J.; Knapp, S.; Kotz, J. D.; Kruger, R. G.; Lowe, D.; Mader, M. M.; Marsden, B.; Mueller-Fahrnow, A.; Müller, S.; O'Hagan, R. C.; Overington, J. P.; Owen, D. R.; Rosenberg, S. H.; Ross, R.; Roth, B.; Schapira, M.; Schreiber, S. L.; Shoichet, B.; Sundström, M.; Superti-Furga, G.; Taunton, J.; Toledo-Sherman, L.; Walpole, C.; Walters, M. A.; Willson, T. M.; Workman, P.; Young, R. N.; Zuercher, W. J. The Promise and Peril of Chemical Probes. *Nat. Chem. Biol.* **2015**, *11* (8), 536–541. <https://doi.org/10.1038/nchembio.1867>.
- (101) Workman, P.; Collins, I. Probing the Probes: Fitness Factors For Small Molecule Tools. *Chem. Biol.* **2010**, *17* (6), 561–577. <https://doi.org/10.1016/j.chembiol.2010.05.013>.
- (102) Li, L.; Zhang, Z. Development and Applications of the Copper-Catalyzed Azide-Alkyne Cycloaddition (CuAAC) as a Bioorthogonal Reaction. *Mol. Basel Switz.* **2016**, *21* (10).

<https://doi.org/10.3390/molecules21101393>.

(103) Sletten, E. M.; Bertozzi, C. R. Bioorthogonal Chemistry: Fishing for Selectivity in a Sea of Functionality. *Angew. Chem. Int. Ed. Engl.* **2009**, *48* (38), 6974–6998. <https://doi.org/10.1002/anie.200900942>.

(104) Grammel, M.; Hang, H. C. Chemical Reporters for Biological Discovery. *Nat. Chem. Biol.* **2013**, *9* (8). <https://doi.org/10.1038/nchembio.1296>.

(105) Huisgen, R. 1,3-Dipolar Cycloadditions. Past and Future. *Angew. Chem. Int. Ed. Engl.* **1963**, *2* (10), 565–598. <https://doi.org/10.1002/anie.196305651>.

(106) Rostovtsev, V. V.; Green, L. G.; Fokin, V. V.; Sharpless, K. B. A Stepwise Huisgen Cycloaddition Process: Copper(I)-Catalyzed Regioselective “Ligation” of Azides and Terminal Alkynes. *Angew. Chem. Int. Ed.* **2002**, *41* (14), 2596–2599. [https://doi.org/10.1002/1521-3773\(20020715\)41:14<2596::AID-ANIE2596>3.0.CO;2-4](https://doi.org/10.1002/1521-3773(20020715)41:14<2596::AID-ANIE2596>3.0.CO;2-4).

(107) Tornøe, C. W.; Christensen, C.; Meldal, M. Peptidotriazoles on Solid Phase: [1,2,3]-Triazoles by Regiospecific Copper(I)-Catalyzed 1,3-Dipolar Cycloadditions of Terminal Alkynes to Azides. *J. Org. Chem.* **2002**, *67* (9), 3057–3064. <https://doi.org/10.1021/jo011148j>.

(108) Neumann, S.; Biewend, M.; Rana, S.; Binder, W. H. The CuAAC: Principles, Homogeneous and Heterogeneous Catalysts, and Novel Developments and Applications. *Macromol. Rapid Commun.* **2020**, *41* (1), 1900359. <https://doi.org/10.1002/marc.201900359>.

(109) Yang, M.; Yang, Y.; Chen, P. R. Transition-Metal-Catalyzed Bioorthogonal Cycloaddition Reactions. *Top. Curr. Chem.* **2015**, *374* (1), 2. <https://doi.org/10.1007/s41061-015-0001-3>.

(110) Chan, T. R.; Hilgraf, R.; Sharpless, K. B.; Fokin, V. V. Polytriazoles as Copper(I)-Stabilizing Ligands in Catalysis. *Org. Lett.* **2004**, *6* (17), 2853–2855. <https://doi.org/10.1021/ol0493094>.

(111) Patel, O.; Kjer-Nielsen, L.; Nours, J. L.; Eckle, S. B. G.; Birkinshaw, R.; Beddoe, T.; Corbett, A. J.; Liu, L.; Miles, J. J.; Meehan, B.; Reantragoon, R.; Sandoval-Romero, M. L.; Sullivan, L. C.; Brooks, A. G.; Chen, Z.; Fairlie, D. P.; McCluskey, J.; Rossjohn, J. Recognition of Vitamin B Metabolites by Mucosal-Associated Invariant T Cells. *Nat. Commun.* **2013**, *4* (1), 1–9. <https://doi.org/10.1038/ncomms3142>.

(112) Crouch, R. D. Selective Deprotection of Silyl Ethers. *Tetrahedron* **2013**, *69* (11), 2383–2417. <https://doi.org/10.1016/j.tet.2013.01.017>.

(113) Speers, A. E.; Adam, G. C.; Cravatt, B. F. Activity-Based Protein Profiling in Vivo Using a Copper(I)-Catalyzed Azide-Alkyne [3 + 2] Cycloaddition. *J. Am. Chem. Soc.* **2003**, *125* (16), 4686–4687. <https://doi.org/10.1021/ja034490h>.

- (114) Speers, A. E.; Cravatt, B. F. Profiling Enzyme Activities In Vivo Using Click Chemistry Methods. *Chem. Biol.* **2004**, *11* (4), 535–546. <https://doi.org/10.1016/j.chembiol.2004.03.012>.
- (115) Kim, C.-S.; Russell, K. C. Rapid Bergman Cyclization of 1,2-Diethynylheteroarenes. *J. Org. Chem.* **1998**, *63* (23), 8229–8234. <https://doi.org/10.1021/jo980879p>.
- (116) Nencka, R.; Votruba, I.; Hřebabeký, H.; Jansa, P.; Tloušťová, E.; Horská, K.; Masojídková, M.; Holý, A. Discovery of 5-Substituted-6-Chlorouracils as Efficient Inhibitors of Human Thymidine Phosphorylase. *J. Med. Chem.* **2007**, *50* (24), 6016–6023. <https://doi.org/10.1021/jm070644i>.
- (117) Cushman, M.; Sambaiah, T.; Jin, G.; Illarionov, B.; Fischer, M.; Bacher, A. Design, Synthesis, and Evaluation of 9-d-Ribitylamino-1,3,7,9-Tetrahydro-2,6,8-Purinetriones Bearing Alkyl Phosphate and α,α -Difluorophosphonate Substituents as Inhibitors of Riboflavin Synthase and Lumazine Synthase. *J. Org. Chem.* **2004**, *69* (3), 601–612. <https://doi.org/10.1021/jo030278k>.

Résumé en français : "Synthesis and study of compounds able to activate MAIT cells"

Résumé du chapitre 1: "Introduction: MAIT cells"

I. Biologie des cellules MAITs

Les cellules MAIT sont des lymphocytes T de l'immunité "innate-like" capables de reconnaître un nombre restreint d'antigènes dérivés du métabolisme de certaines vitamines microbiennes. Ces antigènes sont présentés par la protéine MR1, analogue non polymorphe du complexe majeur d'histocompatibilité (CMH), au TCR (récepteur des cellules T) semi-invariant des cellules MAITs.

Le développement des cellules MAIT a lieu dans le thymus^{1,2,3}. Il est dépendant de MR1 qui présente les antigènes des cellules MAIT aux cellules immatures afin de permettre leur maturation. À la suite de ce développement, la plupart des cellules MAITs expriment le phénotype suivant: CD3⁺ V α 7.2⁺ CD161^{high} et CD8⁺ $\alpha\alpha$ ou double négatif (CD4⁻CD8⁻) (Figure 1). La chaîne α du TCR est associée à un nombre limité de chaînes β (V β 2-13 chez l'homme). Les cellules MAIT expriment d'autres marqueurs tels que des récepteurs aux chimiokines (CCR6, CCR9...), des récepteurs aux cytokines (IL-12R, IL-18R) ou encore les facteurs de croissance PLZF et ROR γ t. Ces mêmes cellules expriment également un phénotype mémoire avec CD45RO et CD95.

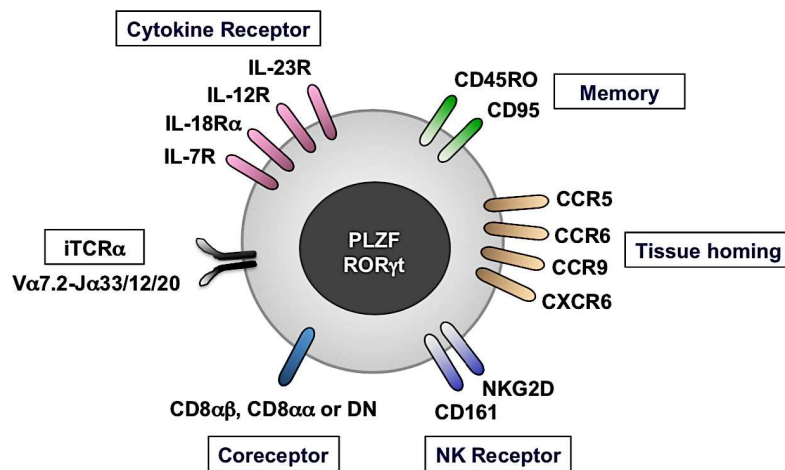


Figure 1: Phénotype des cellules MAIT classiques⁴

Les cellules MAIT constituent une population abondante de cellules T retrouvée principalement dans le foie (20-40% des cellules T), le tractus gastro-intestinal (3-5% des cellules T), les vaisseaux sanguins périphériques (1-10% des cellules T) et les poumons (2-4% des cellules T)⁵.

Lorsque les cellules MAIT sont activées, elles produisent et sécrètent plusieurs cytokines pro-inflammatoires dont $TNF\alpha$, $INF\gamma$ et IL-17 (Figure 2). Ces cellules exercent des fonctions cytotoxiques puisqu'elles sont capables de lyser les cellules infectées par certains micro-organismes (mécanisme dépendant de MR1) en sécrétant des perforines et granzymes^{6,7}. Elles peuvent également induire l'activation d'autres cellules immunitaires telles que des lymphocytes B ou des cellules dendritiques afin de déclencher une réponse immunitaire adaptative⁸.

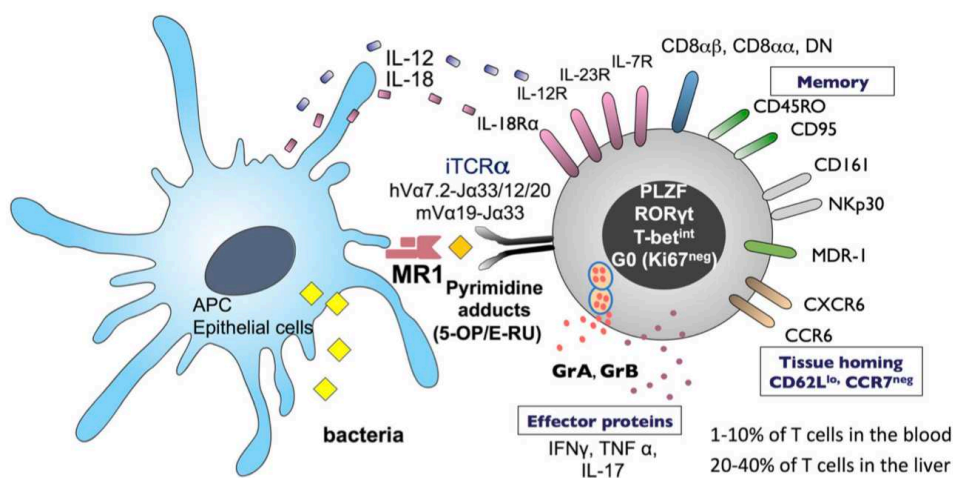


Figure 2: Activation des cellules MAIT⁹

II. Ligands et activation des cellules MAIT

A. Modulation de l'activité des cellules MAIT dépendante du TCR

1. Antigènes des cellules MAIT

L'activité des cellules MAIT est modulée par plusieurs antigènes activateurs ou inhibiteurs dérivés du métabolisme de certaines vitamines microbiennes. Ainsi, l'activation des cellules MAITs est inhibée par des dérivés de la vitamine B9 (acide folique) comme le composé 6-Fp (6-formylpterine) et son analogue acétylé Ac-6-Fp (acetyl-6-formylpterine) (Figure 3).

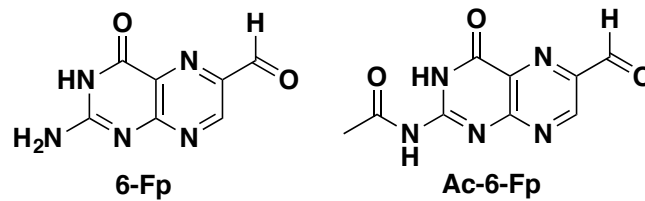


Figure 3: Structure chimique des ligands inhibiteurs des cellules MAIT

L'activation des cellules MAIT est médiée par des dérivés de la riboflavine (vitamine B2). Les deux ligands les plus actifs connus à ce jour sont le 5-OP-RU (5-(2-oxopropylideneamino)-6-D-ribitylaminouracil) et le 5-OE-RU (5-(2-oxoethylideneamino)-6-D-ribitylaminouracil). Ces composés sont produits respectivement à partir d'une réaction de condensation entre le précurseur clé 5-A-RU (5-amino-6-D-ribitylaminouracil) et le methylglyoxal ou le glyoxal (métabolites de la glycolyse) (Figure 4). Ces deux antigènes sont très instables en milieu aqueux et subissent rapidement une cyclisation pour donner des dérivés ribityllumazines présentant un moindre pouvoir antigénique.

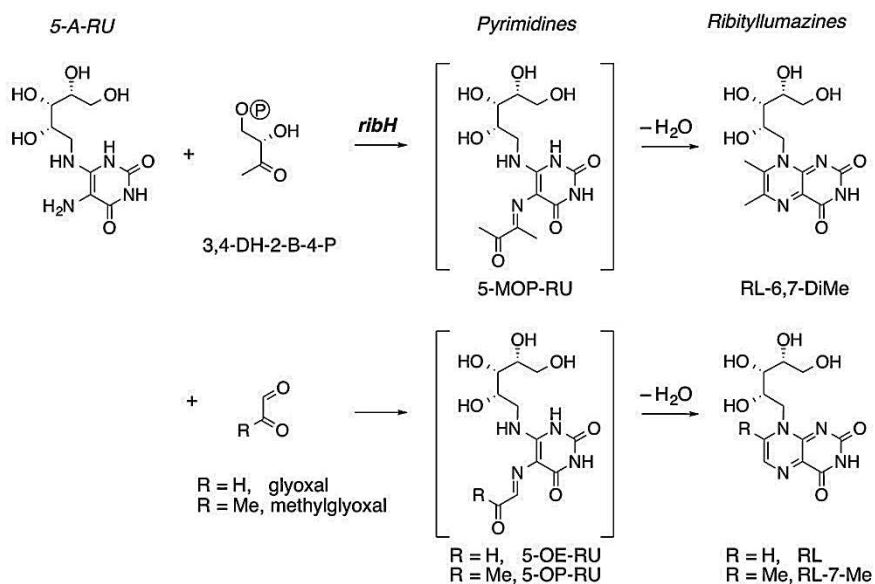


Figure 4: Biosynthèse des ligands agonistes des cellules MAIT¹⁰

2. Présentation antigénique par MR1

La protéine MR1 est responsable de la présentation des antigènes précédemment décrits au TCR des cellules MAIT. La liaison de ces molécules au MR1 est médiée par un certain nombre d'interactions (liaisons hydrogène, interactions de Van der Waals...) et tout particulièrement par la formation d'une imine (base de Schiff) entre la Lys43 de MR1 et le groupement carbonyle de ces ligands (**Erreur ! Source du renvoi introuvable.**). Une fois formé dans le réticulum endoplasmique des cellules présentatrices d'antigènes (CPA), le complexe antigénique migre vers la membrane plasmique

afin d'être présenté au TCR des cellules MAIT. Les ligands agonistes interagissent avec le TCR par le biais d'un important réseau de liaisons hydrogène formé grâce aux groupements hydroxyles de la chaîne ribityle. A l'inverse, les ligands inhibiteurs qui ne possèdent pas de chaîne ribityle n'interagissent pas efficacement avec le TCR et ne peuvent donc pas activer les cellules MAIT.

B. Activation des cellules MAIT indépendante du TCR

Les cellules MAIT présentent également une activation indépendante du TCR orchestrée par certaines cytokines pro-inflammatoires et antivirales (principalement IL-18, IL-12, IL-15, $\text{INF}\alpha\text{-}\beta$)^{11,12}. Ainsi, il est vraisemblable que les cellules MAIT soient impliquées dans la réponse immunitaire aux infections virales et à certaines pathologies auto-immunes et inflammatoires.

III. Cellules MAIT et immunothérapies

Du fait de leur activité antimicrobienne (et antivirale), les cellules MAIT pourraient constituer une cible thérapeutique de choix. Elles pourraient être directement ciblées par de nouveaux vaccins puisqu'elles expriment un phénotype mémoire ou plus indirectement être utilisées en tant qu'adjuvants vaccinaux dans le but d'améliorer la réponse vaccinale. L'implication des cellules MAIT dans d'autres pathologies telles que les cancers ou les maladies auto-immunes et inflammatoires est également à l'étude. En revanche, il n'existe pas de preuves évidentes d'un rôle protecteur ou au contraire néfaste des cellules MAIT dans ces pathologies.

Afin de permettre l'étude approfondie des cellules MAIT comme agents thérapeutiques, il est primordial d'accroître nos connaissances concernant leurs antigènes et de résoudre le problème d'instabilité chimique ces molécules.

IV. Recherche de nouveaux antigènes des cellules MAIT

A. Synthèse de nouveaux analogues stables du 5-OP-RU

Une première étude a décrit la synthèse de trois analogues du 5-OP-RU (Figure 5)¹³. L'étude de ces composés a montré que **9** était très instable en milieu aqueux et que **10** l'était également mais dans une moindre mesure. En revanche, **11** était très stable mais son activité était beaucoup plus faible que celle du 5-OP-RU (EC_{50} 1.6 nM versus 1.6 pM pour le 5-OP-RU).

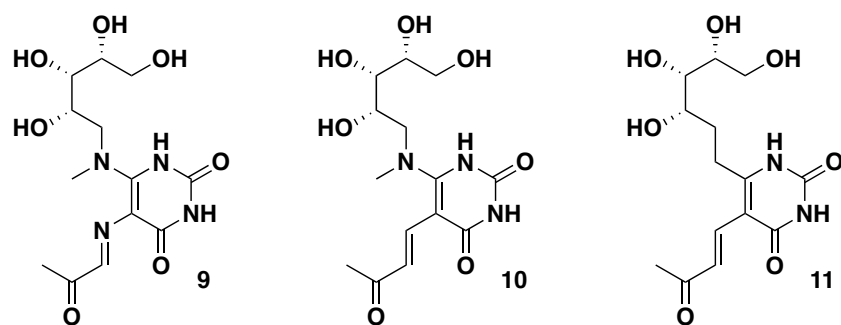


Figure 5: Structure chimique des composés 9-11

Une seconde étude basée sur un screening *in silico* a permis d'identifier un certain nombre de molécules dérivés de médicaments capables de moduler l'activité des cellules MAIT (Figure 6)¹⁴. Parmi ces composés, l'acide 3-formaldehyde-salicylique (3-F-SA), l'acide 5-formaldehyde-salicylique (5-F-SA), le 2-hydroxy-napthaldehyde (2-OH-1-NA) et le 2,4-diamino-6-formylpteridine (2,4-DA-6-Fp) étaient capable d'induire une up-régulation de MR1 à la surface des CPA. Le 3-F-SA et le 2-OH-1-NA sont des inhibiteurs des cellules MAIT alors que le 5-F-SA est un agoniste faible de ces mêmes cellules. Le diclofénac et ses métabolites (4'-hydroxy-diclofenac et 5'-hydroxy-diclofénac) ont également permis une faible activation des cellules MAIT au cours de cette étude. Ainsi, la protéine MR1 peut présenter d'autres composés que les antigènes dérivés de la biosynthèse de vitamines microbiennes au TCR des cellules MAIT. Cette découverte offre des opportunités de découvrir d'autres antigènes des cellules MAIT présentant des structures chimiques originales.

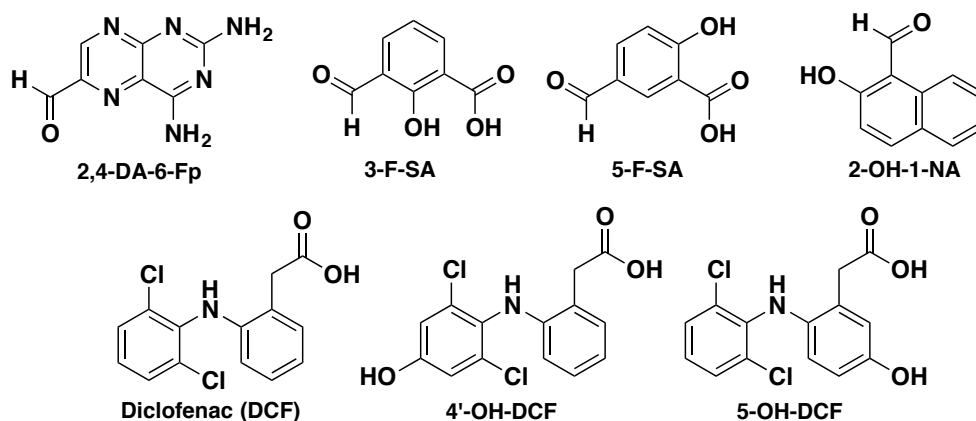


Figure 6: Structure chimique des molécules capables de moduler l'activité des cellules MAIT

Enfin, trois études récentes ont investigué l'importance de la chaîne ribityle (relations structure-activité) et de chacun de ses groupements hydroxyles dans l'activité biologique (up-régulation de MR1 et activation des cellules MAIT)^{15,16,17}. Les résultats montrent que la chaîne ribityle ne semble pas indispensable à la liaison au MR1 induisant l'up-régulation à la membrane cellulaire. C'est la formation de l'imine avec la Lys43 qui présente le plus d'importance pour lier efficacement le

MR1. À l'inverse, la chaîne ribityle est primordiale dans l'interaction avec le TCR. En effet, les résultats de ces études montre que les groupements 2'-OH et 3'-OH semblent essentiels pour induire une activation des cellules MAITs tandis que les groupements 4'-OH et 5'-OH semblent moins importants.

Objectifs de recherche

Le principal objectif de recherche était de synthétiser de nouveaux analogues actifs et stables des antigènes des cellules MAIT. Pour ce faire, nous avons, dans un premier temps, effectué un certain nombre de pharmacomodulations du 5-OP-RU dans le but de stabiliser sa structure chimique. Ensuite, nous avons cherché à synthétiser des prodrugs du 5-A-RU, le précurseur chimique du 5-OP-RU capable de former ce dernier *in situ* par réaction avec du méthylglyoxal endogène.

Le second objectif de recherche était de synthétiser une sonde chimique nous permettant de visualiser et de suivre les antigènes des MAIT dans les cellules et tissus biologiques. Pour ce faire, nous avons synthétisé un analogue du 5-OP-RU comportant un alcyne terminal lié à la chaîne ribityle. Ce composé peut réagir par CuAAC (Cu(I)-catalyzed azide-alkyne cycloaddition) dans des réactions bio-orthogonales permettant de visualiser la molécule liée au MR1 dans les cellules (Figure 7).

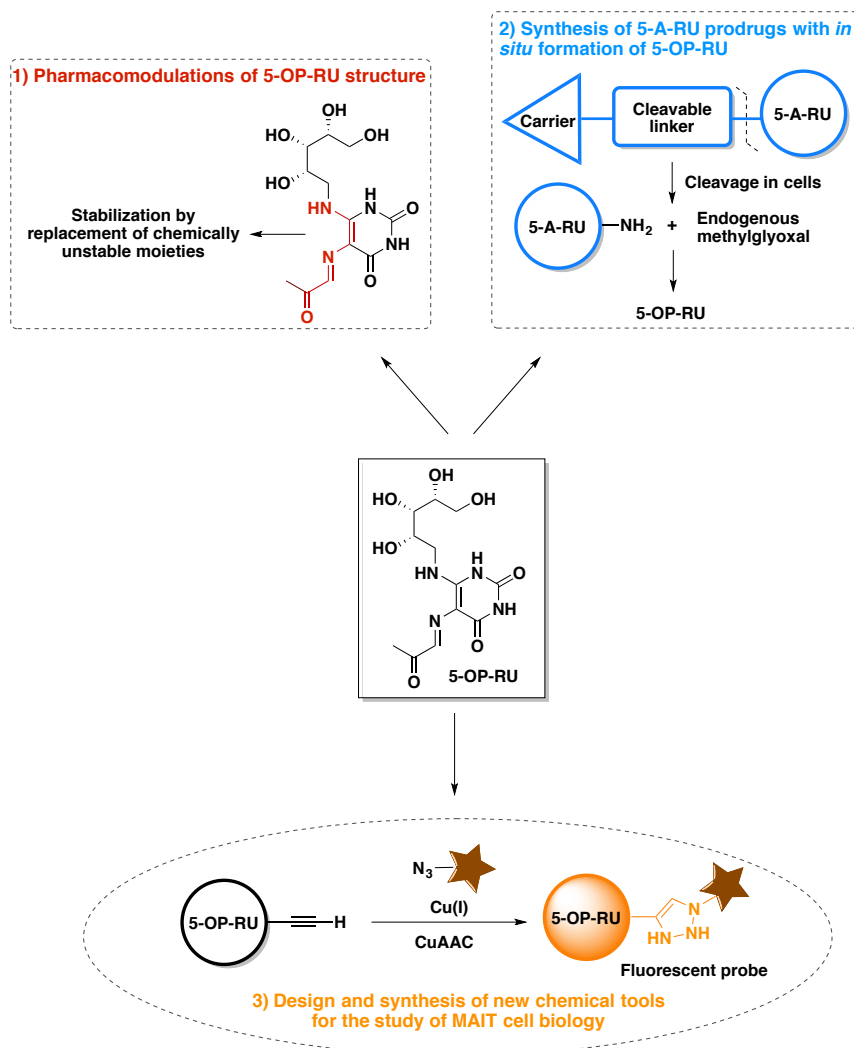


Figure 7: Objectifs du projet de recherche

Résumé du chapitre 2: "Synthesis and study of stable analogues of 5-OP-RU"

I. Synthèse et étude analytique du 5-A-RU et du 5-OP-RU

A. Synthèse du 5-A-RU

De nombreuses voies de synthèse du 5-A-RU sont publiées à ce jour. Nous avons choisi d'adapter une de ces synthèses en série non protégée pour produire de grandes quantités du précurseur stable **4** (5-N-RU)¹⁸ (Schéma 1). Le 5-A-RU est une molécule très instable. C'est pourquoi nous avons dû synthétiser un nouveau batch à chaque fois à partir du stock de **4**. De plus, afin d'améliorer sa stabilité, nous avons isolé le 5-A-RU sous forme de sels hydrochlorés (**5**) par hydrogénation sur Pd/c puis ajout de HCl 1N.

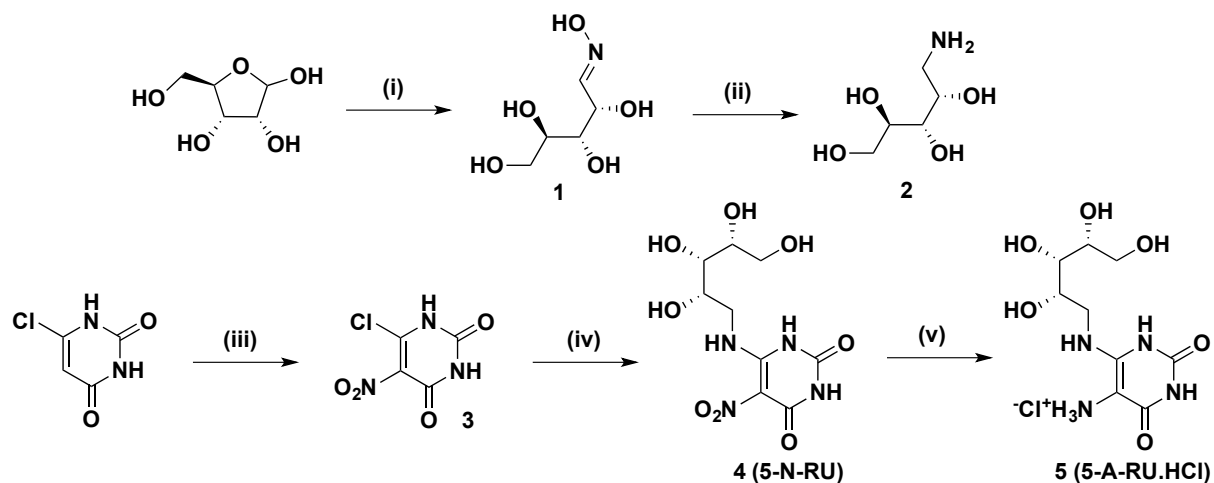


Schéma 1: Synthèse de 5 en série non protégée; Conditions et réactifs: (i) $\text{NH}_2\text{OH.HCl}$, NaOMe dans EtOH, 70°C , 78%; (ii) PtO_2 , H_2 dans AcOH, 103% (impureté mineure); (iii) HNO_3 , H_2SO_4 , 73%; (iv) **2**, KOH 2N dans EtOH/ H_2O , 45%; (v) **1**) Pd/C, H_2 dans H_2O 2) HCl 1N, 94%

Nous avons également développé une synthèse en série protégée visant à produire un analogue protégé de la molécule **2**. Celui-ci a été largement utilisé pour la synthèse d'analogues stables du 5-OP-RU en plus de permettre la synthèse de **5** (Schéma 2).

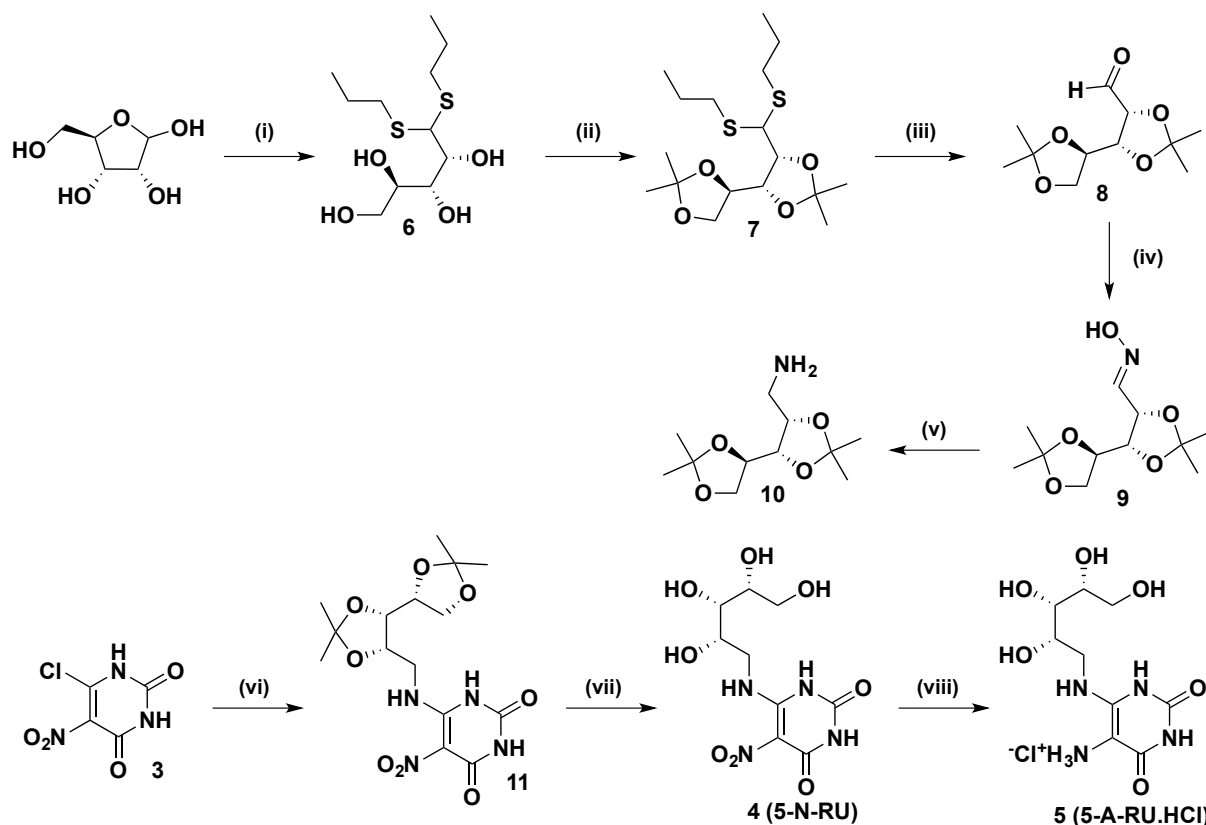


Schéma 2: Synthèse de 5-A-RU 5 en série protégée; Conditions et réactifs: (i) *n*-PrSH dans HCl 37%, 47%; (ii) 2,2-diméthoxypropane, *p*-TsOH dans acétone, 53%; (iii) I₂, NaHCO₃ dans acétone/H₂O, 76%; (iv) NH₂OH.HCl, NaHCO₃ dans EtOH/H₂O, 77%; (v) LiAlH₄ dans THF, reflux, 76%; (vi) **10**, Et₃N dans DCM, 93%, (vii) TFA/H₂O, 94%; (viii) 1) Pd/C, H₂ dans H₂O, 2) HCl 1N, 94%

B. Etude analytique du 5-A-RU

Afin de comprendre les mécanismes de dégradation du 5-A-RU, nous avons réalisé en collaboration avec Sanofi, une étude analytique de ce composé. En combinant des analyses par spectrométrie de masse et RMN ¹H, nous avons pu proposer une hypothèse expliquant la rapide dégradation du 5-A-RU (Figure 8). D'après ce modèle, l'instabilité serait due à une oxydation de l'amine primaire du 5-A-RU en milieu aqueux.

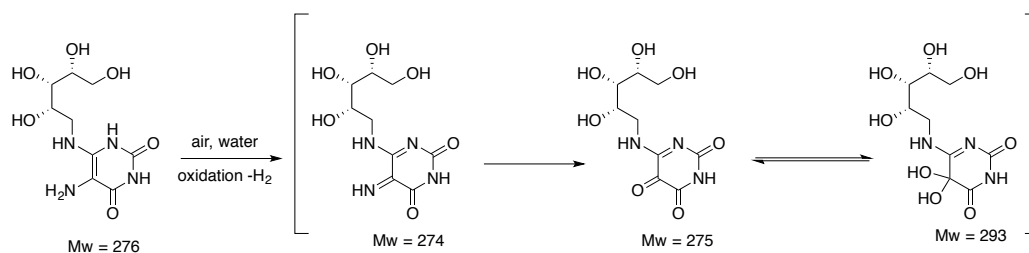


Figure 8: Mécanisme hypothétique de dégradation du 5-A-RU

C. Synthèse du 5-OP-RU

Du fait de son instabilité, le 5-OP-RU est le plus souvent formé juste avant l'addition sur les cellules lors des tests biologiques. La réaction entre le 5-A-RU et le methylglyoxal dans l'eau permet de former une quantité très faible de 5-OP-RU car celui-ci se dégrade très rapidement dans ce solvant¹³. En revanche, dans le DMSO, le 5-OP-RU formé ne subit pas de cyclisation et une conversion totale du 5-A-RU est observée. Nous avons synthétisé du 5-OP-RU dans ces deux solvants afin de comparer leur activité biologique respective (Schéma 3).

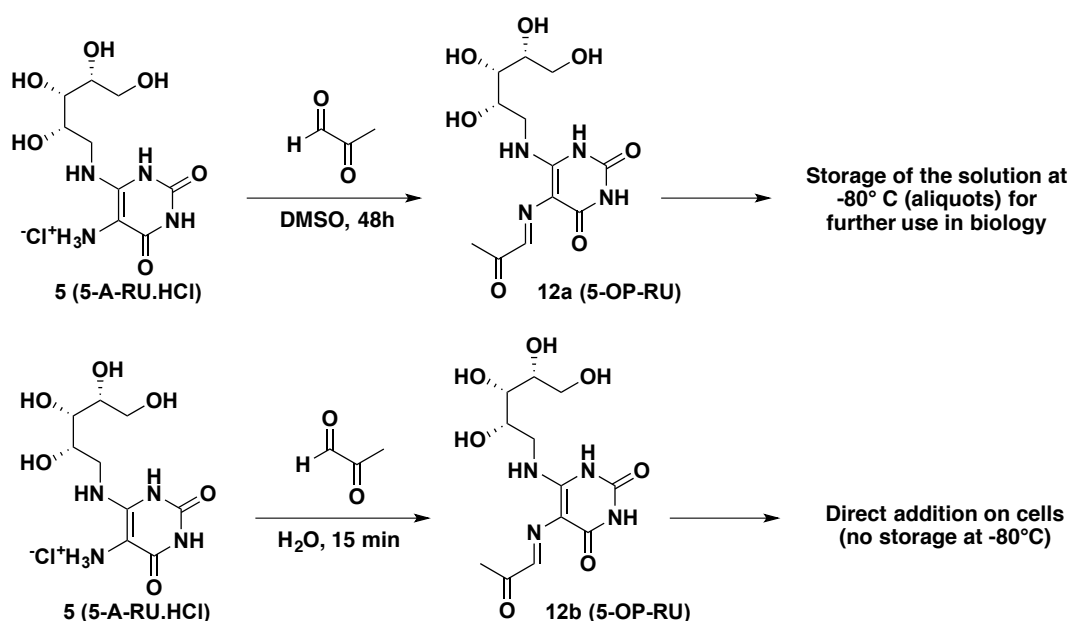


Schéma 3: Synthèse de 12a (DMSO) et 12b (water)

D. Synthèse et évaluation biologique d'analogues stables du 5-OP-RU

1. Stratégie de chimie médicinale

Plusieurs stratégies de chimie médicinale ont été envisagées (Figure 9) :

- Modification de la chaîne D-ribitylamine
- Remplacement du groupement instable α -iminocarbonyl par un alkyl ou un vinylsulfonate (liaison ionique avec lys43 du MR1 au lieu d'une liaison covalente)
- Modification de l'hétérocycle avec synthèse de molécules comportant deux cycles fusionnés stables

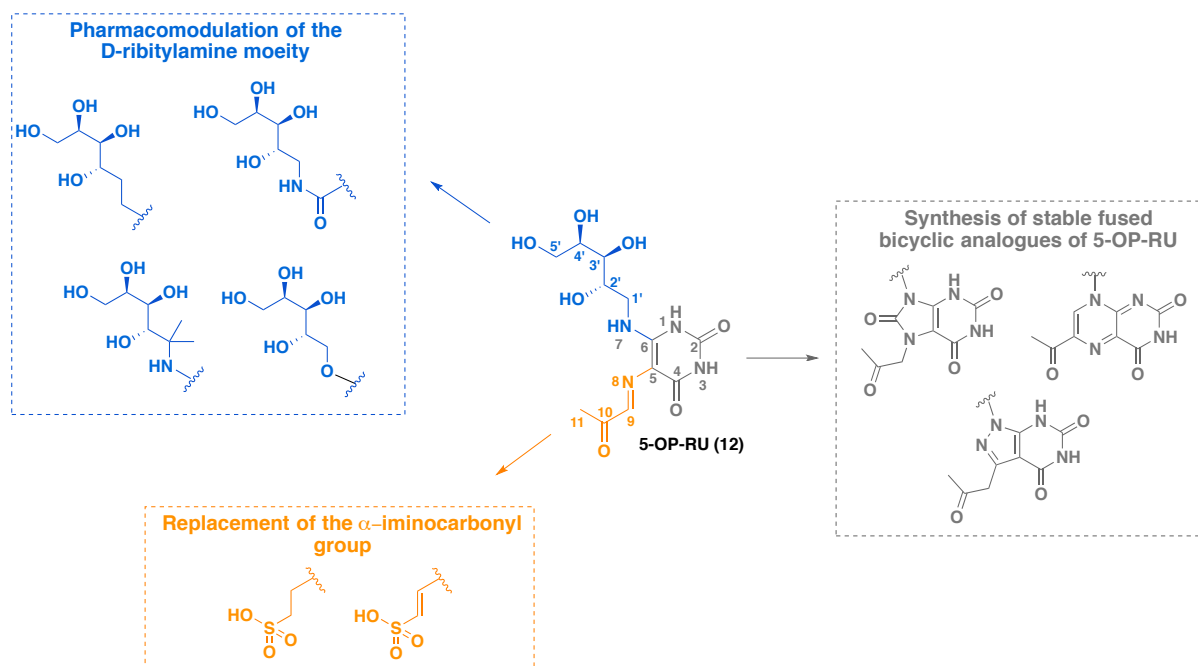


Figure 9: Résumé des différentes pharmacomodulations de 5-OP-RU envisagées

2. Modulation du groupement α -iminocarbonyle

a) Synthèse de l'analogue alkylsulfonate **13**

La molécule **13** a été synthétisée en sept étapes avec l'introduction d'un alcyne par une réaction de Sonogashira puis une réaction d'hydroboration qui a permis de former **16** (Schéma 4). Après introduction du groupement sulfonate, la molécule **19** a été couplée avec **12** et le composé final **13** a été obtenu après déprotection des groupements hydroxyles de la chaîne ribityle.

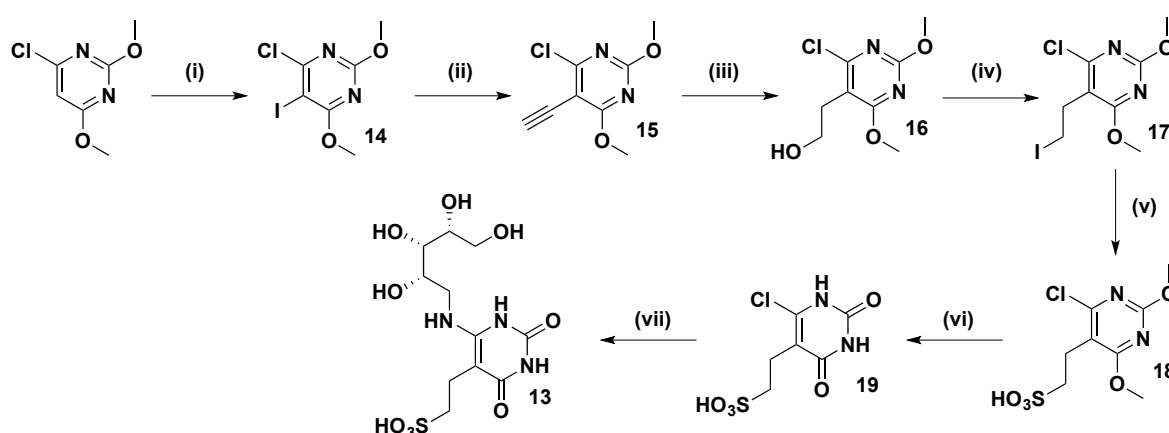


Schéma 4: Synthèse de 13; Réactifs et conditions: (i) N-iodosuccinimide, AcOH, anhydride acétique dans CH_3CN , 80°C , 81%; (ii) 1) TMS-acétylène, $\text{Pd}(\text{PPh}_3)_2\text{Cl}_2$, CuI dans $i\text{Pr}_2\text{NH} / \text{THF}$ 1:1, 70°C ; 2) K_2CO_3 dans MeOH, 64%; (iii) 1) B_2Pin_2 , Cs_2CO_3 , MeOH dans CH_3CN , 100°C , tube scellé; 2) NaOH, H_2O_2 ; 3) NaBH_4 dans MeOH 52%; (iv) PPh_3 , I_2 ,

imidazole dans THF, 74%; (v) Na₂SO₃ dans acétone/H₂O, reflux, 88%; (vi) HCl 37%, AcOH, reflux 65%; (vii) 1) **10** dans EtOH, tube scellé; 2) TFA/H₂O 22%

b) Synthèse de l'analogue vinylsulfonate

Nous avons réussi à obtenir un précurseur protégé (**23**) de la molécule finale par réaction de Wittig entre **20** et **21** puis par un couplage pallado-catalysé de Buchwald-Hartwig entre **10** et **22**. (Schéma 5)

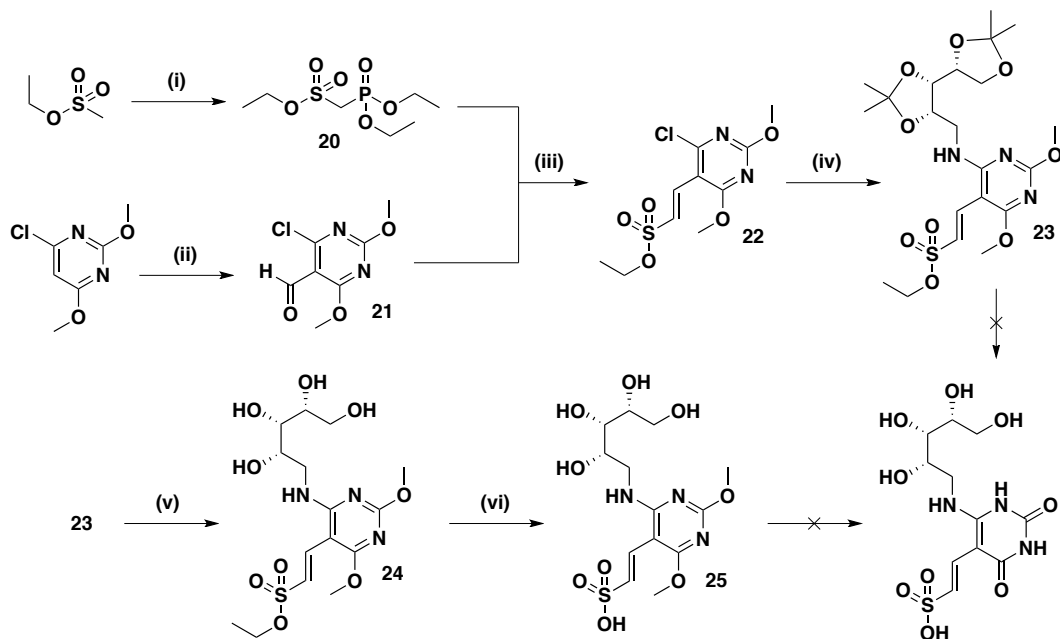


Schéma 5: Synthèse initiale de l'analogue vinylsulfonate; Réactifs et conditions: (i) diéthylphosphochloridate, *n*-BuLi dans THF, -78°C à -50°C, 63%; (ii) *n*-BuLi, DMF dans THF, -78°C, 64%; (iii) *t*-BuOK dans THF, 0°C à ta, 69%; (iv) **10**, Pd(dba)₃, Xantphos, Cs₂CO₃ dans toluène, ta, 66%; (v) TFA/H₂O in CH₃CN, 0°C à ta, 47%; (vi) KI dans acétone, reflux, 40%

Malgré de nombreux essais de déprotection, nous ne sommes pas parvenus à la molécule finale. En effet, un problème d'instabilité du groupement vinylsulfonate a été détecté, rendant difficile la déprotection de l'uracile et du sulfonate.

3. Pharmacomodulation de la chaîne D-ribitylamine

En collaboration avec Sanofi, nous avons synthétisé plusieurs analogues du 5-OP-RU en modifiant la partie ribityle de la molécule (Schéma 6).

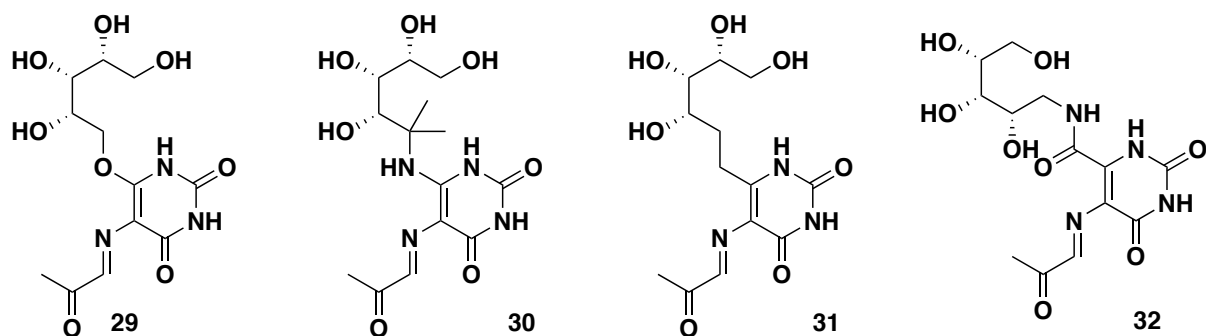


Schéma 6: Structure chimique des analogues 29-32 (modification de la chaîne ribityle)

4. Synthèse d'analogues bicycliques stables du 5-OP-RU

a) *Analogue purinetrione*

La molécule **37** a été obtenu en formant le précurseur protégé du 5-N-RU **34** puis par une cyclisation avec du phosgène pour former l'hétérocycle souhaité. Enfin, une chaîne latérale présentant un groupement carbonyle a été ajouté puis les groupements protecteurs ont été retirés pour donner **37** (Schéma 7).

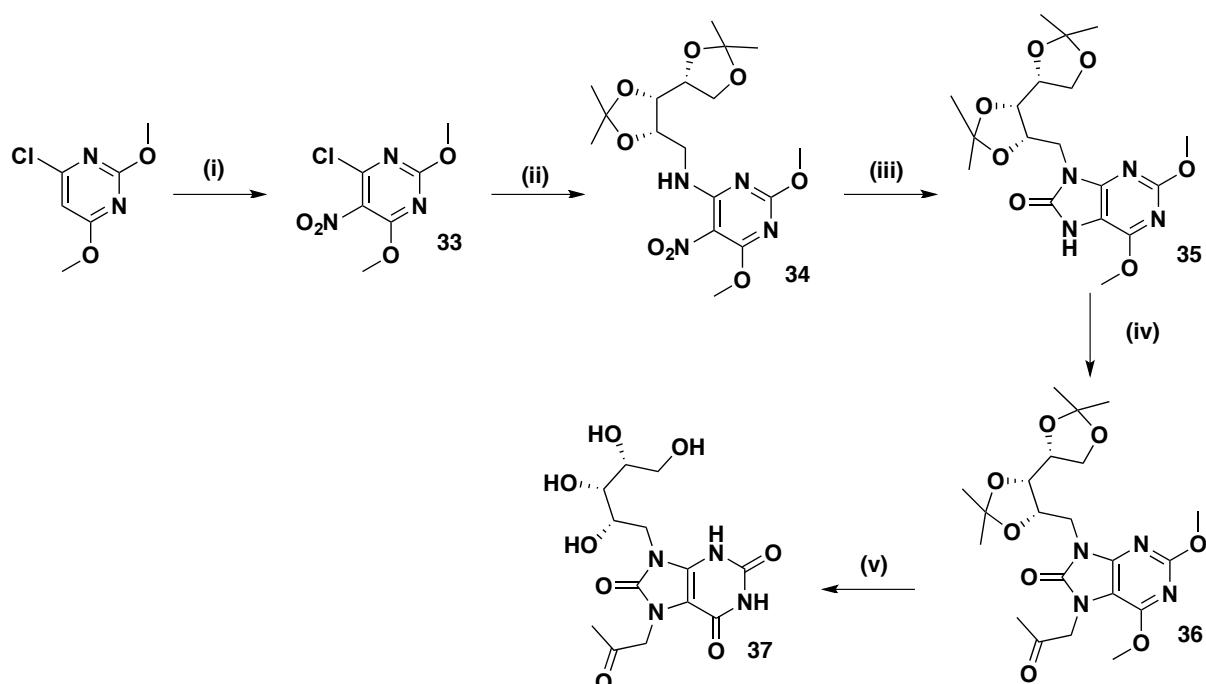


Schéma 7: Synthèse de l'analogue purinetrione 37; Réactifs et conditions: (i) HNO_3 , H_2SO_4 , 80°C , 56%; (ii) **10**, Et_3N dans DMF, 75%; (iii) 1) H_2 , Pd/C dans MeOH; 2) triphosgène, Et_3N dans DCM, 0°C , 72%; (iv) chloroacétone, NaH dans DMF, 94%; (v) HCl 37% dans MeOH, reflux, 84%

b) Synthèse d'un analogue à structure pyrazolo[3,4-d]pyrimidine

La synthèse de **43** est inachevée et seules des traces du produit final ont été obtenues. Le précurseur **42** a pu cependant être obtenu et isolé en couplant les deux molécules **39** et **41** synthétisées séparément au préalable (Schéma 8).

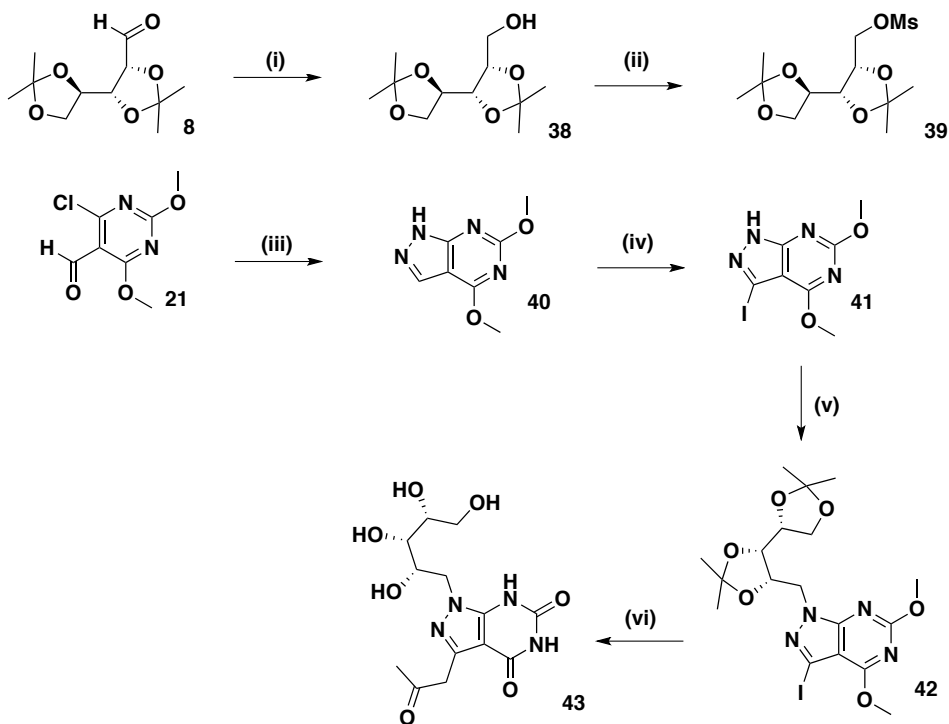


Schéma 8: Synthèse de 43; Réactifs et conditions: (i) NaBH₄ dans MeOH, 48%; (ii) MsCl dans pyridine, 89%; (iii) H₂N-NH₂·H₂O dans MeOH, reflux, 46%; (iv) NIS dans DMF, 46%; (v) **39**, K₂CO₃ dans DMF, 39%; (vi) 1) isopropenyl acétate, (t-Bu)₃SnMeO, P(o-tolyl)₃, PdCl₂(CH₃CN)₂ dans toluène, 120°C tube scellé; 2) HCl 37% dans MeOH, traces du produit obtenues

c) Formyllumazine analogue

L'analogue formyllumazine a pu être formé mais la molécule obtenue était trop instable pour être isolée (dégradation très rapide de la molécule après purification par HPLC) (Schéma 9).

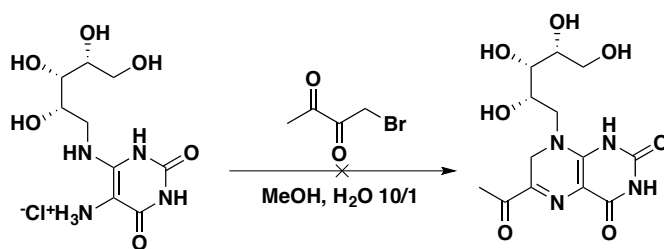


Schéma 9: Synthèse de l'analogue formyllumazine

E. Evaluation biologique

1. Principe des tests

Deux tests différents ont été effectués pour évaluer les molécules :

- Test d'up-régulation de MR1 chez des cellules WT3-m (cellules surexprimant MR1)
- Test d'activation de cellules MAIT de souris transgéniques exprimant le TCR des cellules MAITs (Figure 10).

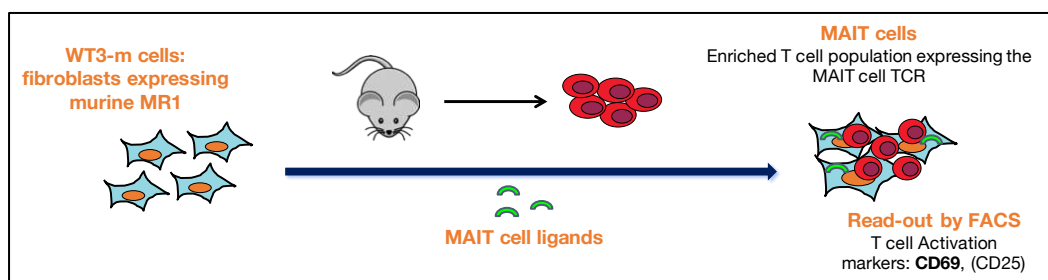


Figure 10: Test d'activation des cellules MAIT

2. Résultats

a) Up-régulation de MR1

Parmi les analogues du 5-OP-RU (**12**) synthétisés, seuls les composés **30** et **31** ont induit une up-régulation de MR1 (Figure 11). Le composé **13** ne franchit probablement pas les membranes plasmiques du fait de son caractère ionique et ne peut donc pas up-réguler MR1. En revanche, il est capable d'induire le refolding de MR1 recombinant, ceci prouvant son affinité pour la protéine.

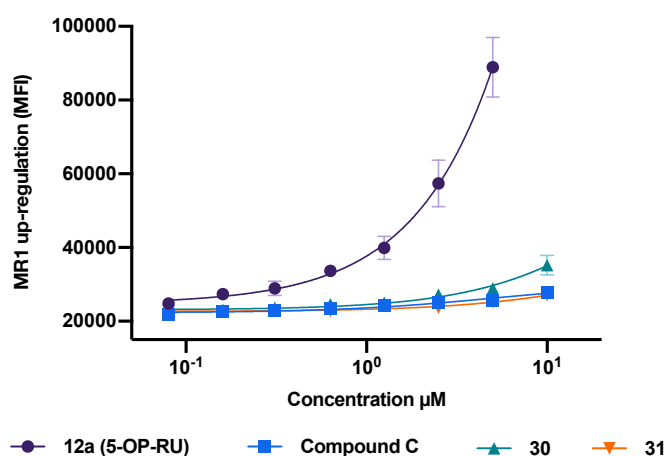


Figure 11: Up-régulation de MR1 par 30 et 31 (chaque mesure a été effectuée en duplicat)

b) *Activation des cellules MAIT*

Les analogues n'ayant pas induit d'up-régulation de MR1 n'ont pas permis l'activation des cellules MAIT tout comme **31**. En revanche, la molécule **30** est capable d'activer les cellules MAITs mais de manière très faible comparée au 5-OP-RU (Figure 12). Ces deux derniers composés peuvent se comporter comme des antagonistes compétitifs du 5-OP-RU comme l'ont démontré les tests de compétition.

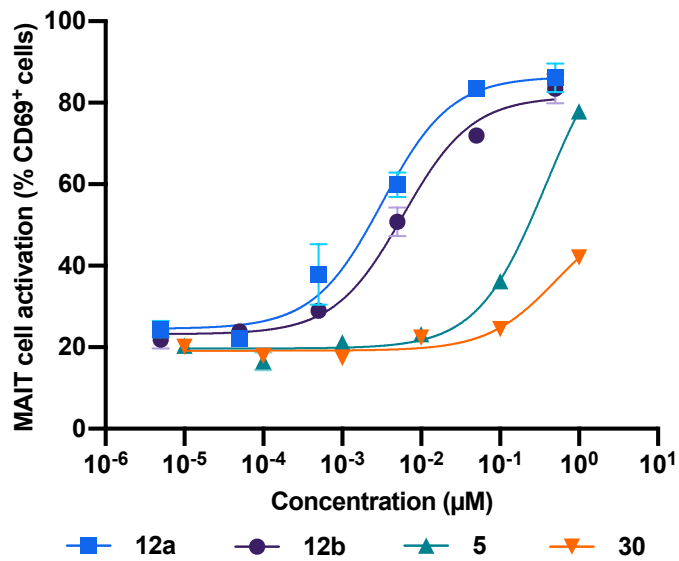


Figure 12: Activation des cellules MAIT par 30 en comparaison avec 5-OP-RU (12a, 12b) et 5-A-RU (5) (chaque mesure a été effectuée en duplicat)

Résumé du chapitre 3 : Prodrug strategy and vectorization of 5-A-

RU

I. Synthèse d'une prodrogue du 5-A-RU sensible au clivage enzymatique

La prodrogue du 5-A-RU est constituée d'un linker phenylalanine-arginine (Phe-Arg) sensible aux cathepsines (Cat B, Cat L, Cat S)¹⁹⁻²¹. Nous avons choisi d'utiliser des billes de latex comme vecteur pour valider notre stratégie et étudier la réponse immunologique induite par la prodrogue. En effet, elles ont montré leur efficacité pour induire une phagocytose/endocytose par des cellules présentatrices d'antigènes²². Une fois la stratégie prodrogue validée, d'autres supports biocompatibles pourront être mis au point. Enfin, un bras espaceur PEG a été inséré entre le motif clivable et les billes pour favoriser le clivage enzymatique (Figure 13).

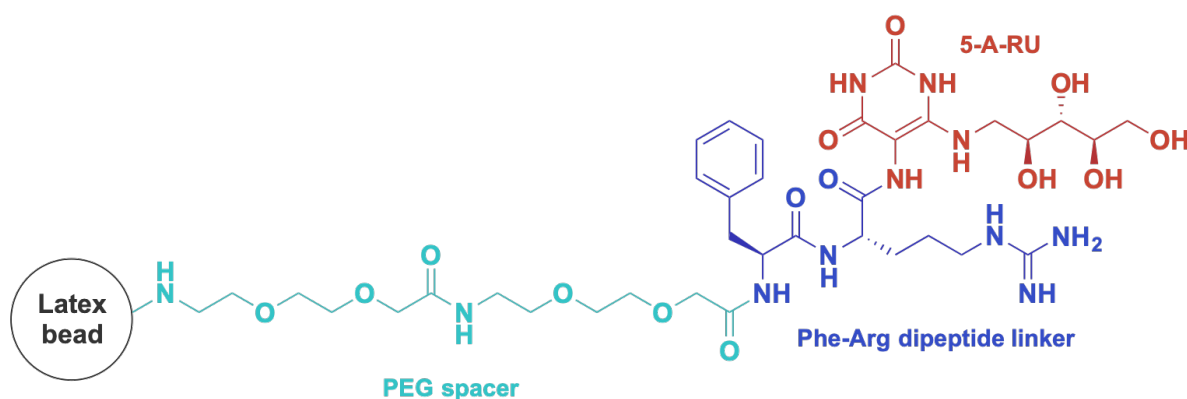


Figure 13: Structure de la prodrogue de 5-A-RU

A. Synthèse chimique

La synthèse du linker **44** a été effectuée sur support solide en utilisant une résine 2-chlorotrityl (Schéma 10).

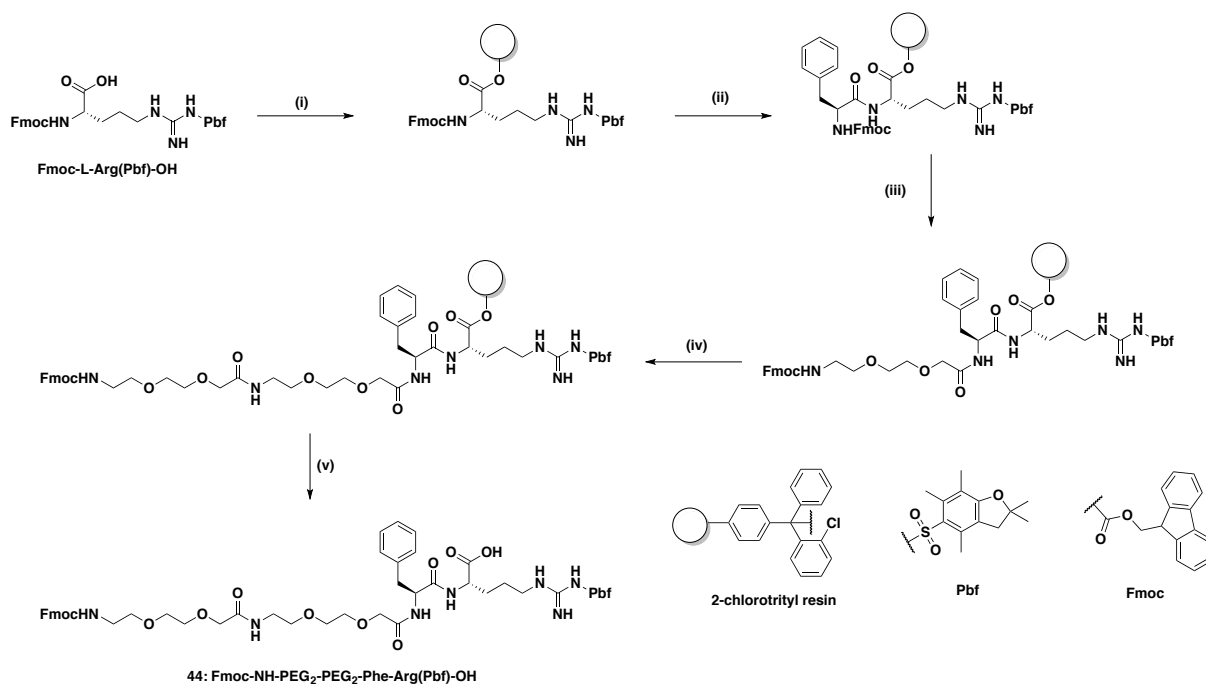


Schéma 10: Synthèse de 44 sur support solide; Réactifs et conditions: (i) résine 2-chlorotrityl chloride, DIEA dans DCM; (ii) 1) pipéridine 20% dans DMF, 2) Fmoc-NH-Phe-OH, DIEA, PyBOP dans DMF; (iii) 1) pipéridine 20% dans DMF, 2) Fmoc-NH-PEG₂-OH, DIEA, PyBOP dans DMF; (iv) 1) pipéridine 20% dans DMF, 2) Fmoc-NH-PEG₂-OH, DIEA, PyBOP dans DMF; (v) TFA/AcOH/H₂O (7/1/2); rendement global : 47%

Dans un premier temps, nous avons souhaité optimiser la réaction de couplage en utilisant la molécule 7-amino-4-méthylcoumarin (AMC). De nombreux essais infructueux ont été effectués avant d'essayer avec un agent de couplage plus réactif, le TCFH (Schéma 11). Le produit de couplage **45** a pu être obtenu bien qu'une épimérisation du centre stéréogénique de l'arginine soit survenue. Après déprotection du groupement protecteur Pbf, nous avons pu isoler le mélange d'épimères **46**.

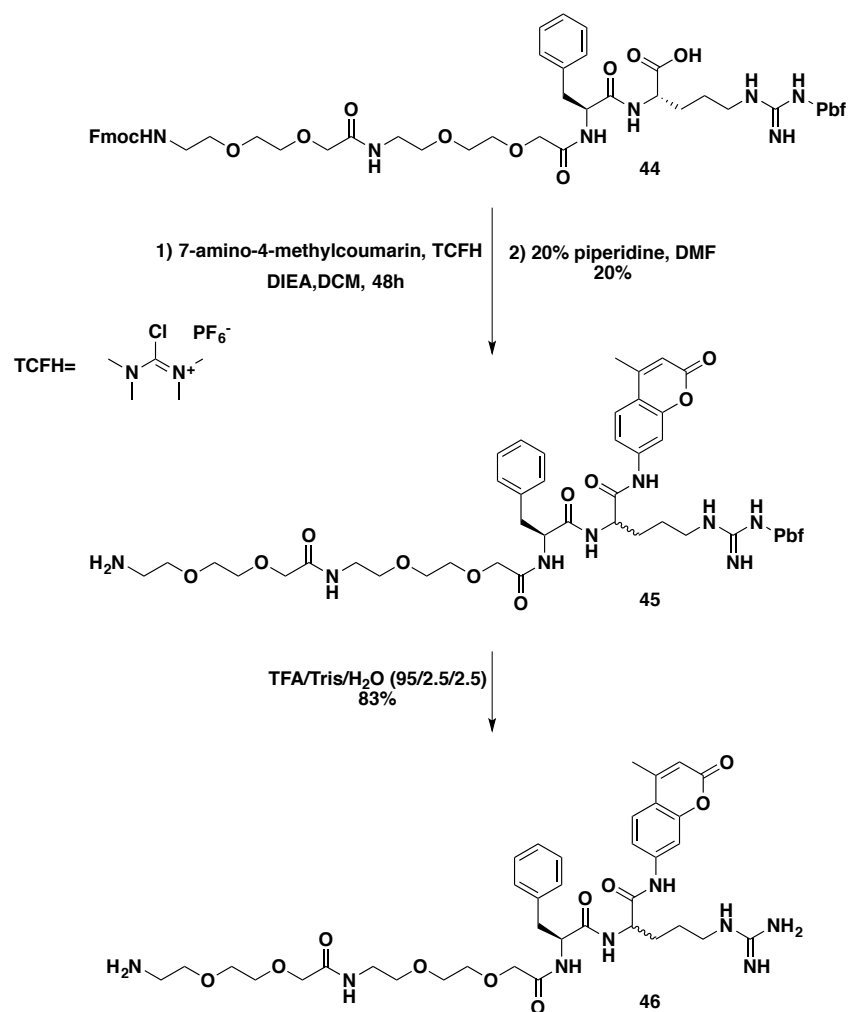


Schéma 11: Synthèse de 46

Les mêmes conditions ont été utilisées pour coupler le 5-A-RU à **44** mais sans réussite du fait de l'insolubilité du 5-A-RU dans le DCM. C'est pourquoi nous avons essayé le couplage avec la molécule **72**, analogue du 5-A-RU qui a montré une meilleure solubilité dans les solvants organiques que ce dernier. Nous avons réussi à coupler **72** à **44** en utilisant le TCFH et un mélange DCM/MeOH comme solvant de réaction. Comme pour **46**, une épimérisation est survenue au cours de la réaction. Malgré tout, le conjugué **47** a bien été obtenu (Schéma 12).

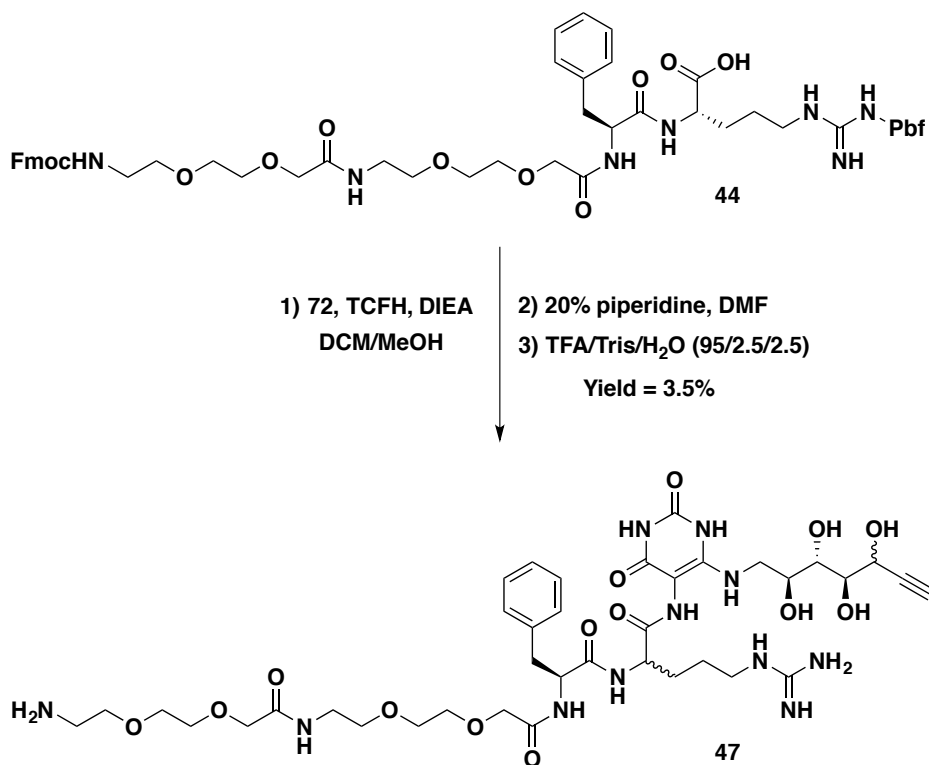


Schéma 12: Synthèse de 47

Finalement, **46** et **47** ont été couplé aux billes de latex par couplage peptidique en milieu aqueux pour donner respectivement **48** et **49** (Schéma 13).

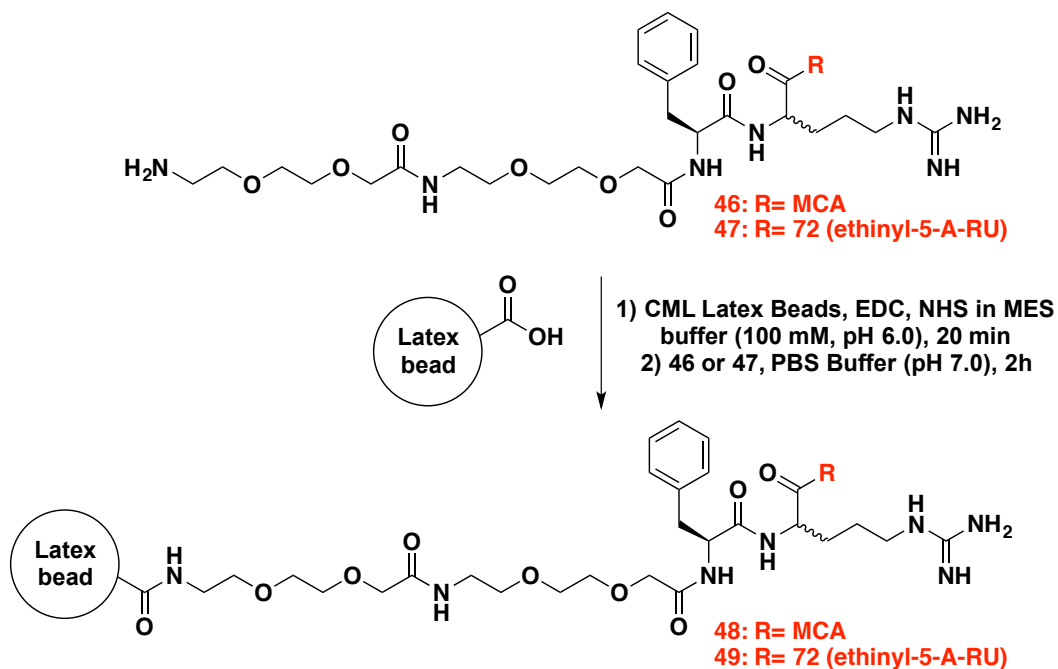


Schéma 13: Synthèse des conjugués CML 48 et 49

B. Evaluation biochimique et biologique des prodrogues de 5-A-RU

1. Evaluation biochimique

L'évaluation biochimique de **46** et **48** a permis de montrer un clivage efficace des deux conjugués par la cathepsine L (Figure 14). En revanche, aucun clivage n'a été détecté avec **47** et **49**.

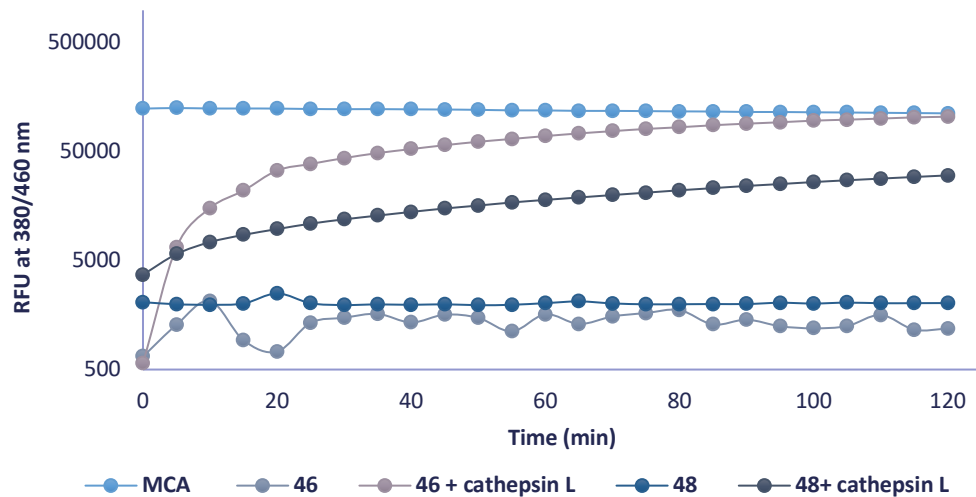


Figure 14: Test de clivage par cathepsine L de 46 et 48. Le clivage a été évalué en mesurant l'intensité de fluorescence à 380/460 nm ($\lambda_{exc}/\lambda_{emi}$) due au relargage d'AMC dans le milieu

2. Evaluation biologique des conjugués

Aucun des produits conjugués aux billes de latex n'a montré d'activité biologique contrairement à **47** qui a induit une légère activation des cellules MAIT (Figure 15). Ce résultat contredit celui obtenu lors de l'évaluation biochimique et cela indique que le conjugué a bien été en partie clivé dans les cellules, probablement par d'autres cathepsines que la cathepsine L.

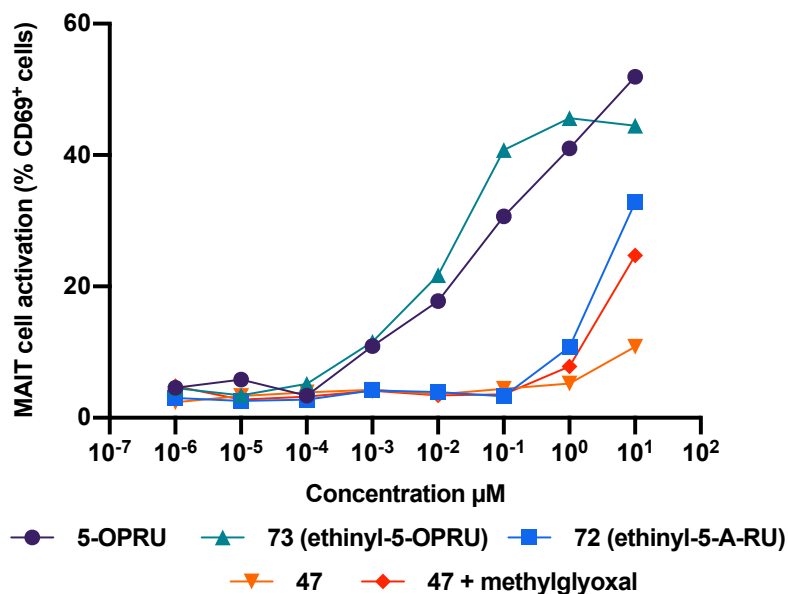


Figure 15: Evaluation biologique de 47

II. Synthèse d'une prodrogue auto-immolable du 5-A-RU

A. Design de la prodrogue

En nous basant sur les travaux d'une autre équipe de recherche qui cherchait à développer des prodrogues de 5-A-RU, nous avons décidé de synthétiser une seconde prodrogue présentant un linker valine-citrulline sensible à la cathepsine B et comportant un espaceur auto-immolable para-aminobenzyl alcohol (PAB)²³. En effet, ce linker a prouvé son efficacité et son utilisation a permis de produire des prodrogues stables et actives du 5-A-RU à visée anti-cancéreuse. Nous avons souhaité produire une autre prodrogue pour étudier les propriétés antimicrobiennes des cellules MAIT (Figure 16).

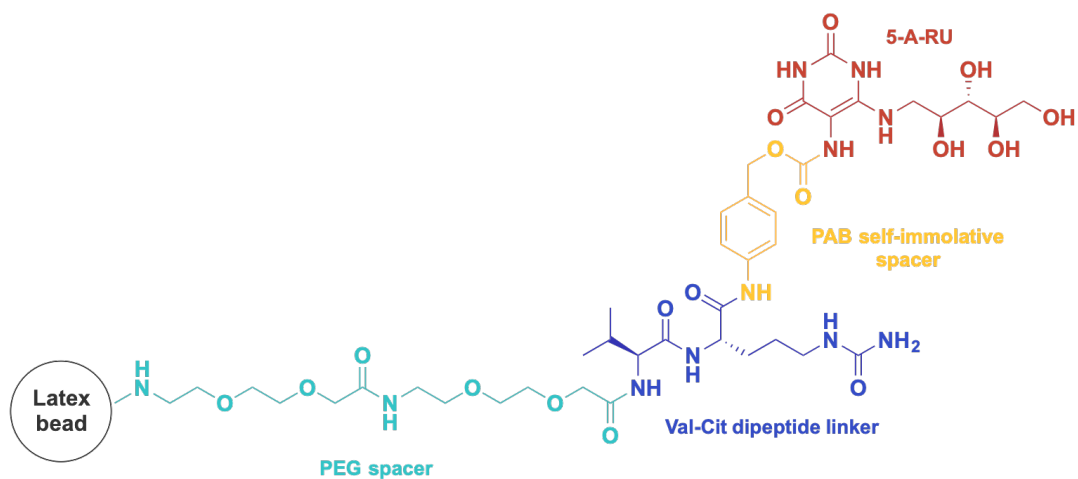


Figure 16: Structure chimique de la prodrogue auto-immolable de 5-A-RU

B. Synthèse de la prodrogue

1. Synthèse du linker

La synthèse des linkers **51** et **53** a été réalisée cette fois en solution (Schéma 14).

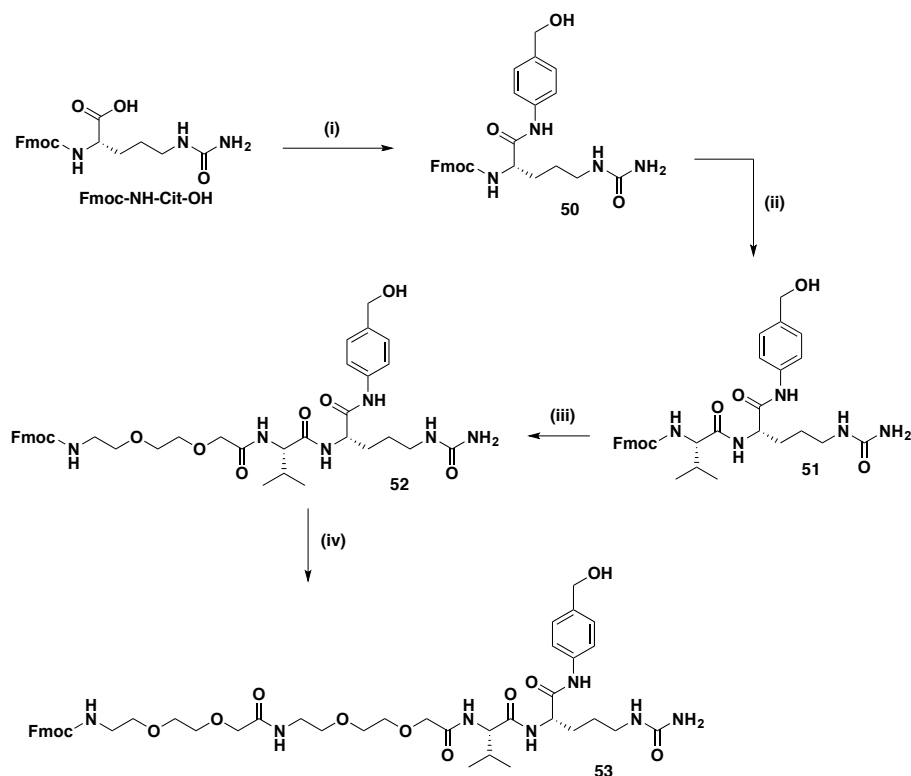


Schéma 14: Synthèse des linkers **51** et **53**; Réactifs et conditions: (i) 4-aminobenzyl alcohol, HATU, DIEA dans DMF, 87%; (ii) 1) pipéridine 20% dans DMF, 2) Fmoc-NH-Val-O-Su dans DMF, 56%; (iii) pipéridine 20% dans DMF, 2) Fmoc-NH-PEG₂-O-Su dans DMF, 47%; (iv) pipéridine 20% dans DMF, 2) Fmoc-NH-PEG₂-O-Su dans DMF, 47%

2. Couplage de 51 et 53 à 5-A-RU

5 (5-A-RU.HCl) a été couplé à **51** (donnant l'analogue déjà décrit **56**²³) et à **53** en utilisant des intermédiaires activés par un ester de paranitrophényle (PNP) (Schéma 15). L'utilisation de pyridine comme solvant pour la réaction de couplage est essentielle car elle permet de neutraliser **5** tout en solubilisant le composé qui peut ensuite réagir avec les linkers pour donner **56** et **57**. Les mêmes réactions réalisées avec la forme neutre du 5-A-RU n'ont pas permis d'obtenir les composés souhaités du fait de l'insolubilité de 5-A-RU dans les solvants organiques. Les composés **58** et **59** ont finalement été obtenus après déprotection de l'amine terminale de la valine.

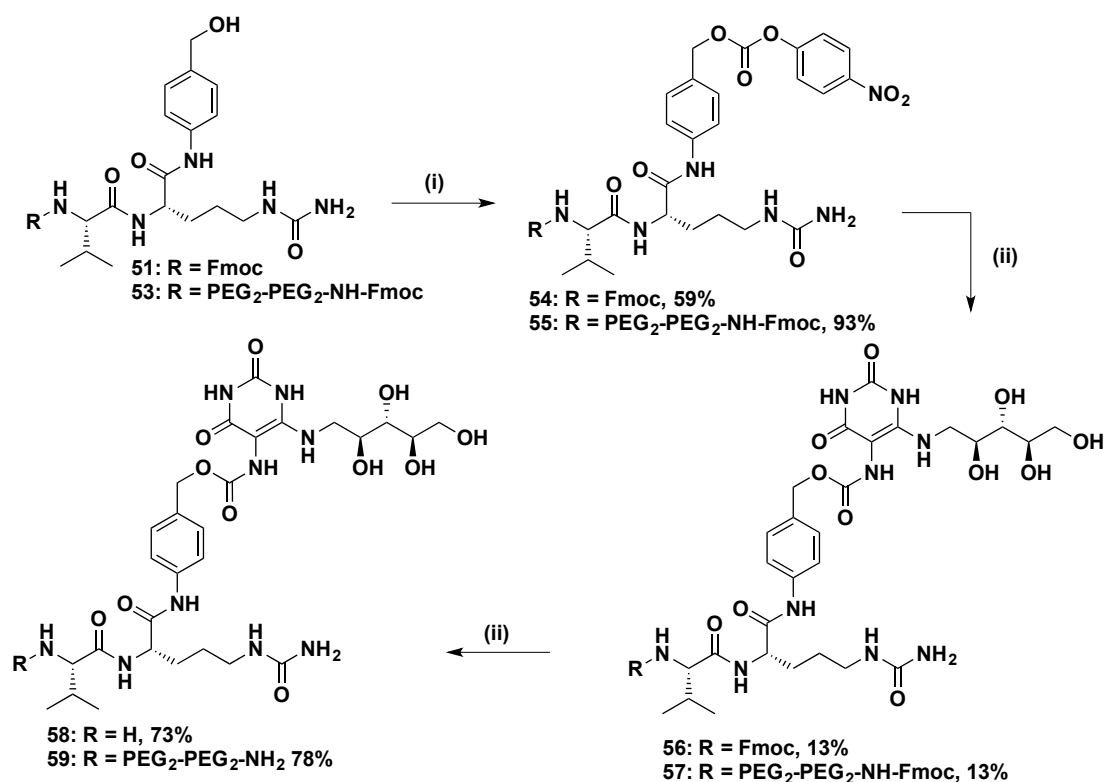


Schéma 15: Synthèse de 58 et 59; Réactifs et conditions: (i) *bis*-4-nitrophényl carbonate, DIPEA dans DMF; (ii) 5-A-RU dans pyridine; (iii) pipéridine dans DMF

3. Couplage de 59 avec les billes de latex

Comme **47**, la molécule **59** a été couplée aux billes de latex par une liaison peptidique pour donner **60** (Schéma 16). Afin d'étudier la réponse immunologique induite par la prodrogue, nous avons également ajouté de l'ovalbumine sur les billes.

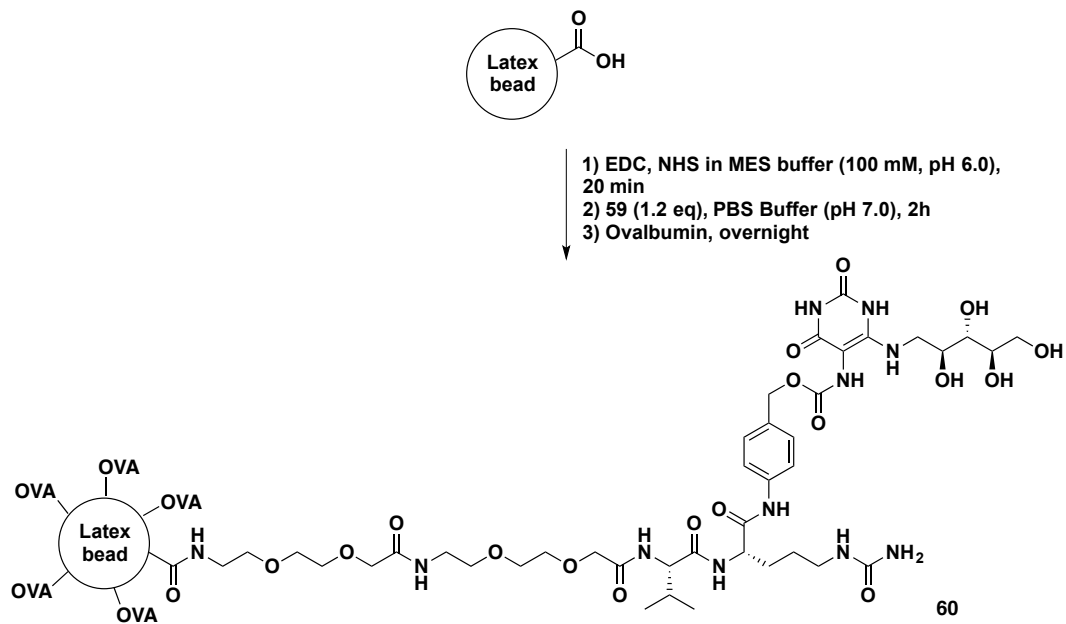


Schéma 16: Synthèse du conjugué 60

C. Evaluation biologique

Malheureusement, le conjugué 60 n'a pas permis une activation des cellules MAIT comme 49. À l'inverse, les conjugués 58 et 59 ont montré une activation modérée des cellules MAITs, plus forte que celle du 5-A-RU et 47 mais moins forte que celle du 5-OP-RU (Figure 17). Ces résultats confirment l'efficacité du vecteur utilisé.

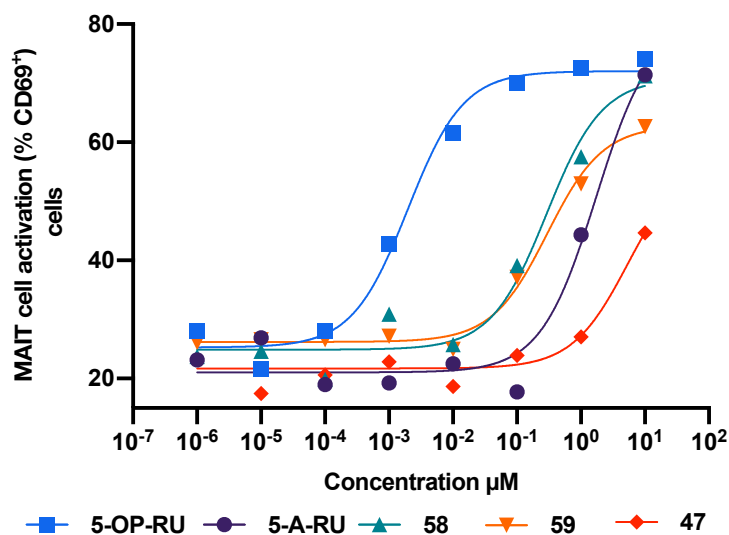


Figure 17: Evaluation biologique des différents prodrogues sur des cellules MAIT d'une souris double transgénique

Résumé du chapitre 3: "Design and synthesis of a new chemical probe for the study of MAIT cell biology"

I. Introduction

L'objectif de ce projet de recherche était de synthétiser une sonde chimique permettant de visualiser et de suivre les antigènes des cellules MAIT dans les cellules et tissus biologiques. Nous avons synthétisé deux analogues (diastéréoisomères) du 5-OP-RU présentant une fonction alcyne au niveau de la chaîne ribityle (Figure 18). L'introduction d'un tel groupement chimique permet de faire réagir ces molécules via CuAAC (copper(I)-catalyzed azide-alkyne cycloaddition) dans des réactions bio-orthogonales *in vitro*, afin de révéler le complexe formé avec MR1 par microscopie à fluorescence.

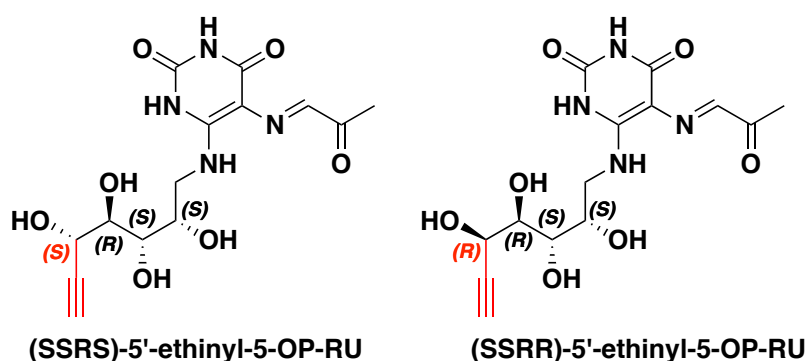


Figure 18: Structure chimique des sondes synthétisées

II. Synthèse des sondes chimiques

Une protection des hydroxyles par groupements TBS a été choisi pour la synthèse (Schéma 17). Nous avons synthétisé un précurseur **66** présentant un azoture afin de donner aisément une amine par réaction de Staudinger. L'étape critique était la déprotection sélective de l'alcool primaire avec l'acide camphorsulfonique donnant **67**. L'addition du groupement TMS-acétylène a permis d'obtenir **69**, mélange de deux diastéréoisomères. Nous avons également découvert qu'une migration d'un groupement TBS s'était produite durant cette réaction du 4'-OH vers le 5'-OH.

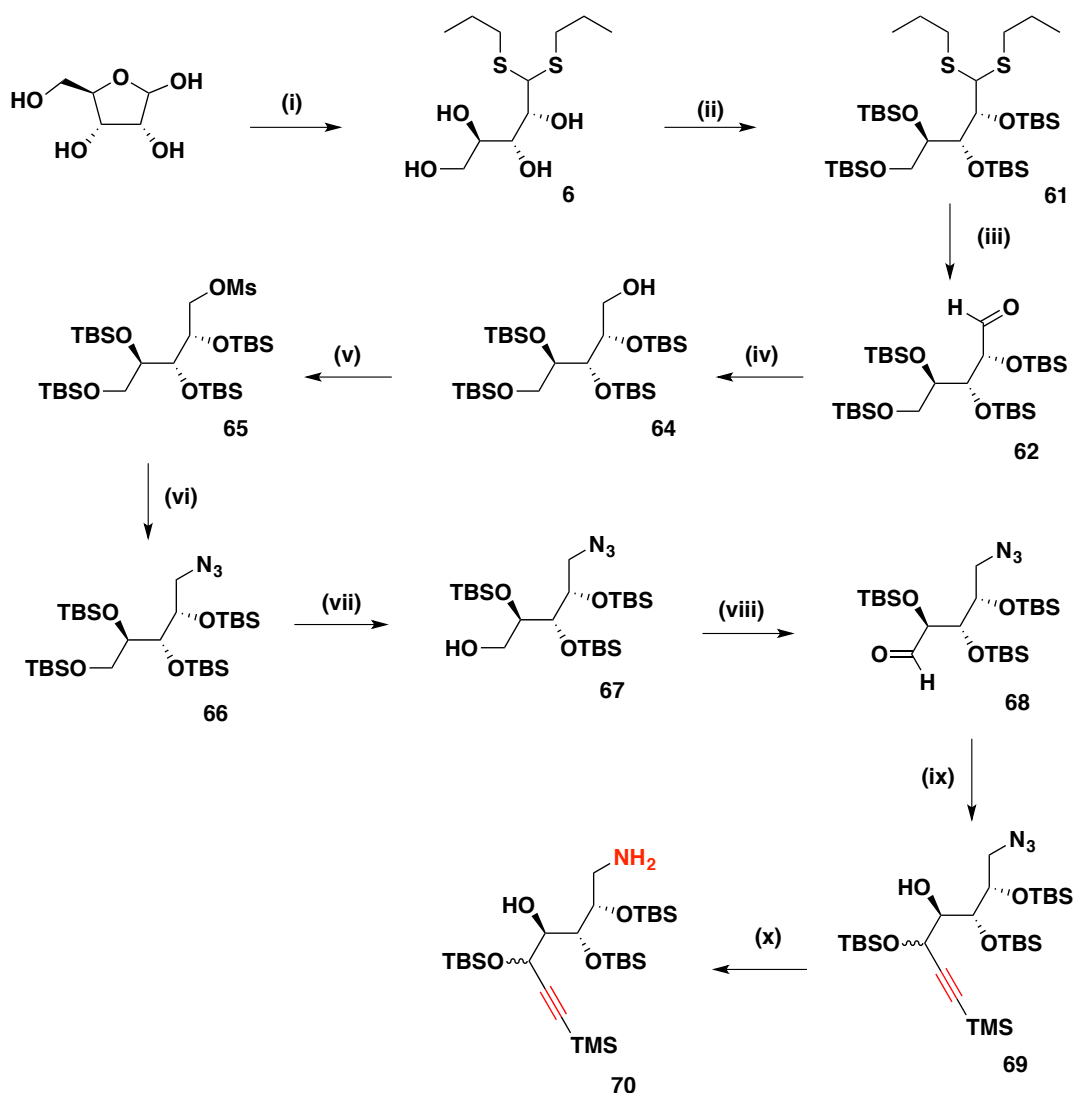


Schéma 17: Synthèse de 70. Conditions et réactifs : (i) *n*-propanethiol dans HCl 37% 0°C à ta, 87%; (ii) TBS-OTf, 2,6-lutidine dans CH₂Cl₂, ta, 54%; (iii) I₂, NaHCO₃ dans acétone/eau, 83%; (iv) NaBH₄ dans MeOH, 0°C à ta, 90% (v) chlorure de mésyle dans pyridine, ta, 95%; (vi) NaN₃ in DMF, 120°C, 99%; (vii) (1*R*)-(-)-acide camphorsulfonique dans MeOH/CH₂Cl₂, ta, 19%; (viii) DMP dans CH₂Cl₂, 0°C à ta, 71%; (ix) TMS-acétylène, *n*-BuLi dans THF -78°C à ta, 45%; (x) PPh₃ dans THF/H₂O, reflux 75%;

Le précurseur ethinyl-5-A-RU **72** a été obtenu après couplage entre **70** et **3** puis réduction du groupement nitro (Schéma 18). La molécule ethinyl-5-OP-RU **73** a été préparée comme **12a**, en faisant réagir **73** avec du methylglyoxal en excès dans du DMSO (48h à température ambiante).

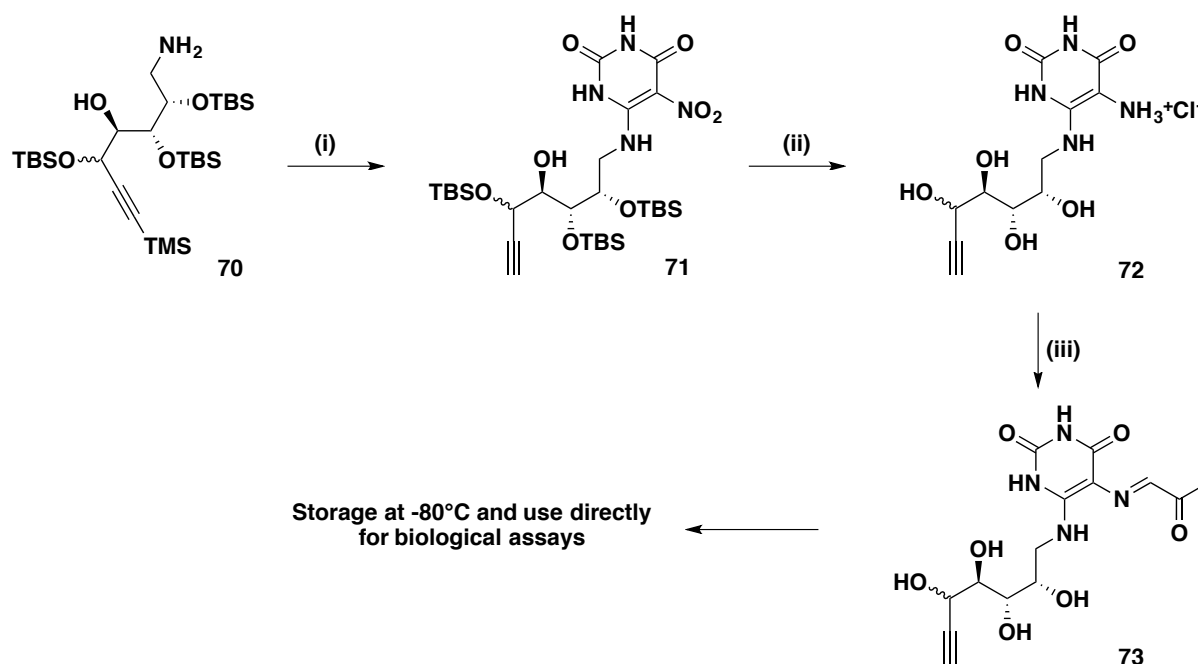


Schéma 18: Synthèse de 73. Réactifs et conditions: (i) 1) 6-chloro-5-nitouracil, Et₃N dans DMF, 50°C; 2) K₂CO₃ dans MeOH, ta, 71%; (ii) 1) Na₂S₂O₄ dans MeOH/H₂O, 90°C; 2) HCl 37% dans MeOH, 0°C à ta, 58%; (iii) methylglyoxal dans DMSO, 48h (produit non isolé)

Des cristaux de **71a** ont été obtenus afin d'effectuer une analyse cristallographique de la molécule et déterminer sa stéréochimie (5'R) (Figure 19). Cette même analyse a également mis en évidence la migration du groupement TBS du 4'-OH vers le 5'-OH comme indiqué précédemment.

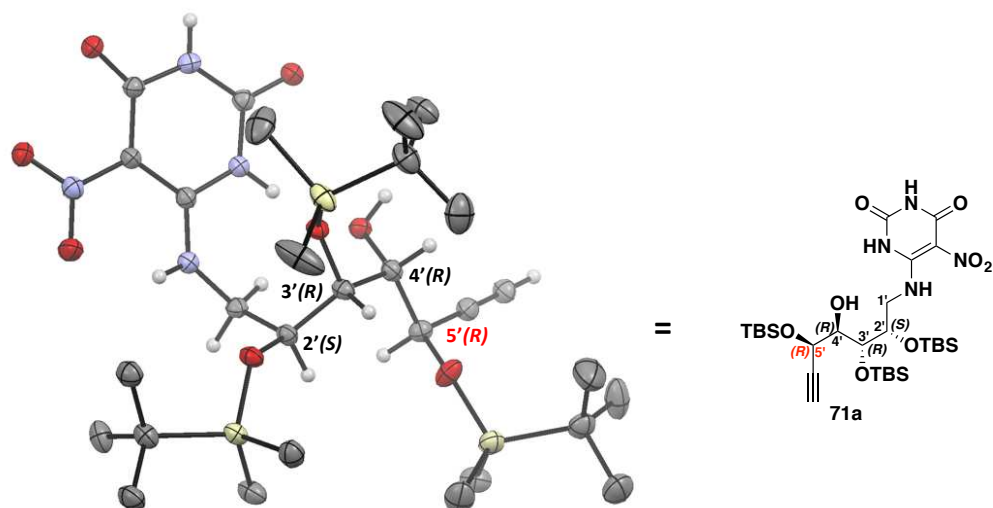


Figure 19: Vue ORTEP d'un conformère de **71a**; les ellipsoïdes thermiques sont dessinées avec un niveau de probabilité de 30%

III. Evaluation biologique

A. Up-régulation de MR1

Les deux diastéréoisomères **73a** et **73b** ont induit une forte up-régulation de MR1, supérieure à celle observée avec le 5-OP-RU (Figure 20).

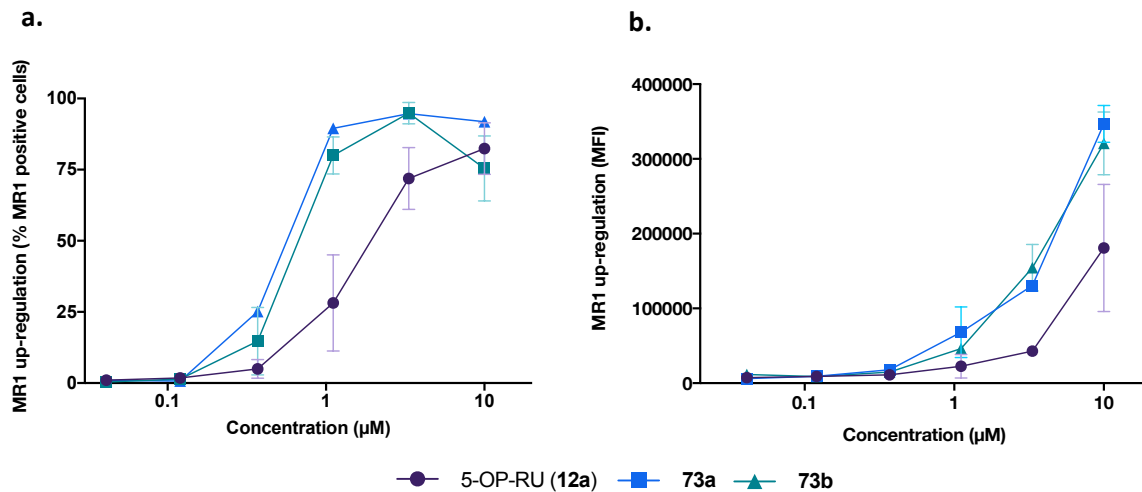


Figure 20: Up-régulation de MR1 en présence de 12a, 73a et 73b; a. pourcentage de cellules MR1 positives; b. MFI : intensité moyenne de fluorescence de l'anticorps anti-MR1-PE; les résultats sont exprimés en moyennes \pm SD de duplicats expérimentaux

B. Activation des cellules MAIT

Les molécules **73a** et **73b** ont activé les cellules MAIT de souris doubles transgéniques (répertoire monoclonal de cellules MAITs) de manière similaire au 5-OP-RU (Figure 21). En revanche, aucune activité n'a été détectée avec des cellules MAIT de souris simple transgéniques (répertoire polyclonal de cellules MAITs). Ces résultats montrent l'importance de la chaîne β du TCR dans la reconnaissance des antigènes des MAIT.

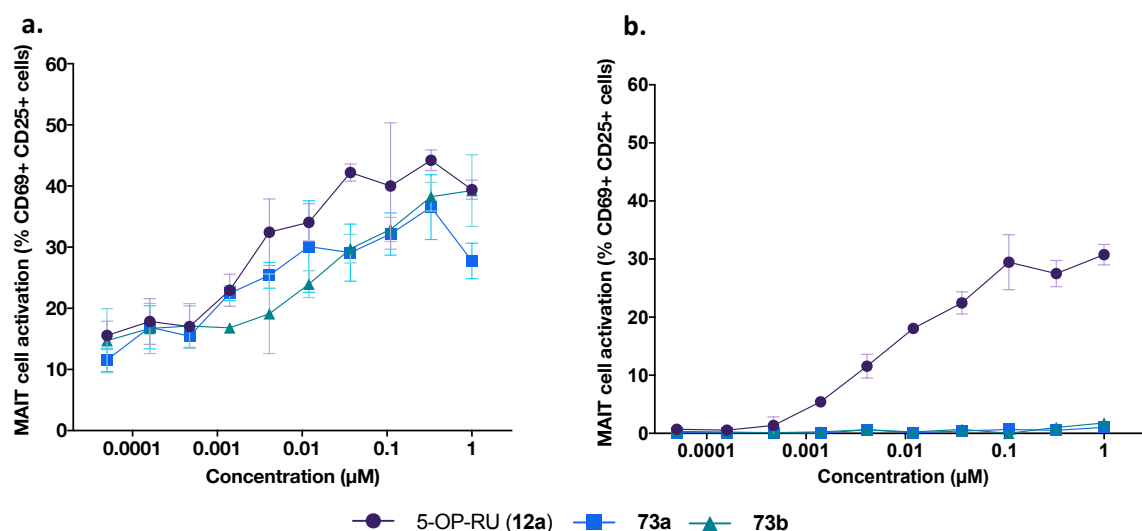


Figure 21: Activation des cellules MAIT par 12a, 73a et 73b; a. cellules MAITs de souris doubles transgéniques $i\alpha 19 V\beta 8$; b. cellules MAITs de souris simples transgéniques; les résultats sont exprimés en moyennes \pm SD de duplicats expérimentaux

C. Utilisation de 73 comme sonde chimique pour l'étude de la biologie des cellules MAIT

Afin de valider notre stratégie de chimie click, nous avons réalisé des expériences de CuAAC *in vitro* avec le mélange de diastéréoisomères **73** (Figure 22). La réaction click a bien fonctionné dans des cellules WT3-m et le complexe MR1-**73** a pu être observé par microscopie à fluorescence (fluorescence localisée autour du noyau après 1h d'incubation). À l'inverse, aucun signal fluorescent n'a été détecté avec la lignée WT3 sauvage (WT3-WT) qui exprime très peu de MR1. Ces résultats suggèrent une liaison spécifique du ligand à MR1 comme recherché et valide l'utilisation de **73** comme sonde chimique pour révéler la présence et la localisation de MR1 *in vitro*.

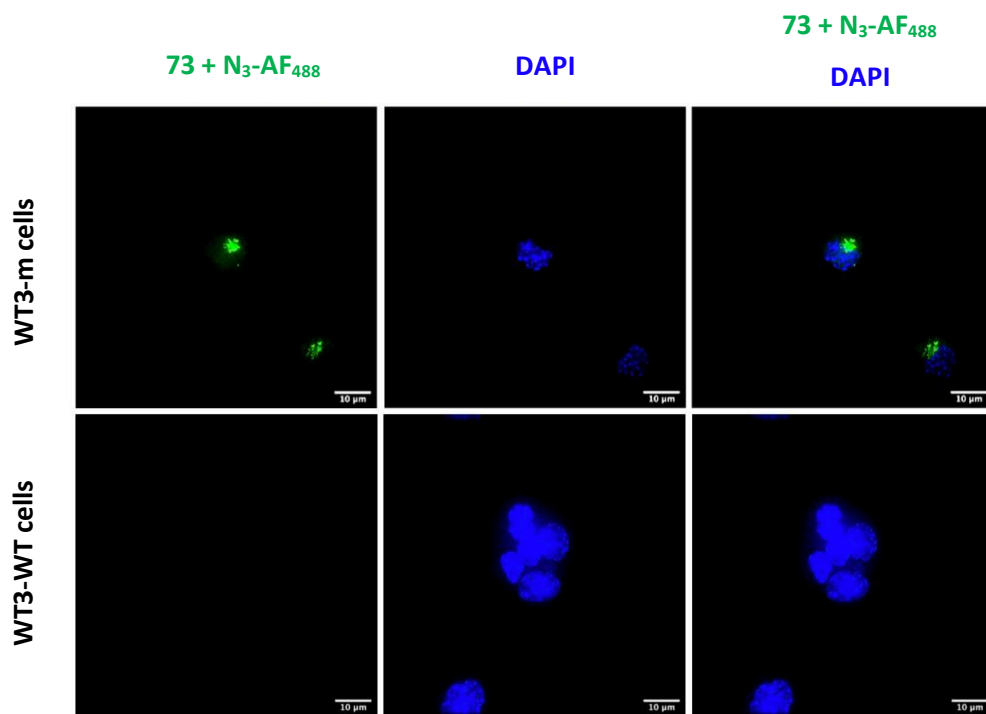


Figure 22: Images de microscopie à fluorescence de 73 conjugué au fluorochrome N₃-AF₄₈₈ (vert) et DAPI (bleu) dans des cellules WT3-m et WT3-WT

Bibliographie

- (1) Seach, N.; Guerri, L.; Le Bourhis, L.; Mburu, Y.; Cui, Y.; Bessoles, S.; Soudais, C.; Lantz, O. Double-Positive Thymocytes Select Mucosal-Associated Invariant T Cells. *J. Immunol. Baltim. Md 1950* **2013**, *191* (12), 6002–6009. <https://doi.org/10.4049/jimmunol.1301212>.
- (2) Martin, E.; Treiner, E.; Duban, L.; Guerri, L.; Laude, H.; Toly, C.; Premel, V.; Devys, A.; Moura, I. C.; Tilloy, F.; Cherif, S.; Vera, G.; Latour, S.; Soudais, C.; Lantz, O. Stepwise Development of MAIT Cells in Mouse and Human. *PLOS Biol.* **2009**, *7* (3), e1000054. <https://doi.org/10.1371/journal.pbio.1000054>.
- (3) Legoux, F.; Bellet, D.; Daviaud, C.; Morr, Y. E.; Darbois, A.; Niort, K.; Procopio, E.; Salou, M.; Gilet, J.; Ryffel, B.; Balvay, A.; Foussier, A.; Sarkis, M.; Marjou, A. E.; Schmidt, F.; Rabot, S.; Lantz, O. Microbial Metabolites Control the Thymic Development of Mucosal-Associated Invariant T Cells. *Science* **2019**, *366* (6464), 494–499. <https://doi.org/10.1126/science.aaw2719>.
- (4) Cui, Y. Biologie Des Cellules MAIT Chez La Souris. thesis, Sorbonne Paris Cité, 2015.
- (5) Kurioka, A.; Walker, L. J.; Klenerman, P.; Willberg, C. B. MAIT Cells: New Guardians of the Liver. *Clin. Transl. Immunol.* **2016**, *5* (8), e98. <https://doi.org/10.1038/cti.2016.51>.
- (6) Kurioka, A.; Ussher, J. E.; Cosgrove, C.; Clough, C.; Fergusson, J. R.; Smith, K.; Kang, Y.-H.; Walker, L. J.; Hansen, T. H.; Willberg, C. B.; Klenerman, P. MAIT Cells Are Licensed through Granzyme Exchange to Kill Bacterially Sensitized Targets. *Mucosal Immunol.* **2015**, *8* (2), 429–440. <https://doi.org/10.1038/mi.2014.81>.
- (7) Bourhis, L. L.; Dusseaux, M.; Bohineust, A.; Bessoles, S.; Martin, E.; Premel, V.; Coré, M.; Sleurs, D.; Serriari, N.-E.; Treiner, E.; Hivroz, C.; Sansonetti, P.; Gougeon, M.-L.; Soudais, C.; Lantz, O. MAIT Cells Detect and Efficiently Lyse Bacterially-Infected Epithelial Cells. *PLOS Pathog.* **2013**, *9* (10), e1003681. <https://doi.org/10.1371/journal.ppat.1003681>.
- (8) Salio, M.; Gasser, O.; Gonzalez-Lopez, C.; Martens, A.; Veerapen, N.; Gileadi, U.; Verter, J. G.; Napolitani, G.; Anderson, R.; Painter, G.; Besra, G. S.; Hermans, I. F.; Cerundolo, V. Activation of Human Mucosal-Associated Invariant T Cells Induces CD40L-Dependent Maturation of Monocyte-Derived and Primary Dendritic Cells. *J. Immunol.* **2017**. <https://doi.org/10.4049/jimmunol.1700615>.
- (9) Mondot, S.; Boudinot, P.; Lantz, O. MAIT, MR1, Microbes and Riboflavin: A Paradigm for the Co-Evolution of Invariant TCRs and Restricting MHCI-like Molecules? *Immunogenetics* **2016**, *68* (8), 537–548. <https://doi.org/10.1007/s00251-016-0927-9>.
- (10) Eckle, S. B. G.; Corbett, A. J.; Keller, A. N.; Chen, Z.; Godfrey, D. I.; Liu, L.; Mak, J. Y. W.; Fairlie, D. P.; Rossjohn, J.; McCluskey, J. Recognition of Vitamin B Precursors and Byproducts by Mucosal Associated Invariant T Cells. *J. Biol. Chem.* **2015**, *290* (51), 30204–30211.

<https://doi.org/10.1074/jbc.R115.685990>.

- (11) Downey, A. M.; Kapłonek, P.; Seeberger, P. H. MAIT Cells as Attractive Vaccine Targets. *FEBS Lett.* **2019**, *593* (13), 1627–1640. <https://doi.org/10.1002/1873-3468.13488>.
- (12) Ussher, J. E.; Willberg, C. B.; Klenerman, P. MAIT Cells and Viruses. *Immunol. Cell Biol.* **2018**, *96* (6), 630–641. <https://doi.org/10.1111/imcb.12008>.
- (13) Mak, J. Y. W.; Xu, W.; Reid, R. C.; Corbett, A. J.; Meehan, B. S.; Wang, H.; Chen, Z.; Rossjohn, J.; McCluskey, J.; Liu, L.; Fairlie, D. P. Stabilizing Short-Lived Schiff Base Derivatives of 5-Aminouracils That Activate Mucosal-Associated Invariant T Cells. *Nat. Commun.* **2017**, *8* (1), 1–13. <https://doi.org/10.1038/ncomms14599>.
- (14) Keller, A. N.; Eckle, S. B. G.; Xu, W.; Liu, L.; Hughes, V. A.; Mak, J. Y. W.; Meehan, B. S.; Pediongco, T.; Birkinshaw, R. W.; Chen, Z.; Wang, H.; D'Souza, C.; Kjer-Nielsen, L.; Gherardin, N. A.; Godfrey, D. I.; Kostenko, L.; Corbett, A. J.; Purcell, A. W.; Fairlie, D. P.; McCluskey, J.; Rossjohn, J. Drugs and Drug-like Molecules Can Modulate the Function of Mucosal-Associated Invariant T Cells. *Nat. Immunol.* **2017**, *18* (4), 402–411. <https://doi.org/10.1038/ni.3679>.
- (15) Awad, W.; Ler, G. J. M.; Xu, W.; Keller, A. N.; Mak, J. Y. W.; Lim, X. Y.; Liu, L.; Eckle, S. B. G.; Nours, J. L.; McCluskey, J.; Corbett, A. J.; Fairlie, D. P.; Rossjohn, J. The Molecular Basis Underpinning the Potency and Specificity of MAIT Cell Antigens. *Nat. Immunol.* **2020**, 1–12. <https://doi.org/10.1038/s41590-020-0616-6>.
- (16) Braganza, C. D.; Shibata, K.; Fujiwara, A.; Motozono, C.; Sonoda, K.-H.; Yamasaki, S.; Stocker, B. L.; Timmer, M. S. M. The Effect of MR1 Ligand Glyco-Analogues on Mucosal-Associated Invariant T (MAIT) Cell Activation. *Org. Biomol. Chem.* **2019**, *17* (40), 8992–9000. <https://doi.org/10.1039/C9OB01436E>.
- (17) Braganza, C. D.; Motozono, C.; Sonoda, K.-H.; Yamasaki, S.; Shibata, K.; Timmer, M. S. M.; Stocker, B. L. Agonistic or Antagonistic Mucosal-Associated Invariant T (MAIT) Cell Activity Is Determined by the 6-Alkylamino Substituent on Uracil MR1 Ligands. *Chem. Commun.* **2020**, *56* (39), 5291–5294. <https://doi.org/10.1039/D0CC00247J>.
- (18) Li, K.; Vorkas, C. K.; Chaudhry, A.; Bell, D. L.; Willis, R. A.; Rudensky, A.; Altman, J. D.; Glickman, M. S.; Aubé, J. Synthesis, Stabilization, and Characterization of the MR1 Ligand Precursor 5-Amino-6-D-Ribitylaminouracil (5-A-RU). *PLOS ONE* **2018**, *13* (2), e0191837. <https://doi.org/10.1371/journal.pone.0191837>.
- (19) Tchoupe, J. R.; Moreau, T.; Gauthier, F.; Bieth, J. G. Photometric or Fluorometric Assay of Cathepsin B, L and H and Papain Using Substrates with an Aminotrifluoromethylcoumarin Leaving Group. *Biochim. Biophys. Acta* **1991**, *1076* (1), 149–151. [https://doi.org/10.1016/0167-4838\(91\)90232-o](https://doi.org/10.1016/0167-4838(91)90232-o).

- (20) Werle, B.; Staib, A.; Jülke, B.; Ebert, W.; Zladoidsky, P.; Sekirnik, A.; Kos, J.; Spiess, E. Fluorometric Microassays for the Determination of Cathepsin L and Cathepsin S Activities in Tissue Extracts. *Biol. Chem.* **1999**, *380* (9), 1109–1116. <https://doi.org/10.1515/BC.1999.138>.
- (21) Kamboj, R. C.; Pal, S.; Raghav, N.; Singh, H. A Selective Colorimetric Assay for Cathepsin L Using Z-Phe-Arg-4-Methoxy- β -Naphthylamide. *Biochimie* **1993**, *75* (10), 873–878. [https://doi.org/10.1016/0300-9084\(93\)90042-Q](https://doi.org/10.1016/0300-9084(93)90042-Q).
- (22) Hoffmann, E.; Kotsias, F.; Visentin, G.; Bruhns, P.; Savina, A.; Amigorena, S. Autonomous Phagosomal Degradation and Antigen Presentation in Dendritic Cells. *Proc. Natl. Acad. Sci. U. S. A.* **2012**, *109* (36), 14556–14561. <https://doi.org/10.1073/pnas.1203912109>.
- (23) Lange, J.; Anderson, R. J.; Marshall, A. J.; Chan, S. T. S.; Bilbrough, T. S.; Gasser, O.; Gonzalez-Lopez, C.; Salio, M.; Cerundolo, V.; Hermans, I. F.; Painter, G. F. The Chemical Synthesis, Stability, and Activity of MAIT Cell Prodrug Agonists That Access MR1 in Recycling Endosomes. *ACS Chem. Biol.* **2020**, *15* (2), 437–445. <https://doi.org/10.1021/acscchembio.9b00902>.

RÉSUMÉ

Les cellules MAIT (mucosal-associated invariant T cells) sont des lymphocytes T de l'immunité "innate-like" capables de reconnaître des antigènes microbiens dérivés de la riboflavine (vitamine B2) qui sont produits exclusivement par des bactéries et certaines levures. L'activation des cellules MAIT dépendante du TCR nécessite une présentation antigénique par la protéine MR1 (MHC-class I related protein), celle-ci étant exprimée principalement par des cellules présentatrices d'antigènes. Une fois activées, les cellules MAIT peuvent exercer des fonctions antimicrobiennes en tuant directement les cellules infectées par un pathogène. Cette activité antimicrobienne suggère un fort intérêt thérapeutique à cibler les cellules MAIT dans des immunothérapies innovantes. Malheureusement, l'antigène le plus actif des MAIT, appelé 5-OP-RU, souffre d'une importante instabilité chimique, ce qui rend l'étude des cellules MAIT difficile. Cette molécule est produite par une réaction de condensation entre son précurseur clé, le 5-A-RU (aussi instable) et du méthylglyoxal endogène. Pour résoudre le problème de l'instabilité chimique, nous avons synthétisé de nouveaux analogues stables du 5-OP-RU en cherchant à maintenir une forte activité biologique sur les cellules MAIT. Nous avons également synthétisé des prodrogues du 5-A-RU capables de libérer la molécule in situ pour former ensuite du 5-OP-RU directement dans les cellules présentatrices d'antigène. Enfin, nous avons développé un analogue "clickable" du 5-OP-RU pouvant être utilisé dans le but de suivre et de visualiser les antigènes des cellules MAIT dans les tissus biologiques et les cellules par microscopie à fluorescence.

MOTS CLÉS

Chimie médicinale, immunologie, vectorisation, chimie bio-orthogonale

ABSTRACT

MAIT cells are innate-like T lymphocytes that recognize a series of microbial antigens derived from the riboflavin (vitamin B2) biosynthesis pathway, which are exclusively present in bacteria and some yeasts. The TCR dependent activation of MAIT cells requires an antigenic presentation mediated by MR1 (MHC-class I related protein) expressed mostly by antigen presenting cells (APCs). Once activated, MAIT cells can exert antimicrobial functions notably by killing pathogen-infected cells. This antimicrobial activity suggest a strong therapeutic interest in targeting MAIT cells in innovative antimicrobial immunotherapies. Unfortunately, the most active antigen discovered yet named 5-OP-RU suffers from a high chemical instability, thus making difficult the study of MAIT cell biology. 5-OP-RU is produced from a condensation reaction between its chemical precursor 5-A-RU (also unstable) and endogenous methylglyoxal. To overcome the stability issues, we designed and synthesized stable analogues of MAIT cells trying to maintain a strong potency of MAIT cells activation. We also synthesized prodrugs of 5-A-RU that were able of releasing the molecule in situ to form 5-OP-RU directly in APCs. Finally, we developed a new clickable analogue of 5-OP-RU that can be used to track and visualize MAIT cell antigens in biological tissues and cells by fluorescence microscopy.

KEYWORDS

Medicinal chemistry, immunology, vectorization, bio-orthogonal chemistry